
THE UNIVERSITY
*of* EDINBURGH

# Activation and catalytic transformation of carbon oxygenates by uranium, yttrium and palladium complexes


**Laura Puig-Urrea**

The University of Edinburgh

Submitted for the degree of Doctor of Philosophy

January 2019

**Declaration**

The work described in this thesis is my own, except where I have given reference to a published source or acknowledged help from a named person. This thesis has not been submitted, in whole or in part, for any degree at this or any other university. The work herein was carried out under the supervision of Professor Dieter Vogt from December 2014 to February 2017 and under the supervision of Professor Polly L. Arnold from February 2017 to January 2019.

Signature:

Date: 30/01/19

# Abstract

In recent years the use of renewable feedstocks, instead of fossil fuels, for the production of industrially important chemicals has drawn increasing attention. An interesting aspect of moving towards low-carbon technologies is the use of carbon dioxide as an appealing carbon source as a cheap, non-toxic and abundantly available $C_1$ building block.

This thesis is divided in two parts in which the activation and the catalytic transformation of small molecules, such as CO and $CO_2$, have been studied with an actinide, a rare-earth and a transition metal catalysts. An introduction examining the chemistry trends across d- and f-block is given in chapter one.

Part A:

Chapter two reviews important uranium and yttrium complexes in the literature that successfully undergo small molecule activation. Boroxide ligands and their properties are introduced and selected examples are provided.

Chapter three reports the synthesis and characterisation of a new U(III) boroxide complex and its reactivity towards small molecules. The synthesis and characterisation of two different yttrium boroxide complexes is reported and the reactivity with small molecules is compared.

Part B:

A very interesting use of carbon dioxide is the catalytic formation of acrylates with alkenes.

Chapter four reviews the catalytic transformation of carbon dioxide and ethene to acrylate, focusing on nickel and palladium catalyst and on the mechanism and the formation of a lactone as an intermediate species.

Chapter five describes the catalytic screening of different parameters such as catalyst precursor, ligands and temperature on the catalytic formation of acrylate using nickel and palladium catalysts.

Chapter six presents the detailed experimental methods used in part A and B.

# Lay Summary

The conversion of carbon oxygenates such as CO and $CO_2$, is a crucial target in order to reduce the use of fossil fuels, as both can be used as starting materials for the synthesis of chemical commodities. Moreover, an alternative to the use of fossil fuels as a form of energy, is the use of nuclear energy, thus developing an understanding in the f-block chemistry is essential.

The aim of this work is to study the structure and reactivity of new uranium and yttrium complexes bearing boroxide ligands. Boroxide ligands are particularly interesting as addition of another possible reactive site into the ligand environment might develop different reactivity. Herein the reactivity towards small molecules and other substrates with uranium and yttrium complexes is examined. Particularly interesting is the activation of arene solvents when the uranium boroxide complex reacts with several phosphines.

Furthermore, the catalytic formation of acrylates from carbon dioxide and ethene is examined and a screening on different parameters such as ligands is carried out.

# Acknowledgments

I would like to start these acknowledgments in order of appearance. Firstly, I would like to thanks to Prof. Dieter Vogt for giving me the opportunity to start my PhD in his group and his guidance in catalysis chemistry.

I would like to thanks all the members of the Vogt group. Thanks to Eszter and Vero with whom I have shared this long journey from day one, we've made it! I am also grateful to Anna, Maria, Viktor, Lewis, Evert and all the "temporary" group members: Bachir, Nicola, Juddith and Dani2, thanks for all the laughs, you all made my arrival to Edinburgh much easier. I would like to specially thanks to my board game and travel partners Dani and George for all the good memories and the future ones! And many many thanks to Dr Jenni Garden, you helped us all in a very difficult time, always with a smile and with your doors wide open until the very end. You are a blessing!

He de fer especial mencio al Dani, sense el qual la meitat d'aquesta tesis no existiría, moltissimes gràcies, i gràcies per suportar-me en els pitjors moments i ajudar-me a tirar endevant.

I am really grateful to Prof. Polly Arnold, for "adopting" me and for sharing her love and enthusiasm for a chemistry that was far from my comfort zone.

I would like to thanks all the Larnolds, past and present, it is not easy to start in a new group halfway through your PhD but you made it much easier. Thanks to Jordann and Cath who helped me lots in the beginning with understanding the "new" chemistry. I am really grateful to Rory and Tatsumi for their corrections and for helping me with the writing process. Lotte, Steven, Max, Megan, Ryan, Connor, Francis, Amy, Brad, Nicola, Jamie, Paul and Liam it's been an absolute pleasure!

I am very grateful for the help in crystallography to Dr Gary Nichol,and the NMR spectroscopy assistance provided by Dr Lorna Murray and Mr Juraj Bella.

I would like to thanks all the friend I made in Edinburgh, specially to Veronika and Adriana. Thanks for all the shared moments, all the listening and the plans. The future awaits!

Finalment vull agrair a tota la meva gent de Barelona, se que en algun moment veu patir una miqueta, però el vostre suport ha fet que això sigui possible. I agraïr especialment a la meva familía, gràcies per aguantar totes les meves neures, sobretot en aquest últims mesos d'escriptura.

# List of abbreviations

## General

| | |
|---|---|
| **18-c-6** | 18-crown-6 |
| **Acac** | Acetylacetonate |
| **Ad** | Adamantyl |
| **An** | Actinide |
| **APPI** | Atmospheric pressure photoionisation |
| **Ar** | Aryl |
| **Avg** | Average |
| **$BAr_4^F$** | Tetrakis[3,5-bis(trifluoromethyl)phenyl]borate |
| **BenzP*** | (R,R)-(+)-1,2-Bis(*tert*-butylmethylphosphino)benzene |
| **BTPP** | *Tert*-Butylimino-tri(pyrrolidino)phosphorane |
| **bpy** | 2,2'-Bipyridyl |
| **Cat** | Catalyst |
| **cdt** | 1,5,9-Cyclododecatriene |
| **CHP** | N-Cyclohexylpyrrolidone |
| **cod** | 1,5-Cyclooctadiene |
| **COT** | Cyclooctatetraenyl |
| **$COT^{TIPS}$** | (Tri-*iso*-propylsilyl)cyclooctatetraenyl |
| **Cp** | Cyclopentadienyl |
| **Cp*** | 1,2,3,4,5-Pentamethylcyclopentadienyl |
| **Crypt** | Cryptand |
| **Cy** | Cyclohexyl |
| **DBF** | N,N-dibutylformamide |
| **DBU** | 1,8-Diazabicyclo[5.4.0]undec-7-ene |
| **DCC** | *N*,*N*′-Dicyclohexylcarbodiimide |
| **dcpb** | 1,2-Bis(dicyclohexylphosphino)butane |
| **dcpe** | 1,2-Bis(dicyclohexylphosphino)ethane |
| **dcpfc** | 1,1'-Bis(dicyclohexylphosphino)ferrocene |
| **dcpm** | 1,2-Bis(dicyclohexylphosphino)methane |
| **dcpp** | 1,2-Bis(dicyclohexylphosphino)propane |
| **DFT** | Density functional theory |

| | |
|---|---|
| **d$^{i}$Prpfc** | 1,1'-Bis(di-*iso*-propylphosphino)ferrocene |
| **dme** | Dimethoxyethane |
| **dmpe** | 1,2-Bis(dimethylphosphino)ethane |
| **dmpm** | 1,2-Bis(dimethylphosphino)methane |
| **dppb** | 1,2-Bis(diphenylphosphino)butane |
| **dppe** | 1,2-Bis(diphenylphosphino)ethane |
| **dppEtPy** | 2-(2-(Diphenylphosphino)ethyl)pyridine |
| **dppfc** | 1,1'-Bis(diphenylphosphino)ferrocene |
| **dppm** | 1,2-Bis(diphenylphosphino)methane |
| **dppp** | 1,2-Bis(diphenylphosphino)propane |
| **dpppa** | 3-(Diphenylphosphino)-1-propylamine |
| **d$^{t}$Bupe** | 1,2-Bis(di-*tert*-butylphosphino)ethane |
| **d$^{t}$Bupfc** | 1,1'-Bis(di-*tert*-butylphosphino)ferrocene |
| **d$^{t}$BupmBz** | 1,2-Bis(di-*tert*-butylphosphinomethyl)benzene |
| **Et** | Ethyl |
| **EPR** | Electron paramagnetic resonance |
| **eq.** | Equivalents |
| **h** | Hours |
| **HBBN** | 9-Bora-9-bicyclononane |
| **IAS** | Inverse arene sandwich |
| **Im** | Bis(trifluoromethanesulfonyl)imide |
| **$^{i}$Pr** | *Iso*-propyl |
| **IR** | Infrared |
| **Ln** | Lanthanide |
| **L$^{TMS}$** | N,N'-Bis(trimethylsilyl)benzamidinate |
| **M** | Metal |
| **Me** | Methyl |
| **Me-bpe** | 1,2-Bis((2S,5S)-2,5-dimethylphospholano)ethane |
| **Mes** | Mesityl |
| **Mes$^{F}$** | 1,3,5-Tris(trifluoromethyl)phenyl |
| **Min** | Minutes |
| **NaBHT** | Sodium 2,6-di-*tert*-butyl-4-methylphenoxide |
| **nb** | 2,5-Norbornadiene |

| | |
|---|---|
| **Neop** | Neopentyl |
| **$NEt_3$** | Triethylamine |
| **NHC** | N-heterocyclic carbene |
| **NMR** | Nuclear Magnetic resonance |
| **OAr** | Aryloxide |
| **ODipp** | 2,6-Di-*iso*-propylphenoxide |
| **ODtbp** | 2,6-Di-*tert*-butylphenoxide |
| **OTf** | Trifluoromethanesulfonate |
| **OTtbp** | 2,4,6-Tri-*tert*-butylphenoxide |
| **Ph** | Phenyl |
| **ppm** | Parts per million |
| **Py** | Pyridine |
| **Py-O** | Pyridine N-oxide |
| **R** | Alkyl |
| **RE** | Rare earth |
| **r.t.** | Room temperature |
| **Solv** | Solvent |
| **SQUID** | Superconducting quantum interference device |
| **syngas** | Equimolar mixture of CO and $H_2$ |
| **$^t$Bu** | *Tert*-butyl |
| **tacn** | 1,4,7-Triazacyclononane |
| **THF** | Tetrahydrofuran |
| **TM** | Transition metal |
| **tmeda** | *N*,*N*,*N*′,*N*′-Tetramethylethylenediamine |
| **TON** | Turnover number |
| **$tren^{DBMS}$** | $\{N(CH_2CH_2NSi^tBuMe_2)_3\}$ |
| **trip** | Triisopropylphenyl |
| **XantPhos** | 4,5-Bis(diphenylphosphino)-9,9-dimethylxanthene |
| **XPhos** | 2-Dicyclohexylphosphino-2',4',6'-triisopropylbiphenyl |
| **XRD** | X-ray diffraction |
| **xs** | Excess |
| **Xy** | 3,5-Dimethylphenyl (xylyl) |

**NMR**

| | |
|---|---|
| **br** | Broad |
| **d** | Doublet |
| **dd** | Doublet of doublets |
| **m** | Multiplet |
| **ppm** | Parts Per Million |
| **s** | Singlet |
| **t** | Triplet |
| **tt** | Triplet of triplets |

# Contents

## Chapter 3: Mesityl-boroxide complexes of $U^{III}$ and $Y^{III}$

## Chapter 6: Experimental details

# Chapter 1 : Carbon oxygenate transformations through d- and f-block metals

The conversion of carbon oxygenates such as CO and $CO_2$ into chemical commodities is a crucial target in order to reduce the use of fossil fuels. Currently these non-renewable resources are the main source of energy (80% of the world's energy demands) and chemical feedstocks (approximately 95% of organic commodities, from pharmaceuticals to polymers).[1, 2] Carbon monoxide has been largely used as a $C_1$ building block in the Fischer-Tropsch process, where hydrocarbons are synthesised by hydrogenation of CO in the presence of transition metals.[3] Carbon dioxide is an abundant and inexpensive $C_1$ building block. Moreover, $CO_2$ is an attractive chemical reagent as the use of a greenhouse gas has the potential to reduce the negative environmental impact of climate change, although chemical industry is still far from achieving this goal. The major drawback in the use of $CO_2$ as a reagent is that a large energy input is required for its transformation due to its thermodynamic and kinetic stability.

A brief summary of the activation of CO and $CO_2$ by d- and f-block metals follows.

## 1.1. Carbon monoxide

### 1.1.1. Activation of carbon monoxide by transition metals

CO has two industrially relevant reactions with transition metal catalysts; hydroformylation and carbonylation.

The hydroformylation reaction consists of the reaction between alkenes and syngas (equimolar mixture of CO and $H_2$) to form aldehydes, and it was first discovered by Otto Rolen in 1938. Nowadays, industrial hydroformylation reactions are carried out with rhodium or cobalt homogeneous catalysts (Scheme 1.1).[4]

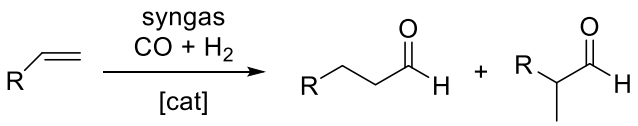


Scheme 1.1. The hydroformylation reaction.

An interesting aspect of this reaction is that even though aldehydes are of little commercial interest, they can be further converted to alcohols via hydrogenation, to carboxylic acids via oxidation, and to amines via reductive amination.

The most active metal in hydroformylation catalysis is rhodium. Concentrations of 10-100 mg/kg and temperatures below 140 °C are usually used. However, Rh is not the only metal that can perform this reaction: Co, Ir, Ru, Os, Tc, Mn, Fe and Re have also been used for hydroformylation reactions.[4]

The carbonylation of methanol by CO to yield acetic acid is another important catalytic reaction with industrial relevance. A simple depiction can be seen in Scheme 1.2.

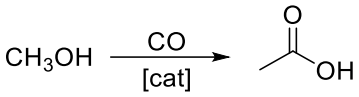


Scheme 1.2. Synthesis of acetic acid by carbonylation of MeOH.

Different industrial approaches have been developed since the 1970s, when the industrial production of acetic acid through carbonylation started. One of these processes was developed by Monsanto. The basic steps of the catalytic reaction by the Monsanto process are: a) the oxidative addition of methyl iodide to $[RhI_2(CO)_2]$; b) ligand migration to generate the acetyl complex followed by CO coordination; and c) reductive elimination of the acetyl iodide, which is then hydrolysed to give acetic acid and HI (Scheme 1.3).[3]

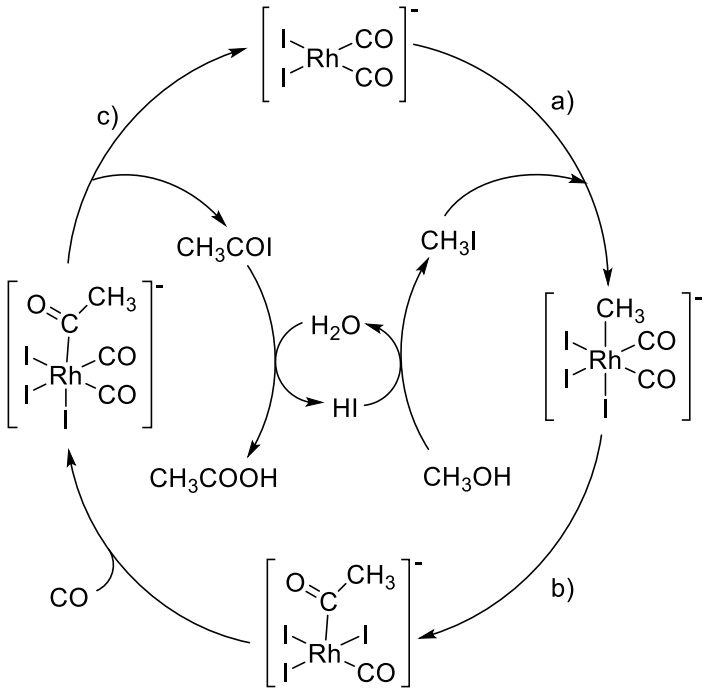


Scheme 1.3. Catalytic cycle for the carbonylation of MeOH through the Monsanto process.[3]

Several metals have proved to be active in the catalytic carbonylation of methanol and other substrates, such as Ru, Ni, Pd, Pt, Ir and Rh; the latter two are the most effective ones.[5] The carbonylation of organic compounds besides alcohols, such as alkenes, alkadienes (compounds containing two or more double bonds) and organic halides, has been widely studied[5, 6] and will not be discussed further in this chapter.

## 1.1.2. Activation of carbon monoxide by lanthanides and actinides

The direct reductive coupling and homologation of carbon monoxide by f-block complexes is not very common. However, a few examples have been reported. In this section, the most important examples are examined.

Evans and co-workers reported the reaction between the divalent samarium complex $[Sm(Cp^*)_2(THF)_2]$ (**A**) ($Cp^* = C_5Me_5$) and carbon monoxide to yield the ketene carboxylate complex $[Sm_2(Cp^*)_4(\mu\text{-}\eta^4\text{-}O_2CCCO)(THF)]_2$ (**C**).[7] The reaction proceeds through a two-electron reduction of three CO molecules to form a ketene carboxylate dianion $(CO)_3^{2-}$.The analogous product was observed few years later when the lanthanum

dinitrogen complex [{(Cp*)$_2$(THF)La}$_2$(μ-η$^2$:η$^2$-N$_2$)] (**B**) was exposed to 90 psi of CO to yield the La complex **C** (Scheme 1.4).[8]

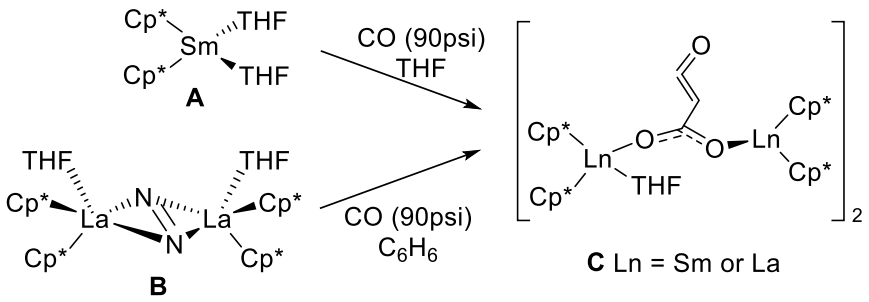


Scheme 1.4. Synthesis of ketene carboxylate complexes **C**.[7, 8]

The synthesis of the dinediolate lutetium complex **E** was also reported by Evans and co-workers when [Lu(Cp)$_2$($^t$Bu)(THF)] (**D**) (Cp = C$_5$H$_5$) was exposed to an excess of CO. Four molecules of CO are coupled to form a dinediolate moiety which bridges two lutetium centres (Scheme 1.5).[9]

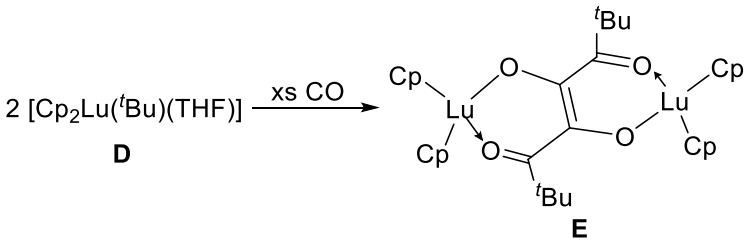


Scheme 1.5. Synthesis of dinediolate complex **E**.[9]

The addition of either an excess or one equivalent of CO to [Y(Cp*)$_2$(η$^2$-pyridyl)] (**F**) to yield the purple complex [{(Cp*)$_2$Y}$_2$(μ-κ$^2$-OC(2-NC$_5$H$_4$)$_2$] (**H**) was reported by Tebuen and co-workers (Scheme 1.6).[10] Neither of the expected complexes, the dinediolate nor the ketene carboxylate, was made. The reaction is proposed to proceeded through nucleophilic attack of the starting compound **F** on the acyl complex **G** to finally yield complex **H**.

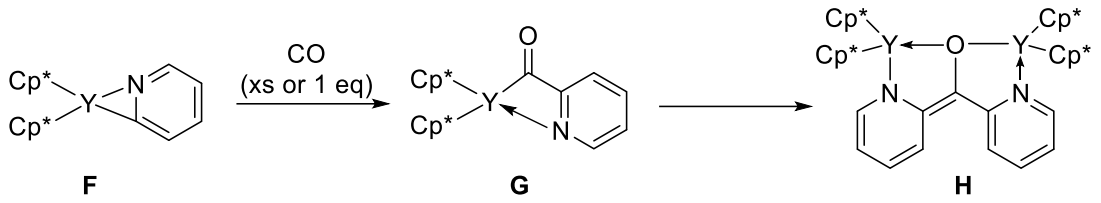


Scheme 1.6. Synthesis of complex **H** via CO activation.[10]

In 2012, Evans and co-workers reported the reduction of CO to the $CO^{1-}$ radical by an in situ generated solution of $Y^{2+}$, obtained from $Y(NR_2)_3/K$ (R = $SiMe_3$).[11] The formation of the polymeric complex $\{[(R_2N)_3Y(\mu\text{-}CO)_2][K_2(18\text{-}c\text{-}6)_2]\}_n$ (**I**) (18-c-6 = 18-crown-6), the ynediolate complex $[\{(R_2N)_3Y\}_2(\mu\text{-}OC{\equiv}CO)][\{K(18\text{-}c\text{-}6)\}_2(18\text{-}c\text{-}6)]$ (**J**), and the insertion/rearrangement product $[(R_2N)_2Y\{OC(=CH_2)Si(Me_2)NSiMe_3\}][K(18\text{-}c\text{-}6)]$ (**K**) were observed when different reaction conditions were used (Scheme 1.7).

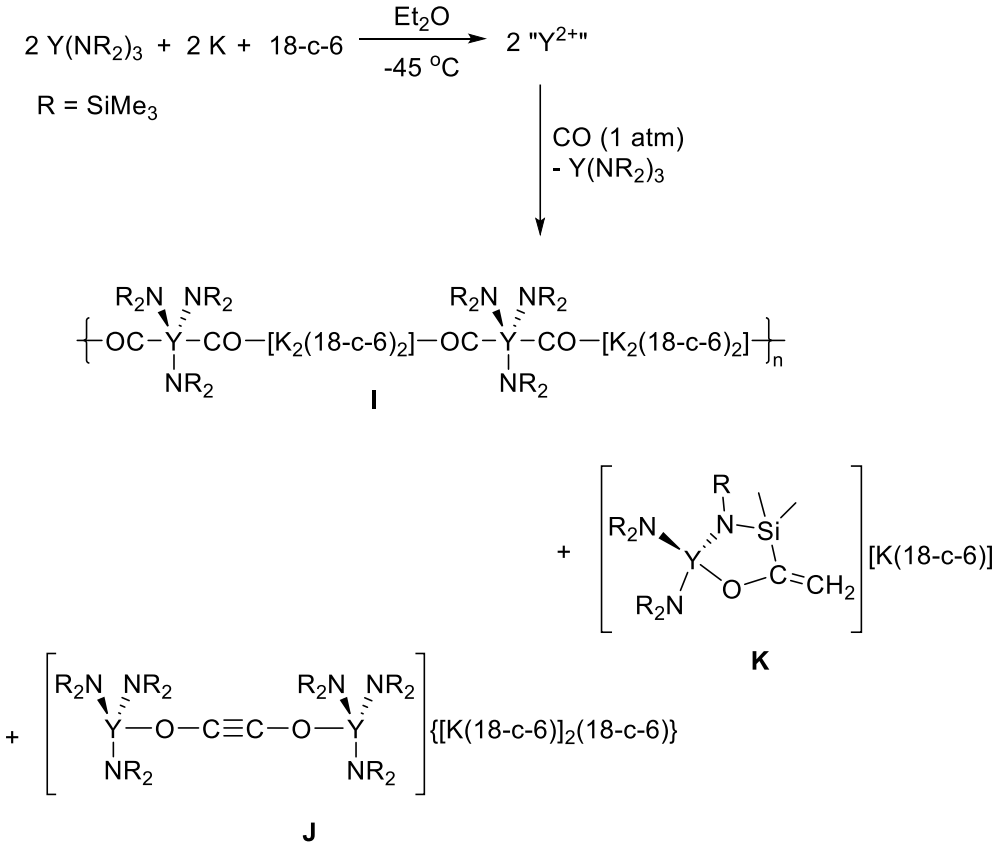


Scheme 1.7. Synthesis of compounds **I**, **J** and **K** by reaction of the $Y(NR_2)_3/K$ (R = $SiMe_3$) system with CO.[11]

Some of the first examples of CO coupling by an actinide, and the insertion of CO into an An–alkyl bond, were reported in 1978 by Turro and co-workers.[12] The reaction of $[An(Cp^*)_2R_2]$ (An = U or Th, and R = Me or $CH_2SiMe_3$) with carbon monoxide provided the monomeric complex $[An(Cp^*)_2(\kappa^2\text{-}O_2C_2(CH_2SiMe_3)_2)]$ (**L**) and the dimeric $[\{(Cp^*)_2An\}_2(\mu\text{-}\eta^1\text{:}\eta^1\text{-}O_2C_2Me_2)]$ (**M**) (Scheme 1.8).

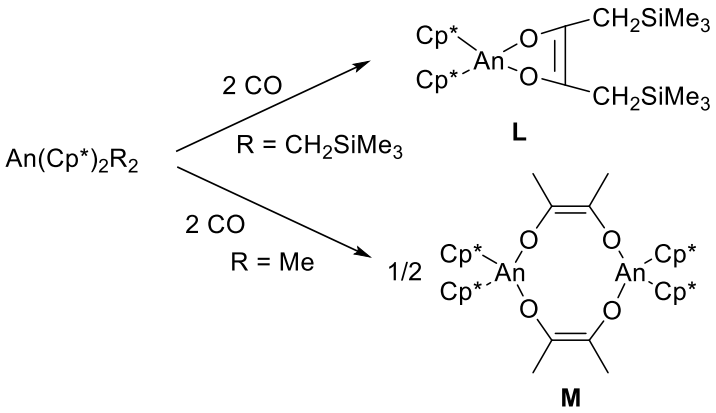


Scheme 1.8. Coupling and insertion of CO into actinide complexes for the synthesis of **L** and **M**.[12]

A remarkable example was reported by Cloke and co-workers in 2006, when exposure of pentane solutions of the uranium(III) complex $[U(Cp^*)(COT^{TIPS})]$ (**N**) ($COT^{TIPS} = C_8H_6(1,4\text{-}Si^iPr_3)$) to one bar of CO provided the dimeric product $[\{(Cp^*)(COT^{TIPS})U\}_2(\mu\text{-}\eta^1\text{:}\eta^2\text{-}C_3O_3)]$ (**O**), which features a cyclic deltate dianion, $C_3O_3^{2-}$, as a bridging ligand (Scheme 1.9).[13]

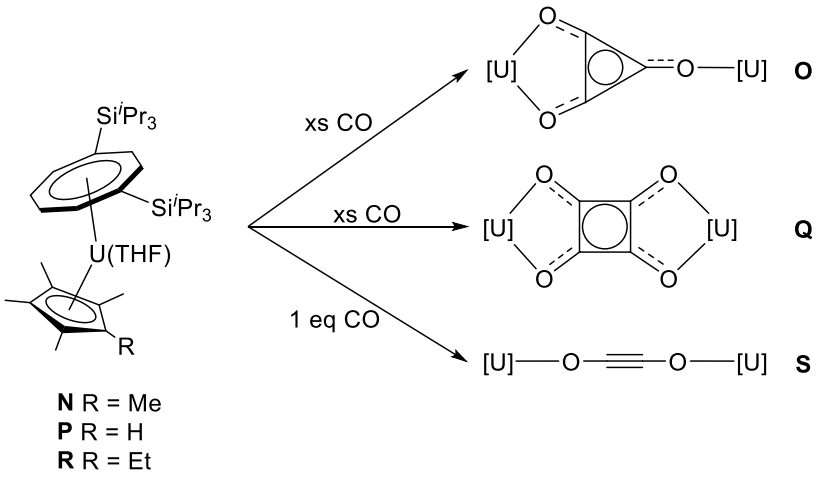


Scheme 1.9. Synthesis of complexes **O**, **Q** and **S** from reaction of **N**, **P** and **R** with CO.[13-15]

Changes in the steric bulk on the Cp* ligand were found to modify the outcome of the CO reduction. The replacement of a methyl group (complex **P**), thereby relieving some of the steric hindrance, led to the formation of complex $[\{(C_5Me_4H)(COT^{TIPS})U\}_2(\mu\text{-}\eta^2\text{:}\eta^2\text{-}C_4O_4)]$ (**Q**), which incorporates the squarate dianion $C_4O_4^{2-}$ from the reductive tetramerization of CO. On the other hand, the addition of an ethyl group (compound **R**), thereby increasing the steric pressure, provided $[\{(C_5Me_4Et)(COT^{TIPS})U\}_2(\mu\text{-}\eta^2\text{:}\eta^2\text{-}C_2O_2)]$ (**S**), which contains the ynediolate dianion, $C_2O_2^{2-}$, by reductive dimerization of CO (Scheme 1.9). Moreover, the oxocarbon moiety in compound **Q** can be removed as $C_4O_2(OSiMe_3)_2$ by quenching with $Me_3SiCl$, providing a new route for future synthesis of organic complexes.[14, 15]

## 1.2. Carbon dioxide

### 1.2.1. Activation of carbon dioxide by transition metals

Pioneering work on the catalytic activation of $CO_2$ was published in the 1970s and 1980s by the research groups of Inoue, Musco, Hoberg, Walther and Behr. Two general reactions were described: a) reaction with alkenes and alkynes; b) the insertion of $CO_2$ into a metal–element bond, which depending on the co-reactants led to different compounds, such as carboxylates, esters or carbonates. Late transition metals such as Fe, Rh, Ni and Pd were used due to their ability to bind a weak ligand like $CO_2$ through backbonding (Scheme 1.10).[16]

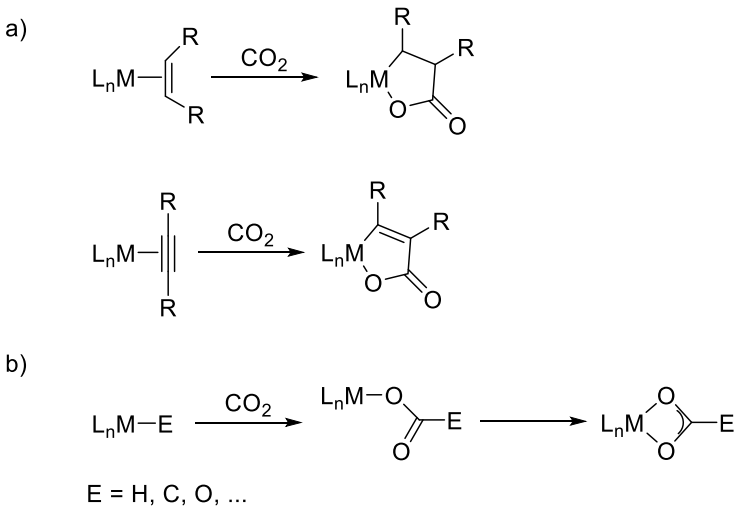


Scheme 1.10. Basic reaction of the catalytic $CO_2$ activation.[16]

Many reviews have been published on the catalytic activation of $CO_2$ with transition metals.[16-20] An example of the catalytic transformation of $CO_2$ and ethene to acrylates is described in Chapter 4. In this section, a selection of examples on the insertion chemistry of $CO_2$ is discussed.

One of the first described $CO_2$ insertions into a transition metal–carbon bond was reported by Vol'pin and co-workers.[21] Treatment of $[(Ph_3P)_3RhPh]$ with an excess of $CO_2$ at room temperature led to the formation of the benzoate complex $[(Ph_3P)_3Rh(OC(=O)Ph)]$. However, $CO_2$ insertion into the Rh complexes $[(Ph_3P)_3RhCl(I)Me]$, $[(Ph_3P)_3Rh(C_2H_5)]$ and $[(Ph_3P)_3Rh(C_2H_5)Cl_2]$ was not successful.

Generally, the catalytic transformation of $CO_2$ via insertion into a TM–C bond requires two steps: in the first one, the insertion takes place, and in the second step, the transformed carboxylate is cleaved and the catalyst is regenerated. However, the second step usually requires hydrolysis or addition of an additive which can destroy or hamper the regeneration of the catalyst.

Fujiwara and co-workers reported one of the first examples of the catalytic conversion of $CO_2$ by insertion into a TM–C bond.[22] The formation of an activated [Ar-Pd-H] species was observed when palladium acetate was treated with aromatic compounds, which were subsequently exposed to $CO_2$ (from 1 to 30 bar) to yield the aromatic carboxylic acids in yields between 2 and 66%. Moreover, biphenyl cross-coupling side-products were observed.

Shi and Nicholas reported the formation of carboxylstannanes from reactions of $[Pd(PR_3)_4]$ (**T**) (R = Ph or Bu) with allylstannanes and $CO_2$ (Scheme 1.11).[23] The oxidative addition of the allylstannanes with the catalyst provided $[(allyl)Pd(SnR'_3)(PR_3)]$ (**V**), which upon exposure to an excess of $CO_2$ led to insertion into the Pd–allyl bond, yielding the carboxylate compound **W**. The carboxylate was then cleaved from **W** by the oxophilic $R'_3Sn$ species.

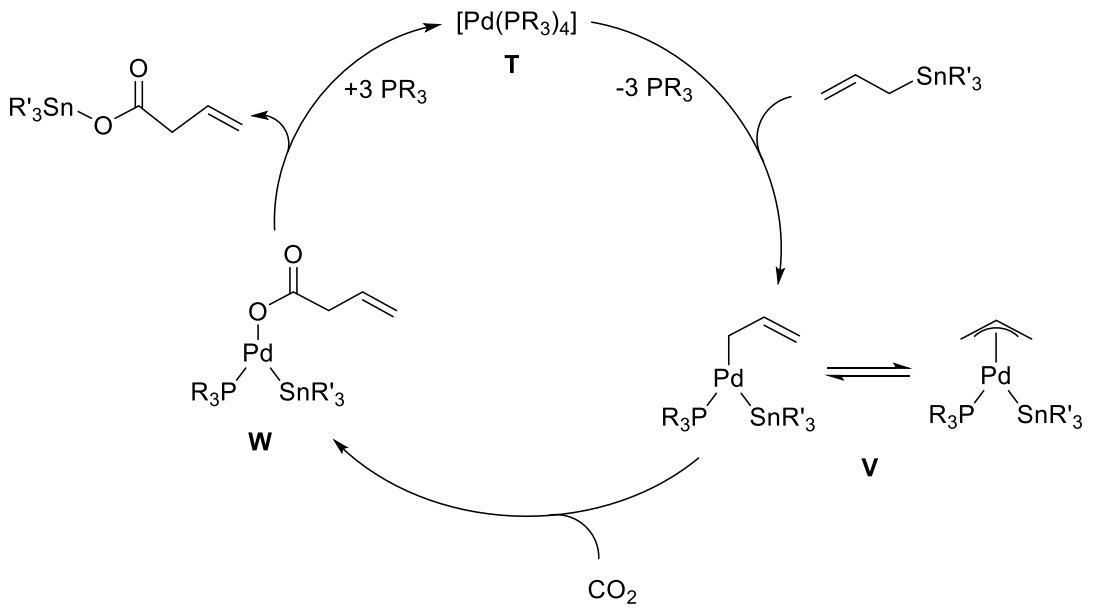


Scheme 1.11. Catalytic formation of carboxylstannanes from allylstannanes and $CO_2$.[23]

## 1.2.2. Activation of carbon dioxide by lanthanides and actinides

In 2012, Boyle, Kemp and co-workers published the insertion reactions of carbon dioxide into several alkoxy lanthanide complexes [Ln(ODtbp)$_3$] (Ln = Ce, Sm, Dy, Y, Er, Yb and Lu; ODtbp = 2,6-di-*tert*-butylphenoxide), which yielded a series of mono-inserted alkoxy lanthanides (compounds **X** and **Y**, Scheme 1.12).[24]

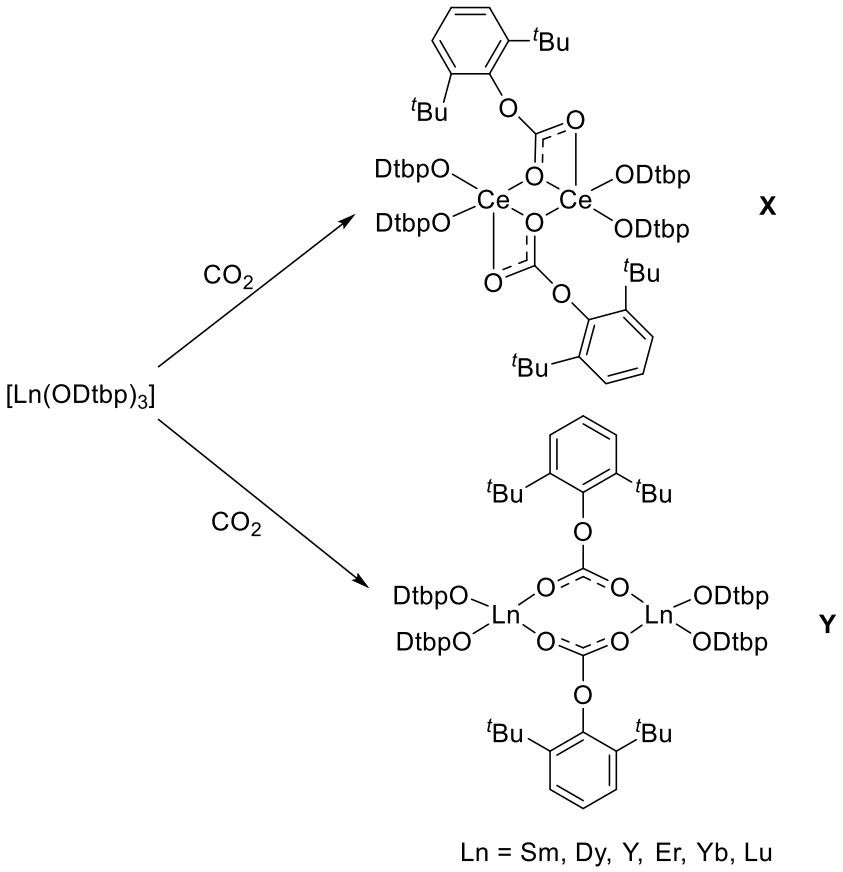


Scheme 1.12. Insertion of $CO_2$ to Ln-O bonds.[24]

Higher $CO_2$ pressures were used in order to achieve a second $CO_2$ insertion. However, no further reactivity was observed. The authors attribute this to steric encumbrance from interactions of the the *tert*-butyl groups with the Ln centre, which might fill open sites and prevent additional $CO_2$ insertions.

Similar reactivity has been previously published by our group with uranium(III) aryloxides.[25] As seen in Scheme 1.13, exposure of uranium complex $[U(ODtbp)_3]$ to 1 bar of $CO_2$ resulted in the formation of the $U^{IV}$ complex $[U(ODtbp)_{4,}]$ from oxidation of the uranium centre followed by ligand redistribution. No reaction was observed for complex $[\{(OTtbp)_3U\}_2(\mu\text{-}\eta^2\text{:}\eta^2\text{-}N_2)]$ (**Z**) (OTtbp = 2,4,6-tri-*tert*-butylphenoxide) upon exposure to an atmosphere of $CO_2$ until the temperature was increased, which allowed the coordinated dinitrogen to be displaced. Complex **AA** was obtained from reduction of $CO_2$ and incorporation of the abstracted oxo atom.

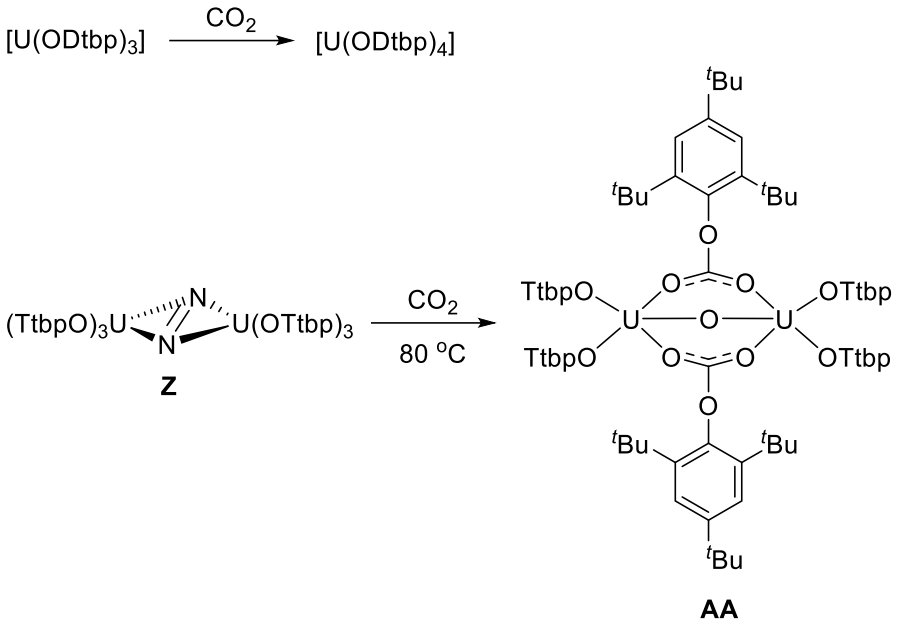


Scheme 1.13. Reactivity of $CO_2$ towards uranium(III) aryloxides.[25]

Interestingly, Meyer and co-workers reported the first example of a linear oxygen-bound $\kappa^1$-OCO complex.[26] When the tris(aryloxide) complex [(($^{Ad}$ArO)$_3$tacn)U] (**AB**) (tacn = 1,4,7-triazacyclononane, Ad = adamantyl) was exposed to $CO_2$ at ambient temperature and pressure, the formation of [(($^{Ad}$ArO)$_3$tacn)U($\mu$-$\kappa^1$-OCO)] (**AC**) was observed (Scheme 1.14).

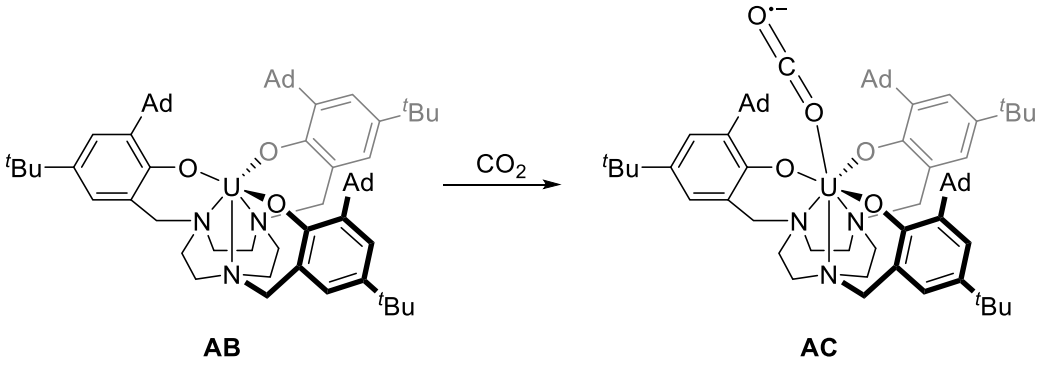


Scheme 1.14. Synthesis of complex **AC** from reaction of tris(aryloxide) complex **AB** with $CO_2$.[26]

However, when the less sterically demanding *tert*-butyl substituted aryloxide [(($^{tBu}$ArO)$_3$tacn)U] was used, the formation of the oxo-bridged complex [{(($^{tBu}$ArO)$_3$tacn)U}$_2$($\mu$-O)] was achieved from reduction of $CO_2$ with one-electron oxidation of each uranium.[27] The authors attributed the driving force for this two-electron

cleavage reaction of $CO_2$ to be the oxidation of the two $U^{III}$ to $U^{IV}$, which is sterically facilitated by the ligand environment.

Several examples of CO and $CO_2$ activation by transition metals, lanthanides and actinides have been reviewed in this chapter. Although some progress has been achieved in the past few years, further research is needed in order to obtain industrially viable uses.

## 1.3. Bibliography

[1] P. L. Arnold, Z. R. Turner, *Nat. Rev. Chem.* **2017**, *1*, 0002.

[2] A. Tortajada, F. Juliá-Hernández, M. Börjesson, T. Moragas, R. Martin, *Angew. Chem. Int. Ed.* **2018**, *57*, 15948-15982.

[3] P. W. N. M. Van Leeuwen, Z. Freixa, Carbon Monoxide as a Chemical Feedstock: Carbonylation Catalysis, Wiley-VCH: Weinheim, Germany, **2006**, pp 319-356.

[4] M. Beller, *Catalytic Carbonylation Reactions, Vol. 18*, Springer-Verlag: Berlin, **2006**, pp 1-37.

[5] B. Cornils, W. A. Herrmann, I. Wiley, *Applied homogeneous catalysis with organometallic compounds : a comprehensive handbook in three volumes*, 2nd, completely rev. and enl. edition. ed., Wiley-VCH: Weinheim, Germany, **2002**, pp 31-182.

[6] M. Röper, *Stud. Surf. Sci. Catal.* **1991**, *64*, 381-429.

[7] W. J. Evans, J. W. Grate, L. A. Hughes, H. Zhang, J. L. Atwood, *J. Am. Chem. Soc.* **1985**, *107*, 3728-3730.

[8] W. J. Evans, D. S. Lee, J. W. Ziller, N. Kaltsoyannis, *J. Am. Chem. Soc.* **2006**, *128*, 14176-14184.

[9] W. J. Evans, A. L. Wayda, W. E. Hunter, J. L. Atwood, *J. Chem. Soc., Chem. Commun.* **1981**, 706-708.

[10] B. J. Deelman, W. M. Stevels, J. H. Teuben, M. T. Lakin, A. L. Spek, *Organometallics* **1994**, *13*, 3881-3891.

[11] M. Fang, J. H. Farnaby, J. W. Ziller, J. E. Bates, F. Furche, W. J. Evans, *J. Am. Chem. Soc.* **2012**, *134*, 6064-6067.

[12] J. M. Manriquez, P. J. Fagan, T. J. Marks, C. S. Day, V. W. Day, *J. Am. Chem. Soc.* **1978**, *100*, 7112-7114.

[13] O. T. Summerscales, F. G. N. Cloke, P. B. Hitchcock, J. C. Green, N. Hazari, *Science* **2006**, *311*, 829-831.

[14] O. T. Summerscales, F. G. N. Cloke, P. B. Hitchcock, J. C. Green, N. Hazari, *J. Am. Chem. Soc.* **2006**, *128*, 9602-9603.

[15] N. Tsoureas, O. T. Summerscales, F. G. N. Cloke, S. M. Roe, *Organometallics* **2013**, *32*, 1353-1362.

[16] M. Cokoja, C. Bruckmeier, B. Rieger, W. A. Herrmann, F. E. Kühn, *Angew. Chem. Int. Ed.* **2011**, *50*, 8510-8537.

[17] T. Sakakura, J. C. Choi, H. Yasuda, *Chem. Rev.* **2007**, *107*, 2365-2387.

[18] K. A. Grice, *Coord. Chem. Rev.* **2017**, *336*, 78-95.

[19] Q. W. Song, Z. H. Zhou, L. N. He, *Green Chem.* **2017**, *19*, 3707-3728.

[20] M. Aresta, Carbon Dioxide Reduction and Uses as a Chemical Feedstock, Wiley-VCH: Weinheim, Germany, **2006** pp 1-41.

[21] I. S. Kolomnikov, A. O. Gusev, T. S. Belopotapova, M. K. Grigoryan, T. V. Lysyak, Y. T. Struchkov, M. E. Vol'pin, *J. Organomet. Chem.* **1974**, *69*, C10-C12.

[22] H. Sugimoto, I. Kawata, H. Taniguchi, Y. Fujiwara, *J. Organomet. Chem.* **1984**, *266*, c44-c46.

[23] M. Shi, K. M. Nicholas, *J. Am. Chem. Soc.* **1997**, *119*, 5057-5058.

[24] L. A. M. Steele, T. J. Boyle, R. A. Kemp, C. Moore, *Polyhedron* **2012**, *42*, 258-264.

[25] S. M. Mansell, N. Kaltsoyannis, P. L. Arnold, *J. Am. Chem. Soc.* **2011**, *133*, 9036-9051.

[26] I. Castro-Rodriguez, H. Nakai, L. Zakharov, A. Rheingold, K. Meyer, *Science* **2004**, *305*, 1757-1759.

[27] I. Castro-Rodriguez, K. Meyer, *J. Am. Chem. Soc.* **2005**, *127*, 11242-11243.

# Chapter 2 : Introduction to $Y^{III}$ and $U^{III}$ chemistry

In the past few years, more and more research has moved towards the search of energy that is not based on fossil fuels. One of the alternatives is the use of nuclear energy. Therefore, developing an understanding of the bonding in the f-block chemistry is crucial and will allow for better nuclear fuels and better custody and remediation of waste from nuclear plants.

## 2.1. Introduction to Yttrium

Yttrium, together with scandium and the lanthanides (La-Lu) form the rare earth elements. The discovery of the rare earth elements started at the end of the 18th century. The first element to be discovered was Yttrium by Finnish chemist J. Gadolin in 1794 as a mixture of different metal oxides and it was first isolated as a metal, although very impure, in 1828 by F. Wöhler by reducing the metal chloride with potassium.[1, 2]

The rare earth elements are silver, silver-white or grey metals; with a high lustre, but tarnish readily in air; have very small differences in solubility and complex formation between themselves and have high electrical conductivity.[2]

Yttrium has an abundance of 31 ppm of earth crustal rocks, being more abundant than more common metals such as lead (crustal abundance of 10 ppm) or gold (0.0031 ppm).[2] With a predominantly oxidation state of $Y^{III}$ has an electronic configuration of [Kr] $4d^1$ $5s^2$. It is associated with the heavier lanthanides due to their similarities in oxidation state and ionic radii. Of importance in the field of electronics, it is used in alloys as standard red colour for tv screens and monitors. Another application is in camera lenses due to its properties in heat and shock resistance, and it is also used in microwave lasers and radar.

Initially, the coordination chemistry of yttrium and the other rare earth ions was only investigated in order to separate these ions from each other. The organolanthanides were first originated as part of a broad survey of the chemistry of cyclopentadienyl ligand with all metals by Wilkinson and Birmingham. Anhydrous $LnCl_3$ (Ln = Sc, Y, La, Ce, Pr, Nd, Sm and Gd) were stirred with cyclopentadienyl sodium in THF to obtain $[Ln(Cp)_3]$ (**A**) complexes (Figure 2.1).[3] Similarly, in 1969-1970 the synthesis of organolanthanides

gained a renewed interested due to the study of cyclooctatetraene (COT) ligand and since the synthesis of uranocene (**F**, Figure 2.4) complex was achieved. The groups of Hayes and Thomas, and Streiweiser and co-workers published a series of organolanthanides bearing cyclooctatetraene ligands. $LnCl_3$ (Ln = Y, La, Ce, Nd, Sm, Eu, Tb, Gd and Yb) were reacted with $K_2COT$ in THF to provide complex [Ln(COT)] (**B**) for Ln = Eu and Yb, and complex $K_2[Ln(COT)_2]$ (**C**) for Ln = Y, La, Ce, Nd, Sm, Tb and Gd.[4-6]

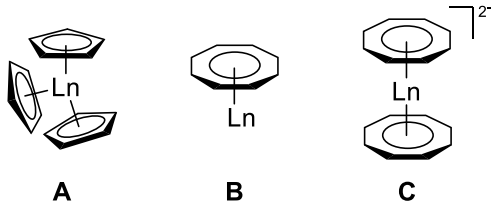


Figure 2.1. First organolanthanide complexes **A**, **B** and **C**.[3-6]

These early studies suggested that organolanthanide chemistry was rather limited and with ionic character. It was thought that they would merely be trivalent versions of alkali and alkaline earth metal organometallic complexes.

## 2.2. Introduction to Uranium

Uranium is one of the three naturally occurring actinides, besides thorium and protactinium. It constitutes 2.3 ppm of the earth's crust and it is usually obtained as uraninite mineral ($U_3O_8$).[7] It is the heaviest element that occurs naturally, with a silver colour and nearly as twice as dense as lead.[8] Uranium has three isotopes: $^{238}U$ which consists in 99.27 % of the uranium extracted from the ores, decays slowly by emitting an α particle and has a half-life of 4.5 billion years; $^{235}U$ which constitutes 0.72 % of the natural uranium; and finally $^{234}U$ which is only a 0.005 %. $^{235}U$ is the most fissile isotope. However, due to its low percentage, before being used as nuclear fuel, the extracted uranium has to undergo an enrichment process in where the portion of $^{235}U$ is increased from 0.72 % to 3 - 5 %. The by-product of the enrichment process is depleted uranium, which has a >99.27 % of $^{238}U$ and it is mostly considered waste. Global stocks are estimated to be 1.6 million tonnes and are increasing every year.[9] With a moderate toxicity and substantial abundance, depleted uranium has proved to be an attractive alternative to expensive transition metals.

Uranium acts distinctively from lanthanides, as the 5*f* orbitals are not as contracted as the 4*f* orbitals. This effect is due to the radial node in the 5*f* electronic wavefunction, which leads to greater orbital participation in actinide bonding. Moreover, the radial node shields the electrons from the nucleus which causes a decrease in the ionisation potential for the 5*f* electrons.

Throughout the actinide series, the 5*f* orbitals decrease in energy, becoming more "core-like" at the same time that the 6*d* orbitals increase in energy, crossing over at uranium as seen in Figure 2.2.[10]

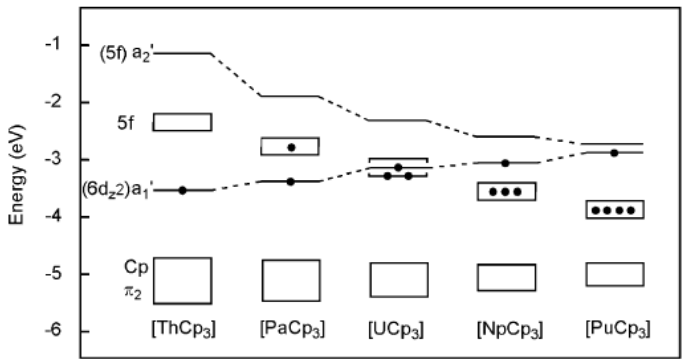


Figure 2.2. Variation of metal-based frontier orbital energies from Th to Pu.[10]

Moreover, because the 5*f* orbitals are more diffuse, overlapping with neighbouring orbitals in other atoms is easier, which leads to more covalency. Radial distribution plots depicted in Figure 2.3 show this effect.

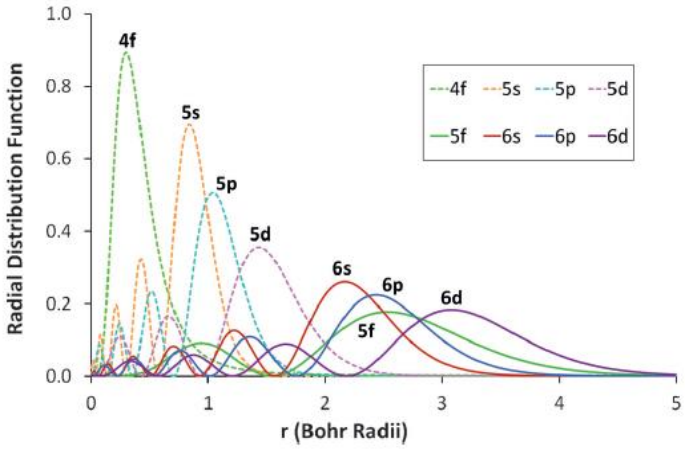


Figure 2.3 Radial distribution functions for 4*f*, 5*s*, 5*p*, 5*d*,5*f*, 6*s*, 6*p* and 6*d* atomic orbitals for $U^{III}$.[10]

This particular behaviour for uranium is sometimes described as if it is acting as a "big transition metal", as it has a range of easily accessible oxidation states from $U^{II}$ to $U^{VI}$.

The different oxidation states and electronic configurations of uranium are shown in Table 2.1.

Table 2.1. Electronic configurations of the different oxidation states of uranium.

| Oxidation state | $U^0$ | $U^{II}$ | $U^{III}$ | $U^{IV}$ | $U^{V}$ | $U^{VI}$ |
|---|---|---|---|---|---|---|
| Electronic configuration | $[Rn]7s^26d^15f^3$ | $[Rn]5f^4$ or $[Rn]6d^15f^3$ | $[Rn]5f^3$ | $[Rn]5f^2$ | $[Rn]5f^1$ | [Rn] |

$U^{II}$ is a rare example, which has only been reported few times in the literature where strongly stabilising ligands are needed.[11-15] The most stable oxidation states are $U^{IV}$ and $U^{VI}$, the latter is the only diamagnetic form of uranium and forms the uranyl ion $UO_2^{2+}$ which is stable under aerobic conditions. $U^{V}$ and $U^{VI}$ are oxidising, whereas $U^{III}$ is strongly reducing, with a redox couple estimated to be between -1.7 and -2.8 V versus ferrocene.[16]

The first investigations of organometallic chemistry of the actinides started with the Manhattan project, where research on the volatile compounds for uranium isotope

separation was carried out. However, organouranium chemistry was limited until the groups of Wilkinson and Fisher reported the first cyclopentadienyl complexes of uranium $[U(\eta^5\text{-}C_5H_5)_3Cl]$ (**D**) and $[U(\eta^5\text{-}C_5H_5)_4]$ (**E**) respectively (Figure 2.4).[17, 18] A few years later, with the discovery of uranocene complex $[(\eta^8\text{-}C_8H_8)_2]$ (**F**), which features one uranium bound to two $\eta^8\text{-}C_8H_8$, some light was shed on the understanding of the δ-bonding in uranium-aromatic ligand systems.[19, 20]

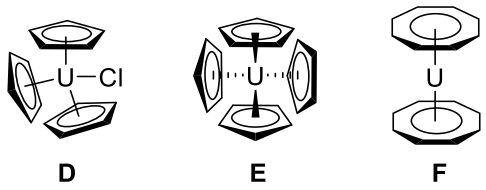


Figure 2.4 First organouranium complexes **D**, **E** and **F**.[17-20]

### 2.2.1. Uranium(III)

The $U^{III}$ ion is strongly reducing which provides it with singular reactivity towards small molecule activation. One electron oxidation from $U^{III}$ to $U^{IV}$ is the most common pathway, often leading to bimetallic structures bridged by a doubly reduced substrate. Common examples are the activation of: carbon monoxide[21, 22] and carbon dioxide,[23] both molecules are of interest due to their potential to act as $C_1$ building blocks. Moreover, activation of arene[24, 25] and dinitrogen[23] has also been reported. However, $U^{III}$ is severely sensitive to air and moisture,[26] therefore needs to be handled carefully, with dry solvents and an inert atmosphere.

Another interesting characteristic of uranium(III) is its extended Van Der Waals radius (1.86 Å) which allows a quite large variety of coordination number and long U–(donor atom) distances.[27] In addition of its hard Lewis acidity, $U^{III}$ has a predisposition towards π and δ-back-bonding, facilitating the coordination and activation of a large range of π-ligands, leading to different coordination modes and reactivity.[28, 29]

A major advance was achieved in 1989 when Clark and co-workers published a robust synthesis for $[UI_3(THF)_4]$ (**G**) from uranium amalgam and iodine in THF (Scheme 2.1),[30] which was an easier synthesis for the main starting material of $U^{III}$ complexes, making its chemistry more accessible. In 2011, an improved synthesis was developed giving $[UI_3(1,4\text{-dioxane})_{1.5}]$ (**H**) with excellent yield and with higher thermal stability than

complex **G**. Moreover, for the synthesis of complex **H** no mercury is needed (Scheme 2.1).[31]

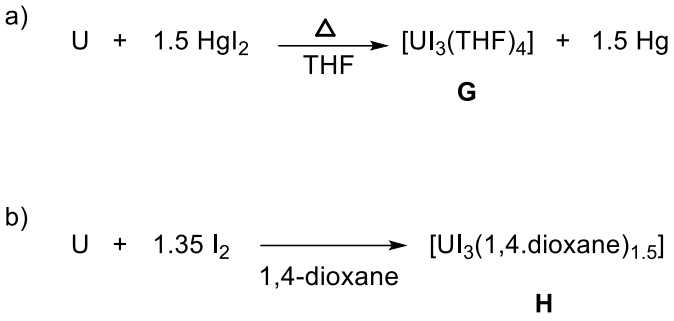


Scheme 2.1. Synthesis of $U^{III}$ iodides with a) THF and b) 1,4-dioxane.[31]

## 2.3. Aryloxide ligands

In the decades of 1980s and 1990s a wide range of alkoxide and aryloxide complexes of the lanthanides were reported, although not much further reactivity of these complexes was pursued.[32]

Pioneering work was done by Lappert and co-workers in 1983 when three- and four-coordinated, hydrocarbon-soluble aryloxides for Sc, Y and lanthanoids were reported.[33] Since then, aryloxide complexes such as $[Y(ODtbp)_3]$ (**I**) and $[Y(OTtbp)_3]$ have been reported.[34, 35] The synthesis of aryloxide complexes can go through either a) salt metathesis of the yttrium chloride and sodium or lithium aryloxide salt; and b) via protonolysis, typically the yttrium tris(silylamide) reacts with the phenol to provide the desired product as seen in Scheme 2.2. Protonolysis is the preferred route, as it is cleaner and $HN(SiMe_3)_2$ can be removed under vacuum.

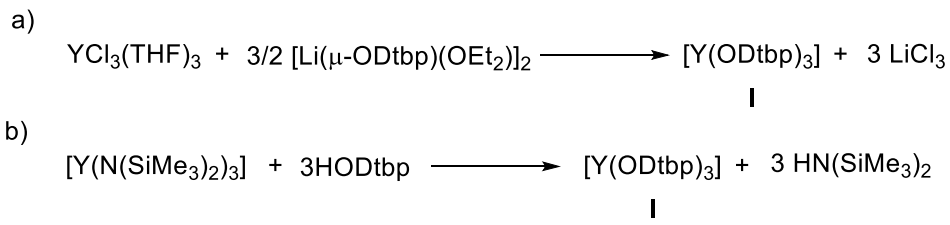


Scheme 2.2. Synthesis of aryloxide yttrium complex **I** through a) salt metathesis, b) protonolysis.[34, 35]

Since early 1990s the use of yttrium aryloxide complexes, such as $[(L^{TMS})Y(OC_6H_2{}^tBu_2Me)]$ ($L^{TMS}$ = N,N'-bis(trimethylsilyl)benzamidinate), as initiators for the polymerisation of lactic acid and related cyclic esters have been studied as new and easily available catalysts. Such complexes have been seen to give a rapid and controlled polymerisation.[36-39]

The interest in organouranium complexes started by focusing on the preparation of uranium compounds where the organic groups were bound to the uranium through oxygen, nitrogen or sulfur.[40] Early reports on the synthesis of monodentate alkoxides were carried out during the 1950s and 1960s.[41-43]

Similar to alkoxides, aryloxides began to gain attention for organouranium chemistry. The first examples reported included heteroleptic systems.[44-46] Pioneering work was done by Lappert and co-workers in 1983 when $[U(NEt_2)(ODtbp)_3]$ (**J**) and $[U(NEt_2)_2(ODtbp)_2]$ (**K**) were synthesised from $[U(NEt_2)_4]_2$ and HODtbp as seen in Scheme 2.3.[47]

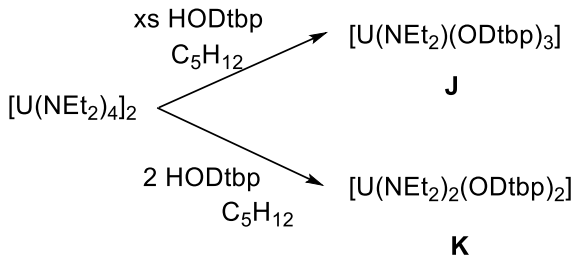


Scheme 2.3. Synthesis of complexes **J** and **K**.[47]

The first homoleptic $U^{III}$ aryloxide was reported in 1988 by Burns and co-workers. The synthesis of $[U(ODipp)_3]_2$ (**L**) (Figure 2.5) and $[U(ODtbp)_3]$ (**M**) was achieved by reaction of $[U(N(SiMe_3)_2)_3]$ with three equivalents of HODipp (2,6-di-*iso*-propylphenol) or HODtbp respectively.[48] It was demonstrated that having sterically bulky aryloxides is key to the synthesis of these type of compounds. Complex **L** forms a dimer which is held together by U···$\eta^6$-arene interactions. The most probable cause for its dimerization is steric effects, as the bulkier complex **M** forms a monomer. The solid-state structure of complex **M** was not confirmed until 2011 in another report by our group.[24] Further reactivity will be discussed in the next sections.

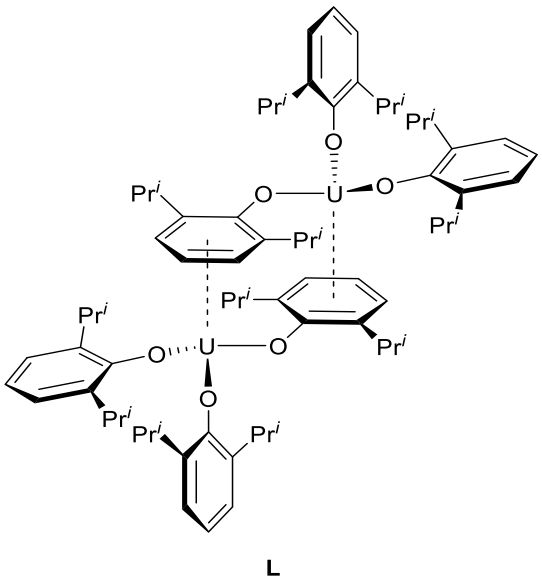


**L**

Figure 2.5. The homoleptic uranium(III) complex **L**.[48]

Other interesting aryloxide ligand systems were developed by Meyers and co-workers, consisting of three aryloxides tethered to an organic linker such as: triazacyclononane [(($^{R}$ArO)$_3$tacn)U] (**N**), amine [(($^{Ad}$ArO)$_3$N)U] (**O**) or mesitylene [(($^{R}$ArO)$_3$Mes)U] (**P**) (Figure 2.6). All complexes are synthesised by protonolysis of the pro-ligands with [U(N(SiMe$_3$)$_2$)$_3$].

In 2002 the synthesis of the aryloxide supported by a macrocyclic poly-amine ligand [(($^{t\text{Bu}}$ArO)$_3$tacn)U] (**Na**) was published. The poly-amine macrocycle acts as an anchor and shields one side of the $U^{III}$ ion while the *tert*-butyl substituents form a protected pocket for further reactivity. The ligand occupies six coordination sites, leaving an axial "free" position for ligand substitution and small molecule activation reactions.[49, 50] A few years later, another uranium complex with a tris(aryloxide) macrocycle ligand was reported [(($^{Ad}$ArO)$_3$N)U] (**O**). This new system includes the substitution of the rigid triazacylononane backbone for an amine allowing for more flexibility in the compound. Moreover, the addition of adamantyl substituents in the aryloxide, provides further protection to the $U^{III}$ reactive centre as a narrow cylindrical cavity above the uranium is formed but adamantyl substituents are flexible enough to let small molecules and other substrates into the reactive cavity.[51] Moreover, adamantyl substituents in the aryloxide motif were also included in the poly-amine macrocyclic ligand system [(($^{Ad}$ArO)$_3$tacn)U] (**Nb**) which was successfully used in: the activation of $CO_2$ and in the synthesis of N-heterocyclic carbene complexes of $U^{III}$.[52, 53] In 2012 the derivative

[(($^{Neop,Me}$ArO)$_3$tacn)U] (**Nc**), which includes a neopentyl phenol and methyl substituents was reported. Complex **Nc** has characteristics in between complexes **Na** and **Nb** as it was designed to have more flexibility next to the uranium reactive centre while providing sufficient steric protection for further reactivity.[54]

Furthermore, $U^{III}$ complexes bearing the mesityl-linked tris(aryloxide) ligand [(($^{t Bu}$ArO)$_3$Mes)U] (**Pa**) and [(($^{Ad}$ArO)$_3$Mes)U] (**Pb**) were reported. These syntheses were inspired by reports about interaction of uranium with arenes by Cummins and co-workers, where a U···η$^6$-arene···U motif is formed.[28, 55] Comparable methodology for activating small molecules was sought by incorporation of an arene ring as part of potential redox active chelating ligand for uranium.[56] Substitution of *tert*-butyl substituents for adamantyl and methyl was carried out in a following report in order to sterically protect the $U^{III}$ reactive centre and increase crystallinity.[57]

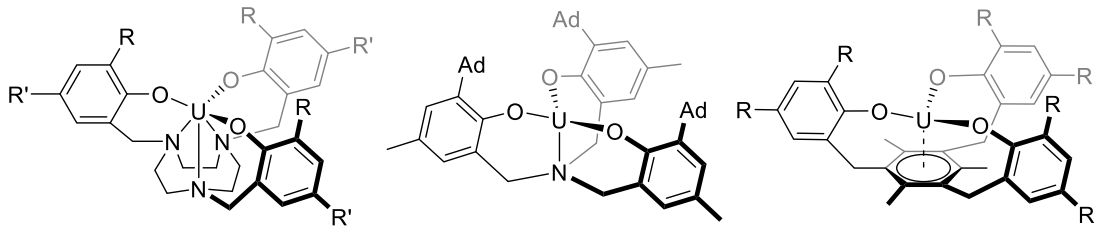


**Na**: R = R' = $^t$Bu
**Nb**: R = Ad, R' = $^t$Bu
**Nc**: R = Neop, R' = Me

**O**

**Pa**: R = $^t$Bu
**Pb**: R = Ad

Figure 2.6. Synthesis of $U^{III}$ tris(aryloxide) complexes **Na-c**, **O** and **Pa-b**.[49-57]

The synthesis of three pre-organised ligands, which could hold two reducing uranium centres was reported by our group in 2016.[58] The idea was developed after noticing that in most cases the activation and transformation of small molecules is achieved almost exclusively by combining two uranium complexes around one substrate.[27, 59] Moreover, it was also seen that the final product actively depends on the steric accessibility of the two uranium centres rather than their redox capability.[60, 61]

Arene bridged tetraphenol ligands **Q**, **R** and **S** were synthesised (Figure 2.7). Ligand **Q** ($H_4L^P$) has an arene *para*-substituted core, with *tert*-butyl and methyl substituents on the phenol rings. Ligand **R** ($H_4L^{P*}$) on the other hand, has the same core structure with *para*-substitution but with 2-phenylpropan-2-yl substituents on the phenols.

Ligand **S** ($H_4L^M$) has *tert*-butyl and methyl substituents on the phenol rings but a *meta*-substituted arene core.

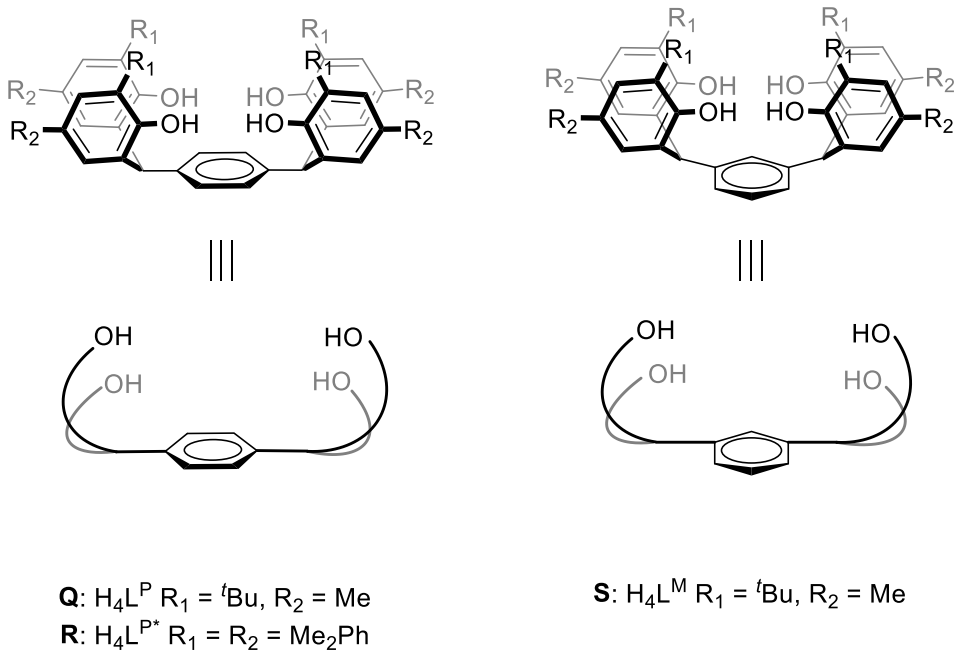


**Q**: $H_4L^P$ $R_1$ = $^t$Bu, $R_2$ = Me
**R**: $H_4L^{P*}$ $R_1$ = $R_2$ = $Me_2Ph$

**S**: $H_4L^M$ $R_1$ = $^t$Bu, $R_2$ = Me

Figure 2.7. The substituted tertraphenols **Q**, **R** and **S**.[58]

The uranium adducts **Qa-b**, **Ra-b** and **Sa-c** were obtained (Figure 2.8). Complexes **Qa** and **Ra** were synthesised by deprotonation of the ligand with $Ca[N(SiMe_3)_2]_2$ followed by reaction with $[UI_4(1,4\text{-dioxane})_2]$. Complex **Sb** follows the same reactions but deprotonation is achieved with $K[N(SiMe_3)_2]$. In contrast, treatment of any of the ligands with two equivalents of $U^{IV}$ metallacycle $[U(N(SiMe_3)_2)_2(\kappa^2C:N\text{-}N(SiMe_3)SiMe_2CH_2)]$ led to deprotonation of all four acidic phenols followed by formation of complexes **Qb**, **Rb** and **Sb**. Finally, compound **Sc** was synthesised by reaction of ligand **S** with $[U(N(SiMe_3)_2)_3]$.

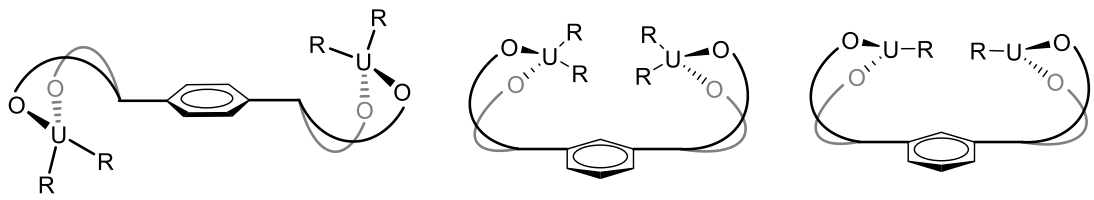

**Qa**: $H_4L^P$ R = I
**Ra**: $H_4L^{P*}$ R = I
**Qb**: $H_4L^P$ R = $N(SiMe_3)_2$
**Rb**: $H_4L^{P*}$ R = $N(SiMe_3)_2$

**Sa**: $H_4L^M$ R = I
**Sb**: $H_4L^M$ R = $N(SiMe_3)_2$

**Sc**: $H_4L^M$ R = $N(SiMe_3)_2$

Figure 2.8. Complexes of bridged tetra(aryloxide) ligands **Qa-b**, **Ra-b**, **Sa-c**.[58]

## 2.4. Siloxide ligands

Siloxide ligands can be regarded as similar to alkoxides and generally are capable of binding to a metal through σ- bonding with π back-bonding. Moreover, because there is also back-bonding from the p orbitals of the oxygen to the $\sigma^*$ of the silicon (negative hyper conjugation), the overall donating power of the siloxide decreases compared to alkoxides or aryloxides. Another consequence of the incorporation of an additional atom in the ligand system is the shift of the R groups of the immediate coordination sphere of the metal.[62]

Although widely used in transition metal chemistry and homogenous catalysis,[62-65] siloxides were first used as ancillary ligands in the early 2010s. The synthesis of the dinitrogen activated complex $[\{(OSiMes_3)_3U\}_2(\mu\text{-}\eta^2\text{:}\eta^2\text{-}N_2)]$, which contains mesityl-substituted siloxide ligands was reported by our group.[66] At the same time, Mazzanti and co-workers reported the synthesis of homoleptic $U^{III}$ siloxide complex $[U(OSi(O^tBu)_3)_2(\mu\text{-}OSi(O^tBu)_3)]_2$ (**T**).[67] Reaction of uranium tris(silylamide) $[U(N(SiMe_3)_2)_3]$ with three equivalents of tris-*tert*-butoxysilanol $HOSi(O^tBu)_3$ yielded complex **T** as seen in Scheme 2.4.

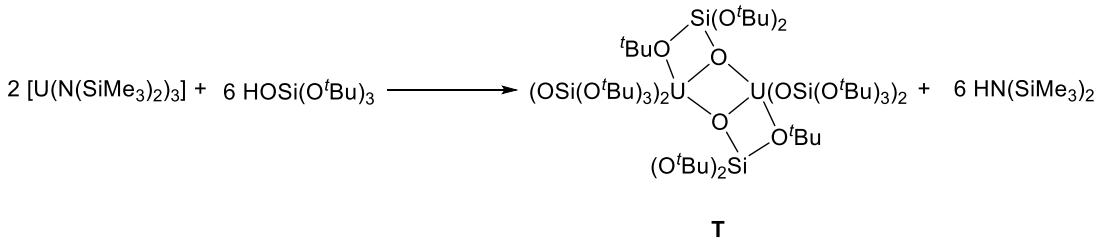

**T**

Scheme 2.4. Synthesis of $U^{III}$ siloxide dimer **T**.[67]

$OSi(O^tBu)_3$ ligand is characterised by a small size, when compared to other silylamide or aryloxide ligands, and its ability to adopt mono- or bidentate forms, which leads to an increased reactivity and stability. Moreover, although $U^{III}$ has a highly reducing character and there is such strongly electron donating environment, complex **T** is stable enough. This is due to the bulky siloxide ligands which by coordinating in both mono- and bidentate forms provide stability towards decomposition.[67]

Moreover, uranium complexes with other oxidation states than $U^{III}$ have been reported with siloxide ligands. For example, the formation of siloxides from uranyl by reductive silylation was first reported by our group in 2008[68] and has since then been described for a variety of co-ligand types and silylating reagents.[69-71]

## 2.5. Boroxide ligands

One of the most important features of the use of ligands is the ability to tune their properties. Usually this is done by modifying either the sterics, through addition of more or less bulky substituents; or by changing the electronic properties, by using electron-withdrawing or electron-donating substituents.

An interesting way to induce an electron-withdrawing effect in an O-donor ligand is the addition of an atom with an empty π-acceptor orbital adjacent to the oxygen, which will modify the extent of the π-donation. One example is the use of boron, where an empty 2*p* orbital is accessible for donation from the oxygen lone-pairs.

Boroxides are usually described as electron-deficient alkoxides. The O-atom lone-pairs are of the correct symmetry to be able to combine with the empty 2*p* orbitals on the boron atom, which results in less electron density available for donation to the metal centre (Figure 2.9).[72]

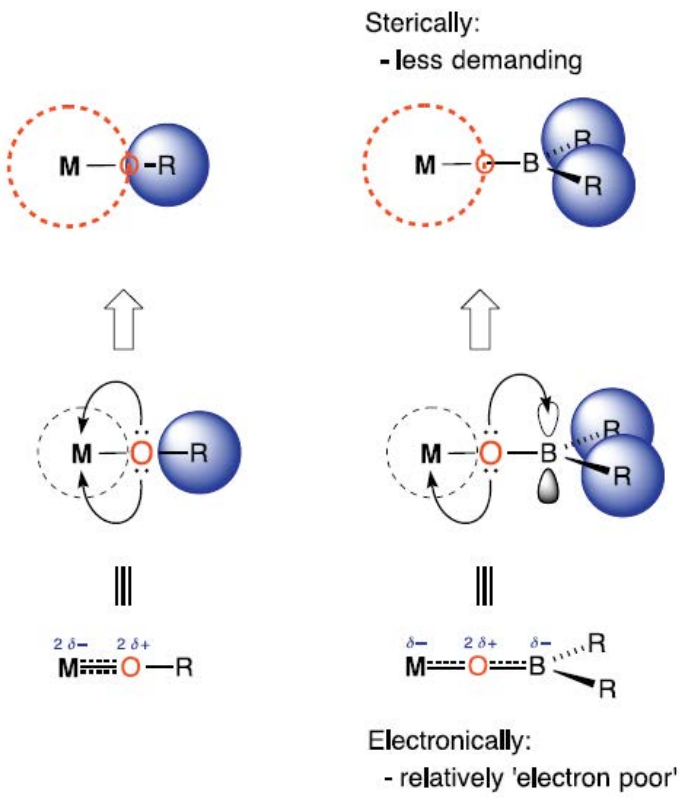


Figure 2.9. Differences in the π-donor ability between alkoxides and boroxides.[72]

A further consequence is the shift from the R groups away from the metal centre, which enables a better access.

There are two different routes for the synthesis of boroxides: a) a salt metathesis approach which consists of two steps. First a generation of a group one metal salt by reaction of the $HOBR_2$ (**U**) borinic acid with commonly an organolithium reagent LiR' (R' = Bu or Me) to generate a lithium boroxide (**V**) which is further reacted with a metal halide (MX) generating the boroxide of the metal used (**W**) and with elimination of LiX. These reactions are usually carried out with in situ generation of **V**. b) Via protonolysis of a suitable organometallic or metal-amido precursor by the borinic acid **U**, providing the boroxide **W**. Being this the most desirable route as it is cleaner, requires one step and does not require further purification (Scheme 2.5).[72]

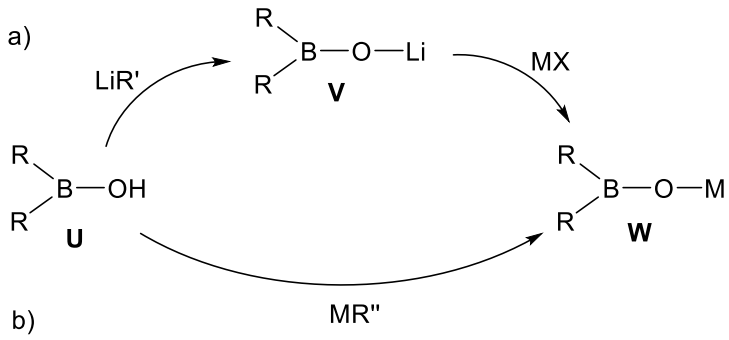


Scheme 2.5. Synthetic routes to boroxides.[72]

In 2002 Coles and co-workers published a study on the differences in the solid-state structure parameters between an alkoxide and a boroxide. Although not all the results agree with the hypothesis due to other effect such as sterics, some differences in bond lengths and angles could be observed in molybdenum complexes $[Mo(^tBu)_2(OCHMes_2)_2]$ (**X**) and $[Mo(^tBu)_2(OBMes_2)_2]$ (**Y**) (Figure 2.10).[73]

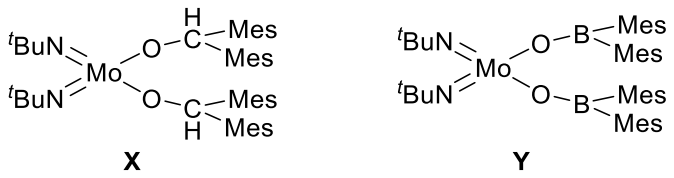


Figure 2.10. Molybdenum complexes **X** and **Y**.[73]

The differences observed were an elongation in the Mo–O bond length, a shortening in the Mo–N distance and a flattening of the Mo–O–B angle, which allows for a greater delocalisation, for the boroxide complex **Y** when compared with the same distances and the Mo–O–C angle in alkoxide complex **X**. All these agrees with the predicted changes if the boroxide is acting as a less effective π-donor to the metal centre.

Boroxides have been used as ligands for main group and transition metal complexes.[72] Moreover, the synthesis of complex $[XSc\{OB(C_6F_5)_2)_2]$ ($X = HC\{H_2NCH_2CH_2NCMe\}_2$) by reaction of $[Sc(Br)(MgBrX)_2]$ with $H_2O{\cdot}B(C_6F_5)_3$ is the only example of a group three boroxide that has been reported in the literature.[74]

## 2.6. Small molecule activation

In the past few years, the binding and activation of industrially and economically important small molecules at rare earth and actinides has gained increased attention. The area has been extensively reviewed recently.[59, 75-78] Selected examples in the $Y^{III}$ and $U^{III}$ small molecule activation are discussed in the following sections.

### 2.6.1. Yttrium(III)

In 2004, Evans and co-workers published the first dinitrogen activation by the yttrium tris(silylamide) complex $[Y(N(SiMe_3)_2)_3]$ (**Z**). Complex **Z** was first synthesised when investigating the reaction pathway of the previously reported thulium complex $[\{(N(SiMe_3)_2)_2(THF)Tm\}_2(\mu\text{-}\eta^2\text{:}\eta^2\text{-}N_2)]$, as it was believed to occur from direct reduction of the trivalent $[Tm(N(SiMe_3)_2)_3]$ precursor with potassium. Therefore, $[Y(N(SiMe_3)_2)_3]$ (**Z**) was treated with one equivalent of potassium graphite in a dinitrogen atmosphere, which led to the formation of diazenido $N_2^{2-}$ bridging complex $[\{(N(SiMe_3)_2)_2(THF)Y\}_2(\mu\text{-}\eta^2\text{:}\eta^2\text{-}N_2)]$ (**AA**) as seen in Scheme 2.6.[79]

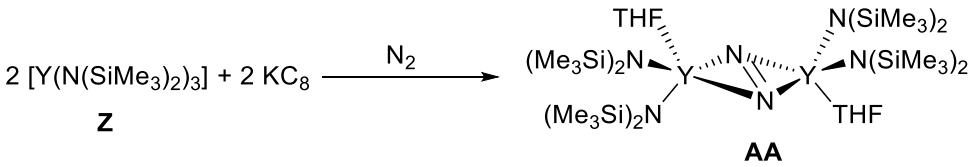


Scheme 2.6. Synthesis of dinitrogen-bridged complex **AA**. [79]

Since then, different ligands and reductants have been used. In 2009 Evans and co-workers published that by varying the method and the rate of addition of the reductant $KC_8$ to a solution of $[Y(N(SiMe_3)_2)_3]$ (**Z**) two new type of reduced dinitrogen complexes were formed, $[K(THF)_6][\{(N(SiMe_3)_2)_2(THF)Y\}_2(\mu\text{-}\eta^2\text{:}\eta^2\text{-}N_2)]$ (**AB**) and $K[\{(N(SiMe_3)_2)_2(THF)Y\}_2(\mu\text{-}\eta^2\text{:}\eta^2\text{-}N_2)]$ (**AC**), besides **AA**, with a similar structure except that an alkali metal cation was also present. The charge balance required that the dinitrogen unit carry a 3- charge, suggesting the presence of a $N_2^{3-}$ radical (Scheme 2.7). Solid-state structure, EPR spectroscopy and DFT calculations confirmed the formation of $N_2^{3-}$.[80]

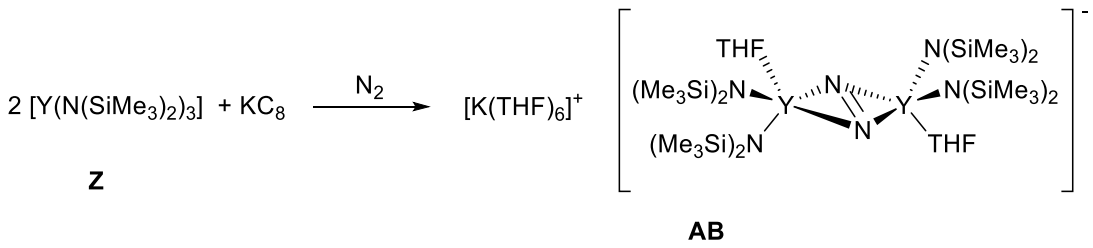


**Z** **AB**

Scheme 2.7. Synthesis of the dinitrogen-bridged complex **AB**.[80]

Similar complexes were obtained with the use of 18-crown-6 and sodium.[81] Moreover, cyclopentadienyl derivative ligands were also used in the synthesis of a dinitrogen-bridged complex, e.g. $[\{(Cp^*)_2(THF)Y\}_2(\mu\text{-}\eta^2\text{:}\eta^2\text{-}N_2)]$ (**AD**) was formed from reaction of $[Y(Cp^*)_2H]$ or $[Y(Cp^*)_2][(\mu\text{-}Ph)BPh_2]$ with $KC_8$.[82] Alternatively, complex **AD** could also be synthesised from either $[Y(Cp^*)_2(C_5Me_4H)]$ or $[Y(Cp^*)_2(\eta^3\text{-}C_3H_5)]$ under and atmosphere of dinitrogen and photolytic conditions.[83, 84] Furthermore, the reaction of $KC_8$ with $[Y(C_5Me_4H)_2][(\mu\text{-}Ph)BPh_2]$, $[Y(C_5H_4Me)_2]$ and $[Y(C_5H_4(SiMe_3))_2]$ under a dinitrogen atmosphere provided complexes $[\{(C_5Me_4H)_2(THF)Y\}_2(\mu\text{-}\eta^2\text{:}\eta^2\text{-}N_2)]$ (**AE**), $[\{(C_5H_4Me)_2(THF)Y\}_2(\mu\text{-}\eta^2\text{:}\eta^2\text{-}N_2)]$ (**AF**) and $[\{(C_5H_4(SiMe_3))_2(THF)Y\}_2(\mu\text{-}\eta^2\text{:}\eta^2\text{-}N_2)]$ (**AG**) respectively.[85-87]

Further reactivity of some of these dinitrogen-bridged complexes was carried out. For instance, the chemistry of complex **AA** with sulfur and selenium was studied, in order to explore if the ligand $N_2^{2-}$ was capable of reducing these chalcogens. Complex **AA** was reacted with elemental sulfur to provided two compounds containing the persulfido $S_2^{2-}$ and sulfido $S^{2-}$ units, $[\{(N(SiMe_3)_2)_2(THF)Y\}_2(\mu\text{-}\eta^2\text{:}\eta^2\text{-}S_2)]$ (**AH**) and $[\{(N(SiMe_3)_2)_2(THF)Y\}_2(\mu\text{-}S)]$ (**AI**), respectively, which co-crystallise together (Scheme 2.8).[88]

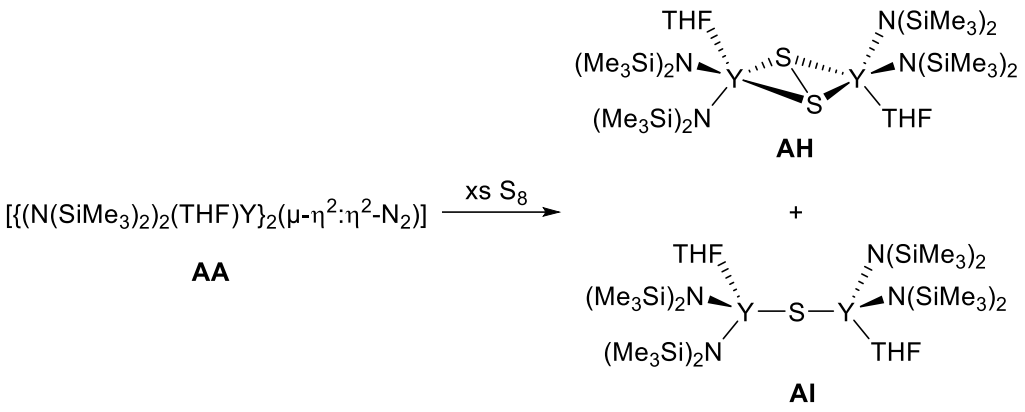


Scheme 2.8. Reactivity of complex **AA** with elemental sulfur.[88]

Studies with elemental selenium showed the formation of the $Se_2^{2-}$ bridged complex $[\{(N(SiMe_3)_2)_2(THF)Y\}_2(\mu\text{-}\eta^2\text{:}\eta^2\text{-}Se_2)]$ (**AJ**). In order to obtain the mono-bridged selenium complex $[\{(N(SiMe_3)_2)_2(THF)Y\}_2(\mu\text{-}Se)]$ (**AK**), the chalcogen transfer reagent $PPh_3Se$ was used.[88]

In a later publication, it was observed that complex $[Y(Cp^*)_2(\eta^3\text{-}C_3H_5)]$ can be reduced by photolysis in the presence of elemental sulfur to yield the sulfido $S^{2-}$ bridged complex $[\{(Cp^*)_2(THF)Y\}_2(\mu\text{-}S)]$ (**AL**).[84]

In an effort to expand the scope of the reactivity of these complexes, reaction with small molecules such as NO and oxygen was carried out. Complex **AC** instantly reacts with 1.5 equivalents of NO gas to provide the one electron reduction product $[\{(N(SiMe_3)_2)_2(THF)Y\}_2(\mu\text{-}\eta^2\text{:}\eta^2\text{-}NO)]$ (**AM**) as major product, and the mono-oxygen bridged complex $[\{(N(SiMe_3)_2)_2(THF)Y\}_2(\mu\text{-}O)]$ (**AN**) as minor by-product. The formation of these complexes was confirmed by solid-state crystal structure, EPR spectroscopy and DFT calculations. The chemical evidence of the presence of $NO^{2-}$ unit was also obtained by reaction of complex **AM** with another equivalent of NO, which led to the formation of complex $[\{(N(SiMe_3)_2)_2Y\}_4(\mu_3\text{-}ON{=}NO)_2(THF)_2]$ (**AO**) (Scheme 2.9). Complex **AO** contains the hyponitritre ion $(ON{=}NO)^{2-}$ as a bridging unit and can be rationalised by the coupling of a NO radical with an $NO^{2-}$ radical in **AM** complex. Moreover, the synthesis of complex **AO** can also be performed by reaction of the dinitrogen-bridged complex **AC** with two equivalents of NO, which also provides the oxo-bridged complex **AN** as a minor by-product. [89, 90]

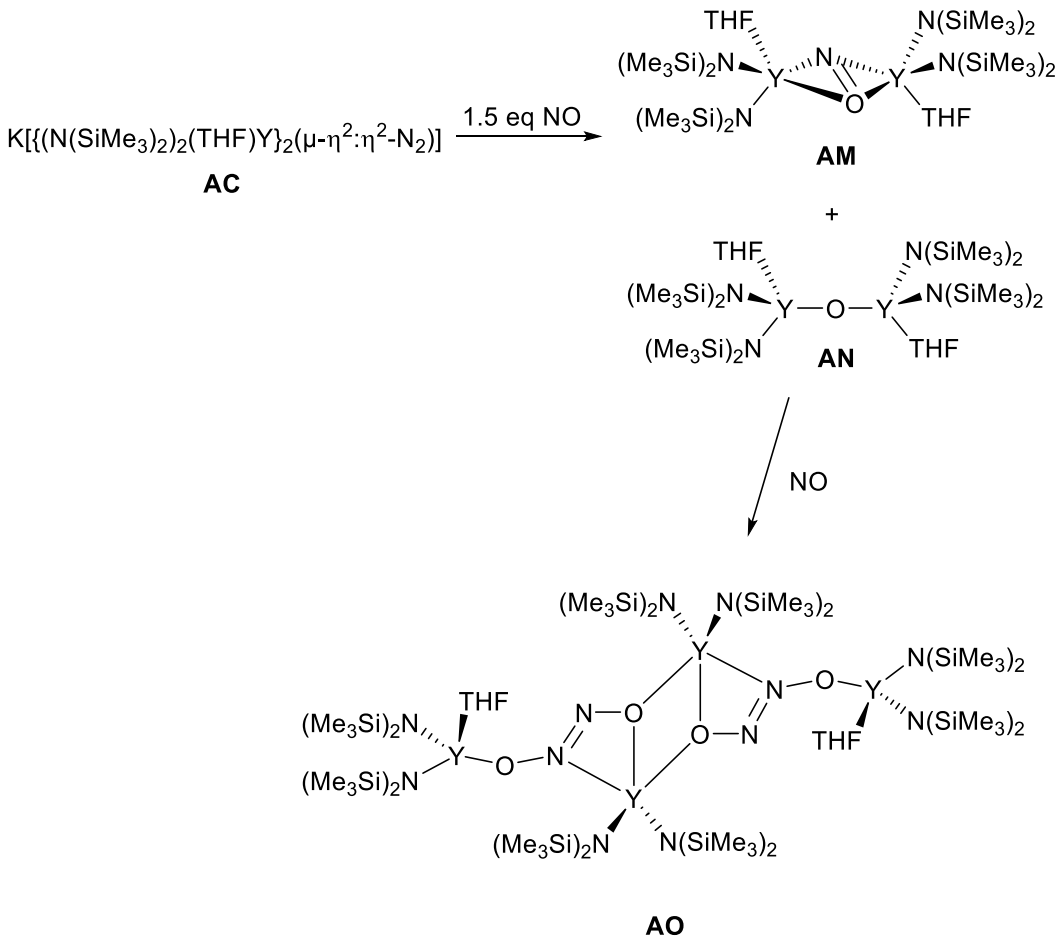


Scheme 2.9. Reactivity of complex **AC** with NO.[89, 90]

Further attempts to synthesise the oxo-bridged complex **AN** by reaction of **AA** with different oxidants such as $N_2O$, $O_2$, pyridine N-oxide, trimethylamine N-oxide, 1,2-epoxybutane, $Ag_2O$ and $K_2O$ did not succeed. However, the reaction of complex **AA** with oxygen provided the peroxide $O_2^{2-}$ bridged complex $[\{(N(SiMe_3)_2)_2(THF)Y\}_2(\mu\text{-}\eta^2\text{:}\eta^2\text{-}O_2)]$ (**AP**) (Scheme 2.10).[90]

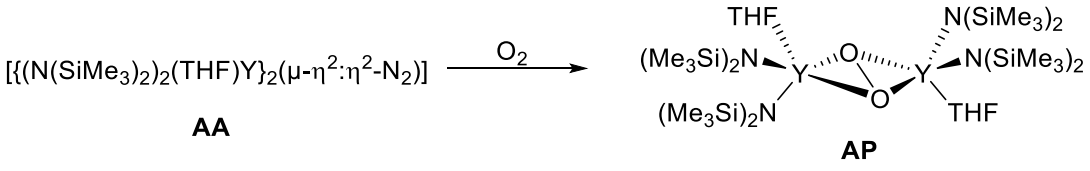


Scheme 2.10. Formation of the oxo-bridged complex **AP**.[90]

## 2.6.2. Uranium(III)

### 2.6.2.1. Reaction with chalcogenides

Although actinide chalcogenide complexes have been known for several years,[91-94] it is only recently that interest in the reactivity of chalcogens and chalcogenides with actinides has gained more attention.[95-98] This interest can be attributed to the different applications of these complexes as fast-ions conductors[99, 100] and thermoelectric energy conversion.[101-103] Moreover, complexes containing the hard uranium ion and the soft sulfur, selenium and tellurium ligands can help with the development of understanding the level of covalency in the metal ligand bond, which is leading to better separation of actinides from lanthanides in nuclear fuel.[104-107]

The first uranium(III) reaction with a chalcogenide-containing reagent was published in 1986 by Andersen and co-workers. $[\{(C_5H_4R)_3U\}_2(\mu\text{-}\eta^2\text{:}\eta^2\text{-}CS_2)]$ (R = Me or $SiMe_3$) was obtained from reaction of $[(C_5H_4R)_3U]$ with $CS_2$.[108]

In 1994 Burns and co-workers reported the reaction of $U^{III}$ aryloxide complex $[U(ODtbp)_3]$ (**M**) with chalcogenide-containing reagents. The reducing nature of complex **M** was examined with the sulfur-containing reagents COS and $PPh_3S$, which yielded the complex with mono-sulfur bridging unit $[\{(ODtbp)_3U\}_2(\mu\text{-}S)]$ (**AQ**) (Scheme 2.11).[109]

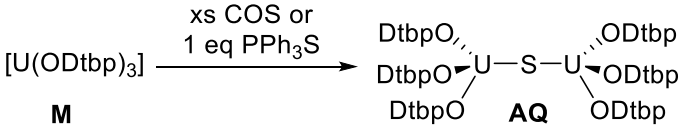


Scheme 2.11. Synthesis of the mono-sulfur bridging complex **AQ**.[109]

A few years later, Meyer and co-workers published the reaction of elemental chalcogenides with $[((^{t\text{Bu}}ArO)_3tacn)U]$ (**Na**) and $[((^{Ad}ArO)_3N)U]$ (**O**). Reaction of 1/8 of elemental sulfur provided the S-bridging complexes $[\{((^{t\text{Bu}}ArO)_3tacn)U\}_2(\mu\text{-}S)]$ (**AR**) and $[\{((^{Ad}ArO)_3N)U\}_2(\mu\text{-}S)]$ (**AT**) and reaction of one equivalent of elemental selenium led to the formation of selenium-bridged compounds $[\{((^{t\text{Bu}}ArO)_3tacn)U\}_2(\mu\text{-}Se)]$ (**AS**) and $[\{((^{Ad}ArO)_3N)U\}_2(\mu\text{-}Se)]$ (**AU**). Moreover, the same complexes were obtained when the chalcogen transfer reagent $PPh_3E$ (E = S or Se) was used (Scheme 2.12).[101]

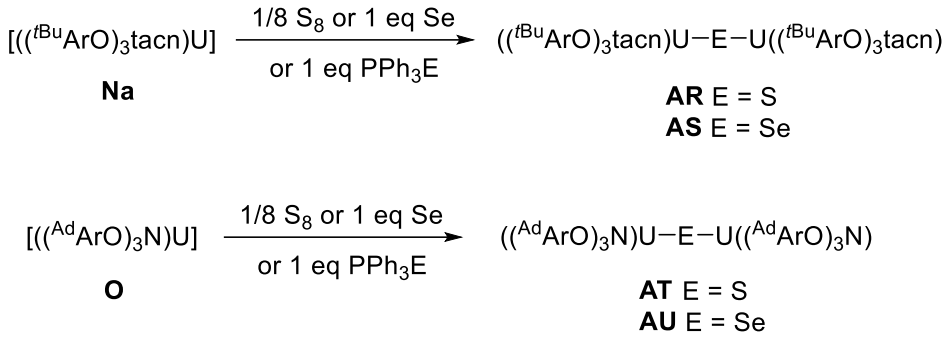


Scheme 2.12. Synthesis of complexes **AR**-**AU** with elemental chalcogenides and $PPh_3E$.[101]

The four complexes feature an $E^{2-}$ motif, complexes **AR** and **AS** present a linear U–E–U in the solid state, which indicates that the chalcogenide group acts as a π-donor. Whereas in complexes **AT** and **AU**, the U–E–U angle is more bent due to the steric congestion induced by the admantyl substituents, preventing optimal overlap in the U–E–U fragment.[101]

In addition, the synthesis of U–$E_2$–U diamond core complexes was achieved by reaction of complex **O** with the elemental chalcogens S, Se and Te, in the presence of sodium amalgam, providing complexes $[\{((^{Ad}ArO)_3N)U\}_2(\mu\text{-}S)_2]$ (**AV**), $[\{((^{Ad}ArO)_3N)U\}_2(\mu\text{-}Se)_2]$ (**AW**), $[\{((^{Ad}ArO)_3N)U\}_2(\mu\text{-}Te)_2]$ (**AX**) (Scheme 2.13).[101]

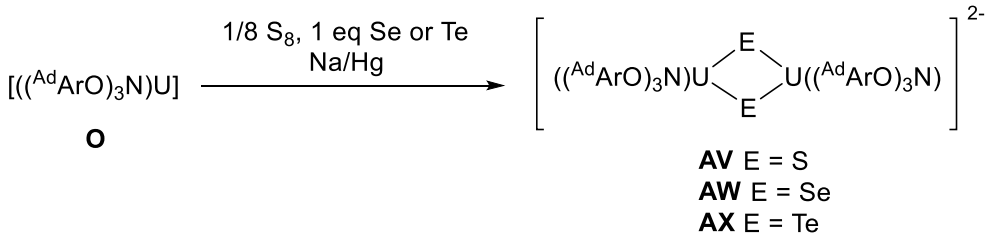


Scheme 2.13. Synthesis of complexes **AV**-**AX** by Na reduction.[101]

Subsequently, complex **O** was reacted with different stoichiometric amounts of elemental sulfur and selenium to yield the mono-, bis- or tetra-chalcogen bridged complexes, as seen in Scheme 2.14.[110]

Addition of one equivalent of selenium to a benzene solution of **O** formed the mono-bridged complex $[\{((^{Ad}ArO)_3N)U\}_2(\mu\text{-}Se)]$ (**AU**). Subsequent addition of one equivalent of elemental selenium to compound **AU** provided the bis-selenium bridged complex $[\{((^{Ad}ArO)_3N)U\}_2(\mu\text{-}Se_2)]$ (**AY**), which can be also obtained by addition of

precisely two equivalents of selenium to a solution of tris(aryloxide) complex **O**. Moreover, the tetra-selenium bridged complex [{((${}^{Ad}$ArO)$_3$N)U}$_2$(μ-η$^3$:η$^3$-Se$_4$)] (**AZ**) can be synthesised by reaction of either two, three or four equivalents of selenium with complexes **AY**, **AU** or **O** respectively.

Similarly, formation of the mono-sulfur bridged complex [{((${}^{Ad}$ArO)$_3$N)U}$_2$(μ-S)] (**AT**) can be achieved by reaction of 1/8 equivalents of $S_8$ with complex **O**, which can react further with addition of 0.375 equivalents of $S_8$ yielding the tetra-sulfur bridging complex [{((${}^{Ad}$ArO)$_3$N)U}$_2$(μ-η$^2$:η$^2$-S$_2$)$_2$] (**BA**). Complex **BA** is also formed by reaction of 1/2 equivalents of $S_8$ with tris(aryloxide) complex **O**.

This reactivity clearly shows the tendency of chalcogens to catenate to rings and chains of various sizes. However, there are not many reports in the literature featuring an actinide with a poly-chalcogenide ligand. Some examples are the thorium complex [(Cp*)$_2$Th(S)$_5$],[92] and uranium complexes [{(N$^t$Bu)$_2$(I)($^t$Bubpy)U}$_2$(μ-η$^2$:η$^2$-E$_4$)] (bpy = 2,2'-bipyridyl, E = S or Se).[111]

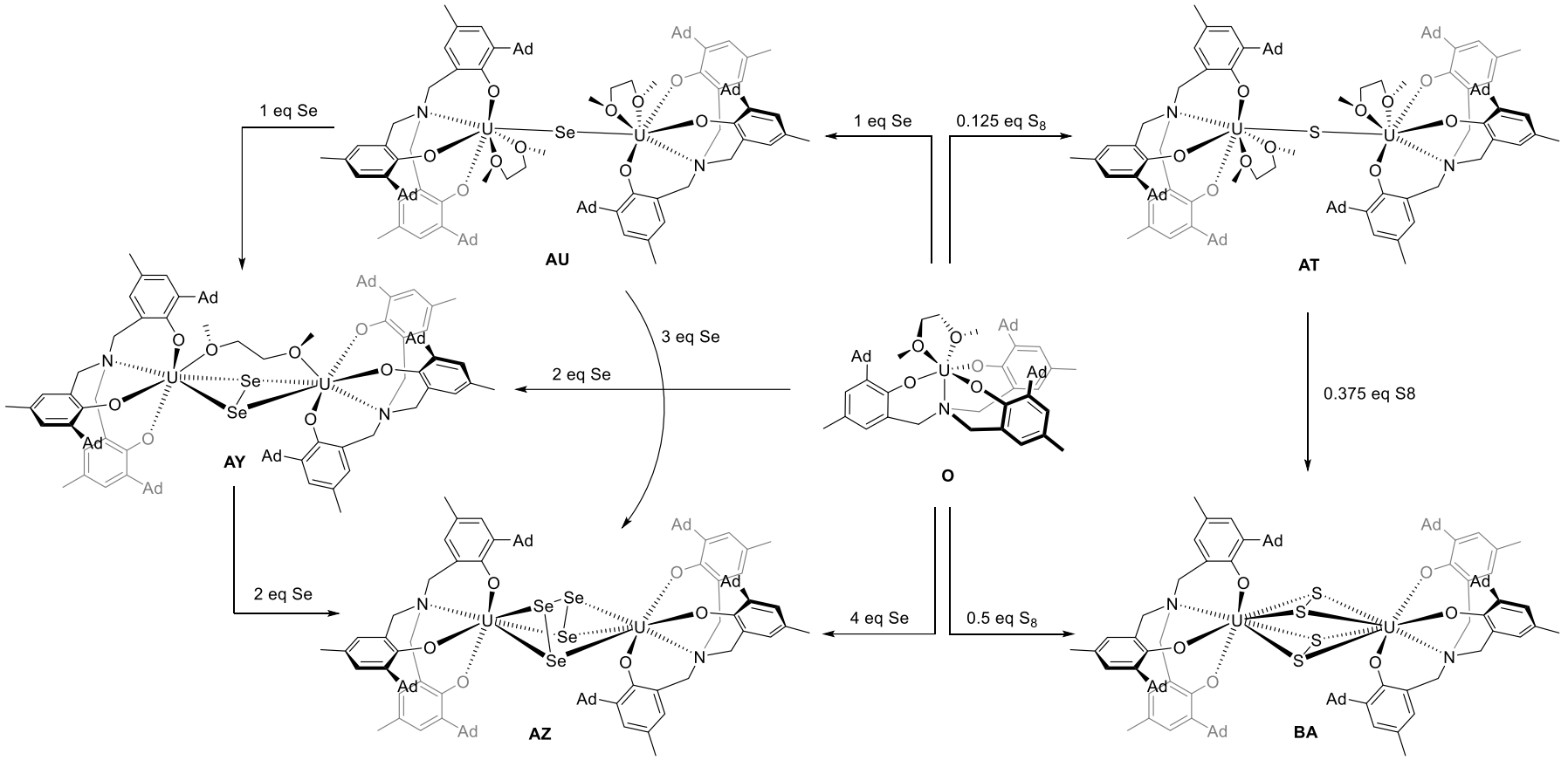


Scheme 2.14. Synthesis of mono-, bis- and tetra-chalcogenide bridging complexes **AT**, **AU**, **AY**, **AZ** and **BA** from elemental chalcogens.[110]

Furthermore, Meyer and co-workers studied the reactivity of tris(aryloxide) complex **O** with $CS_2$ and COS. As seen in Scheme 2.15, exposure of $CS_2$ to a solution of **O** reductively coupled $CS_2$ generating a tetrathiooxalate complex featuring a $C_2S_4^{2-}$ unit, $[\{((^{Ad}ArO)_3N)U\}_2(\mu\text{-}\kappa^2\text{:}\kappa^2\text{-}C_2S_4)]$ (**BB**) , which can be further reduced with sodium amalgam providing the ethylenetetrathiolate complex $[Na(dme)_3]_2[\{((^{Ad}ArO)_3N)U\}_2(\mu\text{-}C_2S_4)]$ (**BC**), featuring a $C_2S_4^{4-}$ moiety.[112, 113] Moreover, it was found that the chalcogenide-bridged complexes $[\{((^{Ad}ArO)_3N)U\}_2(\mu\text{-}S)]$ (**AT**) and $[\{((^{Ad}ArO)_3N)U\}_2(\mu\text{-}Se)]$ (**AU**) could react further with small molecules. Exposure of these complexes to $CS_2$ and COS yielded the insertion products $[\{((^{Ad}ArO)_3N)U\}_2(\mu\text{-}\kappa^2\text{:}\kappa^2\text{-}CS_3)]$ (**BD**), $[\{((^{Ad}ArO)_3N)U\}_2(\mu\text{-}\kappa^2\text{:}\kappa^2\text{-}CS_2Se)]$ (**BE**), and $[\{((^{Ad}ArO)_3N)U\}_2(\mu\text{-}\eta^1\text{:}\kappa^2\text{-}COS_2)]$ (**BF**) and $[\{((^{Ad}ArO)_3N)U\}_2(\mu\text{-}\eta^1\text{:}\kappa^2\text{-}CSSe)]$ (**BG**) respectively. Where **BD** and **BE** feature a chalcogenothiocarbonate $ECS_2^{2-}$ moiety and **BF** and **BG** an $ECOS^{2-}$.

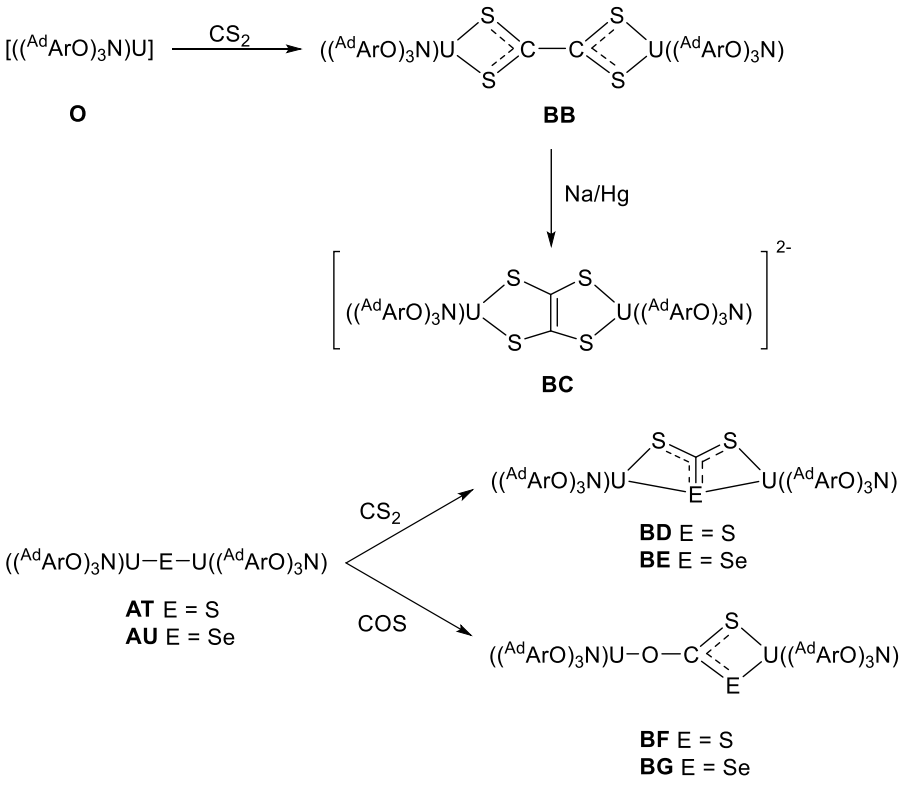


Scheme 2.15. Synthesis of $CS_2$ and COS complexes **BB**-**BG**.[112, 113]

In 2017, our group reported the use of the octadentate Schiff-base pyrrole, anthracene-hinged 'Pacman' ligand $L^A$ to combine two strongly reducing $U^{III}$ centres in the synthesis of complexes $[Na(THF)_4][\{(BH_4)U\}_2(\mu\text{-}BH_4)(L^A)(THF)_2]$ (**BH**) and the

aryloxide substituted [{(OTtbp)U}$_2$(μ-KBH$_4$)(L$^A$)(THF)$_2$] (**BI**) (Figure 2.11), which successfully activate both $S_8$ and $CS_2$.[98]

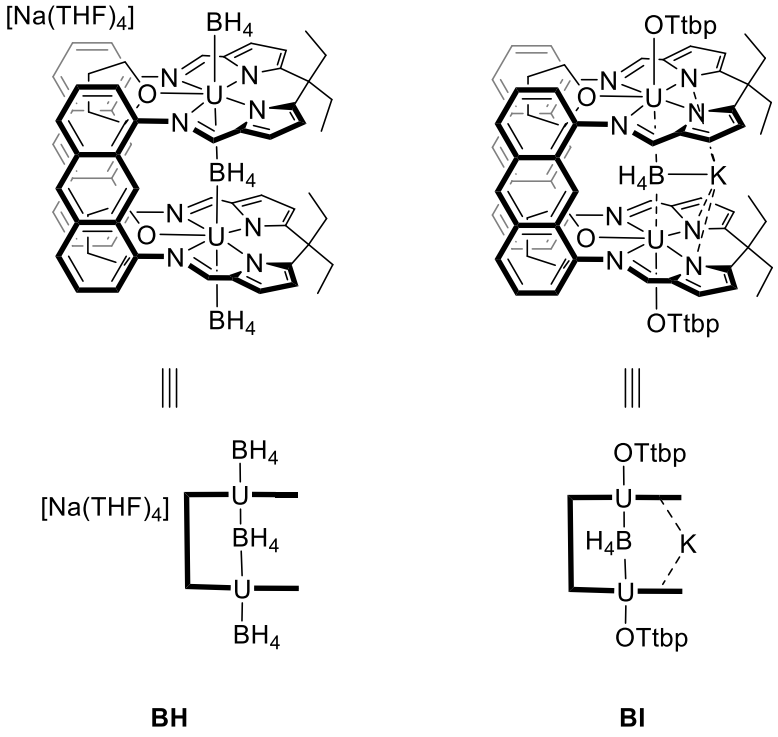


Figure 2.11. Complexes bearing the 'Pacman' ligand L$^A$, **BH** and **BI**.[98]

The addition of 0.75 equivalents of elemental sulfur to complex **BH** provided the polymeric structure **BJ** where S binds as a terminal multiply bonded ligand. Moreover, when complex **BH** was exposed to an excess of $CS_2$ complex [{(CS$_3$)U}$_2$(μ-κ$^2$:κ$^2$-CS$_3$)(L$^A$)] (**BK**) was formed via reductive disproportionation of $CS_2$. Complex **BK** features the rare trithiocarbonate $CS_3^{2-}$ motif in the endo and both exo uranium coordination sites. On the other hand, complex **BI** provided the persulfido $S_2^{2-}$ bridging complex [{(OTtbp)U}$_2$(μ-κ$^2$:κ$^2$-S$_2$)(L$^A$)] (**BL**) when treated with an excess of $S_8$. Moreover, complex [{(OTtbp)U}$_2$(μ-CS$_2$)(L$^A$)] (**BMa**), which features a bent $CS_2^{2-}$ unit, was formed upon exposure of **BI** to an excess of $CS_2$. When complex **BMa** was allowed to stand for 5 days at room temperature, or was heated for 2.5 h the sulfido-bridged complex [{(OTtbp)U}$_2$(μ-S)(L$^A$)] (**BM**) was formed, which provided complex **BL** after addition of an excess of elemental sulfur (Scheme 2.16).[98]

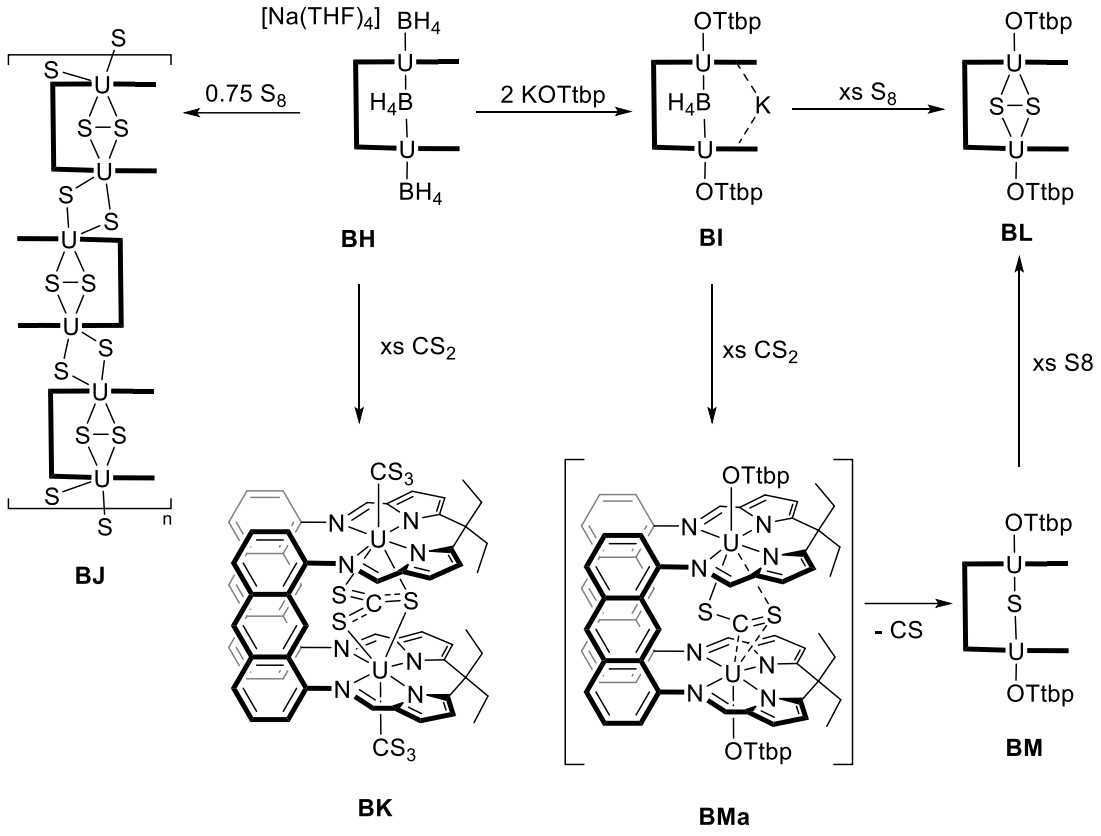


Scheme 2.16. Reactions of complexes **BH** and **BI** with $S_8$ and $CS_2$.[98]

The first example of chalcogen activation with a $U^{III}$ siloxide complex was published by Mazzanti and co-workers, when reaction of complex $[U(OSi(O^tBu)_3)_2(\mu\text{-}OSi(O^tBu)_3)]_2$ (**T**) with one equivalent of $CS_2$ led to the formation of $[\{(OSi(O^tBu)_3)_3U\}_2(\mu\text{-}\eta^2(CS):\eta^2(S,S)\text{-}CS_2)]$ (**BN**) (Scheme 2.17).[67]

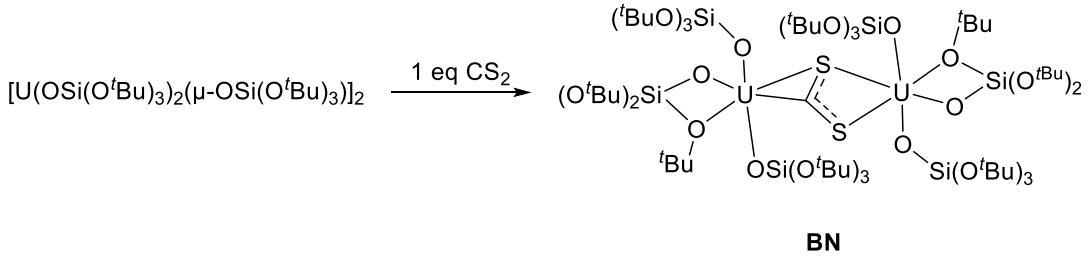


**BN**

Scheme 2.17. Synthesis of complex **BN**.[67]

A few years later, Mazzanti and co-workers published the reactions of $[K(18\text{-}c\text{-}6)][U(OSi(O^tBu)_3)_4]$ (**BO**) and $K[U(OSi(O^tBu)_3)_4]$ (**BP**) with $CS_2$. Reductive disproportionation is favoured when one equivalent of $CS_2$ is added to complex **BO**

yielding the trithiocarbonate complex **BQ** as the major product and the formation of $[U(OSi(O^tBu)_3)_4]$, $[K(18\text{-c-}6)]_2C_2S_4$ (**BR**) and some unidentified species as minor products. Whereas for complex **BP** the dimerization of $CS_2$ is the favoured pathway, providing the tetrathioxalate complex **BS** as the major product and $[U(OSi(O^tBu)_3)_4]$, and unidentified species as by-products (Scheme 2.18).[114]

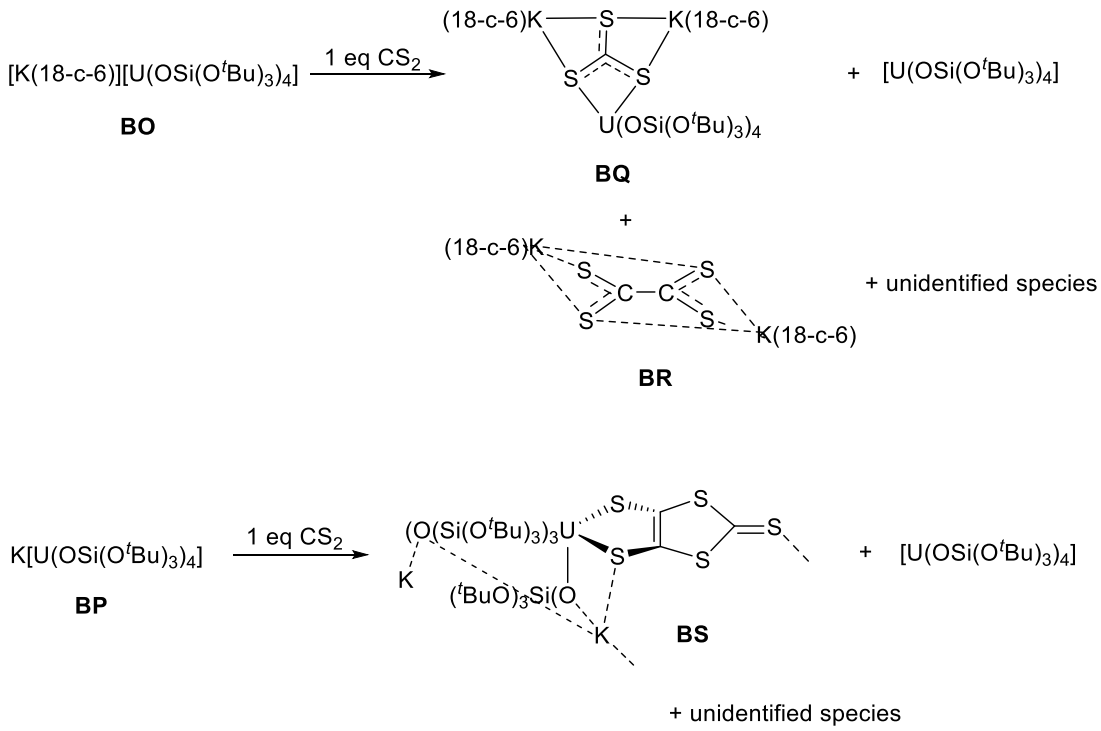


Scheme 2.18. Reaction of siloxide complex **BO** and **BP** with $CS_2$.[114]

Moreover, reaction of stoichiometric amounts of elemental sulfur with $K[U(OSi(O^tBu)_3)_4]$ (**BP**) was also carried out, providing a mixture of complexes. Although isolation of the persulfido unit containing complex $K_2[(S_2)U(OSi(O^tBu)_3)_4]_2$ (**BT**) and complex $[\{K(OSi(O^tBu)_3)_3U\}_2(\mu\text{-}\eta^2\text{:}\eta^2\text{-}S_2)(\mu\text{-}\eta^3\text{:}\eta^3\text{-}S_3)$ (**BU**) which contains both a disulfide and a persulfide unit, was achieved (Scheme 2.19).[115]

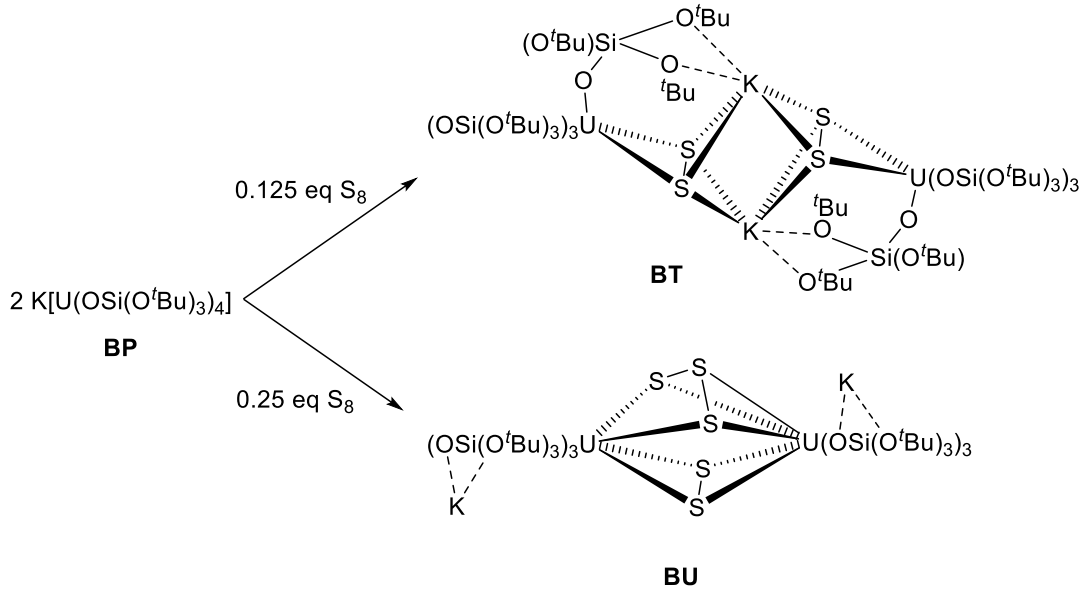


Scheme 2.19. Reaction of siloxide complex **BP** with elemental sulfur. [115]

As seen in the previous examples, $CS_2$ can react in different ways depending on the metal ion and the ancillary ligands. Within lanthanide and actinide chemistry there have been different examples of insertion[95, 116, 117] and reduction reactions of $CS_2$.[108, 112, 113, 118]

The synthesis of complexes containing terminal sulfide ligands in multiple bonding with uranium has increasing interest due to the electronic structures and possible applications in atom transfer chemistry. Although most attempts provided the formation of bridging complexes due to the nucleophilic nature of the terminal sulfide, some examples of terminal sulfido, selenido and tellurido containing a tetravalent $U^{IV}$ ion [93, 119-121] and $U^{V}$ ion [122] have been published.

Treatment of $U^{III}$ siloxide complex $K[U(OSi(O^tBu)_3)_4]$ (**BP**) with atom transfer reagent $PPh_3S$ led to the formation of $K_2[(S)U(OSi(O^tBu)_3)_4K_2]_2$ (**BV**) and to $K_2[(S)(OSi(O^tBu)_3)_4U\}_2(\mu\text{-}K_2(18\text{-c-}6))]$ (**BW**) in the presence of 18-crown-6. Addition of 2.2.2-cryptand to complex **BV** yielded the sulfido terminal complex $K[(S)U(OSi(O^tBu)_3)_4][K\text{cryptand}]$ (**BX**). These complexes are stabilised by the bulky ligand environment created by the siloxide ligands. The sulfur transfer from $PPh_3S$ to the uranium centre is favoured by the presence of Lewis acids like $K^+$. Moreover, the bonding analysis and further calculations revealed that the U–S bond has triple character, and therefore the participation of the *f*-orbitals in the bonding is low (Scheme 2.20).[115]

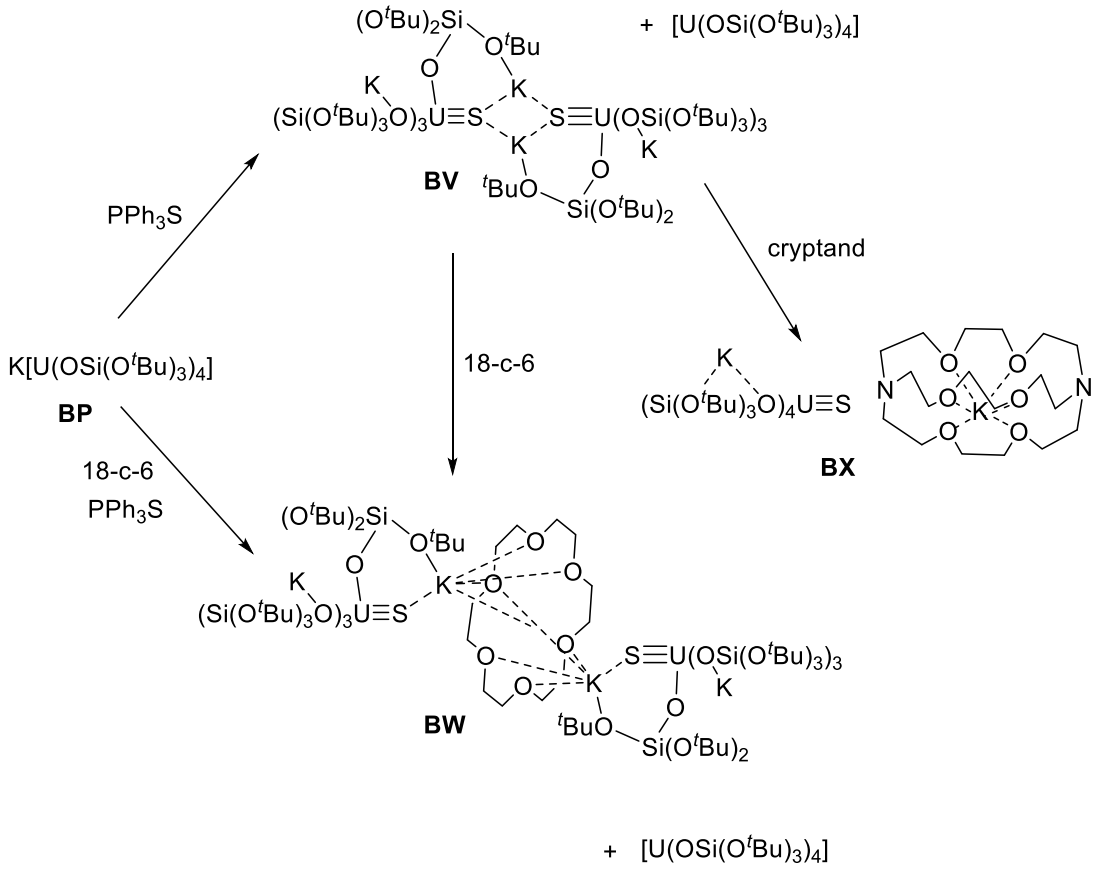


Scheme 2.20. Synthesis of chalcogen-containing complexes **BV**, **BW** and **BX**.[115]

### 2.6.2.2. Reaction with arenes

Since the first report of a uranium-arene interaction complex [U($\eta^5$-$C_5H_5$)$_3$Cl] (**D**) in 1956,[17] the study of complexes with such interactions has gained increased attention, not only to help understand the nature of the bonding, but also for the promising applicability of new reactivity.[24, 123-125] The first uranium complex containing a neutral bound arene [U($\eta^6$-$C_6H_6$)Cl$_4$] (**BY**) was published by Cesari and co-workers in 1971 (Figure 2.12).[126] A few years later, Cotton and co-workers published a similar complex featuring a different arene [U($\eta^6$-Mes)Cl$_4$] (**BZ**),[127] and in 1989 Ephritikhine and co-workers reported the synthesis of [U($\eta^6$-$C_6Me_6$)Cl$_4$] (**CA**).[128] All three complexes feature a piano stool half sandwich and were obtained by refluxing [U(BH$_4$)$_4$] or a mixture of UCl$_4$, AlCl$_3$ and powdered aluminium metal in arene solvent.

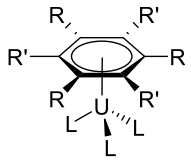


**BY** R = R' = H
**BZ** R = H R' = Me
**CA** R = R' = Me

Figure 2.12. U-arene complexes **BY**-**CA**.[126-128]

Another interesting class of uranium-arene complexes are the so-called uranium inverse arene sandwiches, particularly interesting for the presence of π and δ covalent interactions between the arene and the uranium *d*- and *f*-orbitals.[25] Uranium inverse arene sandwiches were first reported by Cummins and co-workers when reduction of the iodo tris(amido)uranium complex [UI(NAd(Ar))$_3$] (where Ar = 3,5-(Me)$_2$-C$_6$H$_3$) with KC$_8$ in the presence of arene solvent led to the formation of IAS (inverse arene sandwich) complexes [{(NAd(Ar))$_2$U}$_2$(μ-η$^6$:η$^6$-C$_6$H$_6$)] (**CB**) and [{(NAd(Ar))$_2$U}$_2$(μ-η$^6$:η$^6$-C$_7$H$_8$)] (**CC**) (Scheme 2.21).[28]

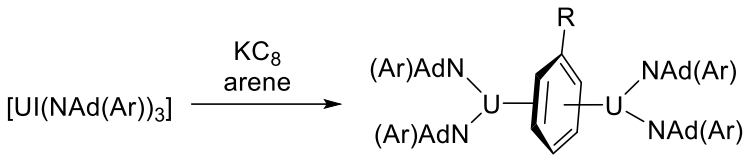


**CB** R = H
**CC** R = Me

Scheme 2.21. Synthesis of the first uranium IAS complexes **CB** and **CC**.[28]

Complexes **CB** and **CC** feature an arene moiety with a η$^6$:η$^6$ fashion with the $^1$H NMR resonances shifted to very low field (~ -80 to -90 ppm). The oxidation states for uranium and arene can be seen in three different ways: a) as an extreme with two formally $U^{II}$ ions with a neutral arene, b) with two trivalent uranium centres and a di-anionic arene, or c) two $U^{IV}$ centres and a tetra-anionic arene (Figure 2.13).[25]

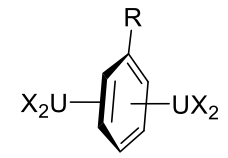


a) $U^{II}$-[$C_6H_5R$]-$U^{II}$
b) $U^{III}$-[$C_6H_5R$]$^{2-}$-$U^{III}$
c) $U^{IV}$-[$C_6H_5R$]$^{4-}$-$U^{IV}$

Figure 2.13. Possible oxidation states for uranium IAS complexes.[25]

Since then many different uranium inverse arene sandwiches have been reported, bearing a range of different ligands. In most cases reduction by K or $KC_8$ is needed.[28, 55, 129-136] Moreover, the formation of IAS complexes of transition metals and lanthanides have also been reported.[137-146]

In 2012 our group published a new route for the synthesis of uranium inverse arene sandwich complexes which does not require a reductant. This new synthetic path gives an opportunity to incorporate functionalised arenes that would be incompatible with the presence of such reductants.[24]

Storage of a solution of aryloxide [U(ODtbp)$_3$] (**M**) in arene solvent (benzene, toluene and biphenyl) for few days at 90 °C provided the inverse arene sandwich complexes [{(ODtbp)$_2$U}$_2$(μ-η$^6$:η$^6$-$C_6H_5R$)] (R = H, Me and Ph) **CDa-b** and **CF**. Analogous reactions happen for the uranium tris(silylamide) [U(N(SiMe$_3$)$_2$)$_3$] complex, which yields complexes [{(N(SiMe$_3$))$_2$U}$_2$(μ-η$^6$:η$^6$-$C_6H_5R$)] (R = H or Me) (**CEa-b**) and [{(N(SiMe$_3$))$_2$U}$_2$(μ-η$^6$:η$^6$-$C_6H_5$Ph)] (**CG**) (Scheme 2.22).

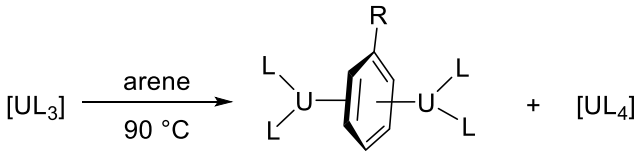


**CDa** L = ODtbp R = H
**CDb** L = ODtbp R = Me
**CEa** L = N(SiMe$_3$)$_2$ R = H
**CEb** L = N(SiMe$_3$)$_2$ R = Me
**CF** L = ODtbp R = Ph
**CG** L = N(SiMe$_3$)$_2$ R = Ph

Scheme 2.22. Direct synthesis of uranium IAS complexes **CD**-**CG**.[24]

Computational studies were carried out in order to understand the reaction mechanism. The overall redox reaction is a partial oxidation of the uranium. Four uranium centres are used to form two $U^{III}$ for the inverse arene sandwich complex and two uranium centres are "lost" in the form of [$UL_4$] by-product, while the arene is reduced to a dianion. The reaction proceeds through two concerted steps. The first step consists in the binding of two [$UL_3$] fragments and an arene molecule with ligand transfer from one [$UL_3$] to another to form an intermediate [$U(\eta^6\text{-}C_6H_6)L_2$] and a [$UL_4$]. The second step involves the binding of a third [$UL_3$] to the other side of the arene-bound intermediate at the same time that a ligand is transferred to another [$UL_3$] to finally form [$\{(L)_2U\}_2(\mu\text{-}\eta^6\text{:}\eta^6\text{-}C_6H_6)$] and two [$UL_4$] (Figure 2.14).[24]

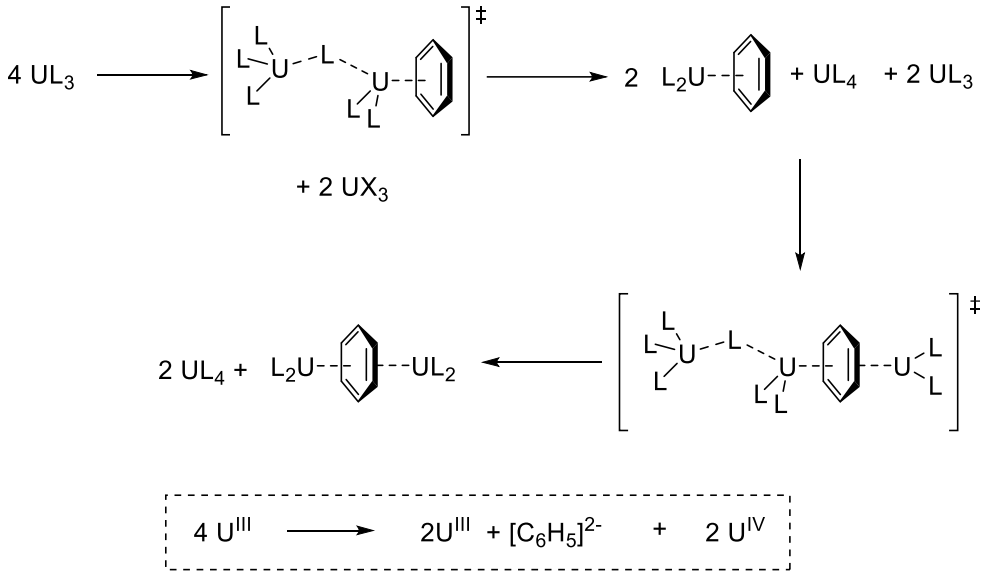


Figure 2.14. Predicted mechanism for the formation of uranium IAS complex.[24]

Despite not constituting considerable changes in the electronic and steric effects, the tri-*tert*-butyl-substituted [$U(OTtbp)_3$] (**CH**) does not react with arenes to form inverse arene sandwich complexes. However, the synthesis of [$\{(OTtbp)_2U\}_2(\mu\text{-}\eta^6\text{:}\eta^6\text{-}C_6H_6)$] (**CI**) could be achieved by treating [$\{(N(SiMe_3))_2U\}_2(\mu\text{-}\eta^6\text{:}\eta^6\text{-}C_6H_6)$] (**CEa**) with HOTtbp as seen in Scheme 2.23.

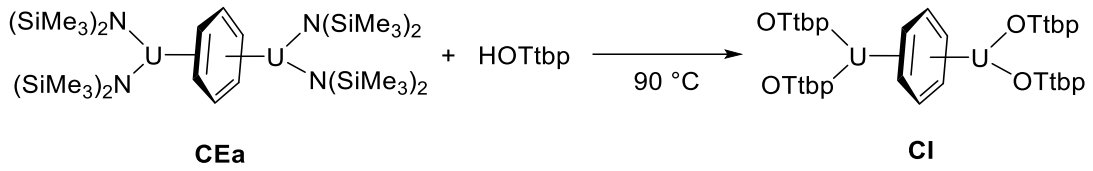


**CEa** **CI**

Scheme 2.23. Synthesis of tri-*tert*-butyl phenol analogue complex **CI**.[24]

Further reactions with functionalised arenes were performed for the aryloxide complex [U(ODtbp)$_3$] (**M**). Reaction with phenylsilane, which is incompatible with group 1 metals, led to the formation of [{(ODtbp)$_2$U}$_2$(μ-η$^6$:η$^6$-C$_6$H$_5$SiH$_3$)] (**CJ**). However, isolation from [U(ODtbp)$_4$] was not possible due to similar solubility properties (Scheme 2.24).

Moreover, borylation of the reduced arene was also possible by adding 9-bora-9-bicyclononane (HBBN) to complex [U(ODtbp)$_3$] **M** in the chosen arene, benzene, toluene, biphenyl or naphthalene affording [{(ODtbp)$_2$U}$_2$(μ-η$^6$:η$^6$-C$_6$H$_5$BBN)] (**CK**), [{(ODtbp)$_2$U}$_2$(μ-η$^6$:η$^6$-C$_7$H$_7$BBN)] (**CL**), [{(ODtbp)$_2$U}$_2$(μ-η$^6$:η$^6$-C$_{12}$H$_9$BBN)] (**CM**) and [{(ODtbp)$_2$U}$_2$(μ-η$^6$:η$^6$-C$_{10}$H$_7$BBN)] (**CN**) respectively. Complex **CK** could also be synthesised from addition of HBBN to inverse arene sandwich complex **CDa**. Storage of complex **CN** in benzene at 90 °C for 6 days gave the benzene inverse sandwich complex **CDa** and free C$_{10}$H$_7$BBN. This methodology has the potential to become catalytic (Scheme 2.24).

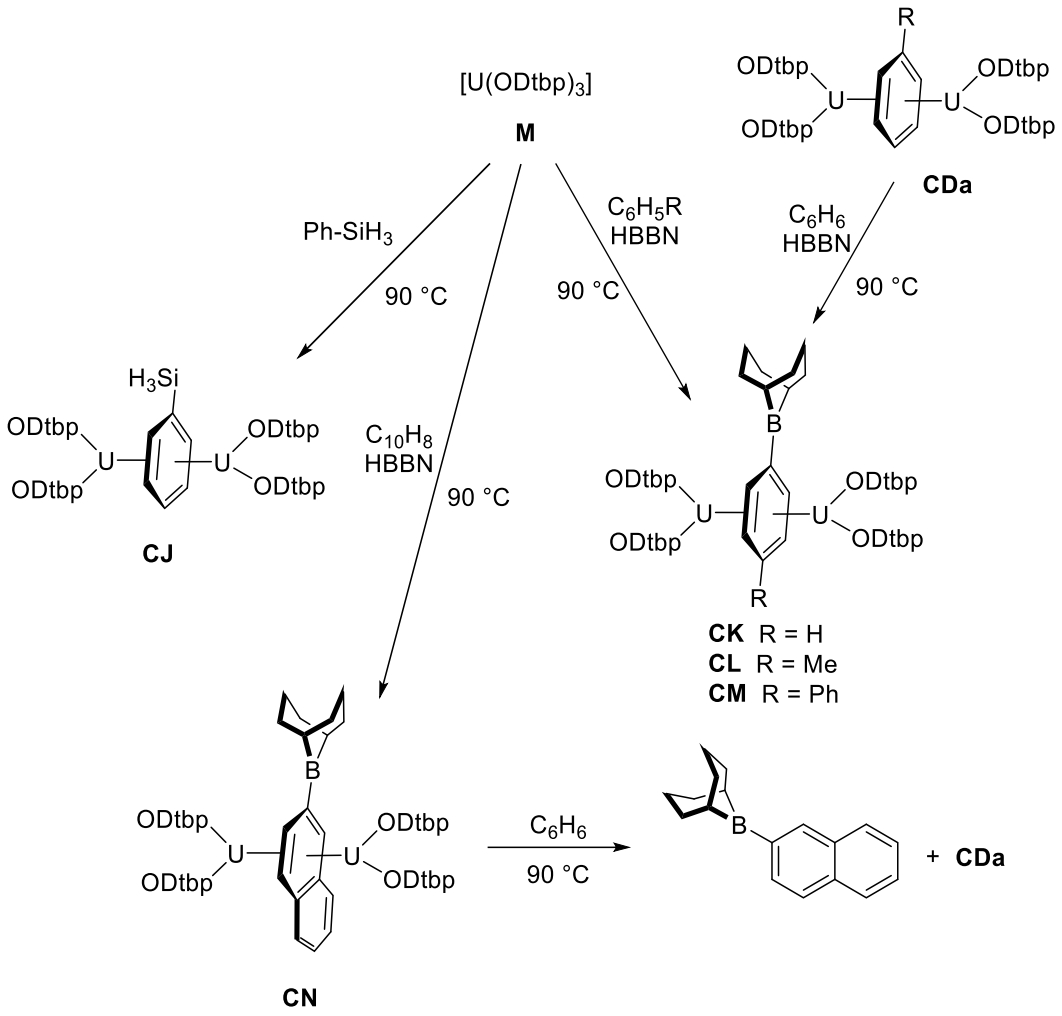


Scheme 2.24. Reactivity of $[U(ODtbp)_3]$ (**M**) with different functionalised arenes.[24]

The borylation reactions are thermodynamically favoured due to the increased stability of the borylated arene complexes when compared to the non-borylated.

In 2012 Mazzanti and co-workers reported the synthesis of a uranium inverse arene sandwich which forms from the siloxide uranium complex **T** in toluene, compound $[\{(OSi(O^tBu)_3)U\}_3(\mu\text{-}\eta^6\text{:}\eta^6\text{-}C_7H_8)]$ (**CO**).[67] One year later an extended study was published with the synthesis of two more inverse arene sandwich complexes, and computational analysis of the electronic structure of those compounds. Complex **CO** can be subsequently reduced with $KC_8$ to yield the mono- and di-anionic inverse arene sandwich complexes $K[\{(OSi(O^tBu)_3)_3U\}_2(\mu\text{-}\eta^6\text{:}\eta^6\text{-}C_7H_8)]$ (**CP**) and $K_2[\{(OSi(O^tBu)_3)_3U\}_2(\mu\text{-}\eta^6\text{:}\eta^6\text{-}C_7H_8)]$ (**CQ**) as seen in Scheme 2.25.[147]

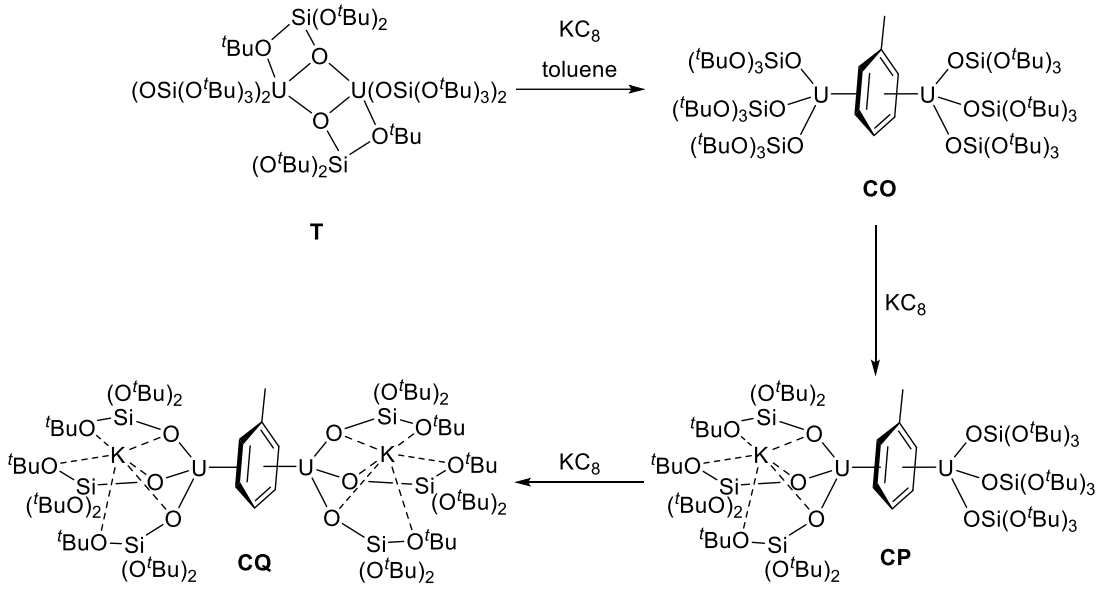


Scheme 2.25. Synthesis of IAS complexes **CO**, **CP** and **CQ**.[147]

DFT studies were carried out in order to reveal the electronic states of complexes **CO**, **CP** and **CQ**. Complex **CO** is best described as high-valent $U^{V}$ centre bridged by a tetra-anionic $(C_7H_8)^{4-}$. In the mono-ionic compound **CP** each uranium centre is in a different oxidation state, $U^{IV}$ and $U^{V}$, with a tetra-anionic arene and complex **CQ** features two $U^{IV}$ and a tetra-anionic toluene moiety.

### 2.6.2.3. Reaction with nitrogen

Dinitrogen is the primary source in both biological and industrial processes. The conversion of dinitrogen to ammonia through the Haber-Bosch process is one of the biggest industrial transformations and requires approximately a 2 % of the world's energy production. Therefore, mild routes to dinitrogen activation and functionalisation are of continuing interest.[59]

The first activation of dinitrogen with a $U^{III}$ centre was reported by Scott and co-workers in 1998. Complex [U(tren$^{DMBS}$)] (**CR**) (tren$^{DBMS}$ = {N($CH_2CH_2NSi^tBuMe_2)_3$}) was found to reversibly bind dinitrogen to afford the weakly bound side-on complex [{(tren$^{DMBS}$)U}$_2$($\mu$-$\eta^2$:$\eta^2$-$N_2$)] (**CS**) upon exposure to an atmosphere of $N_2$ at -20 °C (Scheme 2.26). No reduction of dinitrogen was observed, but a Lewis acidic-type interaction, which is readily removed under vacuum.[148]

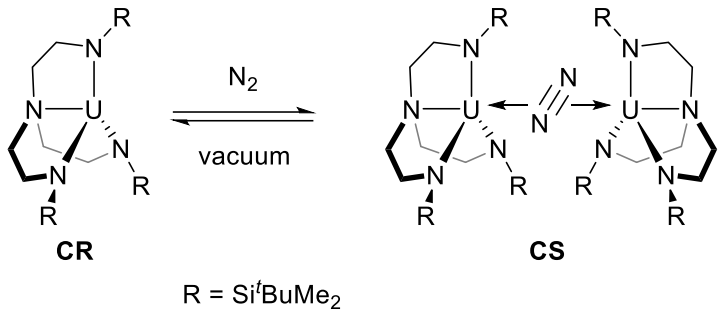


Scheme 2.26. Synthesis of reversibly bind $N_2$ complex **CS**.[148]

Shortly after, Cummins and co-workers published the first heterodinuclear end-on dinitrogen bridging complex $[\{C_6H_3Me_2\text{-}3,5\}_2(^tBu)N\}_3U(\mu\text{-}\eta^1\text{:}\eta^1\text{-}N_2)\text{-}Mo\{N(^tBu)Ph\}_3]$, where dinitrogen is reduced, promoting an elongation of the N–N distance.[149] Moreover, Cp* complex $[U(Cp^*)_3]$ and pentalene complex $[U(Cp^*)(\eta\text{-}C_8H_4\{Si^iPr_3\text{-}1,4\}_2)]$ also showed dinitrogen activation, although some overpressure was necessary in order to stabilise them despite the formal reduction to $N_2^{2-}$.[150, 151]

In addition, in 2011 our group reported the first dinitrogen-bound $U^{III}$ aryloxide complexes. The synthesis of complex $[U(ODtbp)_3]$ (**M**) from $[U(N(SiMe_3)_2)_3]$ and HODtbp under an atmosphere of dinitrogen afforded a minor product which was characterised as $[\{(ODtbp)_3U\}_2(\mu\text{-}\eta^2\text{:}\eta^2\text{-}N_2)]$ (**CT**). Similarly, the reaction between $[U(N(SiMe_3)_2)_3]$ and HOTtbp under a dinitrogen atmosphere provided complex $[\{(OTtbp)_3U\}_2(\mu\text{-}\eta^2\text{:}\eta^2\text{-}N_2)]$ (**CU**) in near quantitative yields (Scheme 2.27).[23]

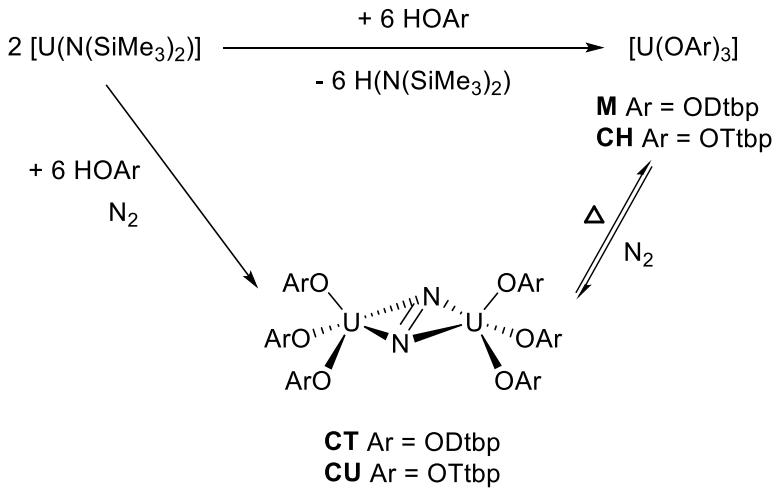


Scheme 2.27. Synthesis of the dinitrogen-bound complexes **CT** and **CU**.[23]

Structural parameters, Raman spectroscopy and computational calculations indicate that the reactions proceeded via reduction of the dinitrogen providing a side-on bound diazenido $N_2^{2-}$ species by the two $U^{III}$ centres to form a $U^{IV}$-$N_2^{2-}$-$U^{IV}$ dimer.

The addition of the third *tert*-butyl substituent increased the electron donation on the aryloxide, which is proposed to be the cause of enhancing the reducing power of the $U^{III}$ centre. As it is observed that complex **CU** is more stable than **CT**, as the coordinated dinitrogen can be reversibly removed upon heating a solution of **CU** to 80 °C, whereas for complex **CT** this can be achieved by freeze-pump-thaw degassing at room temperature. This effect demonstrates the notable control exerted by simple modifications to the aryloxide ligands.

In 2013 our group reported the synthesis of a dinitrogen-bridged complex supported by siloxide ligands. Similarly to the formation of aryloxide complexes **CT** and **CU**, reaction of tris(silylamide) [U(N(SiMe$_3$)$_2$)$_3$] with the bulky trimesitylsilanol HOSiMes$_3$ in a dinitrogen atmosphere afforded complex [{(OSiMes$_3$)$_3$U}$_2$(μ-η$^2$:η$^2$-N$_2$)] (**CV**) (Scheme 2.28).[66]

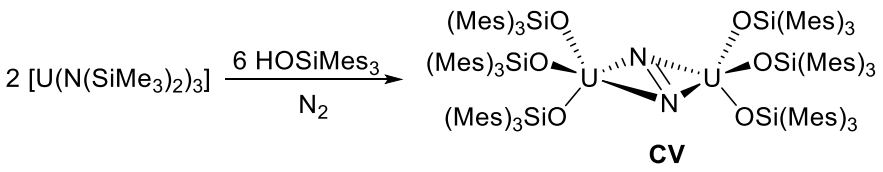


Scheme 2.28. Synthesis of dinitrogen-bridged complex **CV**.[66]

Structural parameters and Raman spectroscopy reveal that dinitrogen is reduced to a diazenido $N_2^{2-}$ species bound in a side-on manner to form a $U^{IV}$-$N_2^{2-}$-$U^{IV}$ dimer.

A few years later, Mazzanti and co-workers published the synthesis of a multimetallic uranium nitride complex which is able to activate and functionalise dinitrogen. Exposing complex K$_3$[{(OSi(O$^t$Bu)$_3$)$_3$U}$_2$(μ-N)] to dinitrogen, both in the solid state and in a toluene solution, yielded complex K$_3$[{(OSi(O$^t$Bu)$_3$)$_3$U}$_2$(μ-N)(μ-η$^2$:η$^2$-N$_2$)] (**CW**) in good yields. Single crystal X-Ray diffraction, EPR spectroscopy and SQUID measures confirmed the formation of complex **CW** with a side-on bound hydrazido $N_2^{4-}$ moiety bridging two $U^{V}$ centres in a diamond-shaped geometry and a nitrido $N^{3-}$ ligand also bridging the two uranium ions.[152]

Further reactivity with complex **CW** was carried out. Addition of acids such as HOTtbp, PyHCl, HCl and $HBAr^F$ ($BAr^F$ = [{3,5-$(CF_3)_2C_6H_3$}$_4$B]$^-$) provided the protonation of the nitride ligand to give complex $K_2$[{(OSi(O$^t$Bu)$_3$)$_3$U}$_2$(μ-NH)(μ-η$^2$:η$^2$-$N_2$)] (**CX**). Moreover, addition of two equivalents of PyHCl led to the formation of the doubly protonated species with the presence of bis(imido)-bridged diuranium(IV/V) complex $K_2$[{(OSi(O$^t$Bu)$_3$)$_3$U}$_2$(μ-NH)$_2$(μ-Cl)] (**CY**) (Scheme 2.29).

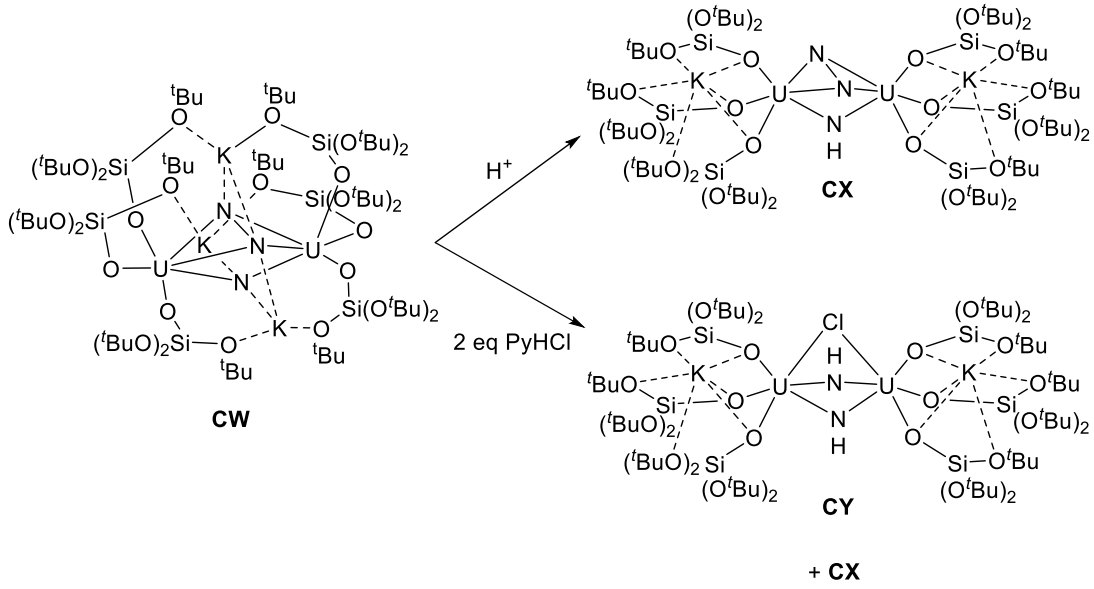


Scheme 2.29. Synthesis of nitrogen-bridged complexes **CX** and **CY.**[152]

Addition of an excess of acid resulted in the formation of ammonium chloride, suggesting that the protonation of complex **CW** can lead to complete cleavage of dinitrogen. Due to these results, the exposure of complex **CW** to $H_2$ was carried out, as the synthesis of ammonia from $N_2$ and $H_2$ is greatly desirable. No formation of ammonia was observed. However, addition of an HCl solution in ether to the product of the reaction provided ammonia in nearly quantitative yield (Scheme 2.30).

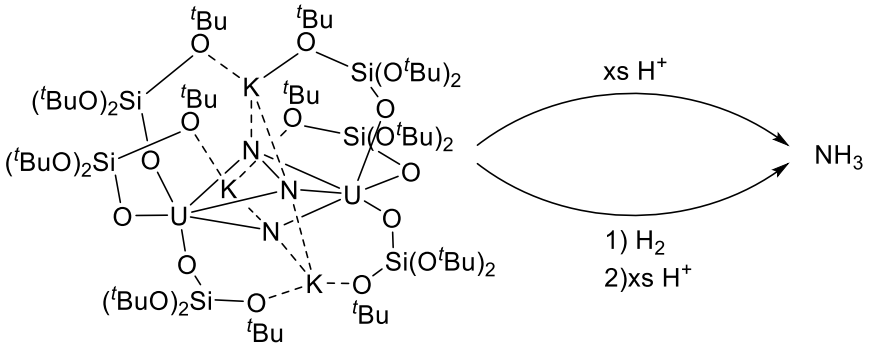


**CW**

Scheme 2.30. Formation of ammonia from siloxide complex **CW**.[152]

## 2.7. Project objectives

As showed before, the amount of transformations performed by uranium(III) complexes bearing either aryloxide and siloxide ligands, is an inspiration to pursue chemistry in this direction. Moreover, the use of other ligands, such as boroxides has proven to be successful in transition metal chemistry.

The primary objective of this project is the synthesis of a uranium boroxide complex and the study of the further reactivity. As mentioned before, the addition of a more electron-accepting atom such as boron into the ligand environment provides a more electron-deficient ligand and displaces the R groups away from the metal centre, which ultimately can give different reactivity. The investigation on the effect of the addition of another Lewis acidic reactive-site into the molecule was our primary target.

Reactivity with small molecules is sought, including arene reduction for the formation of uranium inverse arene sandwich-type complexes.

Finally, the use of a rare earth metal like yttrium in the synthesis of boroxide ligand complexes and further reactivity is investigated.

## 2.8. Bibliography

[1] N. N. Greenwood and A. Earnshaw, *Chemistry of the Elements*, 2nd edn, Butterworth-Heinemann, Burlington, MA, **1997**, pp 944-953.

[2] J. H. L. Voncken, *The Rare Earth Elements: An Introduction*, Springer International Publishing, Cham, Cham, **2016**.

[3] G. Wilkinson, J. M. Birmingham, *J. Am. Chem. Soc.* **1954**, *76*, 6210-6210.

[4] R. G. Hayes, J. L. Thomas, *J. Am. Chem. Soc.* **1969**, *91*, 6876-6876.

[5] F. Mares, K. Hodgson, A. Streitwieser, *J. Organomet. Chem.* **1970**, *24*, C68-C70.

[6] K. O. Hodgson, F. Mares, D. F. Starks, A. Streitwieser, *J. Am. Chem. Soc.* **1973**, *95*, 8650-8658.

[7] N. N. Greenwood, A. Earnshaw, in *Chemistry of the Elements* 2nd edn, Butterworth-Heinemann, Burlington, MA, **1997** pp. 1250-1266.

[8] *Uranium,* Radiological and Chemical Fact Sheets to Support Health Risk Analyses for Contaminated Areas, Argonne National Laboratory, EVS, **2008**

[9] World nuclear association website. http://www.world-nuclear.org/information-library/nuclear-fuel-cycle/uranium-resources/uranium-and-depleted-uranium.aspx (accessed September 2018)

[10] S. T. Liddle, *Angew. Chem. Int. Ed.* **2015**, *54*, 8604-8641.

[11] M. R. MacDonald, M. E. Fieser, J. E. Bates, J. W. Ziller, F. Furche, W. J. Evans, *J. Am. Chem. Soc.* **2013**, *135*, 13310-13313.

[12] H. S. La Pierre, A. Scheurer, F. W. Heinemann, W. Hieringer, K. Meyer, *Angew. Chem. Int. Ed.* **2014**, *53*, 7158-7162.

[13] M. E. Fieser, C. T. Palumbo, H. S. La Pierre, D. P. Halter, V. K. Voora, J. W. Ziller, F. Furche, K. Meyer, W. J. Evans, *Chem. Sci.* **2017**, *8*, 7424-7433.

[14] D. N. Huh, J. W. Ziller, W. J. Evans, *Inorg. Chem.* **2018**, *57*, 11809-11814.

[15] B. S. Billow, B. N. Livesay, C. C. Mokhtarzadeh, J. McCracken, M. P. Shores, J. M. Boncella, A. L. Odom, *J. Am. Chem. Soc.* **2018**, *140*, 17369-17373.

[16] D. E. Morris, R. E. Da Re, K. C. Jantunen, I. Castro-Rodriguez, J. L. Kiplinger, *Organometallics* **2004**, *23*, 5142-5153.

[17] L. T. Reynolds, G. Wilkinson, *J. Inorg. Nucl. Chem.* **1956**, *2*, 246-253.

[18] E. O. Fischer, Y. Hristidu, Z. Naturforsch., **1962**, pp. 275-276.

[19] A. Streitwieser, U. Mueller-Westerhoff, *J. Am. Chem. Soc.* **1968**, *90*, 7364-7364.

[20] A. Zalkin, K. N. Raymond, *J. Am. Chem. Soc.* **1969**, *91*, 5667-5668.

[21] O. T. Summerscales, F. G. N. Cloke, P. B. Hitchcock, J. C. Green, N. Hazari, *Science* **2006**, *311*, 829-831.

[22] P. L. Arnold, Z. R. Turner, R. M. Bellabarba, R. P. Tooze, *Chem. Sci.* **2011**, *2*, 77-79.

[23] S. M. Mansell, N. Kaltsoyannis, P. L. Arnold, *J. Am. Chem. Soc.* **2011**, *133*, 9036-9051.

[24] P. L. Arnold, S. M. Mansell, L. Maron, D. McKay, *Nat. Chem.* **2012**, *4*, 668-674.

[25] S. T. Liddle, *Coord. Chem. Rev.* **2015**, *293-294*, 211-227.

[26] L. Karmazin, M. Mazzanti, J. Pécaut, *Inorg. Chem.* **2003**, *42*, 5900-5908.

[27] I. Korobkov, G. Sandro, *Prog. Inorg. Chem.* **2005,** *54*, 321-349.

[28] P. L. Diaconescu, P. L. Arnold, T. A. Baker, D. J. Mindiola, C. C. Cummins, *J. Am. Chem. Soc.* **2000**, *122*, 6108-6109.

[29] I. Korobkov, S. Gorelsky, S. Gambarotta, *J. Am. Chem. Soc.* **2009**, *131*, 10406-10420.

[30] L. R. Avens, S. G. Bott, D. L. Clark, A. P. Sattelberger, J. G. Watkin, B. D. Zwick, *Inorg. Chem.* **1994**, *33*, 2248-2256.

[31] M. J. Monreal, R. K. Thomson, T. Cantat, N. E. Travia, B. L. Scott, J. L. Kiplinger, *Organometallics* **2011**, *30*, 2031-2038.

[32] R. C. Mehrotra, A. Singh, U. M. Tripathi, *Chem. Rev.* **1991**, *91*, 1287-1303.

[33] P. B. Hitchcock, M. F. Lappert, A. Singh, *J. Chem. Soc., Chem. Commun.* **1983**, 1499-1501.

[34] P. B. Hitchcock, M. F. Lappert, R. G. Smith, *Inorg. Chim. Acta* **1987**, *139*, 183-184.

[35] L. A. M. Steele, T. J. Boyle, R. A. Kemp, C. Moore, *Polyhedron* **2012**, *42*, 258-264.

[36] T. M. Ovitt, G. W. Coates, *J. Am. Chem. Soc.* **1999**, *121*, 4072-4073.

[37] B. J. O'Keefe, M. A. Hillmyer, W. B. Tolman, *J. Chem. Soc., Dalton Trans.* **2001**, 2215-2224.

[38] K. B. Aubrecht, K. Chang, M. A. Hillmyer, W. B. Tolman, *J. Polym. Sci., Part A: Polym. Chem.* **2001**, *39*, 284-293.

[39] X. Wang, J. L. Brosmer, A. Thevenon, P. L. Diaconescu, *Organometallics* **2015**, *34*, 4700-4706.

[40] D. Seyferth, *Organometallics* **2004**, *23*, 3562-3583.

[41] R. G. Jones, G. Karmas, G. A. Martin, H. Gilman, *J. Am. Chem. Soc.* **1956**, *78*, 4285-4286.

[42] R. G. Jones, E. Bindschadler, G. Karmas, F. A. Yoeman, H. Gilman, *J. Am. Chem. Soc.* **1956**, *78*, 4287-4288.

[43] D. C. Bradley, A. K. Chatterjee, *J. Inorg. Nucl. Chem.* **1959**, *12*, 71-78.

[44] K. W. Bagnall, A. M. Bhandari, D. Brown, *J. Inorg. Nucl. Chem.* **1975**, *37*, 1815-1816.

[45] P. G. Edwards, R. A. Andersen, A. Zalkin, *J. Am. Chem. Soc.* **1981**, *103*, 7792-7794.

[46] A. J. Zozulin, D. C. Moody, R. R. Ryan, *Inorg. Chem.* **1982**, *21*, 3083-3086.

[47] P. B. Hitchcock, M. F. Lappert, A. Singh, R. G. Taylor, D. Brown, *J. Chem. Soc., Chem. Commun.* **1983**, 561-563.

[48] W. G. Van der Sluys, C. J. Burns, J. C. Huffman, A. P. Sattelberger, *J. Am. Chem. Soc.* **1988**, *110*, 5924-5925.

[49] I. Castro-Rodriguez, K. Olsen, P. Gantzel, K. Meyer, *Chem. Commun.* **2002**, 2764-2765.

[50] I. Castro-Rodriguez, K. Olsen, P. Gantzel, K. Meyer, *J. Am. Chem. Soc.* **2003**, *125*, 4565-4571.

[51] O. P. Lam, S. C. Bart, H. Kameo, F. W. Heinemann, K. Meyer, *Chem. Commun.* **2010**, *46*, 3137-3139.

[52] I. Castro-Rodriguez, H. Nakai, L. Zakharov, A. Rheingold, K. Meyer, *Science* **2004**, *305*, 1757-1759.

[53] H. Nakai, X. Hu, L. N. Zakharov, A. L. Rheingold, K. Meyer, *Inorg. Chem.* **2004**, *43*, 855-857.

[54] A. C. Schmidt, A. V. Nizovtsev, A. Scheurer, F. W. Heinemann, K. Meyer, *Chem. Commun.* **2012**, *48*, 8634-8636.

[55] P. L. Diaconescu, C. C. Cummins, *J. Am. Chem. Soc.* **2002**, *124*, 7660-7661.

[56] S. C. Bart, F. W. Heinemann, C. Anthon, C. Hauser, K. Meyer, *Inorg. Chem.* **2009**, *48*, 9419-9426.

[57] H. S. La Pierre, H. Kameo, D. P. Halter, F. W. Heinemann, K. Meyer, *Angew. Chem., Int. Ed.* **2014**, *53*, 7154-7157.

[58] J. A. L. Wells, M. L. Seymour, M. Suvova, P. L. Arnold, *Dalton Trans.* **2016**, *45*, 16026-16032.

[59] P. L. Arnold, *Chem. Commun.* **2011**, *47*, 9005-9010.

[60] N. Tsoureas, O. T. Summerscales, F. G. N. Cloke, S. M. Roe, *Organometallics* **2013**, *32*, 1353-1362.

[61] N. Tsoureas, L. Castro, A. F. R. Kilpatrick, F. G. N. Cloke, L. Maron, *Chem. Sci.* **2014**, *5*, 3777-3788.

[62] C. Krempner, *Eur. J. Inorg. Chem.* **2011**, *2011*, 1689-1698.

[63] F. Blanc, C. Copéret, J. Thivolle-Cazat, J.-M. Basset, A. Lesage, L. Emsley, A. Sinha, R. R. Schrock, *Angew. Chem. Int. Ed.* **2006**, *45*, 1216-1220.

[64] M. Bindl, R. Stade, E. K. Heilmann, A. Picot, R. Goddard, A. Fürstner, *J. Am. Chem. Soc.* **2009**, *131*, 9468-9470.

[65] S. Lysenko, J. Volbeda, P. G. Jones, M. Tamm, *Angew. Chem.* **2012**, *124*, 6861-6865.

[66] S. M. Mansell, J. H. Farnaby, A. I. Germeroth, P. L. Arnold, *Organometallics* **2013**, *32*, 4214-4222.

[67] V. Mougel, C. Camp, J. Pécaut, C. Copéret, L. Maron, C. E. Kefalidis, M. Mazzanti, *Angew. Chem., Int. Ed.* **2012**, *51*, 12280-12284.

[68] P. L. Arnold, D. Patel, C. Wilson, J. B. Love, *Nature* **2008**, *451*, 315-317.

[69] E. A. Pedrick, G. Wu, T. W. Hayton, *Inorg. Chem.* **2015**, *54*, 7038-7044.

[70] J. J. Kiernicki, M. Zeller, S. C. Bart, *Angew. Chem. Int. Ed.* **2017**, *56*, 1097-1100.

[71] P. L. Arnold, A. F. Pécharman, E. Hollis, A. Yahia, L. Maron, S. Parsons, J. B. Love, *Nat. Chem.* **2010**, *2*, 1056-1061.

[72] M. P. Coles, *Coord. Chem. Rev.* **2016**, *323*, 52-59.

[73] S. C. Cole, M. P. Coles, P. B. Hitchcock, *J. Chem. Soc., Dalton Trans.* **2002**, 4168-4174.

[74] A. M. Neculai, C. C. Cummins, D. Neculai, H. W. Roesky, G. Bunkòczi, B. Walfort, D. Stalke, *Inorg. Chem.* **2003**, *42*, 8803-8810.

[75] J. Hong, Z. Li, Z. Chen, L. Weng, X. Zhou, L. Zhang, *Dalton Trans.* **2016**, *45*, 6641-6649.

[76] M. Xémard, M. Cordier, E. Louyriac, L. Maron, C. Clavaguéra, G. Nocton, *Dalton Trans.* **2018**, *47*, 9226-9230.

[77] B. M. Gardner, S. T. Liddle, *Eur. J. Inorg. Chem.* **2013**, *2013*, 3753-3770.

[78] S. T. Liddle, *Angew. Chem., Int. Ed.* **2015**, *54*, 8604-8641.

[79] W. J. Evans, D. S. Lee, J. W. Ziller, *J. Am. Chem. Soc.* **2004**, *126*, 454-455.

[80] W. J. Evans, M. Fang, G. Zucchi, F. Furche, J. W. Ziller, R. M. Hoekstra, J. I. Zink, *J. Am. Chem. Soc.* **2009**, *131*, 11195-11202.

[81] M. Fang, J. E. Bates, S. E. Lorenz, D. S. Lee, D. B. Rego, J. W. Ziller, F. Furche, W. J. Evans, *Inorg. Chem.* **2011**, *50*, 1459-1469.

[82] B. M. Schmiege, J. W. Ziller, W. J. Evans, *Inorg. Chem.* **2010**, *49*, 10506-10511.

[83] M. E. Fieser, J. E. Bates, J. W. Ziller, F. Furche, W. J. Evans, *J. Am. Chem. Soc.* **2013**, *135*, 3804-3807.

[84] M. E. Fieser, C. W. Johnson, J. E. Bates, J. W. Ziller, F. Furche, W. J. Evans, *Organometallics* **2015**, *34*, 4387-4393.

[85] S. E. Lorenz, B. M. Schmiege, D. S. Lee, J. W. Ziller, W. J. Evans, *Inorg. Chem.* **2010**, *49*, 6655-6663.

[86] T. J. Mueller, M. E. Fieser, J. W. Ziller, W. J. Evans, *Chem. Sci.* **2011**, *2*, 1992-1996.

[87] M. R. MacDonald, J. W. Ziller, W. J. Evans, *J. Am. Chem. Soc.* **2011**, *133*, 15914-15917.

[88] J. F. Corbey, M. Fang, J. W. Ziller, W. J. Evans, *Inorg. Chem.* **2015**, *54*, 801-807.

[89] W. J. Evans, M. Fang, J. E. Bates, F. Furche, J. W. Ziller, M. D. Kiesz, J. I. Zink, *Nat. Chem.* **2010**, *2*, 644-647.

[90] J. H. Farnaby, M. Fang, J. W. Ziller, W. J. Evans, *Inorg. Chem.* **2012**, *51*, 11168-11176.

[91] D. L. Perry, A. Zalkin, H. Ruben, D. H. Templeton, *Inorg. Chem.* **1982**, *21*, 237-240.

[92] D. A. Wrobleski, D. T. Cromer, J. V. Ortiz, T. B. Rauchfuss, R. R. Ryan, A. P. Sattelberger, *J. Am. Chem. Soc.* **1986**, *108*, 174-175.

[93] L. Ventelon, C. Lescop, T. Arliguie, M. Ephritikhine, P. C. Leverd, M. Lance, M. Nierlich, *Chem. Commun.* **1999**, 659-660.

[94] A. J. Gaunt, B. L. Scott, M. P. Neu, *Inorg. Chem.* **2006**, *45*, 7401-7407.

[95] W. Ren, G. Zi, D. C. Fang, M. D. Walter, *J. Am. Chem. Soc.* **2011**, *133*, 13183-13196.

[96] J. L. Brown, G. Wu, T. W. Hayton, *Organometallics* **2013**, *32*, 1193-1198.

[97] D. E. Smiles, G. Wu, T. W. Hayton, *Inorg. Chem.* **2014**, *53*, 12683-12685.

[98] P. L. Arnold, C. J. Stevens, N. L. Bell, R. M. Lord, J. M. Goldberg, G. S. Nichol, J. B. Love, *Chem. Sci.* **2017**, *8*, 3609-3617.

[99] S. Lange, T. Nilges, *Chem. Mater.* **2006**, *18*, 2538-2544.

[100] N. Zheng, X. Bu, P. Feng, *Nature* **2003**, *426*, 428-432.

[101] O. P. Lam, F. W. Heinemann, K. Meyer, *Chem. Sci.* **2011**, *2*, 1538-1547.

[102] H. Xu, K. M. Kleinke, T. Holgate, H. Zhang, Z. Su, T. M. Tritt, H. Kleinke, *J. Appl. Phys.* **2009**, *105*, 053703.

[103] N. D. Lowhorn, T. M. Tritt, E. E. Abbott, J. W. Kolis, *Appl. Phys. Lett* **2006**, *88*, 022101.

[104] K. I. M. Ingram, N. Kaltsoyannis, A. J. Gaunt, M. P. Neu, *J. Alloys Compd.* **2007**, *444-445*, 369-375.

[105] C. Madic, M. Lecomte, P. Baron, B. Boullis, *C. R. Phys.* **2002**, *3*, 797-811.

[106] S. R. Daly, J. M. Keith, E. R. Batista, K. S. Boland, D. L. Clark, S. A. Kozimor, R. L. Martin, *J. Am. Chem. Soc.* **2012**, *134*, 14408-14422.

[107] D. E. Smiles, G. Wu, P. Hrobárik, T. W. Hayton, *J. Am. Chem. Soc.* **2016**, *138*, 814-825.

[108] J. G. Brennan, R. A. Andersen, A. Zalkin, *Inorg. Chem.* **1986**, *25*, 1756-1760.

[109] L. R. Avens, D. M. Barnhart, C. J. Burns, S. D. McKee, W. H. Smith, *Inorg. Chem.* **1994**, *33*, 4245-4254.

[110] S. M. Franke, F. W. Heinemann, K. Meyer, *Chem. Sci.* **2014**, *5*, 942-950.

[111] L. P. Spencer, P. Yang, B. L. Scott, E. R. Batista, J. M. Boncella, *Inorg. Chem.* **2009**, *48*, 11615-11623.

[112] O. P. Lam, F. W. Heinemann, K. Meyer, *Angew. Chem., Int. Ed.* **2011**, *50*, 5965-5968.

[113] O. P. Lam, L. Castro, B. Kosog, F. W. Heinemann, L. Maron, K. Meyer, *Inorg. Chem.* **2012**, *51*, 781-783.

[114] C. Camp, O. Cooper, J. Andrez, J. Pécaut, M. Mazzanti, *Dalton Trans.* **2015**, *44*, 2650-2656.

[115] J. Andrez, J. Pécaut, R. Scopelliti, C. E. Kefalidis, L. Maron, M. W. Rosenzweig, K. Meyer, M. Mazzanti, *Chem. Sci.* **2016**, *7*, 5846-5856.

[116] E. M. Matson, W. P. Forrest, P. E. Fanwick, S. C. Bart, *J. Am. Chem. Soc.* **2011**, *133*, 4948-4954.

[117] D. Heitmann, C. Jones, D. P. Mills, A. Stasch, *Dalton Trans.* **2010**, *39*, 1877-1882.

[118] W. Ren, H. Song, G. Zi, M. D. Walter, *Dalton Trans.* **2012**, *41*, 5965-5973.

[119] J. L. Brown, S. Fortier, R. A. Lewis, G. Wu, T. W. Hayton, *J. Am. Chem. Soc.* **2012**, *134*, 15468-15475.

[120] D. E. Smiles, G. Wu, T. W. Hayton, *J. Am. Chem. Soc.* **2014**, *136*, 96-99.

[121] M. W. Rosenzweig, A. Scheurer, C. A. Lamsfus, F. W. Heinemann, L. Maron, J. Andrez, M. Mazzanti, K. Meyer, *Chem. Sci.* **2016**, *7*, 5857-5866.

[122] R. P. Kelly, M. Falcone, C. A. Lamsfus, R. Scopelliti, L. Maron, K. Meyer, M. Mazzanti, *Chem. Sci.* **2017**, *8*, 5319-5328.

[123] T. W. Hayton, *Dalton Trans.* **2010**, *39*, 1145-1158.

[124] M. B. Jones, A. J. Gaunt, *Chem. Rev.* **2013**, *113*, 1137-1198.

[125] H.S. La Pierre, K. Meyer, Prog. Inorg Chem. **2014**, *58*, 303–416.

[126] M. Cesari, U. Pedretti, Z. Zazzetta, g. Lugli, W. Marconi, *Inorg. Chim. Acta* **1971**, *5*, 439-444.

[127] F. A. Cotton, W. Schwotzer, *Organometallics* **1987**, *6*, 1275-1280.

[128] D. Baudry, E. Bulot, P. Charpin, M. Ephritikhine, M. Lance, M. Nierlich, J. Vigner, *J. Organomet. Chem.* **1989**, *371*, 155-162.

[129] W. J. Evans, S. A. Kozimor, J. W. Ziller, N. Kaltsoyannis, *J. Am. Chem. Soc.* **2004**, *126*, 14533-14547.

[130] D. P. Mills, F. Moro, J. McMaster, J. van Slageren, W. Lewis, A. J. Blake, S. T. Liddle, *Nat. Chem.* **2011**, *3*, 454-460.

[131] M. J. Monreal, S. I. Khan, J. L. Kiplinger, P. L. Diaconescu, *Chem. Commun.* **2011**, *47*, 9119-9121.

[132] D. Patel, F. Moro, J. McMaster, W. Lewis, A. J. Blake, S. T. Liddle, *Angew. Chem. Int. Ed.* **2011**, *50*, 10388-10392.

[133] P. L. Diaconescu, C. C. Cummins, *Inorg. Chem.* **2012**, *51*, 2902-2916.

[134] B. Vlaisavljevich, P. L. Diaconescu, W. L. Lukens, L. Gagliardi, C. C. Cummins, *Organometallics* **2013**, *32*, 1341-1352.

[135] A. J. Wooles, W. Lewis, A. J. Blake, S. T. Liddle, *Organometallics* **2013**, *32*, 5058-5070.

[136] D. Patel, F. Tuna, E. J. L. McInnes, J. McMaster, W. Lewis, A. J. Blake, S. T. Liddle, *Dalton Trans.* **2013**, *42*, 5224-5227.

[137] A. W. Duff, K. Jonas, R. Goddard, H. J. Kraus, C. Krueger, *J. Am. Chem. Soc.* **1983**, *105*, 5479-5480.

[138] W. M. Lamanna, W. B. Gleason, D. Britton, *Organometallics* **1987**, *6*, 1583-1584.

[139] F. A. Cotton, P. A. Kibala, W. A. Wojtczak, *J. Am. Chem. Soc.* **1991**, *113*, 1462-1463.

[140] Y. C. Tsai, P. Y. Wang, S. A. Chen, J. M. Chen, *J. Am. Chem. Soc.* **2007**, *129*, 8066-8067.

[141] Y. C. Tsai, P. Y. Wang, K. M. Lin, S. A. Chen, J. M. Chen, *Chem. Commun.* **2008**, 205-207.

[142] T. Watanabe, Y. Ishida, T. Matsuo, H. Kawaguchi, *Dalton Trans.* **2010**, *39*, 484-491.

[143] M. C. Cassani, D. J. Duncalf, M. F. Lappert, *J. Am. Chem. Soc.* **1998**, *120*, 12958-12959.

[144] Y. K. Gun'ko, P. B. Hitchcock, M. F. Lappert, *Organometallics* **2000**, *19*, 2832-2834.

[145] C. M. Kotyk, M. E. Fieser, C. T. Palumbo, J. W. Ziller, L. E. Darago, J. R. Long, F. Furche, W. J. Evans, *Chem. Sci.* **2015**, *6*, 7267-7273.

[146] C. T. Palumbo, L. E. Darago, M. T. Dumas, J. W. Ziller, J. R. Long, W. J. Evans, *Organometallics* **2018**, *37*, 3322-3331.

[147] C. Camp, V. Mougel, J. Pécaut, L. Maron, M. Mazzanti, *Chem. – Eur. J.* **2013**, *19*, 17528-17540.

[148] P. Roussel, P. Scott, *J. Am. Chem. Soc.* **1998**, *120*, 1070-1071.

[149] A. L. Odom, P. L. Arnold, C. C. Cummins, *J. Am. Chem. Soc.* **1998**, *120*, 5836-5837.

[150] W. J. Evans, S. A. Kozimor, J. W. Ziller, *J. Am. Chem. Soc.* **2003**, *125*, 14264-14265.

[151] F. G. N. Cloke, P. B. Hitchcock, *J. Am. Chem. Soc.* **2002**, *124*, 9352-9353.

[152] M. Falcone, L. Chatelain, R. Scopelliti, I. Živković, M. Mazzanti, *Nature* **2017**, *547*, 332-335.

# Chapter 3 : Mesityl-boroxide complexes of $U^{III}$ and $Y^{III}$

As discussed in Chapter 2, the use of boroxides differs from more common aryloxide ligand, as the addition of an electron-accepting atom into the ligand environment creates a more electron-deficient ligand, thereby modifying the electronic properties. An extra effect is the shift of the R groups away from the metal centre, creating more space for further reactivity. Moreover, the effect we wanted to investigate was if the addition of another Lewis acid into the complex would modify the reactivity towards small molecules, as there is another possible reactive site in the molecule.

This chapter describes an optimised route for the synthesis of a uranium(III) mesityl boroxide complex, its characterisation and reactivity studies towards small molecules. Two different yttrium boroxide complexes were synthesised and their reactivity towards small molecules was examined.

## $U^{III}$ boroxide complexes

Uranium(III) is known to be able to insert and activate a wide range of small molecules.[1-3] Different types of ligands have been previously described. In Chapter 2, aryloxide and siloxide ligands are reviewed. In the following section, the synthesis and reactivity of the $U^{III}$ boroxide complex $[U(OBMes_2)_2(\mu\text{-}OBMes_2)]_2$ is described.

## 3.1. Synthesis and characterisation of $[U(OBMes_2)_2(\mu\text{-}OBMes_2)]_2$ (1)

Toluene was added to a mixture of $HOBMes_2$ and $[U(N(SiMe_3)_2)_3]$ to yield a purple solution which was allowed to stir at room temperature for 4 hours. $[U(OBMes_2)_2(\mu\text{-}OBMes_2)]_2$ (**1**) was obtained as a dark purple solid after removal of the solvent under reduced pressure, followed by washing and recrystallisation from hexane (Scheme 3.1). Complex **1** was characterised by $^{1}H$ and $^{11}B$ NMR spectroscopies, APPI mass spectrometry, elemental analysis and single crystal XRD analysis.

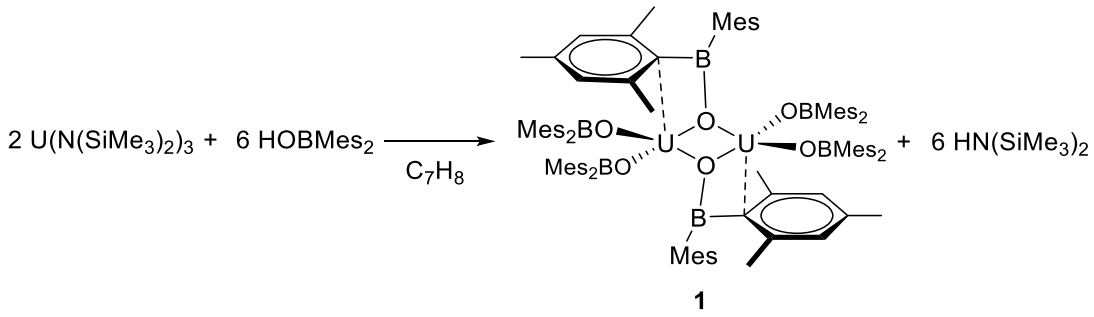


**1**

Scheme 3.1. Synthesis of $U^{III}$ boroxide complex **1**.

The $^{1}$H NMR spectrum of **1** contains paramagnetically shifted resonances from 8 to -15 ppm. The resonances corresponding to the bridging ligands are more shifted (from -3.7 to -15 ppm) due to their closer proximity to the uranium centres, whereas the resonances corresponding to the terminal ligands fall between 8.3 to 2.5 ppm (Figure 3.1). The $^{11}$B NMR spectrum contains two resonances at 51 and 74 ppm corresponding to the two boron environments.

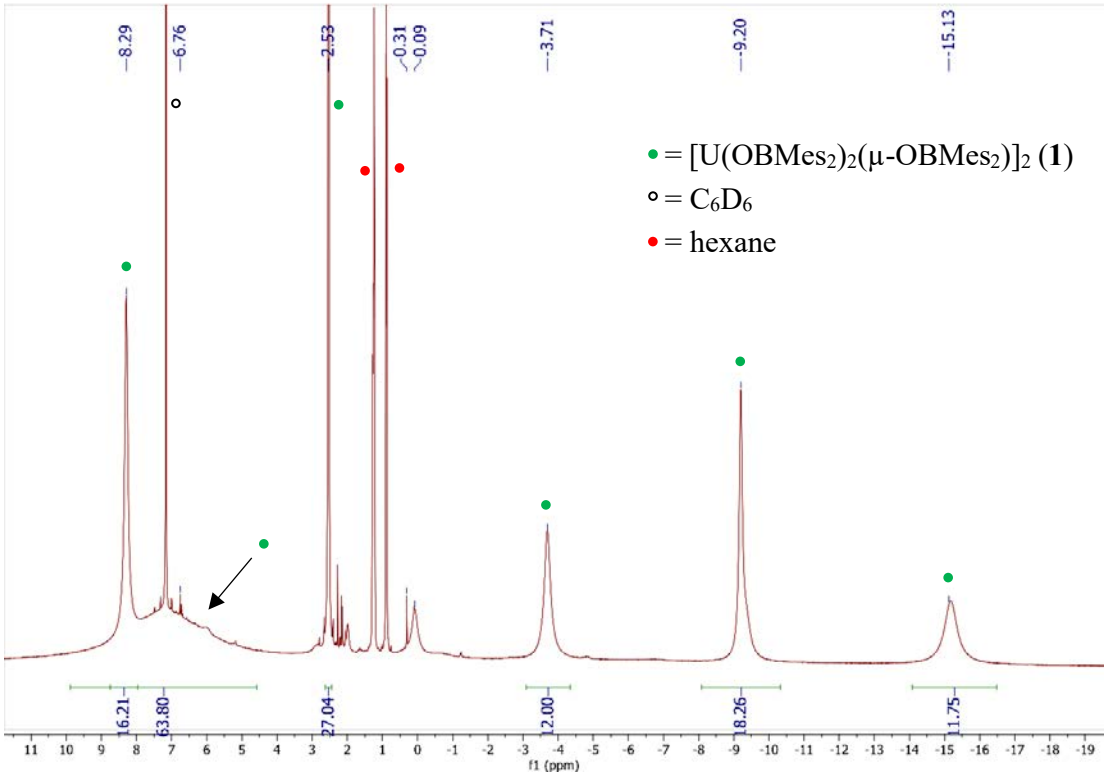


Figure 3.1. $^{1}$H NMR spectrum (298 K, $C_6D_6$, 500 MHz) of complex $[U(OBMes_2)_2(\mu\text{-}OBMes_2)]_2$ **1**.

Mass spectrometric analysis showed the molecular ion at m/z = 1033.56, which corresponds to the $[M]^{+\bullet}$ fragment $[U(OBMes_2)_3]^{+\bullet}$.

Dark purple crystals of **1** suitable for single crystal XRD analysis were obtained from storage of a concentrated hexane solution of **1** at -30 °C for 24 hours.

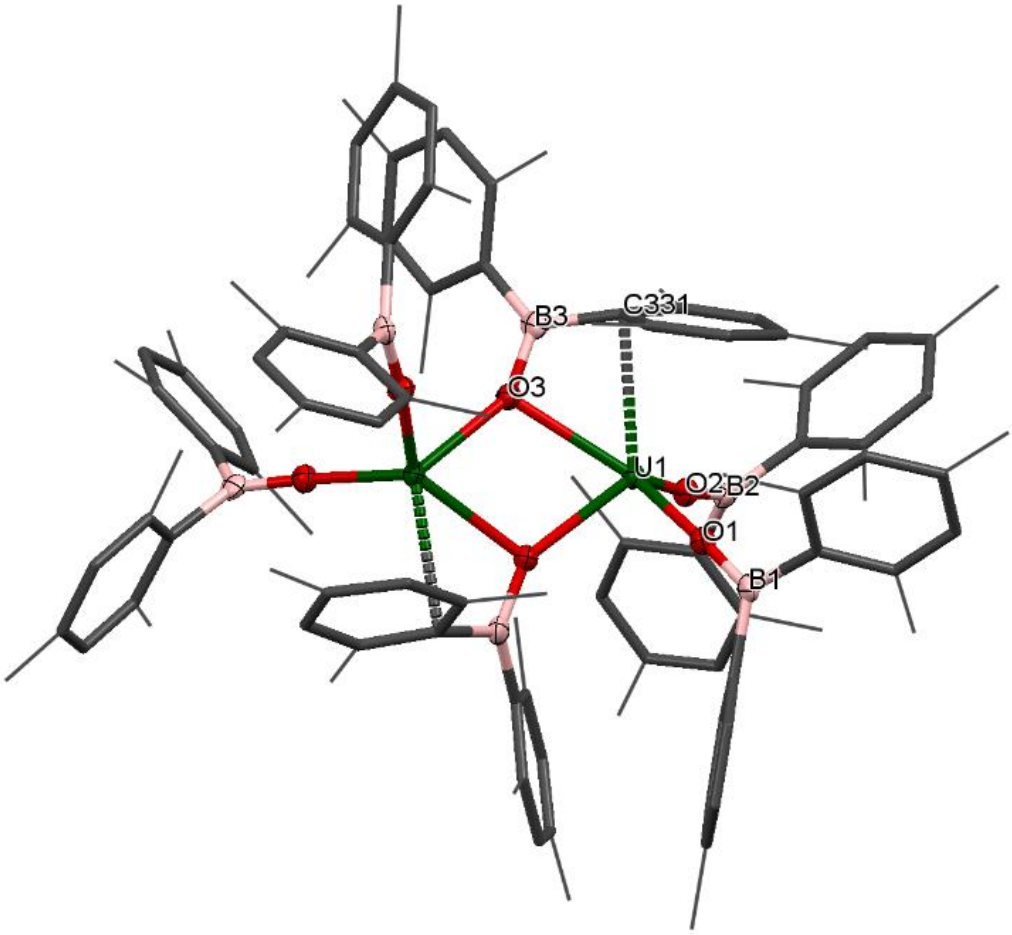


Figure 3.2. Solid-state structure of **1**. The mesityl groups are depicted as wireframe and capped sticks for clarity. The hydrogen atoms are omitted. The thermal ellipsoids are displayed at 50% probability.

The solid-state structure of **1** confirms the formation of a centrosymmetric dinuclear $U^{III}$ complex in which the two uranium centres are bridged by two boroxide ligands (Figure 3.2) in a distorted trigonal bipyramid geometry due to the interaction of the uranium centres with the bridging mesityl groups. The U···C distances for these interactions (U···$C_{avg}$ 2.845 Å) are slightly longer than other $\eta^1$ interactions with uranium, such as the complexes bearing the ligand {1,3[2,5-($^i$Pr)$_2$PhNC(=CH$_2$)]C$_6$H$_4$} reported by Gambarotta and co-workers (Figure 3.3).[4]

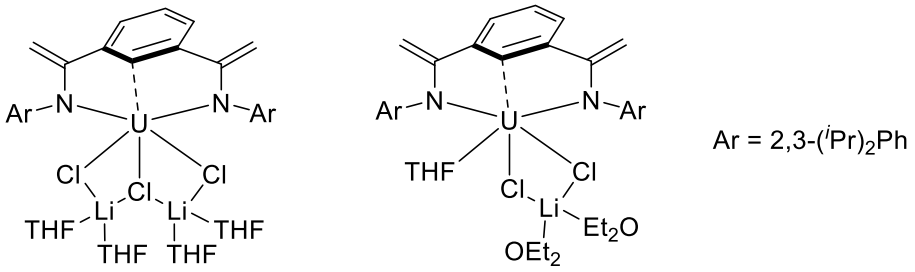


Figure 3.3. $\eta^1$ U···C interactions of complexes bearing the ligand {1,3[2,5-($^i$Pr)$_2$PhNC(=CH$_2$)]C$_6$H$_4$} reported by Gambarotta and co-workers.[4]

The U–O bond lengths for the boroxide ligands are 2.548(10) Å and 2.372(10) Å for the bridging boroxides, and an average U–$O_{avg}$ bond length of 2.196 Å for the terminal boroxides. Both are in the same range as the U–O distances for the siloxide-bridged $U^{III}$ dimer reported by Mazzanti and co-workers, $[U(OSi(O^tBu)_3)_2(\mu\text{-}OSi(O^tBu)_3)]_2$, which features two $U^{III}$ centres with two bridging and two terminal siloxide ligands with U–O distances of 2.549(3) Å and 2.396(3) Å for the bridging siloxides, and a U–$O_{avg}$ of 2.193(4) Å for the terminal ligands. Moreover, the U···U distance for complex **1** is 3.966 Å, which is similar to the $U^{III}$ siloxide complex (U···U 3.9862(2) Å).[5] The U–$O_{avg}$ distance for the terminal ligands is similar to that of $[U(OBTrip)_3]$ (Trip = triisoporpylphenyl) (mean 2.183(7) Å), which was previously prepared by the former group member Dr. Jordann Wells,[6] and slightly longer than that of the uranium tris(aryloxide) complex $[U(ODtbp)_3]$, with U–$O_{avg}$ = 2.159 Å.[1] Together, the nearly linear U–O–B angle for the terminal boroxide ligands (mean 171.6°) and the elongation of the U–O bonds are a direct consequence of the reduced π-donor ability of the ligand compared with a carbocyclic aryloxide, which is decreased by having a boron substituent on the ligand. Electron density from the oxygen is accepted by the boron, leading to a lower degree of π-donation from the boroxide to the uranium centre.

## 3.2. Reactivity of $[U(OBMes_2)_2(\mu\text{-}OBMes_2)]_2$ (1)

Compound **1** was treated with a wide range of small molecules and other reactants (Scheme 3.2). From reductants such as $KC_8$ to typically inert CO and $CO_2$ gases. The most interesting reactions are the formation of different inverse arene sandwich complexes upon treatment with phosphines.

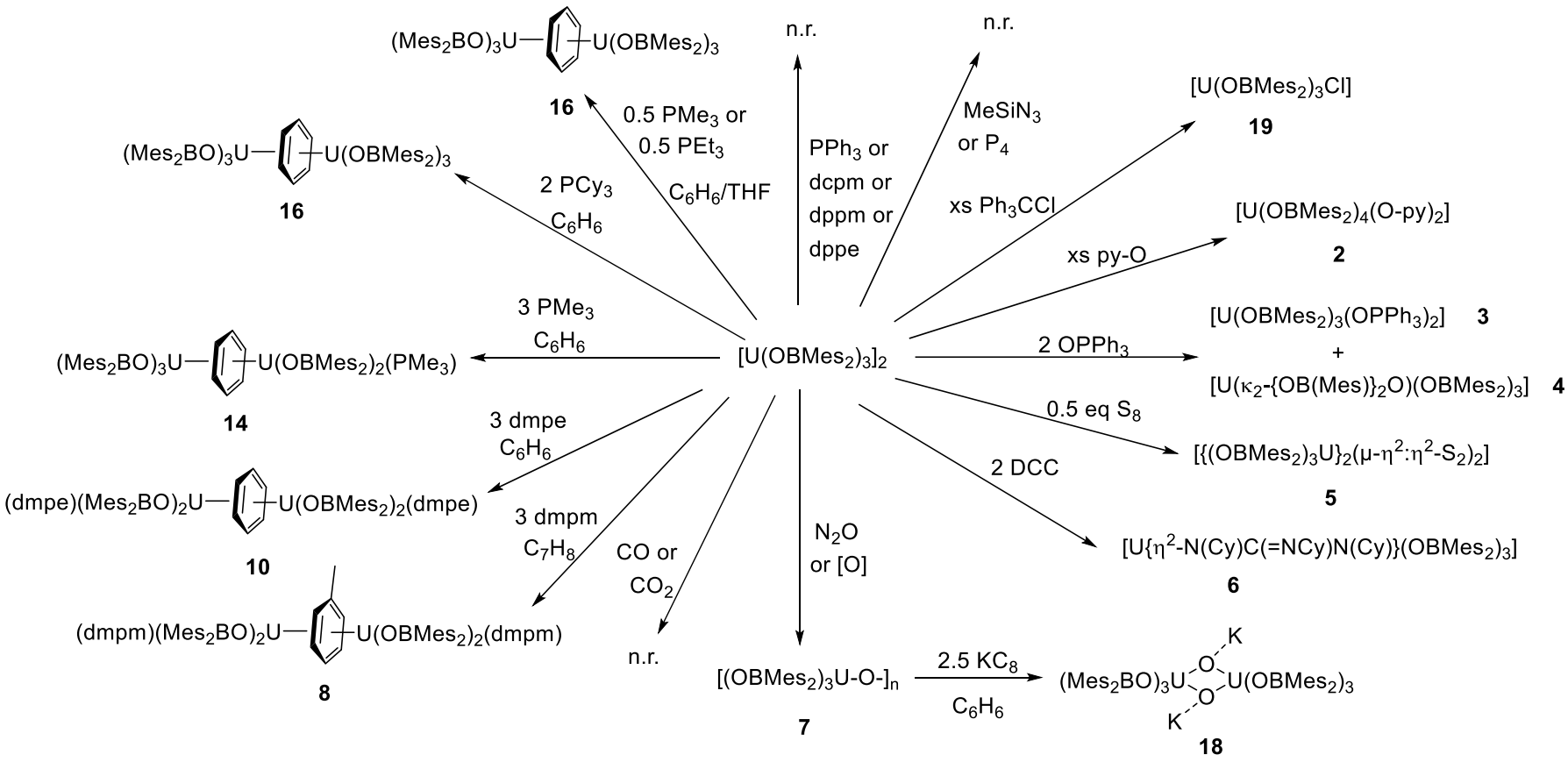


Scheme 3.2. Reactivity of complex **1**.

### 3.2.1. Reaction with pyridine N-oxide

The formation of oxo complexes with structures such as $UL_n{=}O$,[7-9] $L_nU{\equiv}O$[10, 11] or U–O–U[12] by reaction with py-O have been previously reported. However, addition of benzene to a mixture of $[U(OBMes_2)_2(\mu\text{-}OBMes_2)]_2$ (**1**) with an excess of pyridine N-oxide provided a brown solution from which $[U(OBMes_2)_4(py\text{-}O)_2]$ (**2**) was isolated as dark orange crystals after 72 hours. Coordination of pyridine N-oxide to metal complexes is not unique, although there are only a few examples.[11, 13-16]

$$[U(OBMes_2)_3]_2 \xrightarrow[\text{- } U_{(0)}\text{, -2 "(OBMes}_2)^-\text{"}]{\text{xs py-O, } C_6D_6} [U(OBMes_2)_4(O\text{-}py)_2]$$

**2**

Scheme 3.3. Synthesis of complex **2**. The elimination of $(OBMes_2)^-$ was assumed for charge balance, but was not looked for in the product mixture.

The identity of complex **2** was confirmed by $^1H$ and $^{11}B$ NMR spectroscopies, APPI mass spectrometry and single crystal XRD analysis. Mass spectrometric data showed the expected molecular ion at m/z = 1223.65, which corresponds to the $[M]^{+\bullet}$ fragment, $[U(OBMes_2)_4(Py\text{-}O)_2]^{+\bullet}$.

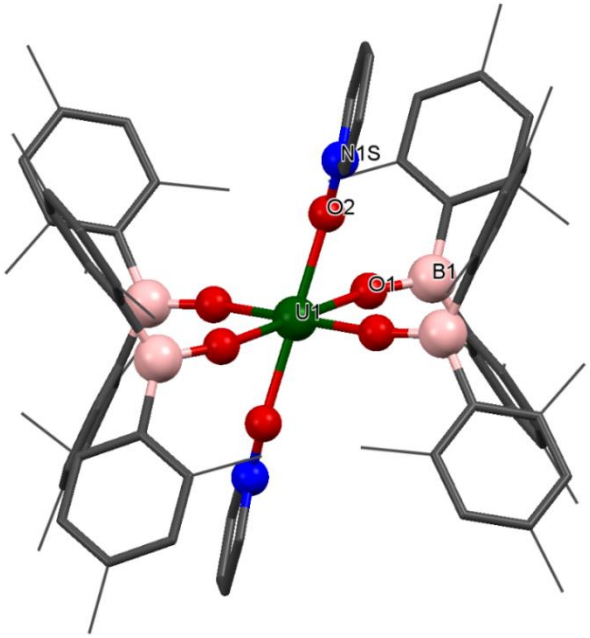


Figure 3.4. Solid-state structure of **2**. Hydrogens atoms are omitted and mesityl groups and pyridine oxide ligands are depicted as wireframe and capped sticks for clarity.

Dark orange crystals suitable for XRD analysis were grown from a concentrated benzene solution. The data are only of sufficient quality to discuss connectivity information but not for bond metrics. The solid-state structure reveals a $U^{IV}$ complex with a distorted octahedral geometry with the boroxide ligands in the equatorial positions and the pyridine N-oxide ligands in the axial positions.

### 3.2.2. Reaction with triphenylphosphine oxide

Phosphine oxides are widely used ligands in f-element chemistry. As a result of the oxophilic and Lewis acidic character of lanthanides and actinides, phosphine oxides coordinate readily, and they are able to stabilise a variety of complexes in low and high oxidation states. [17-22] Moreover, applications in catalysis and liquid-liquid extraction processes have been found.[23] Therefore, the reaction of the uranium boroxide complex **1** with $OPPh_3$ was investigated (Scheme 3.4)

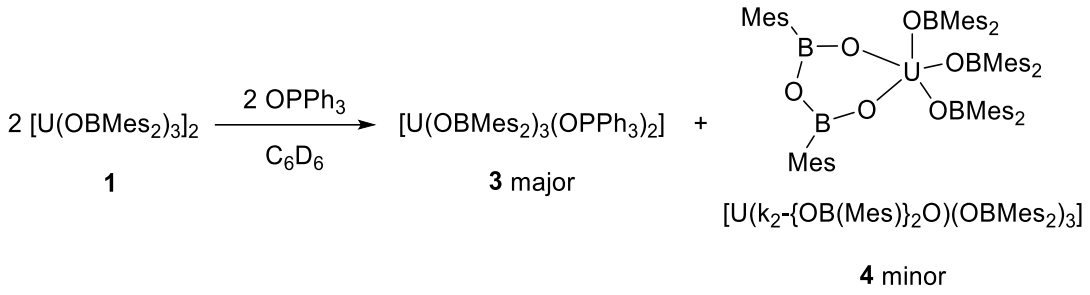


Scheme 3.4. Synthesis of compounds **3** and **4**.

Addition of two equivalents of $OPPh_3$ to a solution of **1** leads to the formation of $[U(OBMes_2)_3(OPPh_3)_2]$ (**3**), which co-crystallised together with $[U(k_2\text{-}\{OB(Mes)\}_2O)(OBMes_2)_3]$ (**4**). The $^1H$ NMR spectrum of **3** in $C_6D_6$ contains six resonances which range from 6.9 to 1.9 ppm. The $^{11}B$ NMR spectrum shows a single broad resonance at 56 ppm, and the $^{31}P$ NMR spectrum shows a single broad resonance at -18 ppm, and this is significantly shifted from the free $OPPh_3$ resonance (~25 ppm) as a result of its proximity to the metal centre. Mass spectrometric analysis (APPI-MS) showed a molecular ion peak at m/z = 1589.77 that corresponds to fragment $[\mathbf{3}]^{+\bullet}$.

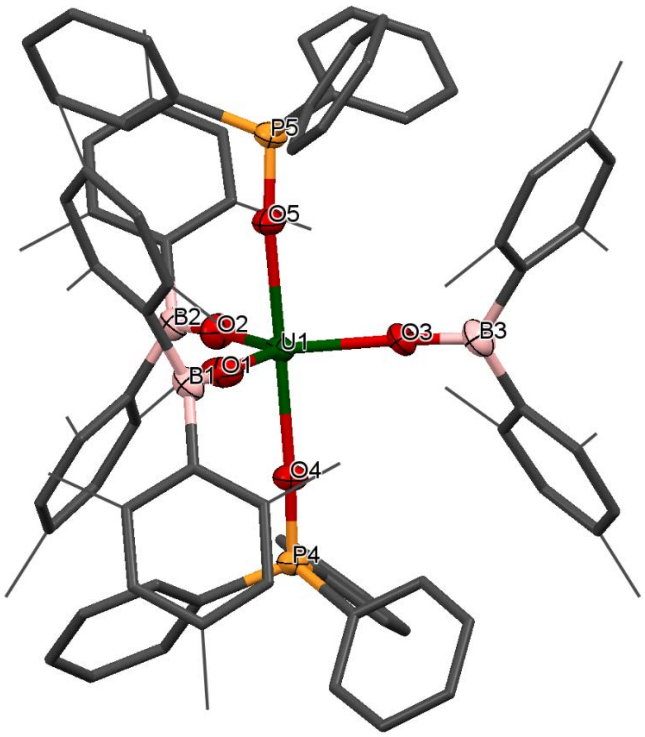


Figure 3.5. Solid-state structure of **3**. Mesityl and phenyl groups are depicted as capped sticks and wireframe for clarity. Hydrogen atoms are omitted. The thermal ellipsoids are displayed at 50% probability.

Single crystals of **3** and **4** were obtained by slow diffusion of hexanes into a benzene solution. Complex **3** has an approximately trigonal bipyramidal coordination geometry (Figure 3.5). The U–$OPPh_3$ bond lengths are 2.273(4) Å and 2.270(4) Å, which are ~0.1 Å shorter than other $U^{III}$–$OPPh_3$ distances previously reported.[17, 24] The U–O–P angles for the phosphine oxide ligands are 170.4(3)° and 174.4(2)° respectively, and the $O_4$–U–$O_5$ angle is 176.62(13)°. These angles are similar to the angles in the known complex $[U(NPhAr^F)_3(OPPh_3)_2]$ ($Ar^F$ = 3,5-bis(trifluoromethyl)phenyl).[24] The $U–O_{avg}$ distance for the boroxide ligands is 2.124 Å, which is ~0.07 Å shorter than the U–O bond lengths for the terminal boroxides in **1** (mean 2.196 Å). Moreover, the mean U–O–B angle is 176.0°, and this is closer to linearity than the terminal boroxide in **1** (mean 171.6°). This might be due to the trigonal bypiramidal geometry which allows for a greater delocalisation of the electron density in the ligand, thus flattening the U–O–B angle.

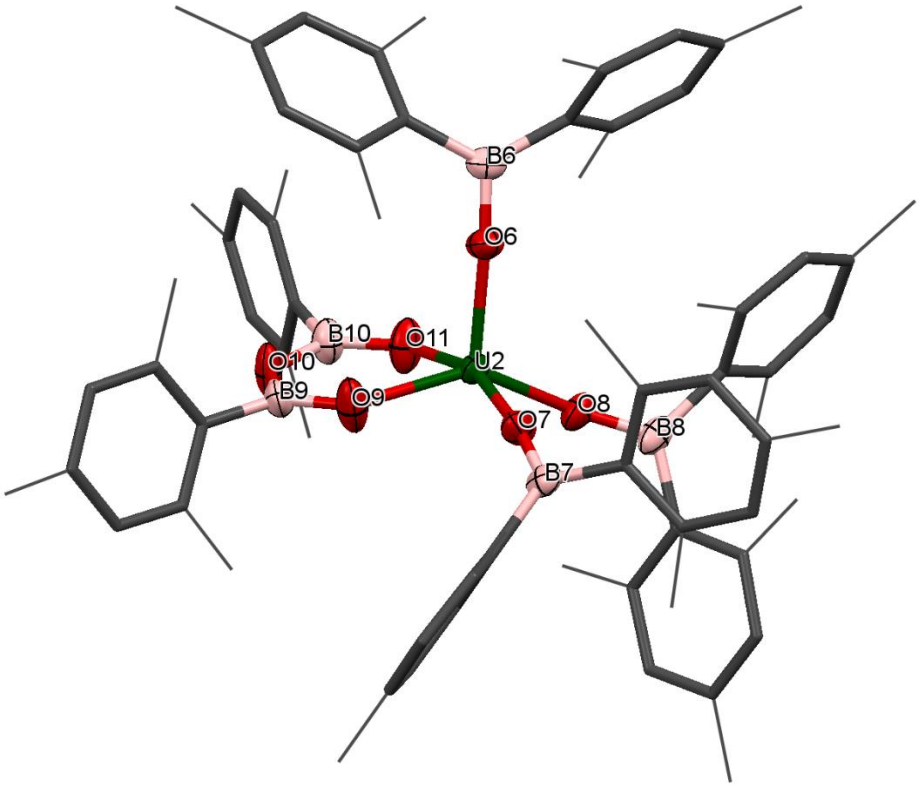


Figure 3.6. Solid-state structure of **4**. The mesityl groups are depicted as wireframe and capped sticks for clarity. Hydrogen atoms are omitted. The thermal ellipsoids are displayed at 50% probability.

Complex **4** has a nearly square pyramidal coordination geometry and contains a coordinated boroxine ligand, cyclic anhydride of borinic acid, which is formally a product of ligand condensation, but probably formed from a contaminant in the ligand. Boroxines are rigid bidentate ligands which have drawn attention recently, mostly by forming complexes of main group elements, e.g. for Al;[25-27] Sn, Sb and Bi;[28-34] but also for transition metals such as Mn,[35] Au[36, 37] and Pt.[38] For the boroxine ligand, the U–O bond distances are 2.193(4) Å and 2.191(4) Å, and these are much longer (~0.2 Å) than those in any previously reported boroxine complex. The B–O distances range from 1.342(9)–1.370(9) Å, which are in the same range as previously reported for main group boroxines. The six-membered ring unit has internal angles close to 120°, except for the $O_9$–U–$O_{11}$ bond which is much smaller, being only 77.40(16)°. The boroxide ligands have similar U–O bond lengths (U–$O_{avg}$ 2.172 Å) to the terminal boroxides in **1** (mean 2.196 Å). Finally, the U–O–B angles for the boroxides range from 155.2(4)° to 168.7(4)°, which are

significantly more bent than for the terminal boroxides in **1** (mean 171.6°). These parameters suggest a formal oxidation state of +V for the uranium centre.

### 3.2.3. Reaction with elemental sulfur

As mentioned in Chapter 2, the reactivity of chalcogens and chalcogenides with actinide complexes has gained attention recently. Of particular interest is the potential of the metal–ligand bonding in these more polarisable systems to advance our understanding of the degree of covalency in uranium–ligand bonds, as this can provide insights into better separation of actinides from lanthanides in spent nuclear fuel.[39-42]

The synthesis of a tetrasulfide-bridged complex from elemental sulfur and the uranium boroxide complex **1** was achieved. Addition of 0.5 equivalents of $S_8$ to a stirred solution of $[U(OBMes_2)_2(\mu\text{-}OBMes_2)]_2$ (**1**) leads to the formation of $[\{(OBMes_2)_3U\}_2(\mu\text{-}\eta^2\text{:}\eta^2\text{-}S_2)_2]$ (**5**), which contains two independent bridging $S_2$ units. Although several complexes bearing $U–S_2$ bridging ligands have been reported, there is only one other example in the literature of a uranium complex featuring two bridging $S_2$ units, $[\{((^{Ad}ArO)_3N)U\}_2(\mu\text{-}\eta^2\text{:}\eta^2\text{-}S_2)_2]$ (Figure 3.8) and it was reported by Meyer and co-workers.[43]

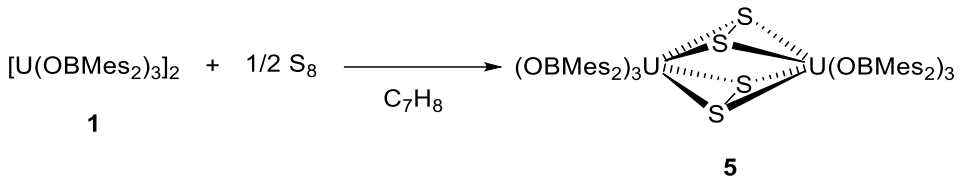


Scheme 3.5. Synthesis of sulfur bridged complex **5**.

The $^1H$ NMR spectrum contains the expected resonances corresponding to the $OBMes_2$ ligand, and the $^{11}B$ NMR spectrum shows one resonance at 50 ppm, indicating one ligand environment. Mass spectrometric analysis showed the molecular ion at m/z =1033.56 that corresponds to the $[M]^{+\bullet}$ fragment, $[\{(OBMes_2)_3U\}(\mu\text{-}\eta^2\text{:}\eta^2\text{-}S_2)]^{+\bullet}$. Translucent red crystals of the sulfur-bridged complex **5** suitable for XRD analysis were grown from a concentrated toluene solution.

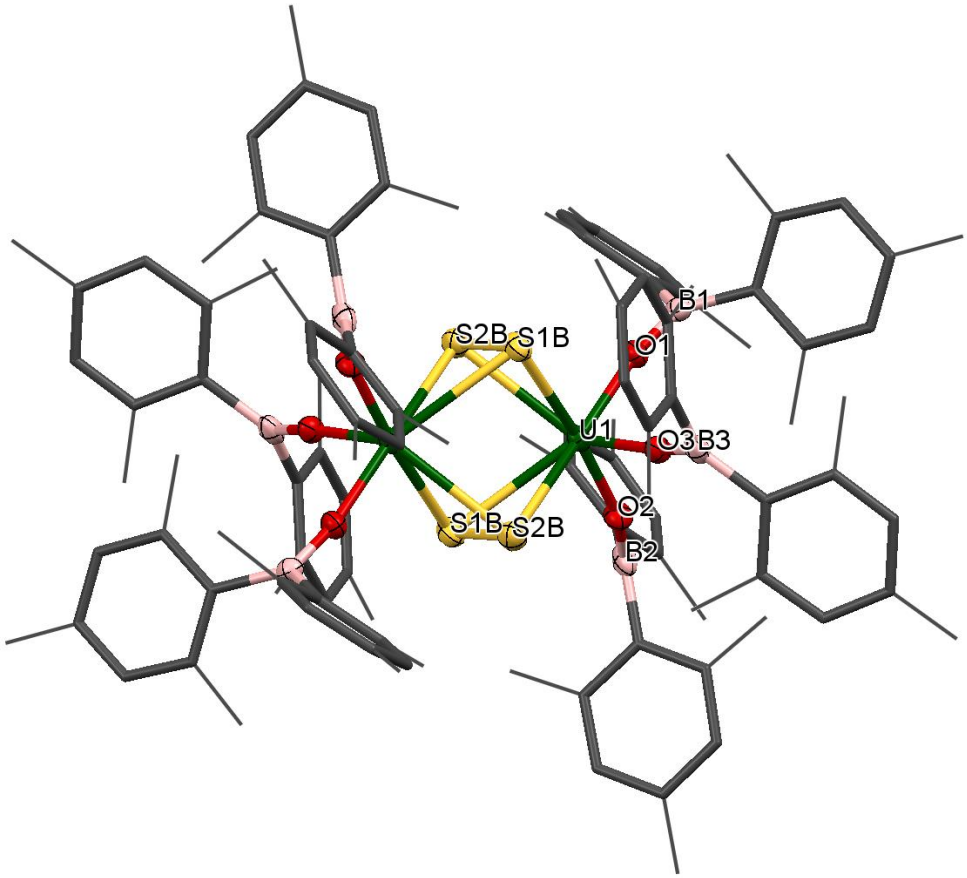


Figure 3.7. Solid-state structure of **5**. The mesityl groups are depicted as wireframe and capped sticks for clarity. Hydrogen atoms are omitted. The thermal ellipsoids are displayed at 50% probability.

Figure 3.7 shows the molecular structure of **5**, confirming the formation of a uranium dimer with two $S_2$ units. Each uranium ion has a distorted pentagonal bipyramidal coordination geometry. The $S_{1B}$–$S_{2B}$ bond length is 2.050(2) Å, which is a typical value for a S–S single bond, and comparable to $H_2S_2$ with a S–S bond length of 2.055 Å.[44] The S···S distance between the two units is 3.491 Å, excluding the possibility of a $S_4^{2-}$ unit.

The ligands are both identified as bridging persulfido $S_2^{2-}$, giving a formal $U^V$ oxidation state for complex **5** by comparison of the U–E bonds. Previously reported uranium persulfido $S_2^{2-}$ complexes show S–S distances from 2.050 Å to 2.103 Å.[45-53] Previously reported transition metal complexes bearing supersulfido $S_2^-$ units range from 1.944 to 2.023 Å.[54-57] Furthermore, the U–$O_{avg}$ bond length is 2.078 Å, which is significantly shorter than the U–O bond lengths for the terminal boroxides in $[U(OBMes_2)_2(\mu\text{-}OBMes_2)]_2$ (**1**) (mean 2.196 Å) and in $U^{IV}$ complex $[U(OBMes_2)_4]$ (**17**)

(mean 2.119 Å), also suggesting a formal oxidation state of +V is most likely. The U–O–B angle is 165(3)°, which is more bent than for the terminal boroxide ligands (mean 171.6°), which is reasonable if more electron density from the O atoms are being distributed into a backdonation from the uranium centres to the sulfido ligands.

Table 1 shows selected bond metrics for compounds $[\{(OBMes_2)_3U\}_2(\mu\text{-}\eta^2\text{:}\eta^2\text{-}S_2)_2]$ **5** and $[\{((^{Ad}ArO)_3N)U\}_2(\mu\text{-}\eta^2\text{:}\eta^2\text{-}S_2)_2]$ (Figure 3.8).[43]

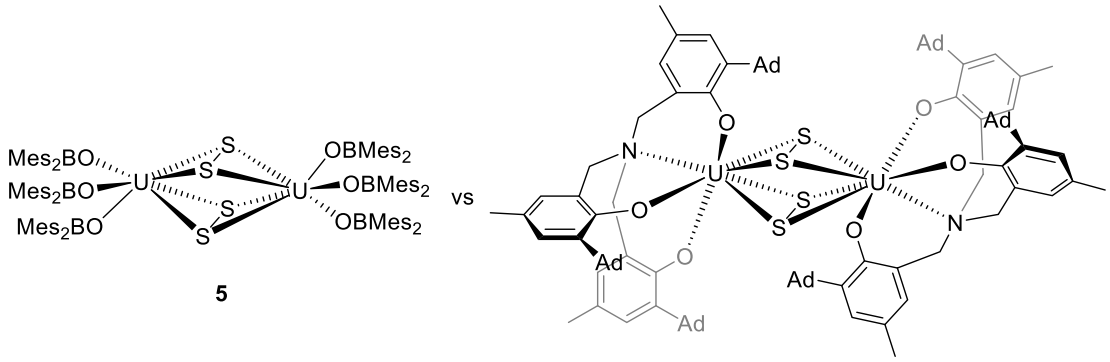


Figure 3.8. Comparison of complexes bearing two independent bridging $S_2$ units, **5** vs $[\{((^{Ad}ArO)_3N)U\}_2(\mu\text{-}\eta^2\text{:}\eta^2\text{-}S_2)_2]$.[43]

Table 1. Selected bond distances (Å) for sulfur bridging complexes $[\{(OBMes_2)_3U\}_2(\mu\text{-}\eta^2\text{:}\eta^2\text{-}S_2)_2]$ (**5**) and $[\{((^{Ad}ArO)_3N)U\}_2(\mu\text{-}\eta^2\text{:}\eta^2\text{-}S_2)_2]$.[43]

| Structural parameters | $[\{(OBMes_2)_3U\}_2(\mu\text{-}\eta^2\text{:}\eta^2\text{-}S_2)_2]$ (**5**) (Å) | $[\{((^{Ad}ArO)_3N)U\}_2(\mu\text{-}\eta^2\text{:}\eta^2\text{-}S_2)_2]$ (Å) |
|---|---|---|
| $U_1–S_{1B}$ | 2.9189(14), 2.9189(14) | 2.741(2), 3.020(2), 2.809(2), 2.767(2) |
| $U_1–S_{2B}$ | 2.7412(13), 2.8601(14) | 2.858(2), 2.763(2), 2.766(2), 2.924(2) |
| S–S | 2.050(2) | 2.050(2), 2.053(2) |
| U–O | 2.082(3), 2.075(3), 2.077(3) | 2.104, 2.106 |
| U···U | 3.8999(4) | 3.8164(3) |

### 3.2.4. Reaction with DCC

The direct reaction of carbodiimides with uranium was first reported by Evans and co-workers in 2009.[58] The aim of these reactions was to insert the carbodiimides into a U–C ligand bond in order to change the steric crowding in organouranium complexes. The simple addition of these carbodiimides can lead to ligands with more donor atoms and greater steric bulk. Since then, several examples of insertion of carbodiimides into metal–ligand σ-bonds have been reported,[59-62] as well as further reactivity towards small molecules with these ligands.[63-65] Moreover, reactions of carbodiimides have also led to the formation of metallacycles, which have been extensively studied by Zi and co-workers.[66-69] These metallacycles are of importance because of their unique structural properties and possible applications in catalysis.

Dropwise addition of a toluene solution of DCC (*N*,*N*′-Dicyclohexylcarbodiimide) to a dark purple toluene solution of **1** produced a green solution which was stirred overnight. The solution was then filtered and evaporated to dryness. The formation of $[U\{\eta^2\text{-}N(Cy)C(=NCy)N(Cy)\}(OBMes_2)_3]$ (**6**, Cy = *cyclo*-$C_6H_{11}$) (Scheme 3.6) was confirmed by $^1H$ and $^{11}B$ NMR spectroscopies. Mass spectroscopic analysis confirmed the formation of complex **6** as the molecular ion at m/z = 1337.85, that corresponds to $[M + H]^+$, was observed. Despite our best efforts, single crystals for XRD characterisation could not be obtained.

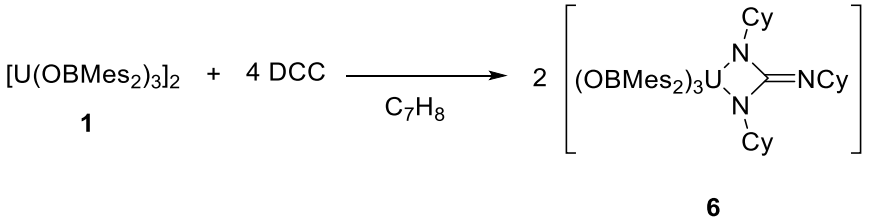


Scheme 3.6. Synthesis of complex **6**.

The $^1H$ NMR spectrum of **6** has resonances from 58 to -11 ppm, widely shifted out of the diamagnetic region by proximity to the paramagnetic uranium centre. Taken together, the characterising data show that the carbodiimide has been coupled by the reducing U centre to form the rearranged cyclohexyl-substituted guanidinate ligand via loss of *cyclo*-hexylisonitrile. This presumably occurs similarly to the procedure reported by Zi and co-workers, for the reaction that converts $[U(\eta\text{-}C_5Me_5)_2(\eta^2\text{-bpy})]$ to

$[U(\eta\text{-}C_5Me_5)_2\{\eta^2\text{-}N(Cy)C(=NCy)N(Cy)\}]$ via extrusion of CyNC from a coordinated DCC ligand then a [2+2] addition to the transiently formed U=NCy group (Scheme 3.7).[66] The fact that this forms from the $U^{IV}$ product again supports the stabilising effect of this ligand on the higher formal oxidation states of uranium.

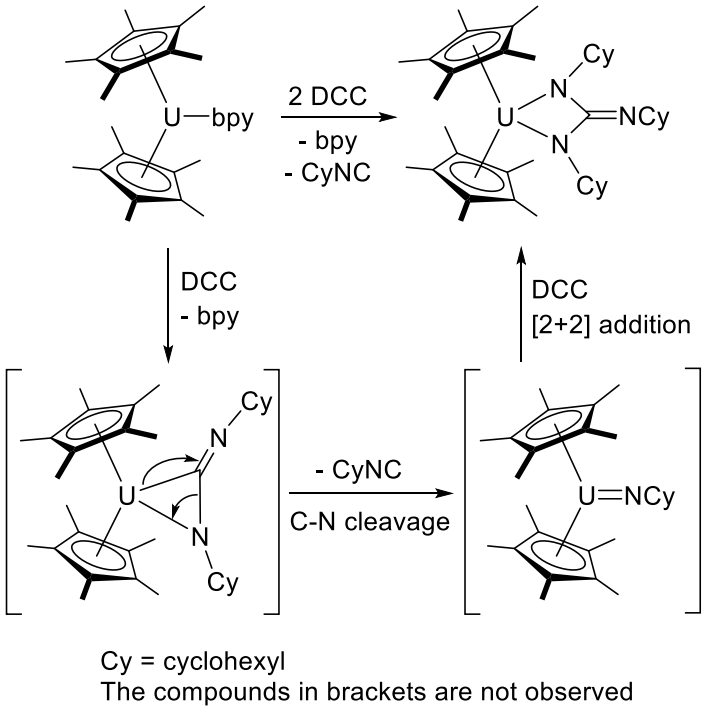


Scheme 3.7. Proposed mechanism for the formation of $[U(\eta\text{-}C_5Me_5)_2\{\eta^2\text{-}N(Cy)C(=NCy)N(Cy)\}]$ by Zi and co-workers.[66]

## 3.2.5. Reaction with gases

Organometallic uranium(III) complexes have been shown to effect reductive transformations of small unsaturated gaseous molecules such as CO, $CO_2$, $N_2O$ and even $N_2$.[1, 70-74]

### 3.2.5.1. Reaction with $N_2O$

Upon exposure of a benzene solution of complex **1** to one atmosphere of $N_2O$, a rapid colour change from dark purple to light brown was observed due to the formation of a bridging oxo complex, $[U(OBMes_2)_3\text{-}O\text{-}]_n$ (**7**), as seen in Scheme 3.8.

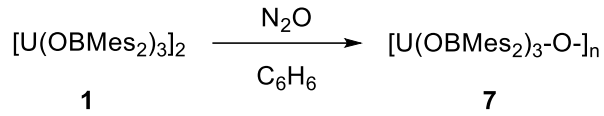


**1** **7**

Scheme 3.8. Formation of oxo complex **7**.

The $^{1}H$ and $^{13}C$ NMR spectra show resonances corresponding to one mesityl environment, which is slightly shifted due to paramagnetic contributions. The $^{11}B$ NMR spectrum contains one resonance at 89 ppm, which confirms the presence of only one boron environment. The elemental analysis result is in agreement with the formation of complex **7**.

Complex **1** is extremely sensitive to the presence of oxygen, rapidly forming complex **7** when is stored as a solution or when solutions are heated, due to reaction with traces of oxygen. Therefore, the formation of complex **7** can be regarded as a decomposition pathway, which is observed in the reactions that do not work due to the instability of complex **1**, thus complex **7** is always formed if no other suitable reagent is present.

### 3.2.5.2. Reaction with CO

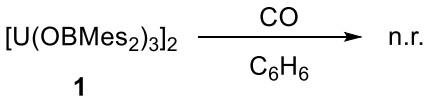


**1**

Scheme 3.9. Exposure of CO to complex **1**.

Exposing a degassed benzene solution of **1** to 1 bar of CO did not result in the formation of any new complex, but complex **7** which was formed due to presence of traces of oxygen. Confirmed by the $^{1}H$ and $^{13}C$ NMR spectra, which show the same resonances as for formation of complex **7**.

### 3.2.5.3. Reaction with $CO_2$

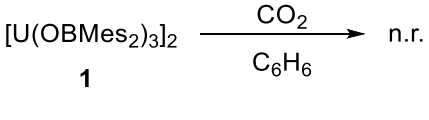


**1**

Scheme 3.10. Exposure of $CO_2$ to complex **1**.

A degassed purple solution of **1** was exposed to 1 bar of $CO_2$. No change was evident in the $^{1}H$ or the $^{11}B$ NMR spectra. Heating the sample to reflux at 80 °C for 24 hours did not result in a change in the NMR spectra, except for the formation of complex **7** due to the presence of traces of oxygen.

The fact that complex **1** does not react with CO and $CO_2$ could be due to the dimerization of complex **1**, whereas for the tri-*iso*-propyl substituted complex $[U(OBTrip_2)_3]$, $[U(OBTrip_2)_4]$ and the carbonate complex $[\{(OBTrip_2)_3U\}_2(\mu\text{-}CO_3)]$ were obtained upon exposure to an atmosphere of CO and $CO_2$ respectively.[6] The increased sterics when substituting the methyl for isopropyl groups seem to create more space for CO and $CO_2$ activation, thus allowing the formation of these complexes.

### 3.2.6. Reactions with phosphines

Although the first examples of phosphine coordination to uranium centres date back to the 1980s, the area is still very much underdeveloped.[75-77] Most reports contain a phosphine ligand where P acts as a donor due to its Lewis basicity, donating electron density into vacant orbitals of the Lewis acidic uranium. Particularly prevalent are the use of bis(dimethylphosphino)ethane (dmpe) and trimethylphosphine ($PMe_3$).[21, 78-81]

The formation of uranium inverse arene sandwich complexes was first reported by Cummins and co-workers, when the iodo tris(amido)uranium complex $[UI(NAd(Ar))_3]$ (Ar = 3,5-$(Me)_2$-$C_6H_3$) was treated with $KC_8$ in arene solvents, which provided $[\{(NAd(Ar))_2U\}_2(\mu\text{-}\eta^6\text{:}\eta^6\text{-}C_6H_6)]$ and $[\{(NAd(Ar))_2U\}_2(\mu\text{-}\eta^6\text{:}\eta^6\text{-}C_7H_8)]$.[82] Since then, the synthesis of other uranium inverse arene sandwich complexes by reduction with $KC_8$ has been reported.[83-86]

Moreover, the formation of uranium inverse arene sandwich complexes has been reported via disproportionation of $[U(ODtbp)_3]$ and $[U(N(SiMe_3)_2)_3]$[87] and via the spontaneous reduction of toluene by the dinuclear $U^{III}$ siloxide precursor $[U(OSi(O^tBu)_3)_2(\mu\text{-}OSi(O^tBu)_3)]_2$.[5]

Here, the first synthesis of uranium inverse arene sandwich complexes supported by stabilisation of phosphine ligands is reported. A range of different mono- and diphosphine ligands have been studied. It is proposed that the phosphines act as stabilizers

for complex **1**, preventing a fast decomposition towards complex **7** and therefore allowing the reaction with the arene solvent and formation of the inverse arene sandwich complex.

### 3.2.6.1. Reactions with diphosphines dmpm and dmpe

The reaction of uranium boroxide complex **1** with diphosphines was first investigated in order to understand if the addition of a Lewis base would interact with both Lewis acidic uranium and boron as seen in Figure 3.9.

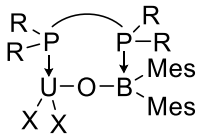


Figure 3.9. Possible interaction of diphosphines with complex **1**.

However, the addition of diphosphine ligands, bis(dimethyphosphino)methane (dmpm) and bis(dimethylphosphino)ethane leads to the formation of uranium inverse arene sandwich complexes (Scheme 3.11).

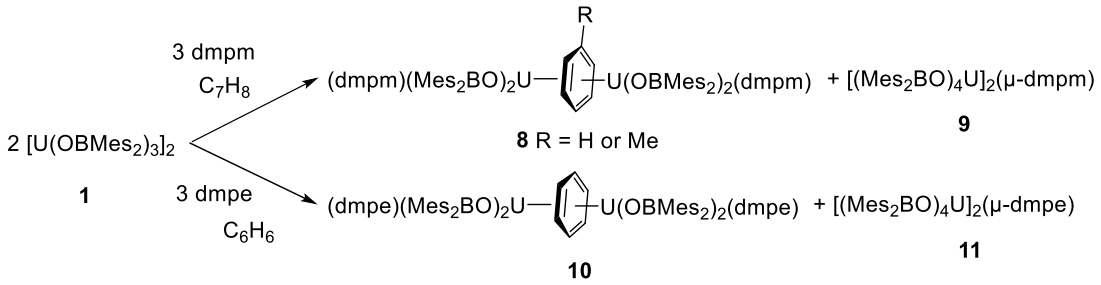


Scheme 3.11. Synthesis of uranium IAS complexes **8** and **10**.

Addition of two equivalents of dmpm or dmpe to an arene solution of **1** leads to the formation of [{(dmpm)(OBMes$_2$)$_2$U}$_2$(μ-η$^6$:η$^6$-C$_6$H$_5$R)] (**8benz** R = H, **8tol** R = Me) and [{(dmpe)(OBMes$_2$)$_2$U}$_2$(μ-η$^6$:η$^6$-C$_6$H$_6$)] (**10**), respectively. To the best of our knowledge, uranium inverse arene sandwich complexes with phosphine coordination have not been previously reported.

As mentioned earlier, the formation of uranium inverse arene sandwich complexes via disproportionation was first reported by our group in 2012.[87] Storage of arene solutions of [U(ODtbp)$_3$] and [U(N(SiMe$_3$)$_2$)$_3$] at 90 °C provided the inverse arene sandwich complexes [{(ODtbp)$_2$U}$_2$(μ-η$^6$:η$^6$-C$_6$H$_5$R)] and

[{(N(SiMe$_3$)$_2$)U}$_2$(μ-η$^6$:η$^6$-C$_6$H$_5$R)] (R = H, Me or Ph), and the oxidized [U(ODtbp)$_4$] and [U(N(SiMe$_3$)$_2$)$_2$(κ$^2$C:N-N(SiMe$_3$)SiMe$_2$CH$_2$)]. Similarly, the reaction of **1** with dmpm leads to the formation of complex **8** with concomitant formation of [{(OBMes$_2$)$_4$U}$_2$(μ-dmpm)] (**9**). Analogously, for the reaction of uranium complex **1** with dmpe, **10** and [{(OBMes$_2$)$_4$U}$_2$(μ-dmpe)] (**11**) are formed, as confirmed by $^1$H and $^{11}$B NMR spectroscopies.

Synthesis of complexes with a diphosphine acting as bridging ligand between two uranium centres have been previously reported. [{(Me$_2$Pz)$_4$U}$_2$(μ-dmpe)], synthesised from [U(Me$_2$Pz)$_4$] and dmpe, and the formation of [{(Me$_2$Pz)$_4$U}$_2$(μ-dppe)] (dppe = bis(diphenylphosphino)ethane) from [U(Me$_2$Pz)$_4$] and dppe are some examples.[88] Recently, Connor Halliday, a member of our group has been able to crystallographically characterise [{ODipp$_4$U}$_2$(μ-dmpe)] as by-product of the reaction of [U(ODipp)$_2$(μ-ODipp$_2$)]$_2$ with dmpe for the formation of uranium inverse arene sandwich complex [(ODipp)$_3$U(μ-η$^6$:η$^6$-C$_6$H$_6$)U(dmpe)(ODipp)$_2$].

The $^1$H and $^{11}$B NMR spectra confirmed the formation of both complexes **8** and **10**. Mass spectrometric analysis showed the molecular ion at m/z = 905.47 that corresponds to the [M + H]$^+$ fragment, [U(dmpm)(OBMes$_2$)$_3$ + H]$^+$.

The formation of inverse arene sandwich complex **8benz** was monitored by $^1$H NMR spectroscopy. The formation of an intermediate species involved in this reaction was observed, and this was assigned to [U(η$^6$-C$_6$H$_6$)(dmpm)(OBMes$_2$)$_2$] (**12**) by $^1$H and $^{11}$B NMR spectroscopies. The $^1$H NMR spectra for the formation of **8benz** over time are represented in Figure 3.10. The formation of the intermediate **12** can be clearly seen through the resonance at -114 ppm which started appearing almost immediately, reaching a maximum between 24 and 48 hours. Then the resonance of intermediate **12** started to fade, whereas the resonances corresponding to the inverse arene sandwich product **8benz** and the oxidation by-product **9** increased in intensity over time. In the same direction, resonances corresponding to consumption of **1** could also be seen. Moreover, a new set of resonances appeared after 24 hours, which were assigned to [U(dmpm)(OBMes$_2$)$_3$].

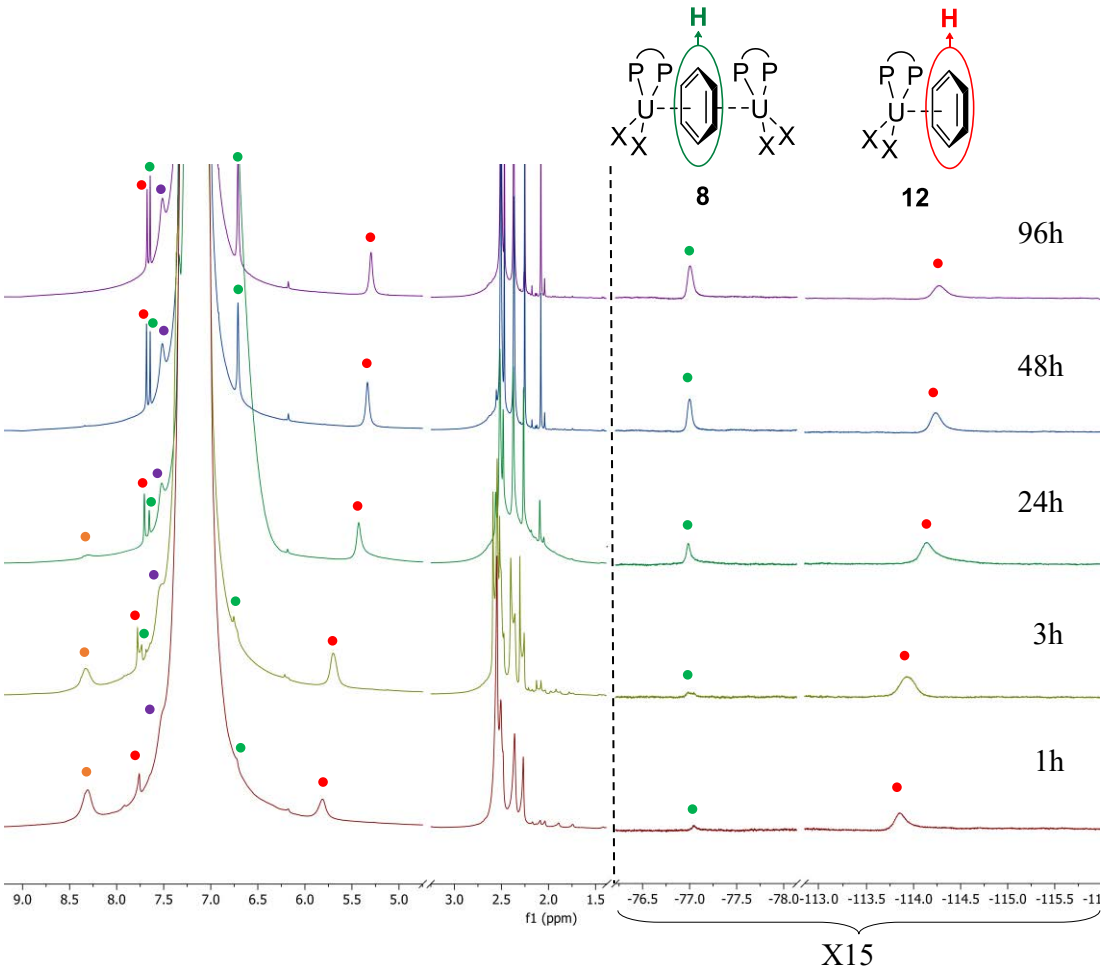


Figure 3.10. $^1$H NMR spectra (298K, $C_6H_6$, 500MHz) of formation of complex **8benz** where ● = $[U(OBMes_2)_2(\mu\text{-}OBMes_2)]_2$ **1**, ● = $[\{(dmpm)(OBMes_2)_2U\}_2(\mu\text{-}\eta^6\text{:}\eta^6\text{-}C_6H_6)]$ **8benz**, ● = $[\{(OBMes_2)_4U\}_2(\mu\text{-}dmpm)]$ **9** and ● = $[U(\eta^6\text{-}C_6H_6)(dmpm)(OBMes_2)_2]$ **12**.

Behaving similarly, the reaction of uranium complex **1** with dmpe gives the uranium inverse arene sandwich complex **10** and complex **11**. Monitoring the reaction by $^1$H NMR spectroscopy, the formation of the intermediate species $[U(\eta^6\text{-}C_6H_6)(dmpe)(OBMes_2)_2]$ (**13**) could also be observed. However, the reaction proceeds much slower, with formation of product **10** only seen after four days.

Although there is not enough information to confirm the mechanism, a possible pathway for these reactions might first consist of coordination of the phosphine ligand and an arene to two $[U(OBMes_2)_3]$ fragments, with ligand transfer from one fragment to another to form intermediate **12** and $[U(dmpm)(OBMes_2)_4]$. The second step could involve the binding of a third $[U(OBMes_2)_3]$ fragment to the intermediate **12** and another phosphine, with another $(OBMes_2)$ transfer to a fourth $[U(OBMes_2)_3]$ moiety to form

complex **8** and two $[U(OBMes_2)_4]$ fragments linked by a phosphine ligand, i.e. complex **9** (Scheme 3.12). Therefore, the overall redox is a partial oxidation of the uranium with arene reduction and ligand transfer. The four $U^{III}$ centres (**1**) react to form two $U^{III}$ centres that have trapped an arene dianion (**8**), and two $U^{IV}$ centres (**9**).

This pathway is similar to the previously reported mechanism for the formation of $[\{(ODtbp)_2U\}_2(\mu\text{-}\eta^6\text{:}\eta^6\text{-}C_6H_6)]$.[87]

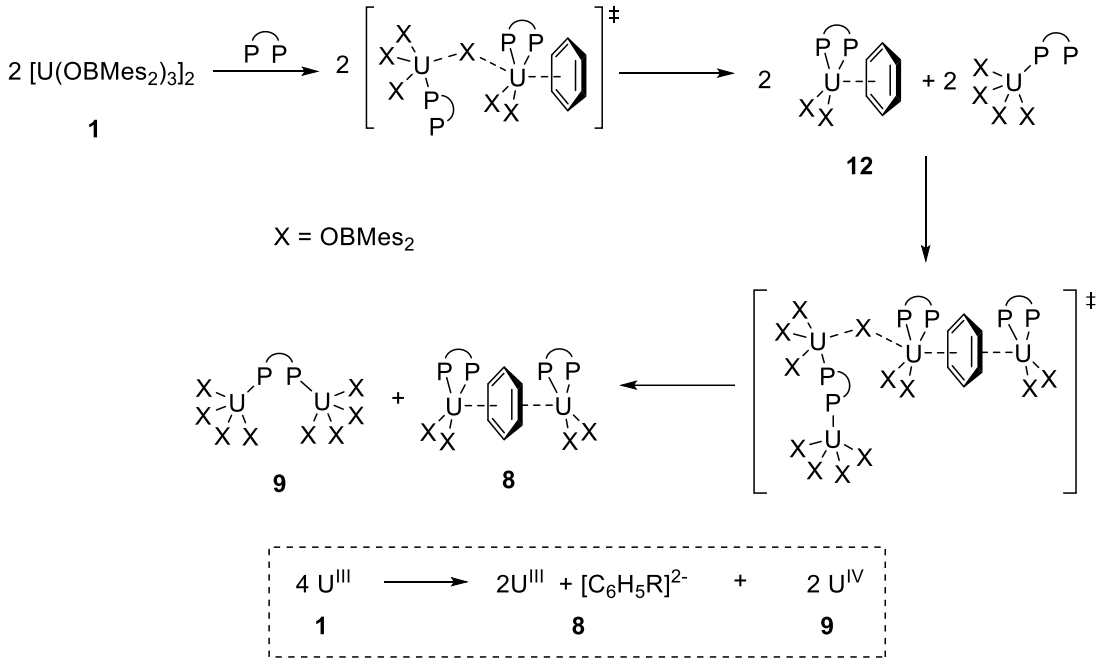


Scheme 3.12. Proposed mechanism for the formation of inverse arene sandwich complexes with diphosphines. When coordination of phosphine is unknown is drawn as monodentate.

### 3.2.6.2. Reactions with diphosphines dcpm, dppm and dppe

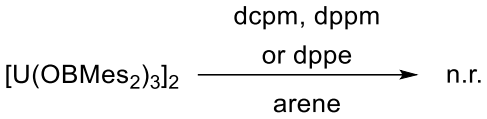


Scheme 3.13. No reactivity of complex **1** with diphosphines dcpm, dppm and dppe.

Reactivity with diphosphines with bigger substituents, i.e. cyclohexyl or phenyl, was investigated for both methyl- and ethyl-bridged phosphines. Addition of dcpm (1,2-bis(dicyclohexylphosphino)methane), dppm (1,2-bis(diphenylphosphino)methane)

or dppe to a dark purple solution of complex **1** in arene solvent overnight did not provide an inverse arene sandwich complex.

### 3.2.6.3. Reactions with monophosphines $PMe_3$, $PEt_3$, $PCy_3$

Reactions of complex **1** with phosphines $PMe_3$, $PEt_3$ (triethylphosphine) and $PCy_3$ (tricyclohexylphosphine) were carried out.

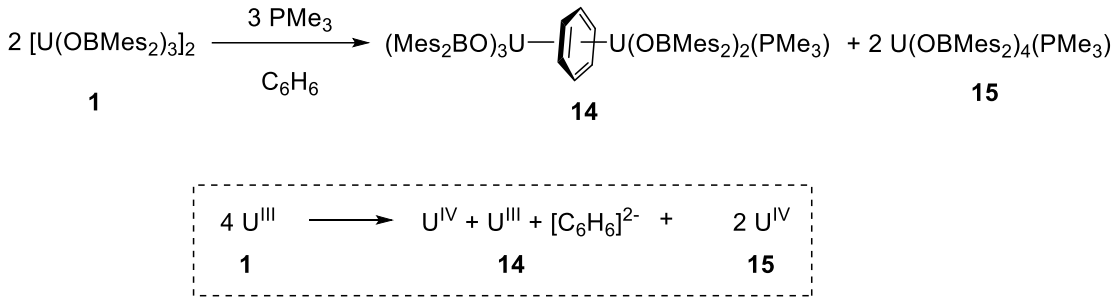


Scheme 3.14. Synthesis of complex **14**.

Comparable to the reaction with diphosphines, the addition of three equivalents or an excess of $PMe_3$ to a benzene solution of **1** provides the desired inverse arene sandwich complex $[(OBMes_2)_3U(\mu\text{-}\eta^6\text{:}\eta^6\text{-}C_6H_6)U(PMe_3)(OBMes_2)_2]$ (**14**) and $[U(OBMes_2)_4](PMe_3)$ **15** (Scheme 3.14). Moreover, the formation of an unidentified by-product was observed, which might contain $U^{II}$ species that have decomposed. Only one phosphine ligand is coordinated to the uranium in complex **14**, as seen in the $^1H$ and $^{11}B$ NMR spectra. Monitoring of the reaction did not show the formation of the mononuclear intermediate seen with the bidentate ligands. The overall redox is a partial oxidation where the four $U^{III}$ centres (**1**) react to form a $U^{IV}$ and a $U^{III}$ that have trapped an arene dianion (**14**), two equivalents of $U^{IV}$ (**15**), and a $U^{II}$ by-product.

The reaction of uranium complex **1** with $PMe_3$ carried out in the presence of a small quantity of THF (1:0.03, benzene:THF) showed different reactivity, giving the targeted inverse arene sandwich complex, $[\{(OBMes_2)_3U\}_2(\mu\text{-}\eta^6\text{:}\eta^6\text{-}C_6H_6)]$ (**16**), without any coordinated phosphine, and $[U(OBMes_2)_4(THF)_2]$ (**17THF**), of which green crystals were deposited on the walls of the reaction vessel in an 8:2 (**16**:**17THF**) ratio (Scheme 3.15).

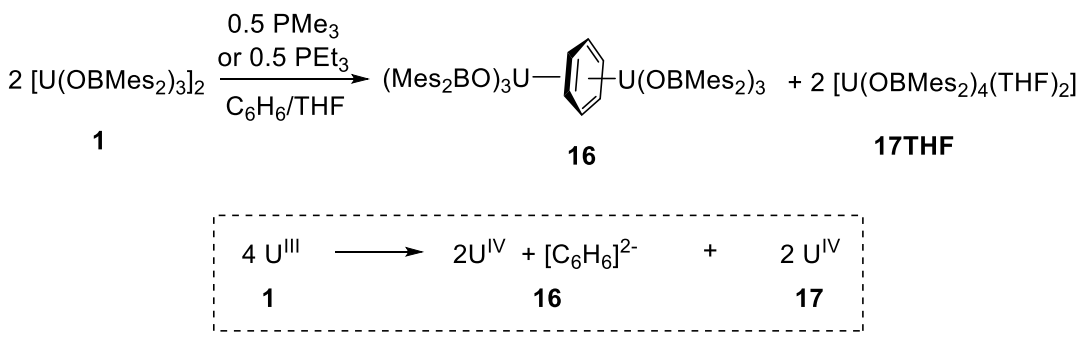


Scheme 3.15. Synthesis of IAS complex **16** with $PMe_3$ and $PEt_3$.

Analogous behaviour was observed for the reaction of complex **1** with $PEt_3$ in the presence of THF, which provided the inverse arene sandwich complex **16**, along with **17THF**. Different stoichiometries of the phosphine ligands (0.5, 1 or 2 equivalents) did not affect the outcome of the reactions.

The most probable path for these reactions is, on one hand the phosphine coordinates to complex **1**, breaking the dimer and providing enough stabilisation to the monomer $UX_3$ to persist in solution long enough to further react with the arene and another $UX_3$ for the formation of uranium inverse arene sandwich **16**.

Moreover, THF might be blocking the ligand transfer between the uranium centres that is needed to form a uranium inverse arene complex like $X_2U$-arene-$UX_2$. We assume the formation of $[U(OBMes_2)_4]$ is a direct consequence of the decomposition of **1** in the presence of THF. Therefore, two different reactions are taking place at the same time: the formation of the inverse arene sandwich complex **16** from the reaction with phosphines, and the formation of complex **17THF** through oxidation due to the presence of THF. Thus, the ratio of complexes **16** and **17THF** is not dependent on the reaction mechanism.

Finally, the reaction with a bulkier monophosphine, such as $PCy_3$, was studied as seen in Scheme 3.16.

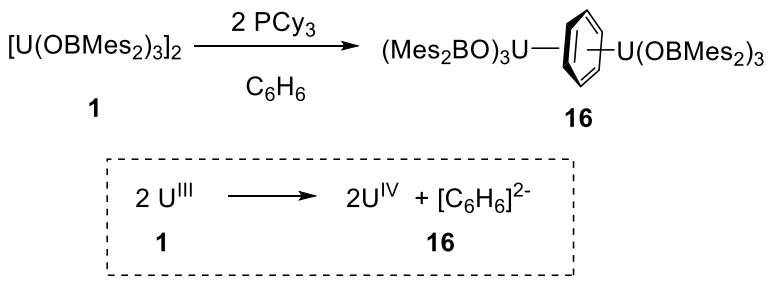


Scheme 3.16. Synthesis of inverse arene sandwich complex **16** with $PCy_3$.

Addition of two equivalents of $PCy_3$ to a benzene solution of **1** leads to the formation of $[\{(OBMes_2)_3U\}_2(\mu\text{-}\eta^6\text{:}\eta^6\text{-}C_6H_6)]$ (**16**) in 19% yield. Complex **16** seems to be formed similarly to the reactions of complex **1** with $PMe_3$ and $PEt_3$, where the coordination of the phosphine seems to break the dimer **1** and to provide stabilisation to enable the formation of complex **16** by reduction of benzene, which features two $U^{IV}$ and a benzene dianion. Moreover, $PCy_3$ might be too bulky to achieve coordination to the inverse arene sandwich complex.

Characteristic $^1H$ NMR shifts for the trapped arenes and $^{11}B$ NMR shifts for the ligands of the different inverse arene sandwich complexes are given in Table 2.

Table 2. $^1H$ and $^{11}B$ NMR chemical shifts (ppm) for the arene and boroxide ligand in complexes **8benz**, **10**, **14** and **16**.

| Compound | $^1H$ Ar (ppm) | $^{11}B$ ligand (ppm) |
|---|---|---|
| **8benz** | -77 | -17 |
| **10** | -75 | -17 |
| **14** | -80 | -16 |
| **16** ($C_6H_6$/THF) | -80 | -16 |
| **16** ($C_6H_6$) | -82 | - |

### 3.2.6.4. Reaction with monophosphine $PPh_3$

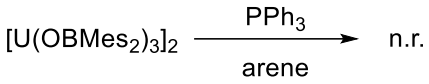


Scheme 3.17. No reaction between complex **1** and monophosphine $PPh_3$.

Similarly to the diphosphines dcmp, dppm and dppe, the monophosphine $PPh_3$ (triphenylphosphine) did not react with complex **1**.

### 3.2.6.5. Structural comparisons

Dark brown crystals of **8** from the reaction of uranium boroxide complex **1** and dmpm were grown by slow diffusion of hexane into a concentrated toluene solution (Figure 3.11).

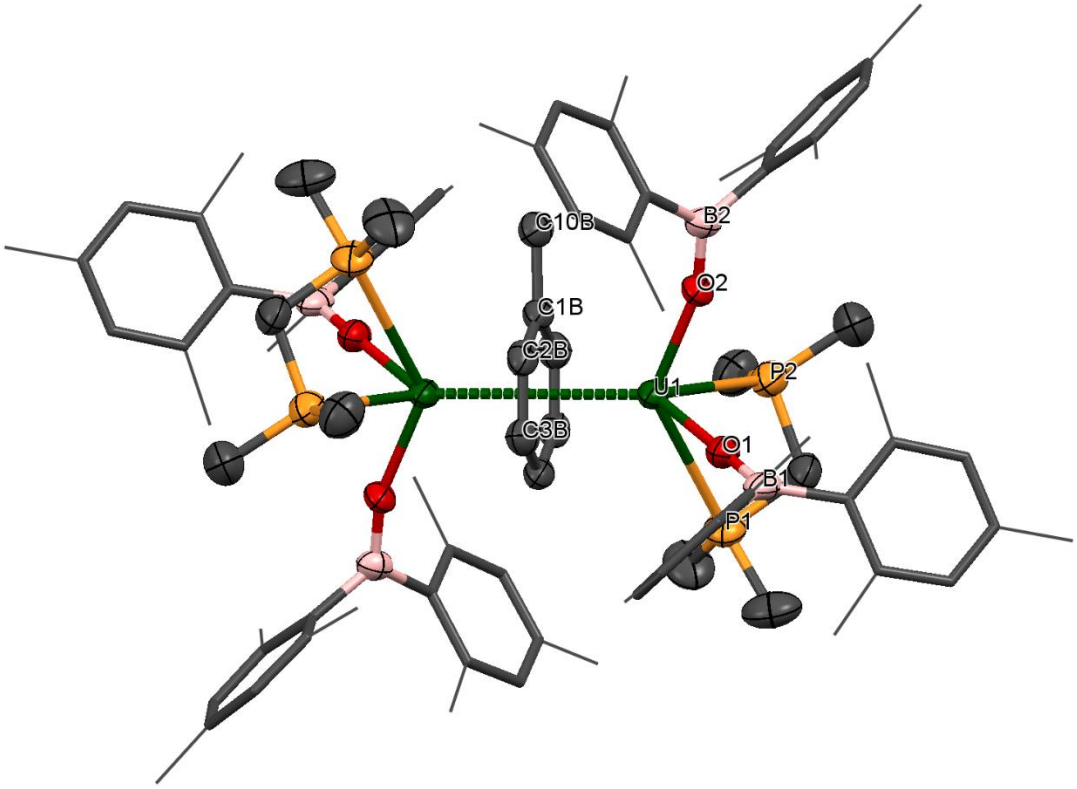


Figure 3.11. Solid-state structure of **8**. The mesityl groups are depicted as wireframe and capped sticks for clarity. Hydrogen atoms are omitted. The thermal ellipsoids are displayed at 50% probability.

The structure of complex **8** shows formation of a uranium inverse arene sandwich complex where each uranium ion is coordinated to two terminal, monodentate $OBMes_2$ ligands, one bidentate dmpm ligand, and a planar $\mu$-$\eta^6$:$\eta^6$ bridging arene.

The average C–C bond distance of the toluene in complex **8** is 1.444 Å, 0.05 Å longer than in free toluene,[89] which is in agreement with previously reported uranium inverse arene sandwich complexes.[87, 90, 91]

In addition, the central arene ring is planar, with a deviation from planarity of 0.003 Å and a $U–C_{centroid}$ distance of 2.161 Å. The mean $U–C_{arene}$ distance is 2.599 Å, which is significantly shorter than those found in other $U^{III}$ neutral arene complexes (~2.93 Å), such as $[U(\eta^6\text{-}C_6Me_6)Cl_4]$, which was reported by Ephritikhine and co-workers in 1989,[4, 91, 92] and in the same range as previously reported arene-bridged complexes often formulated as $U^{III}$-(arene$^{2-}$)-$U^{III}$, $[\{X_2U\}_2(\mu\text{-}\eta^6\text{:}\eta^6\text{-}C_6H_5R]$ (X = bulky amido, methanide or aryloxide; R = H or $CH_3$),[82-84, 87] thus indicating the same oxidation states. The U–O distances (mean 2.194 Å) of the boroxide ligands are almost identical to the terminal boroxides in complex **1** with a $U–O_{avg}$ distance of 2.196 Å.

There are no previous reports of a dmpm ligand coordinated to uranium. However, the U–P distances found in complex **8** (from 3.088(2) Å to 3.208(2) Å) are in the same range as those found in uranium dmpe complexes.[79, 80, 93]

Brown crystals of **16**, which is formed by the reaction of complex **1** with $PCy_3$, were also obtained from slow diffusion of hexane into a concentrated benzene solution (Figure 3.12).

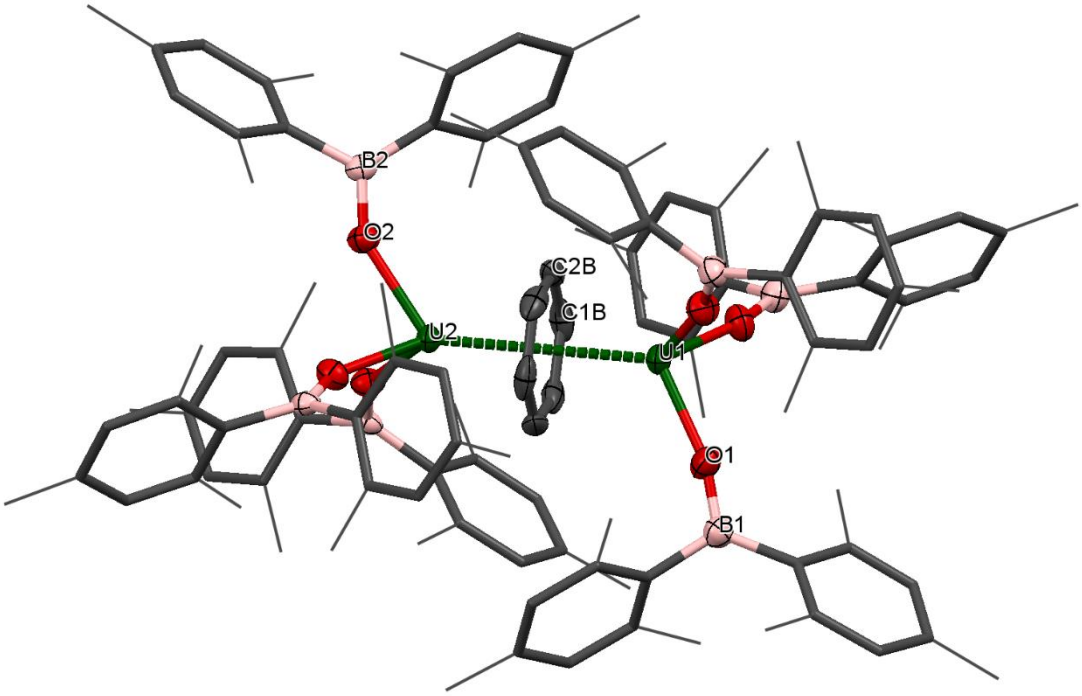


Figure 3.12. Solid-state structure of **16**. The mesityl groups are depicted as wireframe and capped sticks for clarity. Hydrogen atoms are omitted. The thermal ellipsoids are displayed at 50% probability.

The structure of inverse arene sandwich complex **16** presents the coordination of three $OBMes_2$ ligands in a monodentate, terminal fashion and a planar $\mu$-$\eta^6$:$\eta^6$ bridging benzene.

The average C−C bond distance for the benzene in complex **16** is 1.434 Å, 0.04 Å longer than in free benzene[94] and in agreement with previously reported benzene inverse arene sandwich complexes.[86, 87] Moreover, complex **16** has an average U–$C_{arene}$ distance of 2.632 Å, which is ~0.04 Å longer than the dmpm-coordinated inverse arene sandwich complex **8**, and considerably shorter than those reported for $U^{IV}$ neutral arene complexes (~2.90 Å).[95, 96] These differences could suggest the formation of a $U^{IV}$-(arene$^{2-}$)-$U^{IV}$ or $U^{III}$-(arene)-$U^{III}$ complex. In addition, the formation of a $U^{V}$-(arene$^{4-}$)-$U^{V}$ should not be ruled out without further studies, although the U–C distance for the known complex $[K\{(OSi(O^tBu)_3)_3U\}_2(\mu\text{-}\eta^6\text{:}\eta^6\text{-}C_7H_8)]$[90] is ~0.06 Å longer than in complex **16**. Therefore, the suggested formal oxidation state is two $U^{IV}$ centres and an arene dianion. The average U–$C_{centroid}$ distance is 2.210 Å and the central benzene has a deviation from planarity of 0.007 Å.

The $U–O_{avg}$ distance of the boroxide ligands is 2.20 Å, which is almost identical to the distance in the terminal boroxides in complex **1** and the boroxide ligands in the dmpm inverse arene sandwich complex **8**.

Table 3 shows the most significant structural parameters for complexes **8** and **16**.

Table 3. Structural parameters of IAS complexes [{(dmpm)$(OBMes_2)_2U\}_2(\mu\text{-}\eta^6,\eta^6\text{-}C_7H_8)$] (**8**), and [{$(OBMes_2)_3U\}_2(\mu\text{-}\eta^6,\eta^6\text{-}C_6H_6)$] (**16**).

| Structural parameter | [{(dmpm)$(OBMes_2)_2U\}_2(\mu\text{-}\eta^6\text{:}\eta^6\text{-}C_7H_8)$] (**8**) (Å) | [{$(OBMes_2)_3U\}_2(\mu\text{-}\eta^6\text{:}\eta^6\text{-}C_6H_6)$] (**16**) (Å) |
|---|---|---|
| U–O range | 2.184(3)–2.203(4) | 2.155(6)–2.256(6) |
| $U–O_{avg}$ | 2.194 | 2.20 |
| U–P range | 3.088(2)–3.208(2) | - |
| $U–P_{avg}$ | 3.15 | - |
| C–C range | 1.431(8)–1.453(8) | 1.416(13)–1.447(13) |
| $C–C_{avg}$ | 1.444 | 1.434 |
| U–C range | 2.576(6)–2.610(5) | 2.623(8)–2.644(8) |
| $U–C_{avg}$ | 2.599 | 2.637 |
| U–U | 4.321 | 4.432 |
| Dev. from planarity | 0.003 | 0.007 |

### 3.2.7. Reaction with $KC_8$

As mentioned earlier, the first uranium inverse arene sandwich complexes, $[\{(NAd(Ar))_2U\}_2(\mu\text{-}\eta^6\text{:}\eta^6\text{-}C_6H_6)]$ and $[\{(NAd(Ar))_2U\}_2(\mu\text{-}\eta^6\text{:}\eta^6\text{-}C_7H_8)]$, were reported in 2000 by Cummins and co-workers via reduction with $KC_8$.[82] Since then, several uranium inverse arene sandwich complexes formed upon reaction with a reductant, such as $KC_8$, in arene solution have been published.[83, 84, 97-102] To target the formation of a uranium inverse arene sandwich complex, reactions of complex **1** with $KC_8$ in toluene and benzene were carried out.

Surprisingly, no inverse arene sandwich complex was obtained, but a reduced form of the decomposition product **7** was isolated instead, $K_2[\{(OBMes_2)_3U\}_2(\mu\text{-}O)_2]$ (**18**). Complex **18** was formed upon addition of 2.5 equivalents of $KC_8$ to a purple solution of **1** in benzene (Scheme 3.18). The reaction of complex **1** with traces of oxygen first, followed by reduction with $KC_8$ is rare, but has been seen previously for complex $[((^{Neop,Me}ArO)_3tacn)U]$, which forms the bis(μ-oxo) bridged complex $[\{((^{Neop,Me}ArO)_3tacn)U\}_2(\mu\text{-}O)_2]$ in the presence of traces of oxygen, and its reduction with $KC_8$ yields $K_2[\{((^{Neop,Me}ArO)_3tacn)U\}_2(\mu\text{-}O)_2]$.[11]

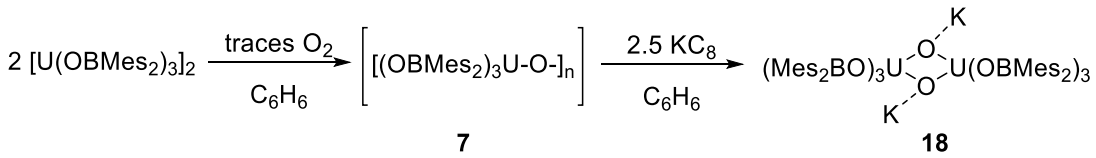


Scheme 3.18. Formation of anionic complex **18**.

Compound **18** crystallised as pale brown plates from the slow diffusion of hexane into a concentrated benzene solution; the structure is shown in Figure 3.13.

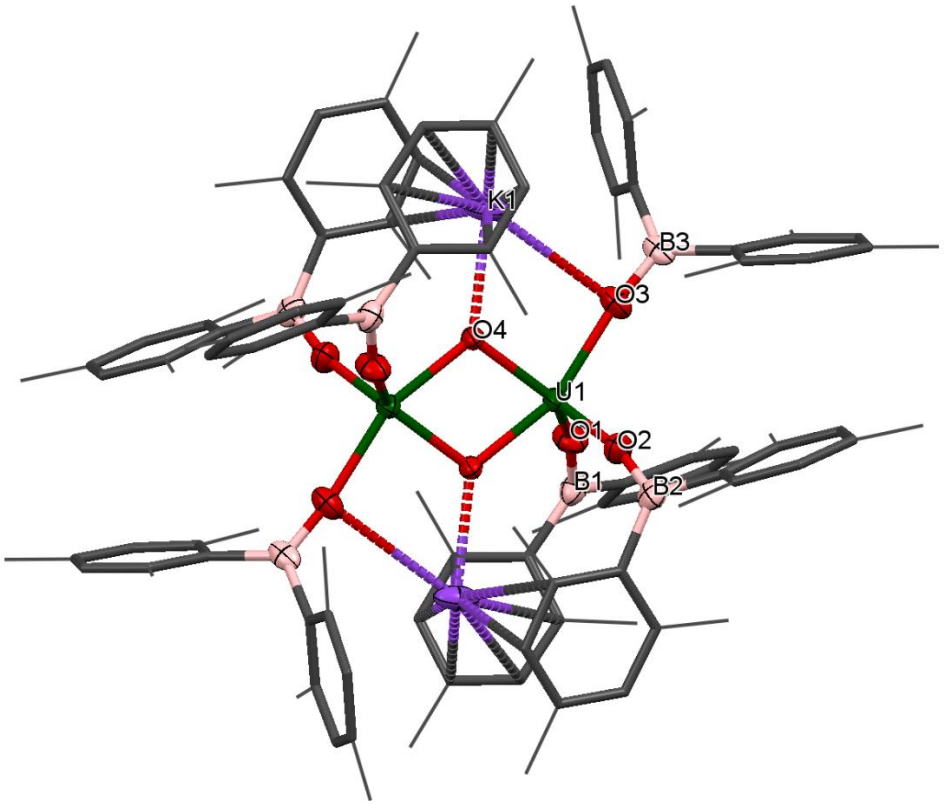


Figure 3.13. Solid-structure of **18**. The mesityl groups are depicted as wireframe and capped sticks for clarity. Hydrogen atoms are omitted. The thermal ellipsoids are displayed at 50% probability.

Complex **18** exhibits a dinuclear structure, where each uranium is five-coordinate with a distorted square pyramidal coordination environment. It features a diamond core structural motif [U(μ-O)$_2$U] with one $K^+$ interacting with each bridging oxygen.

Uranium complex **18** presents U–O bond distances of 2.154(2) Å and 2.127(2) Å for the bridging unit. The U···U distance is 3.4346(3) Å, which is in shorter than the U···U distance in complex **1** (3.966 Å). Moreover, the angles for the bridging oxygens are 73.29(9)° and 106.71(9)° for the O–U–O and the U–O–U respectively. Structural comparison of the bis(μ-oxo) bridged complex **18** with previously reported uranium bis(μ-oxo) bridged compounds shows that the bond metrics and angles are in agreement.[11, 103-106] Each potassium ion is coordinated to one of the bridging oxygens , to one boroxide ligand and to two mesityl moieties, one in a $\eta^5$ fashion and the other one in a $\eta^2$ fashion.

In addition, the U–$O_{boroxide}$ average bond length is 2.21 Å, which is similar to the U–O distance for the terminal boroxides in complex **1** (mean 2.196 Å). Moreover, the U–O–B angles are quite different within the bis(μ-oxo) bridged complex, as the two boroxide ligands which the mesityl groups interact with the potassium are more bent, with U–O–B angles of 151.8(3) and 163.0(3)°, whereas the $U_1$–$O_3$–$B_3$ angle for the other boroxide ligand, which oxygen interacts with the potassium, is 172.2(3)°.

### 3.2.8. Reaction with $P_4$

Activation of white phosphorus, $P_4$, is still the major commercial route to P-containing products utilised by the detergent, food, speciality chemical and pharmaceutical industries.[107]

Although the activation of $P_4$ by uranium complexes is not common, some examples have been reported with concomitant formation of clusters. The addition of $P_4$ to a solution of [U(N[Xy]R)$_3$(I)] (Xy = 3,5-dimethylphenyl, R = $^t$Bu or Ad) provided complex [{(N[Xy]R)$_3$U}$_2$(μ-η$^4$:η$^4$-P$_4$)], which includes an η$^4$:η$^4$ [P$_4$]$^{2-}$ unit.[108] Treatment of [U(η-Cp*)(η-C$_8$H$_6${Si$^i$Pr$_3$-1,4}$_2$)(THF)] resulted in the formation of complex [{(η-Cp*)(η-C$_8$H$_6${Si$^i$Pr$_3$-1,4}$_2$)U}$_2$(μ-η$^2$:η$^2$-P$_4$)] , which contains the square planar η$^2$:η$^2$ [P$_4$]$^{2-}$ unit (Figure 3.14).[109]

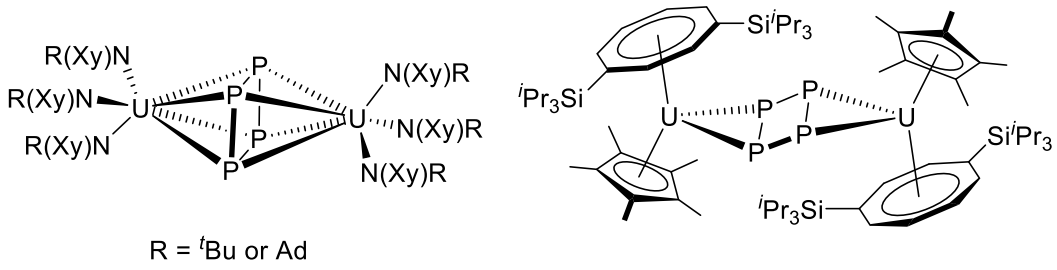


Figure 3.14. The [P$_4$]$^{2-}$ complexes formed after reaction of [U(N[Xy]R)$_3$(I)] (R = $^t$Bu or Ad) and [U(η-Cp*)(η-C$_8$H$_6${Si$^i$Pr$_3$-1,4}$_2$)(THF)] with P$_4$.[108, 109]

The activation of $P_4$ by [{[HC(SiMe$_2$NAr)$_3$]U}$_2$(μ-η$^6$:η$^6$-C$_6$H$_5$Me)] (Ar = toluene) led to the formation of [{[HC(SiMe$_2$NAr)$_3$]U}$_2$(μ-η$^2$:η$^2$:η$^2$-P$_7$)] through an unusual catenation which generates a η$^2$:η$^2$:η$^2$ [P$_7$]$^{3-}$ unit (Figure 3.15).[110]

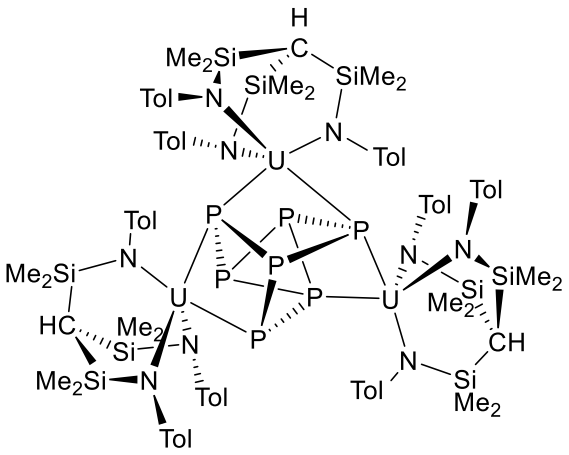


Figure 3.15. The $[P_7]^{3-}$ complex formed after reaction of $[\{[HC(SiMe_2NAr)_3]U\}_2(\mu\text{-}\eta^6\text{:}\eta^6\text{-}C_6H_5Me)]$ (Ar = toluene) with $P_4$.[110]

Addition of one equivalent of white phosphorus to a solution of complex **1** did not lead to the formation of a cluster or any new complex.

### 3.2.9. Reaction with $Me_3SiN_3$

Since the first reported azide activation by uranium by Andersen and co-workers in 1985 which yielded $[U(C_5H_4Me)NR]$ (R = Ph or $SiMe_3$) (Scheme 3.19) from direct reaction of $[U(C_5H_4Me)(THF)]$ with $Me_3SiN_3$ or $PhN_3$,[111] uranium azides have been investigated because of their potential to form U–N multiple bonds.

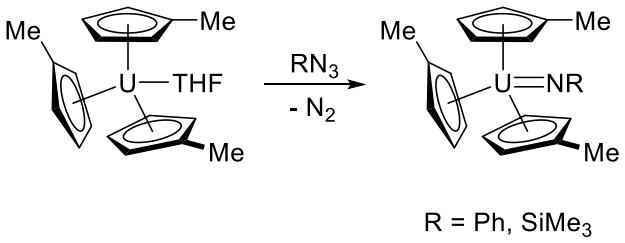


Scheme 3.19. Synthesis of uranium imido complexes by reaction with $RN_3$.[111]

The addition of three equivalents of $Me_3SiN_3$ to a purple solution of complex **1** did not provide a new complex.

### 3.2.10. Reaction with $Ph_3CCl$

Oxidation of uranium boroxide complex **1** was carried out with the use of trityl chloride. Addition of an excess of trityl chloride to a purple solution of **1** provided a pale

red solution which contained the oxidised complex [U(OBMes$_2$)$_3$Cl] (**19**). $^1$H and $^{11}$B NMR spectroscopies confirmed the formation of **19** as seen in Scheme 3.20.

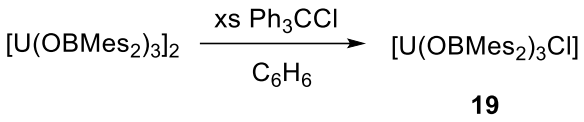


Scheme 3.20. Synthesis of complex **19**.

## 3.3. Synthesis and characterization of [U(OBMes$_2$)$_4$] (17)

The reaction of NaOBMes$_2$ with [UI$_4$(1,4-dioxane)$_2$] in toluene affords [U(OBMes$_2$)$_4$(dioxane)$_{0.5}$]$_2$ (**17diox**). The reaction was stirred overnight and colourless crystals of **17diox** suitable for XRD analysis were obtained from slow diffusion of hexanes into the reaction mixture. Complex **17diox** was characterised by $^1$H and $^{11}$B NMR spectroscopies, mass spectrometry (APPI-MS) and single crystal XRD analysis.

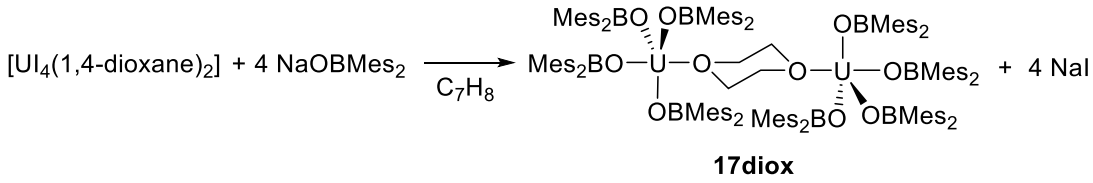


Scheme 3.21. Synthesis of $U^{IV}$ boroxide complex **17**.

The $^1$H and $^{11}$B NMR spectra show a set of resonances for a single boroxide ligand environment. Mass spectrometric analysis showed the molecular ion at m/z = 1298.76 that corresponds to $[M]^{+\bullet}$ fragment $[U(OBMes_2)_4]^{+\bullet}$.

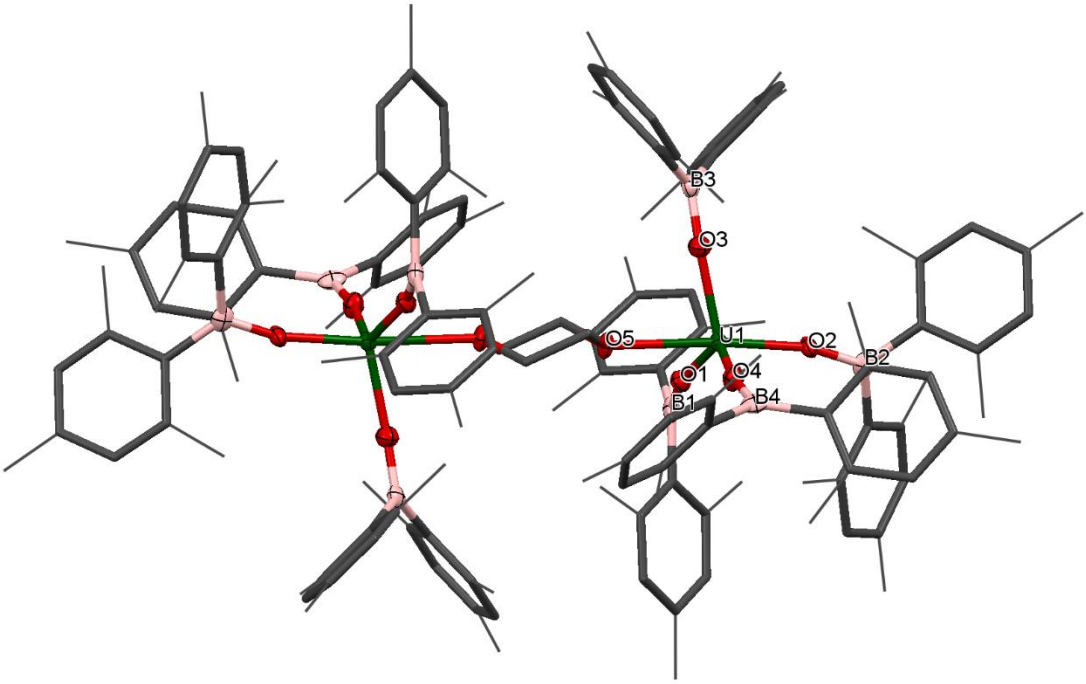


Figure 3.16. Solid-state structure of **17diox**. Mesityl groups and dioxane solvent are depicted as capped sticks and wireframe for clarity. Hydrogen atoms are omitted. The thermal ellipsoids are displayed at 50% probability.

The solid-state structure of **17diox** reveals two $U^{IV}$ ions both in a distorted trigonal bipyramidal coordination environment. Each uranium centre is ligated by one end of a bridging dioxane molecule in an axial position with a U–O distance of 2.577(3) Å, which is considerably longer than in $[UI_4(1,4\text{-dioxane})_2]$ or the $[UI_2(\text{dioxane})_2(\text{aryloxide})]$ previously reported by our group (mean = 2.333(6) Å and 2.087(5) Å respectively).[112, 113] The boroxide ligands in the equatorial positions have a $U–O_{avg}$ distance of 2.144 Å, which is shorter than in the uranium(III) complex **1**, consistent with a $U^{IV}$ centre, and similar to the U–O bond length for $[U(OBTrip)_4]$ with a U–O distance of 2.159(5) Å.[6] The boroxide ligands in the axial positions have a U–O distance of 2.095 Å, which is much shorter than the equatorial boroxides. The $U–O–B_{avg}$ angles are 167.1°, which is comparable to the U–O–B angles of the terminal boroxide ligands in **1** (mean 171.6°).

## 3.4. Synthesis and characterisation of $[U(N(SiMe_3)_2)_3(OBMes_2)]$ (20)

Addition of just one equivalent of $HOBMes_2$ to an orange-brown solution of the uranium metallacycle $[U(N(SiMe_3)_2)_2(\kappa^2C:N\text{-}N(SiMe_3)SiMe_2CH_2)]$ provided a brown

solution from which brown crystals of complex $[U(N(SiMe_3)_2)_3(OBMes_2)]$ (**20**) suitable for XRD analysis were obtained from a concentrated toluene solution (Scheme 3.22). Formation of complex **20** was confirmed by $^{1}H$ and $^{29}Si$ NMR spectroscopies, elemental analysis and single crystal XRD analysis. This synthesis had been also carried out by the former group member Dr. Rowan Young.

$$[U(N(SiMe_3)_2)(\kappa^2C{:}N\text{-}N(SiMe_3)SiMe_2CH_2)] \xrightarrow[C_6H_6]{HOBMes_2} \underset{\mathbf{20}}{[U(N(SiMe_3)_2)_3(OBMes_2)]} + H(N(SiMe_3)_2)$$

Scheme 3.22. Synthesis of heteroleptic complex **20**.

As seen in Figure 3.17, the $^{1}H$ NMR spectrum shows a paramagnetically shifted resonance at -6.6 ppm, which corresponds to the methyl groups in the tris(silylamide) ligand, and three smaller sets of resonances for the boroxide ligand. Moreover, the $^{29}Si$ NMR resonances shift from -74 and -82 ppm for the uranium metallacycle to -132 ppm for complex **20**.

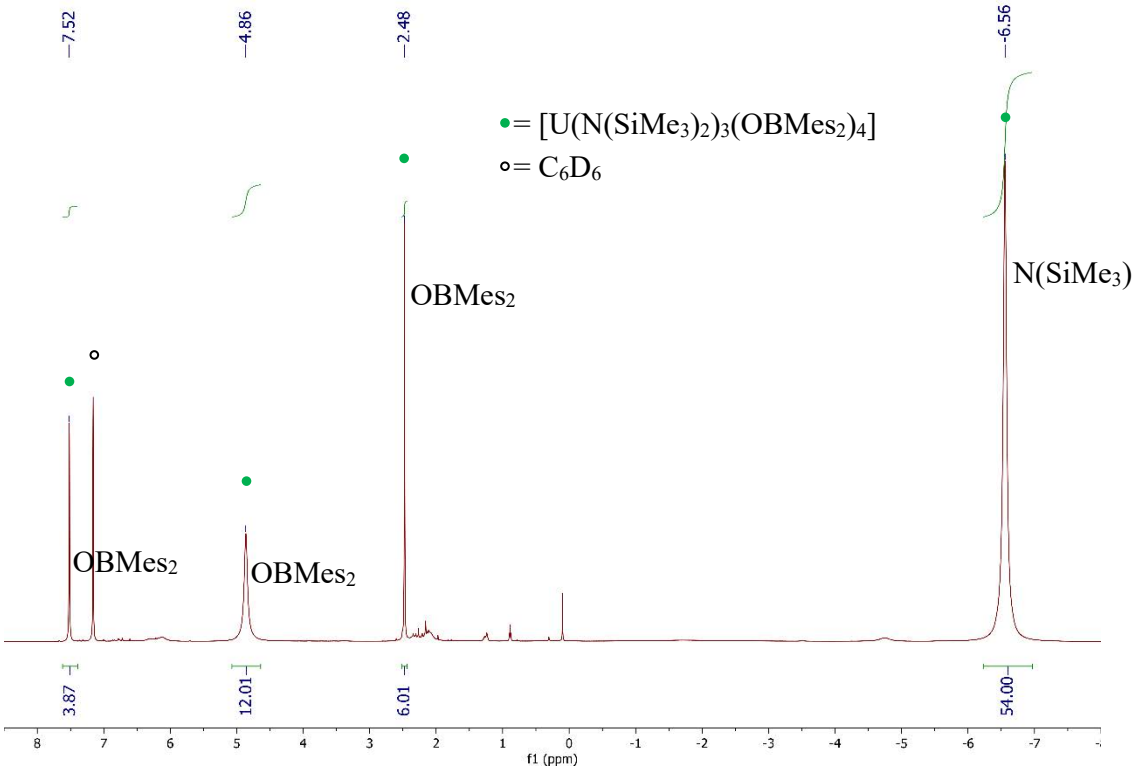


Figure 3.17. $^{1}H$ NMR spectrum (298K, $C_6D_6$, 500 MHz) of complex **20**.

Single crystal XRD analysis revealed that the solid-state structure of complex **20** has a distorted tetrahedral coordination environment (Figure 3.18). The average $U–N_{avg}$ bond length is 2.268 Å, which is ~0.03 Å shorter than that of the previously reported complex $[U(N(SiMe_3)_4]$,[114] which is reasonable if more electron density is being distributed to the boroxide ligand and more electron density is being pulled from the tris(silylamide) ligands, thus decreasing the U–N bond length. Moreover, the N–U–N angles are 105.00(8)°, 113.72(8)° and 116.96(9)°, which are in the same range as for $[U(N(SiMe_3)_4]$. The U–O distance is 2.1559(18) Å, which is slightly shorter than the U–O distance in the terminal boroxides for complex **1** ($U–O_{avg}$ is 2.196 Å) but longer than the $U–O_{avg}$ for $[U(OBMes_2)_4(dioxane)_{0.5}]$ (2.144 Å). The U–O–B angle is 167.23(19)°, which is in the same range as U–O–B angles for the terminal boroxides in complex **1** (mean 171.6°).

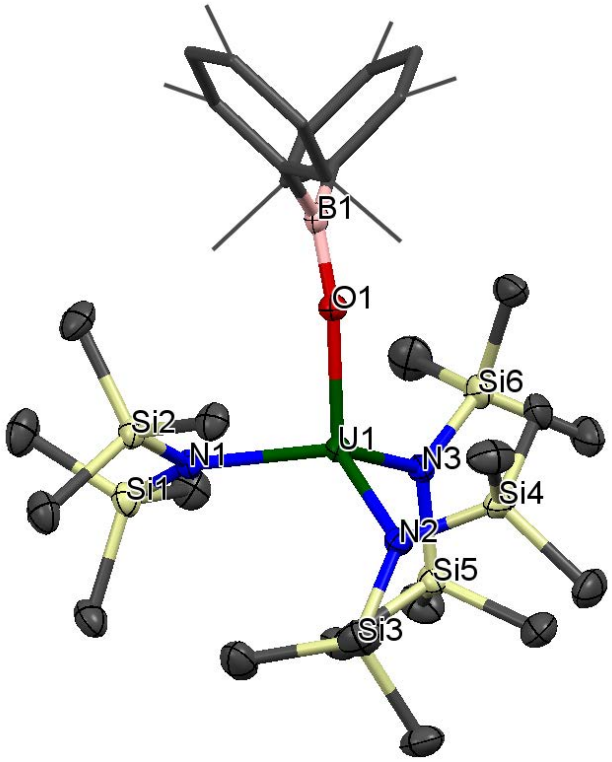


Figure 3.18. Solid-state structure of **20**. Mesityl group is depicted as capped sticks and wireframe for clarity. Hydrogen atoms are omitted. The thermal ellipsoids are displayed at 50% probability.

## 3.5. Targeted synthesis of $[U(OBMes_2^F)_3]$

In an attempt to modify the electronic properties of uranium boroxide complexes, the synthesis of the fluorinated substituted boroxide ligand $HOBMes_2^F$ ($Mes_2^F$ = 1,3,5-tris(trifluoromethyl)benzyl) was carried out according to literature procedures.[115] Treating a purple solution of $[U(N(SiMe_3)_2)_3]$ in benzene with three equivalents of $HOBMes_2^F$ provided a dark brown solution (Scheme 3.23).

$$[U(N(SiMe_3)_2)_3] + 3\ HOBMes_2^F \xrightarrow[C_6H_6]{} [U(OBMes_2^F)_3] + 3\ H(N(SiMe_3)_2)$$

Scheme 3.23. Targeted synthesis of $[U(OBMes_2^F)_3]$.

A possible outcome of this reaction would be the uranium mediated C–F bond activation to provide an $X_3UF$ complex such as compound $[(C_5H_4Me)_3UF]$ reported by Andersen and co-workers.[116] Treatment of $[U(C_5H_4Me)_3]$ with two equivalents of hexaflurorbenzene produced the $U^{IV}$ fluoride complex $[(C_5H_4Me)_3UF]$ and the C–C coupled product $C_6F_5CMe_3$. However, the $^1H$ and $^{19}F$ NMR spectra show a complex mixture, displaying numerous broad and sharp resonances, indicating that a mixture of compounds had been formed.

## Y(III) boroxide complexes

As mentioned in Chapter 2, yttrium alkoxides and aryloxides have been widely explored, mostly used as catalysts for polymerisation of lactide and other monomers.[117-119] Here, the synthesis and characterisation of two new boroxide yttrium complexes and their reactivity towards small molecules is detailed.

## 3.6. Synthesis and characterisation of $[Y(OBMes_2)_3]$ (21)

Only one structurally characterised group three metal boroxide has been reported in the literature. Complex $[XSc\{OB(C_6F_5)_2\}_2]$ (X = $HC\{H_2NCH_2CH_2NCMe\}_2$) was formed by reaction of $[Sc(Br)(MgBrX)_2]$ with $H_2O{\cdot}B(C_6F_5)_3$ as a method of controlled hydrolysis. The water was reduced and the metal oxidised to $Sc^{III}$.[120]

Treating an ice cold, colourless THF solution of $[YCl_3(THF)_2]$ with 2.8 equivalents of $NaOBMes_2$ provided $[Y(OBMes_2)_3]$ (**21**) as a colourless solid in 83% yield after stirring

at r.t. overnight. The reaction mixture was evaporated to dryness and washed with hexane. Complex **21** was characterised by $^{1}H$ and $^{11}B$ NMR spectroscopies and elemental analysis. Despite considerable effort, single crystals for XRD characterisation were not obtained. The $^{1}H$ and $^{11}B$ NMR spectra show the corresponding resonances of the mesityl ligand in a diamagnetic environment.


Scheme 3.24. Synthesis of yttrium boroxide complex **21**.

## 3.7. Reactivity of [Y(OBMes$_2$)$_3$] (21)

As mentioned in Chapter 2, Evans and co-workers have published the activation of dinitrogen,[121, 122] carbon monoxide,[123, 124] carbon dioxide,[124, 125] nitrogen monoxide[126, 127] and sulfur[124, 128] with yttrium complexes.

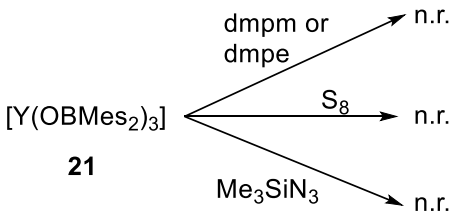


Scheme 3.25. No-reactivity of yttrium complex **21**.

Reactivity towards elemental sulfur, $Me_3SiN_3$, and the diphosphines dmpm and dmpe was examined with [Y(OBMes$_2$)$_3$]. However, addition of stoichiometric amounts of these reagents to solutions of **21** did not result in any observable change in the $^{1}H$ and $^{11}B$ NMR spectra.

## 3.8. Synthesis and characterisation of [Y(OBMes$_2^F$)$_3$] (22)

Addition of three equivalents of an off-white HOBMes$_2^F$ solution to an ice cold solution of [Y(N(SiMe$_3$)$_2$)$_3$] in toluene provided an off-white solution which was evaporated to dryness, followed by washing of the solids with cold (-78 °C) toluene. Complex [Y(OBMes$_2^F$)$_3$] (**22**) was obtained in 46% yield as colourless crystals after

recrystallisation from toluene. Complex **22** was characterised by $^{1}H$, $^{11}B$ and $^{19}F$ NMR spectroscopies, elemental analysis and single crystal XRD analysis.

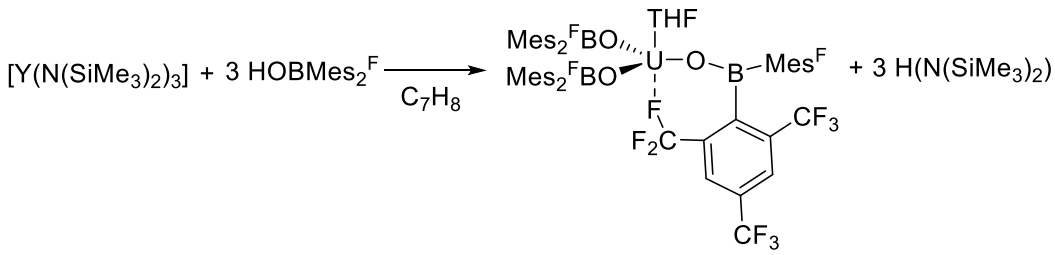


**22**

Scheme 3.26. Synthesis of fluorinated complex **22**.

Complex **22** crystallised with a molecule of coordinated THF, which came from the synthesis of the reagents, and three boroxide ligands. The five-coordinate Y centre is bound to one oxygen atom from the THF, three oxygen atoms from the boroxide ligands, and one fluorine atom from a $CF_3$ group on one of the boroxide ligands, affording a distorted trigonal bipyramidal coordination geometry (Figure 3.19).

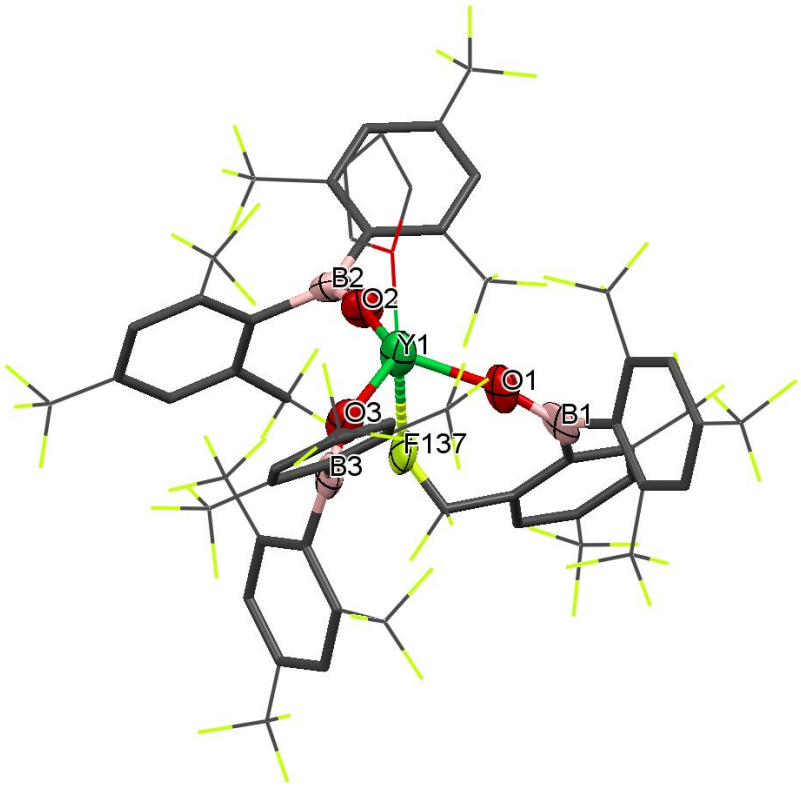


Figure 3.19. Solid-state structure of **21**. Fluorine-substituted mesityl groups and THF solvent are depicted as capped sticks and wireframe for clarity. Hydrogen atoms are omitted. The thermal ellipsoids are displayed at 50% probability.

The Y–$O_{avg}$ bond length of the boroxide ligands is 2.119 Å, which has a similar range to previously reported yttrium tris(aryloxide) complexes[129-131] such as [Y(OMes)$_3$], with a Y–$O_{avg}$ bond length of 2.108(6) Å.[132] In addition, the O–Y–O angles (105.5(3)°, 115.6(3)° and 128.4(3)°) are comparable to previously reported ones. Moreover, the interaction between a fluorine from a ligand and the yttrium centre is not unprecedented, although rare. The Y···$F_{137}$ distance is 2.520(6) Å which is similar to complex [HC{SiMe$_2$N(2-FC$_6$H$_4$)}$_3$Y(OEt$_2$)], in which the three fluorine atoms interact with the yttrium centre (Y···$F_{avg}$ distance is 2.48(4) Å),[133] and complex [(C$_5$H$_4$SiMe$_3$)$_2$Y][MeB(C$_6$F$_5$)$_3$], in which the anion interacts in a chelating fashion via one *ortho*-fluorine atom (Y···F distance is 2.336(3) Å).[134] In addition F–Y–O angle is 73.1(2)° which is in agreement with previously reported F–Y–Ligand angles.[133, 135]

## 3.9. Reactivity of [Y(OBMes$_2^F$)$_3$] (22)

Similarly to complex **21**, the reactivity of fluorine-substituted complex **22** towards small molecules was investigated (Scheme 3.27).

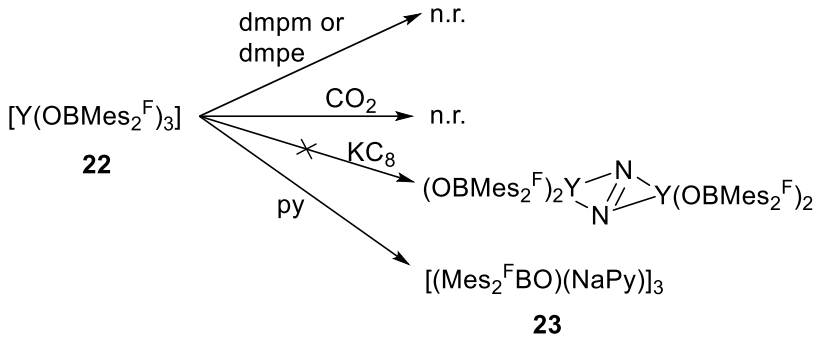


Scheme 3.27. No-reactivity of complex **22**.

Exposure of a yellow solution of [Y(OBMes$_2^F$)$_3$] to one atmosphere of $CO_2$ did not give any appreciable change in the $^1$H, $^{11}$B and $^{19}$F NMR spectra. The most probable cause for the lack of reactivity is the smaller size of yttrium when compared to uranium which makes it inaccessible for small molecule activation. The addition of one equivalent of $KC_8$ in the presence of 18-crown-6 resulted in the formation of pale pink crystals which contained a mixture of [Y(OBMes$_2^F$)$_3$] and other minor products.

Moreover, the addition of stoichiometric amounts of the diphosphines, dmpm or dmpe, to a solution of complex **22** did not produce any observable changes in the $^1$H, $^{11}$B and $^{19}$F NMR spectra. However, colourless crystals suitable for single-crystal X-ray crystallography were grown from slow diffusion of hexane into a pyridine reaction mixture, which showed the formation of the boroxine, [(Mes$_2^F$BO)(NaPy)]$_3$ (**23**) (Figure 3.20).

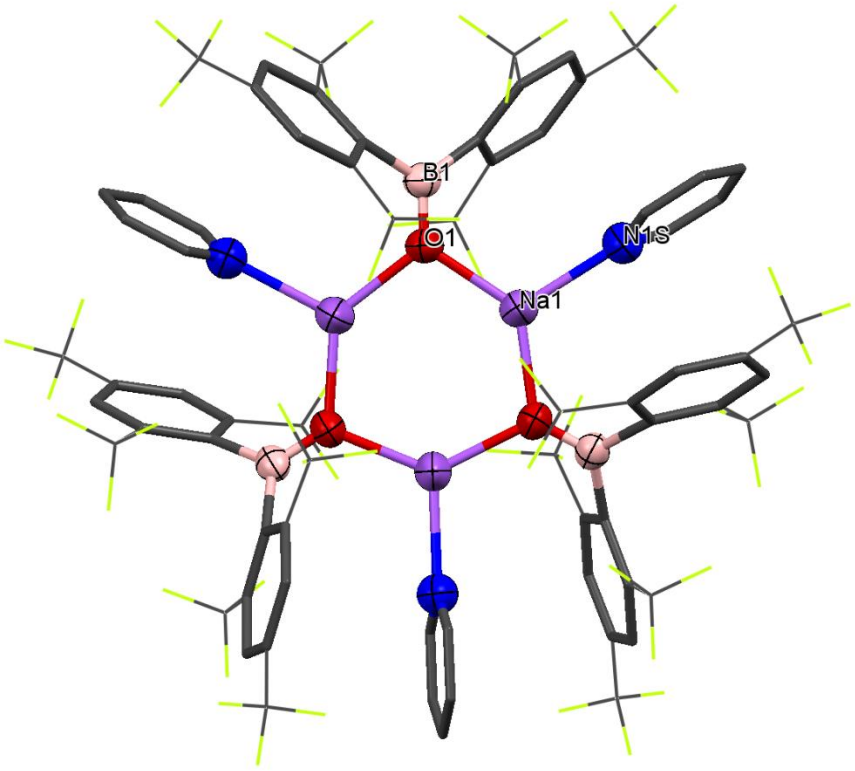


Figure 3.20. Solid-state structure of **23**. Fluorine-substituted mesityl groups and pyridine solvent are depicted as capped sticks and wireframe for clarity. Hydrogen atoms are omitted. The thermal ellipsoids are displayed at 50% probability.

The solid-state structure of complex **23** presents an almost planar six-membered ring of Na–O units. The Na–O distance is 2.076(14) Å, which is shorter than the previously reported Na–O rings in $[Na_6(Ph_2CHO)_6]$ (mean 2.25(5) Å).[136] Moreover, the Na–O–Na angles are 108.86° and the O–Na–O angles are 131.14°, confirming the formation planar six-membered ring.

## 3.10. Chapter summary and conclusions

The new $U^{III}$ boroxide complex $[U(OBMes_2)_2(\mu\text{-}OBMes_2)]_2$ (**1**) has proven to be able to activate a wide range of molecules. Complex **1** is able to coordinate oxygen donor molecules such as pyridine N-oxide and triphenylphosphine oxide to form complexes **2** and **3** respectively.

Moreover, complex **1** is capable of reducing elemental sulfur to yield the tetra-chalcogenide bridged complex **5**, which contains two uranium(V) centres. Reaction with carbodiimide DCC provided the metallacycle **6** via coupling by the U centres to form the rearranged cyclohexyl-substituted guanidinate ligand.

Reactivity towards small gaseous molecules such as CO and $CO_2$ was investigated. However, no reaction was observed upon exposure of complex **1** to an atmosphere of CO or $CO_2$ due to the inaccessibility of the uranium centres.

Interestingly, the reaction of complex **1** with phosphines $PMe_3$, $PEt_3$, $PCy_3$ and diphosphines dmpm and dmpe provided the synthesis of different uranium inverse arene sandwich complexes with and without coordinated phosphine, complexes **8**, **10**, **14** and **16**. This is the first time that phosphine coordination has played a role in the formation of uranium inverse arene sandwich complexes as stabiliser towards intermediates and preventing decomposition, thus this coordination is crucial in the reaction mechanism.

Complex **1** is extremely sensitive to the presence of oxygen and it rapidly forms the oxygen-bridged complex **7** upon contact with traces of oxygen. Exposure of complex **1** to an atmosphere of oxidant gas $N_2O$ also provides complex **7**.

Finally, yttrium boroxide complex **21** and fluorine-substituted complex **22** were synthesised. However, neither showed further reactivity towards chalcogens, $CO_2$, azides or phosphines, indicating that yttrium might be too small, thus being inaccessible for small molecule activation.

## 3.11. Bibliography

[1] S. M. Mansell, N. Kaltsoyannis, P. L. Arnold, *J. Am. Chem. Soc.* **2011**, *133*, 9036-9051.

[2] P. L. Arnold, *Chem. Commun.* **2011**, *47*, 9005-9010.

[3] S. T. Liddle, *Angew. Chem. Int. Ed.* **2015**, *54*, 8604-8641.

[4] I. Korobkov, S. Gorelsky and S. Gambarotta, *J. Am. Chem. Soc.*, 2009, **131**, 10406-10420.

[5] V. Manguel, C. Camp, J. Pécaut, C. Copéret, L. Maron, C. E. Kefadilis, M. Mazzanti, *Angew. Chem. Int. Ed.* **2012**, *51*, 12280-12284.

[6] J. A. L. Wells, *Ph.D. thesis*, University of Edinburgh **2018**.

[7] D. S. J. Arney, C. J. Burns, *J. Am. Chem. Soc.* **1995**, *117*, 9448-9460.

[8] D. S. J. Arney, C. J. Burns, *J. Am. Chem. Soc.* **1993**, *115*, 9840-9841.

[9] O. Cooper, C. Camp, J. Pécaut, C. E. Kefalidis, L. Maron, S. Gambarelli, M. Mazzanti, *J. Am. Chem. Soc.* **2014**, *136*, 6716-6723.

[10] S. J. Kraft, J. Walensky, P. E. Fanwick, M. B. Hall, S. C. Bart, *Inorg. Chem.* **2010**, *49*, 7620-7622.

[11] A.C. Schmidt, F. W. Heinemann, W. W. Lukens, K. Meyer, *J. Am. Chem. Soc.* **2014**, *136*, 11980-11993.

[12] L. R. Avens, D. M. Barnhart, C. J. Burns, S. D. McKee, W. H. Smith, *Inorg. Chem.* **1994**, *33*, 4245-4254.

[13] A. J. Lewis, U. J. Williams, J. M. Kikkawa, P. J. Carroll, E. J. Schelter, *Inorg. Chem.* **2012**, *51*, 37-39.

[14] N. L. Bell, P. L. Arnold, J. B. Love, *Dalton Trans.* **2016**, *45*, 15902-15909.

[15] J. A. Pool, B. L. Scott, J. L. Kiplinger, *J. Am. Chem. Soc.* **2005**, *127*, 1338-1339.

[16] N. A. Sildake, J. Le Duc, J. W. Ziller, W. J. Evans, *Chem. – A Eur. J.* **2012**, *18*, 14820-14827.

[17] J.C. Berthet, M. Nierlich, M. Ephritikhine, *Dalton Trans.* **2004**, 2814-2821.

[18] S. Kannan, M. A. Moody, C. L. Barnes, P. B. Duval, *Inorg. Chem.* **2006**, *45*, 9206-9212.

[19] J. J. Kiernicki, J. S. Harwood, P. E. Fanwick, S. C. Bart, *Dalton Trans.* **2016**, *45*, 3111-3119.

[20] T. W. Hayton, J. M. Boncella, B. L. Scott, E. R. Batista, P. J. Hay, *J. Am. Chem. Soc.* **2006**, *128*, 10549-10559.

[21] R. E. Jilek, L. P. Spencer, R. A. Lewis, B. L. Scott, T. W. Hayton, J. M. Boncella, *J. Am. Chem. Soc.* **2012**, *134*, 9876-9878.

[22] R. E. Jilek, N. C. Tomson, B. L. Scott, J. M. Boncella, *Inorg. Chim. Acta* **2014**, *422*, 78-85.

[23] J.C. Berthet, M. Nierlich, M. Ephritikhine, *Polyhedron* **2003**, *22*, 3475-3482.

[24] H. Yin, A. J. Lewis, U. J. Williams, P. J. Carroll, E. J. Schelter, *Chem. Sci.* **2013**, *4*, 798-805.

[25] Z. Yang, X. Ma, R. B. Oswald, H. W. Roesky, M. Noltemeyer, *J. Am. Chem. Soc.* **2006**, *128*, 12406-12407.

[26] X. Ma, Z. Yang, X. Wang, H. W. Roesky, F. Wu, H. Zhu, *Inorg. Chem.* **2011**, *50*, 2010-2014.

[27] Z. Yang, P. Hao, Z. Liu, X. Ma, H. W. Roesky, J. Li, *J. Organomet. Chem.* **2014**, *751*, 788-791.

[28] M. Kořenková, B. Mairychová, R. Jambor, Z. Růžičková, L. Dostál, *Inorg. Chem. Commun.* **2014**, *47*, 128-130.

[29] M. Kořenková, M. Erben, R. Jambor, A. Růžička, L. Dostál, *J. Organomet. Chem.* **2014**, *772-773*, 287-291.

[30] B. Mairychová, T. Svoboda, P. Štěpnička, A. Růžička, R. W. A. Havenith, M. Alonso, F. D. Proft, R. Jambor, L. Dostál, *Inorg. Chem.* **2013**, *52*, 1424-1431.

[31] B. Mairychová, P. Štěpnička, A. Růžička, L. Dostál, R. Jambor, *Organometallics* **2014**, *33*, 3021-3029.

[32] B. Mairychová, I. V. Kityk, A. Maciag, F. Bureš, M. Klikar, A. Růžička, L. Dostál, R. Jambor, *Inorg. Chem.* **2016**, *55*, 1587-1594.

[33] L. Dostál, R. Jambor, A. Růžička, R. Jirásko, A. Lyčka, J. Beckmann, S. Ketkov, *Inorg. Chem.* **2015**, *54*, 6010-6019.

[34] M. Kořenková, B. Mairychová, A. Růžička, R. Jambor, L. Dostál, *Dalton Trans.* **2014**, *43*, 7096-7108.

[35] U. Bossek, H. Hummel, T. Weyhermüller, K. Wieghardt, S. Russell, L. van der Wolf, U. Kolb, *Angew. Chem. Int. Ed.* **1996**, *35*, 1552-1554.

[36] A. R. Browne, N. Deligonul, B. L. Anderson, M. Zeller, A. D. Hunter, T. G. Gray, *Chem. Commun.* **2015**, *51*, 15800-15803.

[37] N. A. Ayoub, A. R. Browne, B. L. Anderson, T. G. Gray, *Dalton Trans.* **2016**, *45*, 3820-3830.

[38] I. Pantcheva, K. Osakada, *Organometallics* **2006**, *25*, 1735-1741.

[39] K. I. M. Ingram, N. Kaltsoyannis, A. J. Gaunt, M. P. Neu, *J. Alloys Compd.* **2007**, *444-445*, 369-375.

[40] H. H. Dam, D. N. Reinhoudt, W. Verboom, *Chem. Soc. Rev* .**2007**, *36*, 367-377.

[41] S. R. Daly, J. M. Keith, E. R. Batista, K. S. Boland, D. L. Clark, S. A. Kozimor, R. L. Martin, *J. Am. Chem. Soc.* **2012**, *134*, 14408-14422.

[42] D. E. Smiles, G. Wu, P. Hrobárik, T. W. Hayton, *J. Am. Chem. Soc.* **2016**, *138*, 814-825.

[43] S. M. Franke, F. W. Heinemann, K. Meyer, *Chem. Sci.* **2014**, *5*, 942-950.

[44] B. Meyer, *Chem. Rev.* **1976**, *76*, 367-388.

[45] B. M. Gardner, D. M. King, F. Tuna, A. J. Wooles, N. F. Chilton, S. T. Liddle, *Chem. Sci.* **2017**, *8*, 6207-6217.

[46] D. E. Smiles, G. Wu, T. W. Hayton, *New J. Chem.* **2015**, *39*, 7563-7566.

[47] D. L. Perry, A. Zalkin, H. Ruben, D. H. Templeton, *Inorg. Chem.* **1982**, *21*, 237-240.

[48] D. J. Grant, Z. Weng, L. J. Jouffret, P. C. Burns, L. Gagliardi, *Inorg. Chem.* **2012**, *51*, 7801-7809.

[49] J. L. Brown, G. Wu, T. W. Hayton, *Organometallics* **2013**, *32*, 1193-1198.

[50] M. E. Maston., D. M. Goshert., J. J. Kiernicki., S. B. Newell., E. P. Fanwick., P. M. Shores., R. J. Walensky., C. S. Bart., *Chem. – A Eur. J.***2013**, *19*, 16176-16180.

[51] A. C. Sutorik, M. G. Kanatzidis, *Polyhedron* **1997**, *16*, 3921-3927.

[52] J.E. Kwak, D. L. Gray, H. Yun, J. A. Ibers, *Acta Cryst. Sect. E* **2006**, *62*, i86-i87.

[53] C. Camp, M. A. Antunes, G. Garcia, I. Ciofini, I. C. Santos, J. Pecaut, M. Almeida, J. Marcalo, M. Mazzanti, *Chem. Sci.* **2014**, *5*, 841-846.

[54] A. Terzis, R. Rivest, *Inorg. Chem.* **1973**, *12*, 2132-2136.

[55] R. C. Elder, M. Trkula, *Inorg. Chem.* **1977**, *16*, 1048-1051.

[56] T. J. York., C. E. Brown., B. W. Tolman., *Angew. Chem. Int. Ed.* **2005**, *44*, 7745-7748.

[57] S. Yao, C. Milsmann, E. Bill, K. Wieghardt, M. Driess, *J. Am. Chem. Soc.* **2008**, *130*, 13536-13537.

[58] W. J. Evans, J. R. Walensky, J. W. Ziller, A. L. Rheingold, *Organometallics* **2009**, *28*, 3350-3357.

[59] W. J. Evans, M. K. Takase, J. W. Ziller, A. L. Rheingold, *Organometallics* **2009**, *28*, 5802-5808.

[60] M. K. Takase, N. A. Siladke, J. W. Ziller, W. J. Evans, *Organometallics* **2011**, *30*, 458-465.

[61] O. J. Cooper, D. P. Mills, W. Lewis, A. J. Blake, S. T. Liddle, *Dalton Trans.* **2014**, *43*, 14275-14283.

[62] M. A. Boreen, B. F. Parker, T. D. Lohrey, J. Arnold, *J. Am. Chem. Soc.* **2016**, *138*, 15865-15868.

[63] W. J. Evans, J. R. Walensky, J. W. Ziller, *Organometallics* **2010**, *29*, 101-107.

[64] W. J. Evans, J. R. Walensky, J. W. Ziller, *Inorg. Chem.* **2010**, *49*, 1743-1749.

[65] N. A. Siladke, J. W. Ziller, W. J. Evans, *J. Am. Chem. Soc.* **2011**, *133*, 3507-3516.

[66] L. Zhang, C. Zhang, G. Hou, G. Zi, M. D. Walter, *Organometallics* **2017**, *36*, 1179-1187.

[67] L. Zhang, G. Hou, G. Zi, W. Ding, M. D. Walter, *J. Am. Chem. Soc.* **2016**, *138*, 5130-5142.

[68] L. Zhang, B. Fang, G. Hou, G. Zi, W. Ding, M. D. Walter, *Organometallics* **2017**, *36*, 898-910.

[69] G. Zi, *Chem. Commun.* **2018**, *54*, 7412-7430.

[70] F. G. N. Cloke, P. B. Hitchcock, *J. Am. Chem. Soc.* **2002**, *124*, 9352-9353.

[71] O. T. Summerscales, F. G. N. Cloke, P. B. Hitchcock, J. C. Green, N. Hazari, *Science* **2006**, *311*, 829-831.

[72] O. T. Summerscales, F. G. N. Cloke, P. B. Hitchcock, J. C. Green, N. Hazari, *J. Am. Chem. Soc.* **2006**, *128*, 9602-9603.

[73] S. M. Mansell, J. H. Farnaby, A. I. Germeroth, P. L. Arnold, *Organometallics* **2013**, *32*, 4214-4222.

[74] P. L. Arnold, Z. R. Turner, *Nat. Rev. Chem.* **2017**, *1*, 0002.

[75] J. G. Brennan, A. Zalkin, *Acta Cryst. Sect. C* **1985**, *41*, 1038-1040.

[76] P. G. Edwards, R. A. Andersen, A. Zalkin, *J. Am. Chem. Soc.* **1981**, *103*, 7792-7794.

[77] M. R. Duttera, V. W. Day, T. J. Marks, *J. Am. Chem. Soc.* **1984**, *106*, 2907-2912.

[78] L. P. Spencer, R. L. Gdula, T. W. Hayton, B. L. Scott, J. M. Boncella, *Chem. Commun.* **2008**, 4986-4988.

[79] D. L. Swartz Ii, L. P. Spencer, B. L. Scott, A. L. Odom, J. M. Boncella, *Dalton Trans.* **2010**, *39*, 6841-6846.

[80] B. S. Newell, T. C. Schwaab, M. P. Shores, *Inorg. Chem.* **2011**, *50*, 12108-12115.

[81] S. R. Daly, G. S. Girolami, *Inorg. Chem.* **2010**, *49*, 5157-5166.

[82] P. L. Diaconescu, P. L. Arnold, T. A. Baker, D. J. Mindiola, C. C. Cummins, *J. Am. Chem. Soc.* **2000**, *122*, 6108-6109.

[83] D. P. Mills, F. Moro, J. McMaster, J. van Slageren, W. Lewis, A. J. Blake, S. T. Liddle, *Nat. chem.* **2011**, *3*, 454-460.

[84] M. J. Monreal, S. I. Khan, J. L. Kiplinger, P. L. Diaconescu, *Chem. Commun.* **2011**, *47*, 9119-9121.

[85] W. J. Evans, S. A. Kozimor, J. W. Ziller, N. Kaltsoyannis, *J. Am. Chem. Soc.* **2004**, *126*, 14533-14547.

[86] S. T. Liddle, *Coord. Chem. Rev.* **2015**, *293-294*, 211-227.

[87] P. L. Arnold, S. M. Mansell, L. Maron, D. McKay, *Nat. chem.* **2012**, *4*, 668-674.

[88] J. D. Rinehart, T. D. Harris, S. A. Kozimor, B. M. Bartlett, J. R. Long, *Inorg. Chem.* **2009**, *48*, 3382-3395.

[89] O. Madelung, Ed *Landolt-Börnstein : Numerical Data and Functional Relationship in Science and Technology, Vol. 15*, Springer, Berlin, **1987**.

[90] C. Camp, V. Mougel, J. Pécaut, L. Maron, M. Mazzanti, *Chem. – A Eur. J.* **2013**, *19*, 17528-17540.

[91] F. A. Cotton, W. Schwotzer, C. Q. Simpson, *Angew. Chem. Int. Ed.* **1986**, *25*, 637-639.

[92] D. Baudry, E. Bulot, P. Charpin, M. Ephritikhine, M. Lance, M. Nierlich, J. Vigner, *J. Organomet. Chem.***1989**, *371*, 155-162.

[93] M. R. Duttera, P. J. Fagan, T. J. Marks, V. W. Day, *J. Am. Chem. Soc.* **1982**, *104*, 865-867.

[94] J. Plíva, J. W. C. Johns, L. Goodman, *J. Mol. Spectrosc.* **1990**, *140*, 214-225.

[95] F. A. Cotton, W. Schwotzer, *Organometallics* **1985**, *4*, 942-943.

[96] G. C. Campbell, F. A. Cotton, J. F. Haw, W. Schwotzer, *Organometallics* **1986**, *5*, 274-279.

[97] P. L. Diaconescu, C. C. Cummins, *J. Am. Chem. Soc.* **2002**, *124*, 7660-7661.

[98] D. Patel, F. Moro, J. McMaster, W. Lewis, A. J. Blake, S. T. Liddle, *Angew. Chem. Int. Ed.* **2011**, *50*, 10388-10392.

[99] P. L. Diaconescu, C. C. Cummins, *Inorg. Chem.* **2012**, *51*, 2902-2916.

[100] B. Vlaisavljevich, P. L. Diaconescu, W. L. Lukens, L. Gagliardi, C. C. Cummins, *Organometallics* **2013**, *32*, 1341-1352.

[101] A. J. Wooles, W. Lewis, A. J. Blake, S. T. Liddle, *Organometallics* **2013**, *32*, 5058-5070.

[102] D. Patel, F. Tuna, E. J. L. McInnes, J. McMaster, W. Lewis, A. J. Blake, S. T. Liddle, *Dalton Trans.* **2013**, *42*, 5224-5227.

[103] J. G. Reynolds, A. Zalkin, D. H. Templeton, N. M. Edelstein, *Inorg. Chem.* **1977**, *16*, 1090-1096.

[104] P. C. Blake, M. F. Lappert, R. G. Taylor, J. L. Atwood, H. Zhang, *Inorg. Chim. Acta* **1987**, *139*, 13-20.

[105] A. Zalkin, S. M. Beshouri, *Acta Cryst. Sect. C* **1988**, *44*, 1826-1827.

[106] K. C. Mullane, T. Cheisson, E. Nakamaru-Ogiso, B. C. Manor, P. J. Carroll, E. J. Schelter, *Chem. – A Eur. J.* **2018**, *24*, 826-837.

[107] B. M. Cossairt, N. A. Piro, C. C. Cummins, *Chem. Rev.* **2010**, *110*, 4164-4177.

[108] F.H. Stephens, *Ph.D. thesis*, Massachusetts Institute of Technology, Cambridge **2004**.

[109] A. S. P. Frey, F. G. N. Cloke, P. B. Hitchcock, J. C. Green, *New. J. Chem.* **2011**, *35*, 2022-2026.

[110] D. Patel, F. Tuna, E. J. L. McInnes, W. Lewis, A. J. Blake, S. T. Liddle, *Angew. Chem. Int. Ed.* **2013**, *52*, 13334-13337.

[111] J. G. Brennan, R. A. Andersen, *J. Am. Chem. Soc.* **1985**, *107*, 514-516.

[112] M. J. Monreal, R. K. Thomson, T. Cantat, N. E. Travia, B. L. Scott, J. L. Kiplinger, *Organometallics* **2011**, *30*, 2031-2038.

[113] J. A. L. Wells, M. L. Seymour, M. Suvova, P. L. Arnold, *Dalton Trans.* **2016**, *45*, 16026-16032.

[114] A. J. Lewis, U. J. Williams, P. J. Carroll, E. J. Schelter, *Inorg. Chem.* **2013**, *52*, 7326-7328.

[115] S. M. Cornet, K. B. Dillon, C. D. Entwistle, M. A. Fox, A. E. Goeta, H. P. Goodwin, T. B. Marder, A. L. Thompson, *Dalton Trans.* **2003**, 4395-4405.

[116] M. Weydert, R. A. Andersen, R. G. Bergman, *J. Am. Chem. Soc.* **1993**, *115*, 8837-8838.

[117] K. B. Aubrecht, K. Chang, M. A. Hillmyer, W. B. Tolman, *J. Polym. Sci. A Polym. Chem.* **2001**, *39*, 284-293.

[118] K. C. Hultzsch, T. P. Spaniol, J. Okuda, *Angew. Chem., Int. Ed.* **1999**, *38*, 227-230.

[119] X. Wang, J. L. Brosmer, A. Thevenon, P. L. Diaconescu, *Organometallics* **2015**, *34*, 4700-4706.

[120] A.M. Neculai, C. C. Cummins, D. Neculai, H. W. Roesky, G. Bunkòczi, B. Walfort, D. Stalke, *Inorg. Chem.* **2003**, *42*, 8803-8810.

[121] W. J. Evans, D. S. Lee, J. W. Ziller, *J. Am. Chem. Soc.* **2004**, *126*, 454-455.

[122] M. E. Fieser, C. W. Johnson, J. E. Bates, J. W. Ziller, F. Furche, W. J. Evans, *Organometallics* **2015**, *34*, 4387-4393.

[123] B. J. Deelman, W. M. Stevels, J. H. Teuben, M. T. Lakin, A. L. Spek, *Organometallics* **1994**, *13*, 3881-3891.

[124] M. Fang, J. H. Farnaby, J. W. Ziller, J. E. Bates, F. Furche, W. J. Evans, *J. Am. Chem. Soc.* **2012**, *134*, 6064-6067.

[125] M. R. MacDonald, R. R. Langeslay, J. W. Ziller, W. J. Evans, *J. Am. Chem. Soc.* **2015**, *137*, 14716-14725.

[126] W. J. Evans, M. Fang, J. E. Bates, F. Furche, J. W. Ziller, M. D. Kiesz, J. I. Zink, *Nat. Chem.* **2010**, *2*, 644-647.

[127] I. J. Casely, Y. Suh, J. W. Ziller, W. J. Evans, *Organometallics* **2010**, *29*, 5209-5214.

[128] J. F. Corbey, M. Fang, J. W. Ziller, W. J. Evans, *Inorg. Chem.* **2015**, *54*, 801-807.

[129] S. Hamidi, G. B. Deacon, P. C. Junk, P. Neumann, *Dalton Trans.* **2012**, *41*, 3541-3552.

[130] G. B. Deacon, T. Feng, C. M. Forsyth, A. Gitlits, D. C. R. Hockless, Q. Shen, B. W. Skelton, A. H. White, *J. Chem. Soc., Dalton Trans.* **2000**, 961-966.

[131] L. A. M. Steele, T. J. Boyle, R. A. Kemp, C. Moore, *Polyhedron* **2012**, *42*, 258-264.

[132] G. B. Deacon, P. C. Junk, G. J. Moxey, *Chem. – Asian J.* **2009**, *4*, 1717-1728.

[133] H. Memmler, K. Walsh, L. H. Gade, J. W. Lauher, *Inorg. Chem.* **1995**, *34*, 4062-4068.

[134] X. Song, M. Thornton-Pett, M. Bochmann, *Organometallics* **1998**, *17*, 1004-1006.

[135] A. Lara-Sanchez, A. Rodriguez, D. L. Hughes, M. Schormann, M. Bochmann, *J. Organomet. Chem.* **2002**, *663*, 63-69.

[136] J. Geier, H. Rüegger, H. Grützmacher, *Dalton Trans.* **2006**, 129-136.

# Chapter 4 : Introduction to the catalytic formation of acrylates from $CO_2$ and $C_2H_4$

As seen in Chapter one, the use of carbon dioxide as a renewable $C_1$ feedstock has gained increasing attention in industry and academic research as an abundant, renewable and low-cost source.[1, 2]

## Introduction to acrylates

The oxidative coupling of carbon dioxide with ethene to synthesise acrylic acid and its derivates is an attractive reaction with industrial relevance due to their vast applications, e.g. in plastics, coatings, adhesives, textiles and super absorbent polymers among others, with a worldwide production over 5 million tons per year.[3] This new route could offer a cost-competitive alternative to the traditional propylene route. One of the advantages of the direct synthesis of acrylates from carbon dioxide and ethene is the atom efficiency, as both reactants are fully incorporated in the product and 62% of the mass comes from the $CO_2$ (Scheme 4.1).

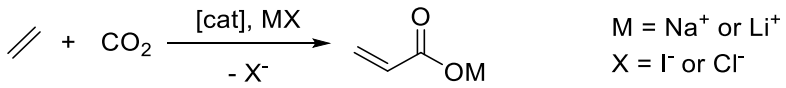


Scheme 4.1. Catalytic formation of acrylates from $CO_2$ and $C_2H_4$.

## 4.1. Nickel-based system

The synthesis of acrylates from carbon dioxide and ethene started in the early 1980s when Hoberg and co-workers synthesised a Ni-lactone from direct coupling of $CO_2$ and $C_2H_4$.[4] Since then only two catalytic approaches have been successful, one reported by Limbach, Schaub and co-workers and one by the Vogt group.[5-11] In 2006 Walther and co-workers proposed a hypothetical catalytic cycle involving: a) coordination of ethene, b) oxidative coupling of the substrates to form the Ni-lactone (**A**), c) β-hydride elimination with subsequent d) reductive elimination and e) the release of the acrylic acid (Figure 4.1).[12]

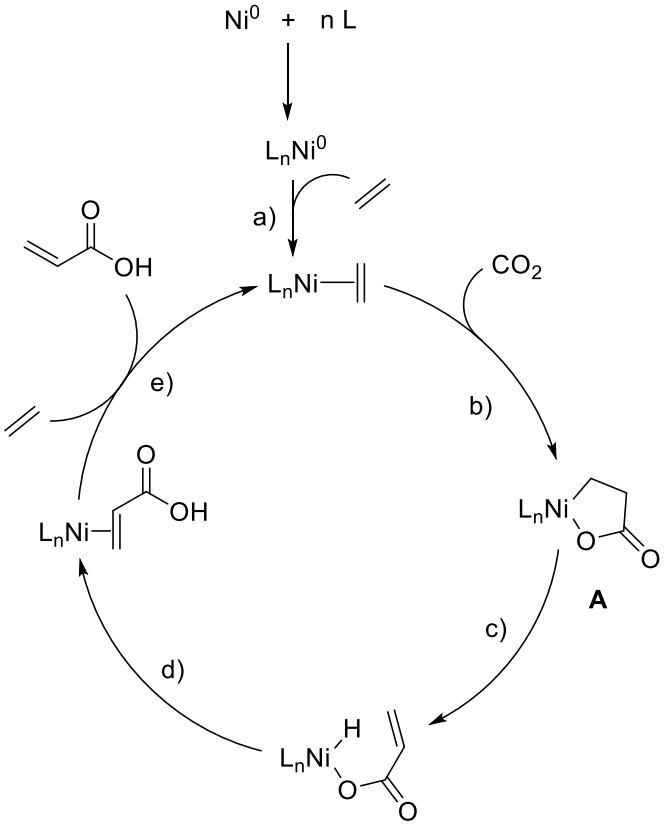


Figure 4.1. Hypothesised catalytic cycle.[12]

The main obstacles of the reaction are the endergonic nature of the overall reaction, and the high activation barrier for the β-H elimination, due to the high stability of the Ni-lactones (**A**).

### 4.1.1. Formation of Ni-lactone

Hoberg and co-workers revealed that Ni-mediated reactions of $CO_2$ and $C_2H_4$ lead to the formation of stable and isolable γ-Ni-lactone intermediates (**A**). The stability of the Ni-lactones largely depends on the ligands coordinated to the Ni centre. The first isolated Ni-lactone was synthesised as a coupling product from ethene, $CO_2$ and $Ni^0$ complex in the presence of 1,8-Diazabicyclo[5.4.0]undec-7-ene (DBU).[4] Since then many efforts have been made to understand the coupling reaction, either experimentally or by quantum mechanical studies.

Early reports on theoretical studies by Dedieu and co-workers compare the differences in the pathways of the formation of a Ni-lactone by either an alkene attacking a $CO_2$-coordinated moiety or $CO_2$ attacking on an alkene pre-coordinated in a bis-amine

$Ni^0$ system.[13]. The first conclusion was that, in both cases, the ligand has to undergo a $\eta^2 \rightarrow \eta^1$ coordination change, as the geometry of the Ni-lactone corresponds either to an $\eta^1$–$CO_2$ or to an $\eta^1$–$C_2H_4$ unit. The different coordination modes of $CO_2$ and $C_2H_4$ were analysed.

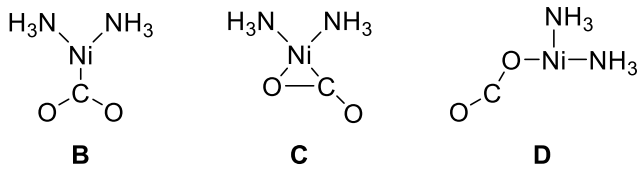


Figure 4.2. Structures for $CO_2$ coordination to bis-amine $Ni^0$ complex.[13]

It was found that the $\eta^1$ structure of a $CO_2$ coordinated (**D**, Figure 4.2) is only 1.3 kcal $mol^{-1}$ higher than the $\eta^2$ structure **C**. Both structures are therefore close in energy, whereas structure **B** was computed to be much higher in energy than **C** (by 46.8 kcal $mol^{-1}$). Moreover, the $\eta^1$ geometry for the corresponding ethene complex lies 29.0 kcal $mol^{-1}$ over the $\eta^2$-$C_2H_4$ ground state structure. Therefore, they concluded that the coupling reaction between $CO_2$ and $C_2H_4$ might involve a coordinated $CO_2$ attacked by an incoming alkene.

However, these findings were later contradicted by Pápai, Aresta and co-workers through more extensive DFT calculations. The C–C coupling between $CO_2$ and $C_2H_4$ was studied by reaction with [Ni(cdt)] (cdt = 1,5,9-Cyclododecatriene) and bipyridine (bpy) (Scheme 4.2).[14]

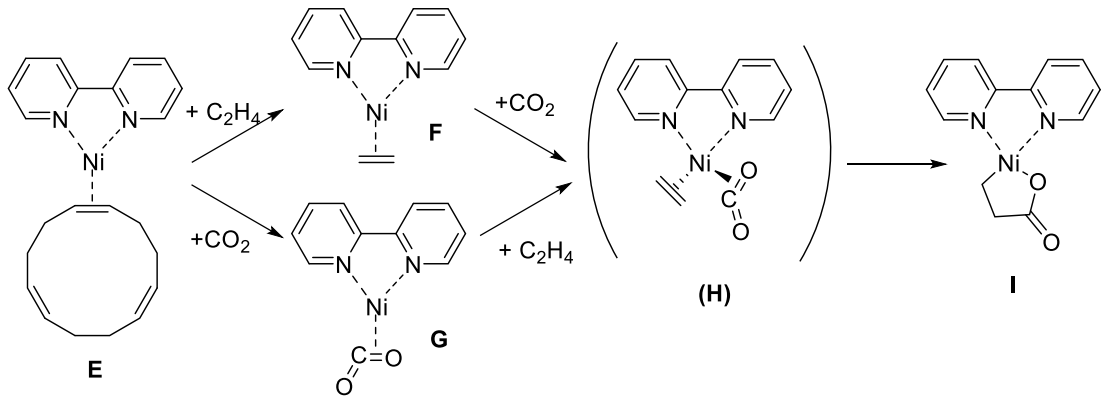


Scheme 4.2. Possible pathways for the formation of a Ni-lactone from [Ni(cdt)], bpy, $CO_2$ and $C_2H_4$.[14]

Comparing the formation of complexes **F** and **G** via the replacement of the

$\eta^2$-coordinated cdt ligand complex **E** showed that formation of **F** is energetically favoured by 8.4 kcal $mol^{-1}$, whereas the reaction of **E** with $CO_2$ is predicted to be endothermic by 1.4 kcal $mol^{-1}$. The formation of the $CO_2$ and $C_2H_4$ coordinated complex (**H**) was also studied as a possible precursor for the formation of the Ni-lactone complex **I**. However, $CO_2$ was found to be labile with a dissociation barrier of 0.8 kcal $mol^{-1}$. Moreover, the energy profile indicates that the C–C coupling does not take place through the intermediate (**H**), but occurs in a single step where $CO_2$ attacks the ethene-bound species **F**.

Several years later, Butine and co-workers investigated the formation of the Ni-lactone using DFT calculations for a [Ni(DBU)] complex. The formation of the Ni-lactone through the approach of $CO_2$ to [(DBU)Ni($C_2H_4$)] was calculated to be favoured by 85 kJ $mol^{-1}$.[15]

The effect of the ligand was investigated by Pidko and co-workers. The relative stability of the optimised structures of Ni-lactones bearing different diphosphines was examined through DTF calculations (Figure 4.3).[16]

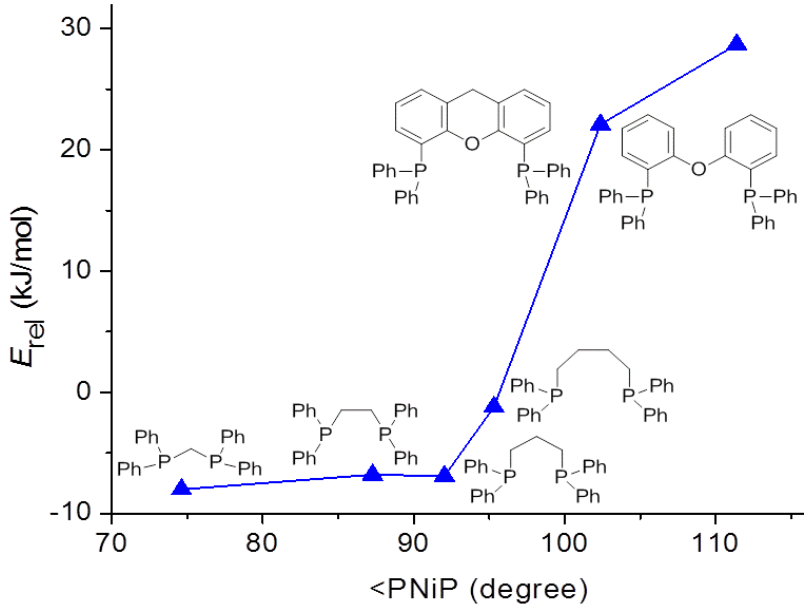


Figure 4.3. Correlation between the relative stability of the Ni-lactone intermediates and the bite angles of the respective diphosphines.[16]

A critical threshold value of 92° in the bite angle of the ligand was found, as shown in Figure 4.3. Below this threshold value the relative stability of the Ni-lactones are

similar. However, increasing of the ligand bite angle leads to substantial destabilization.

Limbach and co-workers published an extensive study on the formation of Ni-lactones combining both experimental and theoretical studies. The effect of the ligand was considered by reaction of $Ni(cod)_2$ (cod = 1,6-cyclooctadiene) and a diphosphine ligand with $CO_2$ and $C_2H_4$. Diphosphine ligands bearing diphenylphosphino substituents led to the formation of $Ni^0$ bischelate complexes **L**, whereas bulkier substituents such as *tert*-butyl provided the Ni-lactone (**J**) and the ethene coordinated complexes (**K**) (Scheme 4.3).[5]

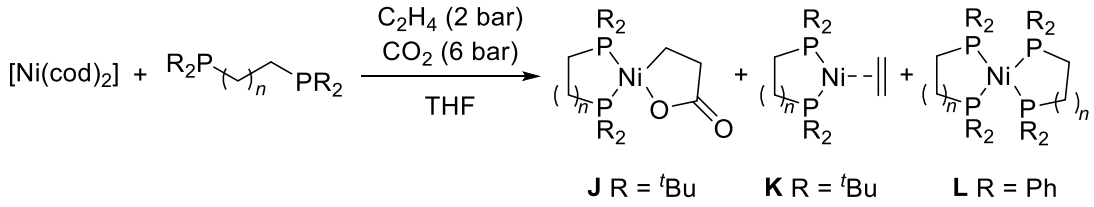


Scheme 4.3. Direct synthesis of Ni-lactones **J**, ethene complexes **K** and tetracoordinated diphosphine complexes **L**.[5]

Complementary theoretical studies, where ligand and solvent influence was taken into account, revealed an alternative mechanism for Ni-lactone formation. A competition between two mechanisms, the literature known "inner sphere" and a new "outer sphere" mechanism, was found (Scheme 4.4).[17]

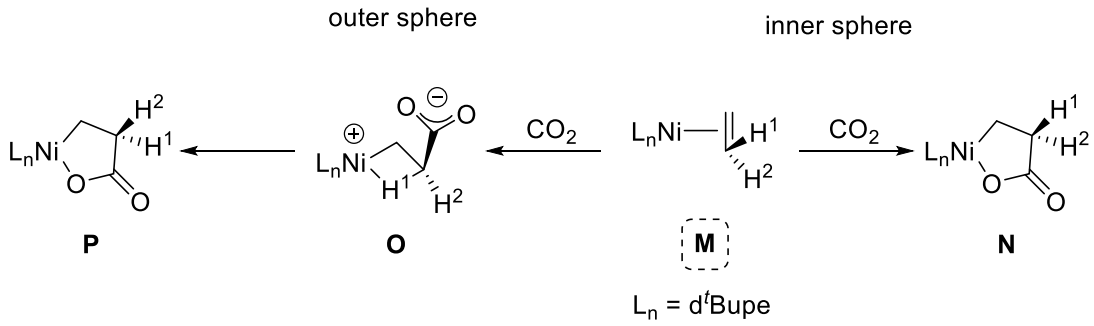


Scheme 4.4. Outer sphere and inner sphere mechanisms for the formation of a Ni-lactone with 1,2-bis(di-*tert*-butylphosphino)ethane ($d^t$Bupe) ligand.[17]

Both mechanisms were assumed to start with the ethene coordinated complex **M**, as previous reports have shown this to be the most stable starting point.[5, 14, 15] The "inner sphere" mechanism consists of the coordination of $CO_2$ to the Ni complex **M**,

followed by the insertion to the Ni–C bond, resulting in the formation of the Ni-lactone complex **N**. A weak associative pre-coordination of the $CO_2$ was found, which depends on the ligand and the level of theory used in the calculations. However, it does not indicate in any case the formation of a stable compound. On the other hand, the "outer sphere" mechanism occurs via attack of $CO_2$ to complex **M** to form the zwitterionic intermediate **O** without pre-coordination of the $CO_2$.

Although general trends were observed, straightforward assumptions on the preferences of each mechanism cannot be made, as the mechanism may vary from ligand to ligand and depending on the reaction conditions. For example, in the gas phase the "inner sphere" mechanism is preferred, but it changes when typical organic solvents such as THF are considered, although the difference is only about 4 kJ $mol^{-1}$. Moreover, electron-rich ligands lead to low barriers for both mechanisms. However, the "outer sphere" mechanism is favoured for sterically hindered ligands. According to computational calculations, the outer sphere mechanism is significantly more favoured in case of steric hindrance, since energetic barriers of the inner sphere mechanism would be more affected by steric obstacles.

### 4.1.2. Cleavage of Ni-lactone and final ligand exchange

The next step on the synthesis of acrylates from $CO_2$ and $C_2H_4$ is the productive cleavage of the Ni-lactone in order to release the acrylate derivative. Different strategies to overcome the crucial β-hydride elimination step have been used, such as addition of different auxiliaries, e.g. methylating reagents, Lewis acids or Brønsted bases.

The first evidence of a β-H elimination was described by Walther and co-workers by reacting Ni-lactones with numerous ligands as potential activators for the reaction.[12] The investigations with diphosphine ligands showed that the reaction route is strongly dependent on the length of the bridge between the two P donor atoms. Simple ligand exchange reactions were observed in most cases. Thermally stable Ni-lactone **R** (Scheme 4.5) was observed when dppe was used, whereas longer bridged diphosphines such as dppp (1,2-bis(diphenylphosphino)propane) and dppb (1,2-bis(diphenylphosphino)butane) led to the formation of unstable Ni-lactones which decomposed into bischelate $Ni^0$ complexes **S** after heating to 60 °C.

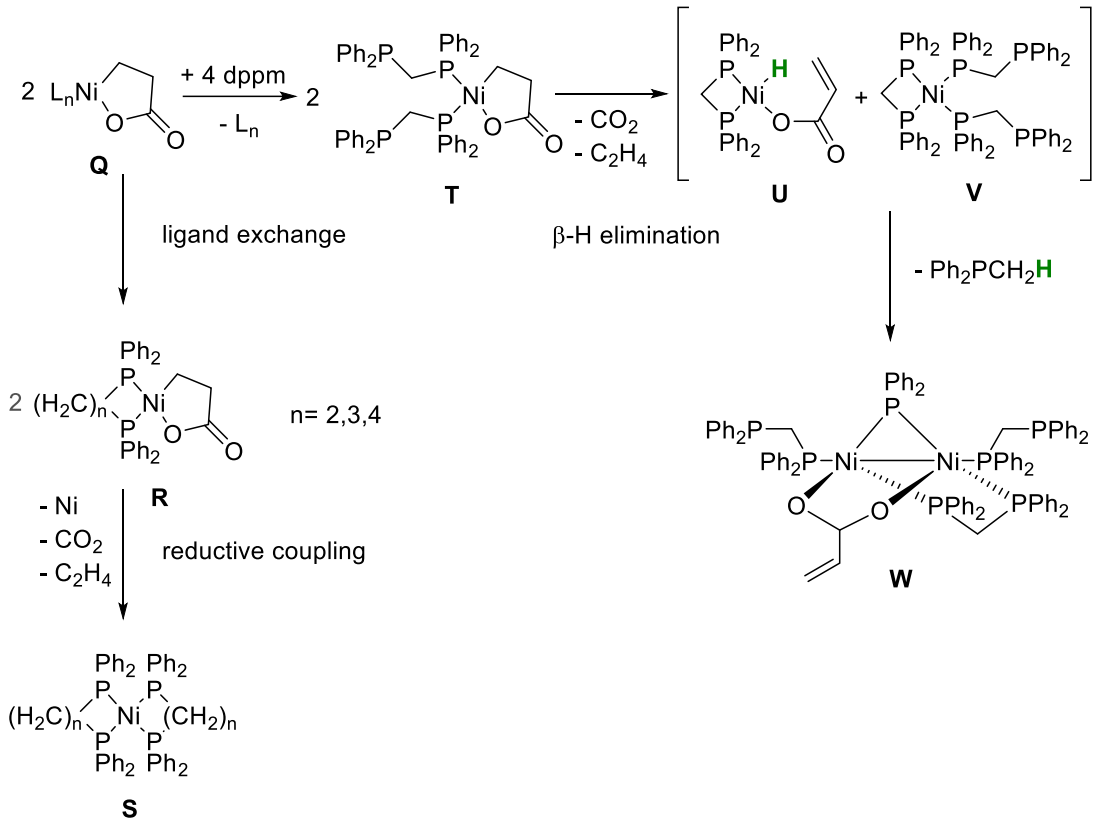


Scheme 4.5. First report of β-hydride elimination.[12]

The smaller diphosphine dppm had different reactivity, as addition of dppm to Ni-lactone complex **Q** provided the binuclear complex **W**. In order to understand the mechanism this was further investigated by reacting [(py)$_2$Ni(CH$_2$CH$_2$COO)] with excess dppm, which led to the formation of complex **T**. Subsequent β-H elimination gave the Ni-H intermediate **U**. One of the dppm ligands serves as hydride acceptor for the intermediate **U** forming the final binuclear complex **W**. This whole process is only possible with dppm as a ligand, due to the chain length and flexibility of dppm, which enables different coordination modes. However, the release of acrylic acid or acrylate was not achieved.

In 2010, Rieger and co-workers reported the liberation of methyl acrylate from Ni-lactones by addition of methylating reagents.[18] The purpose of using MeI was to activate the Ni–O bond by electrophilic attack of the Me cation with subsequent β-H elimination. The [(dppp)Ni(CH$_2$CH$_2$COO)] Ni-lactone was chosen as it does not undergo β-H elimination by thermal reaction. The addition of two equivalents of MeI to a solution of the Ni-lactone provided 10 % of methyl acrylate. The yield of the reaction increased

when the concentration of MeI was increased with a maximum yield of 33 % in neat MeI. Heating the reaction lead to decomposition of the precursor complex into $CO_2$ and $C_2H_4$. The use of other methylating agents such as $MeO^+BF_4^-$ and MeOTf (OTf = trifluoromethanesulfonate) gave 1% and no acrylate respectively. These results can be due to the low methylating activity under the applied conditions, the possible influence of sterics, and coordination features of the leaving groups. All in all, these studies showed for the first time the liberation of acrylate products from Ni-lactones.

Later on, Kühn and co-workers investigated the effect of the ligand in the cleavage of Ni-lactones when using MeI.[19] Different ligands such as tmeda (*N*,*N*,*N*′,*N*′-tetramethylethylenediamine), dppe, dppb and pyridine were used. The different ligand substituted Ni-lactones **X** (Scheme 4.6) were treated with either ten or one hundred equivalents of MeI. It was found that the ligand has a profound influence on the reactivity as tmeda-Ni-lactone delivers higher yields of methyl acrylate when compared to dppe or dppp; while dppb and py Ni-lactones do not react with MeI. NMR and *in situ* IR spectroscopies were used to study the kinetics of the reaction. A new band in the IR spectrum was observed around $\nu$ = 1680 $cm^{-1}$ and attributed to the formation of the intermediate **Y**, resulting from the cleavage of the Ni–O bond by MeI.

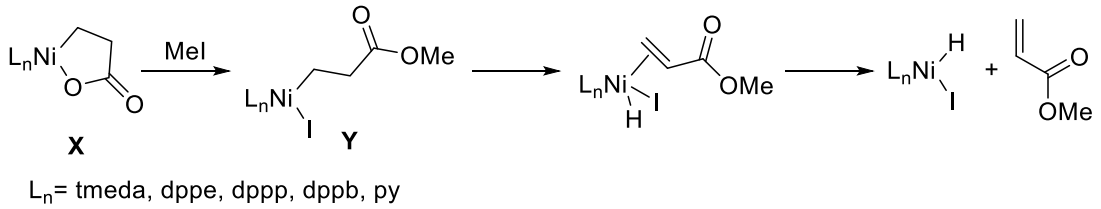


**X** **Y**

$L_n$= tmeda, dppe, dppp, dppb, py

Scheme 4.6. Reaction pathway for MeI and Ni-lactones.[19]

It was concluded that the ligand has a notable influence on the yield of methyl acrylate. Generation of methyl acrylate is favoured by Ni-lactones bearing chelating diamines or diphosphines. Moreover, loosely bound ligands created a favourable environment for the approach of the β-H elimination towards the Ni centre through partial dissociation. Therefore, the reductive elimination of the Ni-lactone to form methyl acrylate was found to be dependent on the electronic and steric effects of the ligands coordinated to the nickel atom.

Bernskoetter and co-workers investigated the effect of the neutral Lewis acid

$BAr_3^F$ as an additive in the activation of the Ni-lactone [(dppfc)Ni($CH_2CH_2COO$)] (**Z**) (dppfc = 1,1'-bis(diphenylphosphino)ferrocene) at ambient temperature (Scheme 4.7).[20]

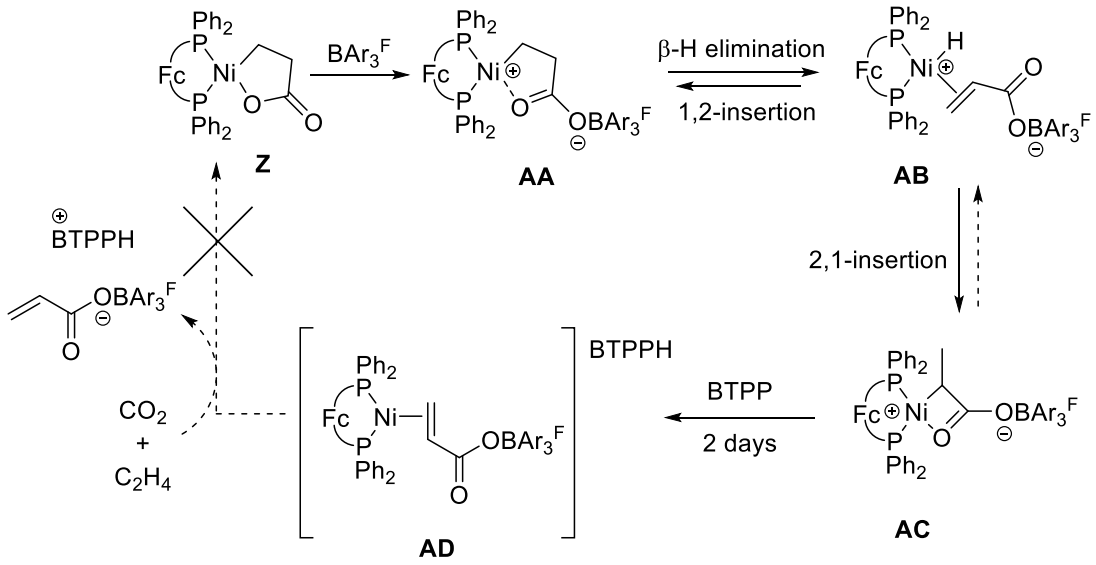


Scheme 4.7. Hypothesised catalytic cycle activated by the Lewis acid $BAr_3^F$.[20]

The reaction of the Ni-lactone **Z** with $BAr_3^F$ led to the formation of the activated Ni-lactone complex **AA**, which converted to thermodynamically stable 2,1-acryl borate complex **AC** through β-H elimination and subsequent insertion of complex **AB**. Complex **AC** was found to undergo more facile deprotonation by an external base than the starting Ni-lactone **Z**. The addition of the phosphazene base *tert*-butyliminotri (BTPP) provided the acrylate complex **AD** after two days. However, the catalytic cycle could not be closed. The treatment of **AD** with $CO_2$ and $C_2H_4$ led to the formation of the ethene bound complex [(dppfc)Ni($H_2C{=}CH_2$)] but the formation of the Ni-lactone was not detected. Nevertheless, the ability of Lewis acids to promote the ring-opening and mild bases to allow the acrylate liberation was proven, which envisaged a new path on the study involving new co-catalysts.

These findings inspired further investigations on the role of the Lewis acids in promoting the cleavage of Ni-lactones through β-H elimination. $Na^+$ was chosen as it was hypothesised to be the weakest Lewis acid that could assist the β-H elimination step. An isomerisation of the Ni-lactone from γ (**AE**) to β (**AF**) lactone was observed, both experimentally and by DFT calculations (Scheme 4.8). This process is formally equivalent to a β-H elimination followed by a 2,1-insertion.[21]

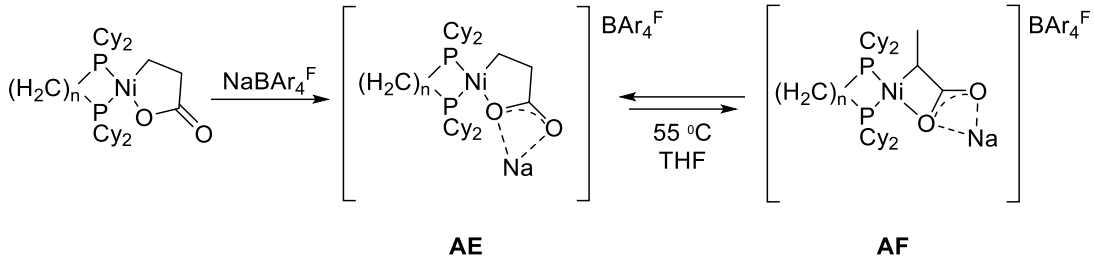


Scheme 4.8. γ-to-β isomerisation of Ni-lactones stabilised by $Na^+$.[21]

The addition of Lewis acidic $Na^+$ cation gave thermodynamic stabilisation to the β-Ni-lactone by lowering the ring strain and stabilisation of the charge on the high energy carboxylate anion intermediates, therefore lowering the overall reaction energy.

Limbach, Hofmann and co-workers carried out an extensive study on the mechanistic details of acrylate formation from Ni-lactones and MeI.[22] The methylation reaction of Ni-lactone was suggested to proceed via an $S_N2$ mechanism with a calculated activation barrier lower than 100 kJ $mol^{-1}$. This might explain the fast reaction of MeI and Ni-lactones even under mild conditions. The cationic lactone intermediates exist in equilibrium between four- and five-membered ring species, similar to the equilibrium observed by Bernskoetter.[21] The use of a weak base such as $NEt_3$ was also investigated. Deprotonation of the cationic Ni-lactones in the presence of $NEt_3$ not only led to the acrylate complex, but also to the protonated Ni-lactone, which is a strong acid that induces side reactions. Moreover, the final step in order to achieve a complete catalytic cycle is a ligand exchange reaction of the methyl acrylate with ethene. However, this step was calculated to be endergonic.

Kühn and co-workers expanded the scope of methylating reagents by using the milder dimethyl carbonate, trimethyl phosphate and 2,2-dimethoxypropane; the stronger Meerwein's reagent analogue trimethyl oxonium tetrafluoroborate; the sulfur containing MeOTf and the highly toxic dimethyl sulfate and methanesulfonate.[23] MeOTF proved to be the most effective in the ring opening and subsequent β-H elimination to finally release acrylate, being more efficient than MeI. As seen in Scheme 4.9 there is an equilibrium between the intermediate complex **AF** and the final acrylate, which is fast for all the ligands except for tmeda.

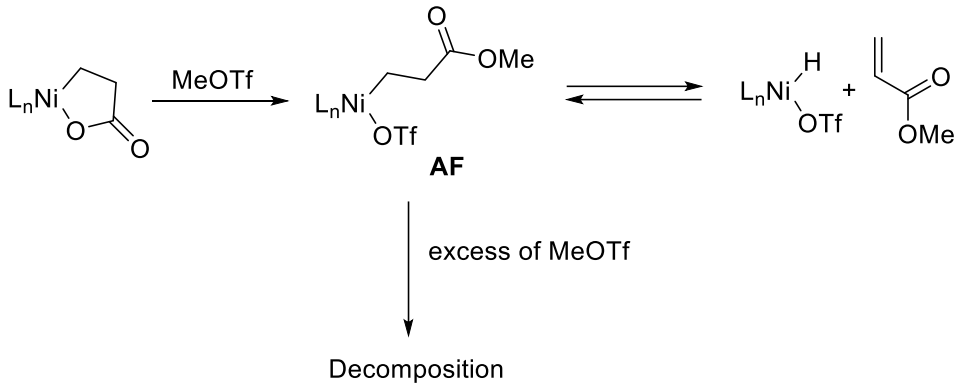


$L_n$= tmeda, dppe, dppp, dppb, d$^t$Bupe, bpy

Scheme 4.9. Proposed reaction pathway for the cleavage of Ni-lactones with MeOTf.[23]

This gave the opportunity to study in depth not only the final product, but also the intermediate via spectroscopic characterization. These findings supported the mechanism of the ring opening of the metallacycle induced by the electrophilic attack of the alkylating reagent, followed by β-H elimination. However, an excess of MeOTf led to decomposition due to coordination to the Ni centre, thus blocking the coordination site necessary for the β-H elimination.

Pidko and co-workers thorough investigations on the effect of different ligands on the catalysis confirmed that the β-H elimination should be the rate determining step in the catalytic cycle. Moreover, reductive decomposition of Ni-lactones was proved to be energetically disfavoured.[16] In addition, the electronic and steric effects on the cleavage of the Ni-lactone were studied, concluding that complexes with widely different ligand bite angles had similar energy barriers, and that the ligand environment did not significantly influence relative energies of transition states.

Moreover, the effect of bases as co-reagents was corroborated by DFT calculations. MeONa was used as a base in a dppe coordinated Ni-lactone system. The activation barrier was lowered by half when compared to the non-assisted catalysis. The formation of an adduct between between MeONa and the Ni-lactone was observed, where $Na^+$ was coordinated to the carbonyl. This coordination was preserved during the reaction. A stabilization through solvation of the $Na^+$ in MeOH was calculated, which decreased the interaction of $Na^+$ with $MeO^-$, and thus increased the effective basicity of MeONa. Finally, a study on the effect of the counter ion was conducted by switching to MeOLi, which

showed higher energy barriers indicating that not only the intrinsic base strength is a matter of choice, but also the choice of the cation.

In addition, Limbach, Hofmann and co-workers investigated possible paths for the β-H elimination of neutral Ni-lactones by DFT calculations.[17] It was concluded that β-H elimination might be possible at room temperature, giving an equilibrium between a 5- and 4-membered Ni-lactone (**AH** and **AJ** respectively, Scheme 4.10). However, formation of acrylate complex was not achieved even at high temperatures. This might be due to the absence of a low-energy path for this step.

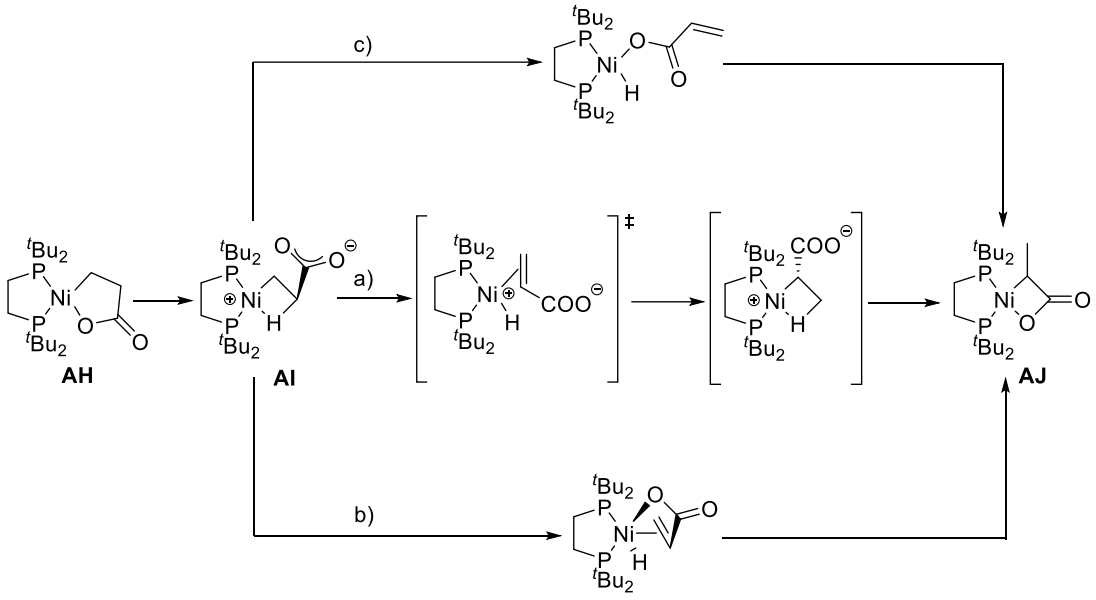


Scheme 4.10. Mechanistic rearrangement of Ni-lactones.[17]

As seen in Scheme 4.10, three different paths were proposed for the equilibrium of the 4- and 5-membered Ni-lactones. The first path a) consists of the dissociation of the carboxylate oxygen bound to the Ni and subsequent rotation of the acrylate moiety to form the 4-membered lactone. In the second path b) the oxygen stays coordinated and a trigonal bipyramidal intermediate is formed. An insertion of one of the carbons forms the 4-membered species **AI** or **AJ**. The last path c) involves the formation of the $\kappa^1$-O-coordinated hydride complex. Again, an insertion of the carbon gives either **AI** or **AJ**. Overall, the activation barrier for both directions, formation of the 4- membered and formation of the 5-membered Ni-lactones are only feasible at higher temperatures.

### 4.1.3. Catalysis with nickel

The first catalytic conversion to acrylates from $CO_2$ and ethene was reported by Limbach and co-workers, in a two-step process with a TON of 10.[5] Several bases were tested in order to deprotonate the Ni-lactone, for the subsequent release of acrylates. It was seen that strong anionic alkali-metal bases, such as NaO$^t$Bu or Na hexamethyldisilazide easily convert the Ni-lactone; while less strong bases like NaOMe or aq. NaOH required higher temperatures and longer time. Moreover, it was observed that the cation played an important role, as the Lewis acidity and the coordinative ability of sodium seemed necessary to stabilize the carboxylate formed during the course of the elimination reaction.

The proposed catalytic cycle can be divided into two parts (Scheme 4.11). The lactone formation a) occurs under $CO_2$ pressure. However, the subsequent steps b) and c) need to be carried out in absence of $CO_2$. This is due to the use of alkoxides as bases, as they irreversibly form fairly stable carbonic acid half-esters with $CO_2$. While the oxidative coupling step proceeds quickly under high pressure of $CO_2$ (40 bar), the cleavage of the Ni-lactone and subsequent release of sodium acrylate is performed in the absence of $CO_2$. A consecutive 18 cycles were needed to achieve a yield of 1.02 % of Na-acrylate, which corresponded to a catalytic turnover number of 10.

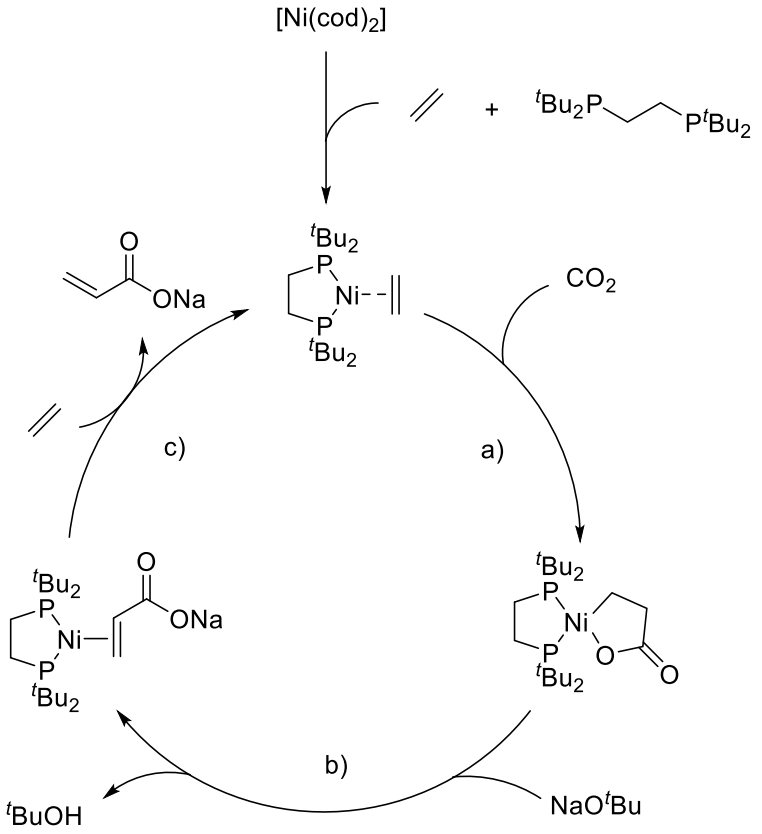


Scheme 4.11. Catalytic formation of Na-acrylate from $CO_2$, $C_2H_4$ and base.[5]

Several years later, the Vogt group reported the first one-pot catalytic formation of acrylate from ethene and $CO_2$.[11] The addition of a hard Lewis acid such as $Li^+$ was found to facilitate the β-H elimination through coordination to the carbonyl moiety, decreasing the overall free energy barrier. It was calculated that the effect of $Li^+$ led to lower energy barriers than $Na^+$. Moreover, the addition of a reductant such as Zn dust was found to be favourable as it allowed the regeneration of the catalyst by reducing the side-product $[L_nNiI_2]$ back to $[(L_n)Ni^0]$ ($L_n$ = diphosphine).

The first catalytic reaction was carried out with $Ni(cod)_2$ as catalyst precursor, 1,2-bis(dicyclohexylphosphino)ethane (dcpe) as ligand and LiI as Lewis acid salt to promote the elimination step (Scheme 4.12). $NEt_3$ was added in order to regenerate the active catalyst species by reductive elimination of HI. Moreover, after addition of Zn-dust as reducing agent higher TONs of up to 8 were achieved. TONs up to 21 were reached with dcpp as ligand.

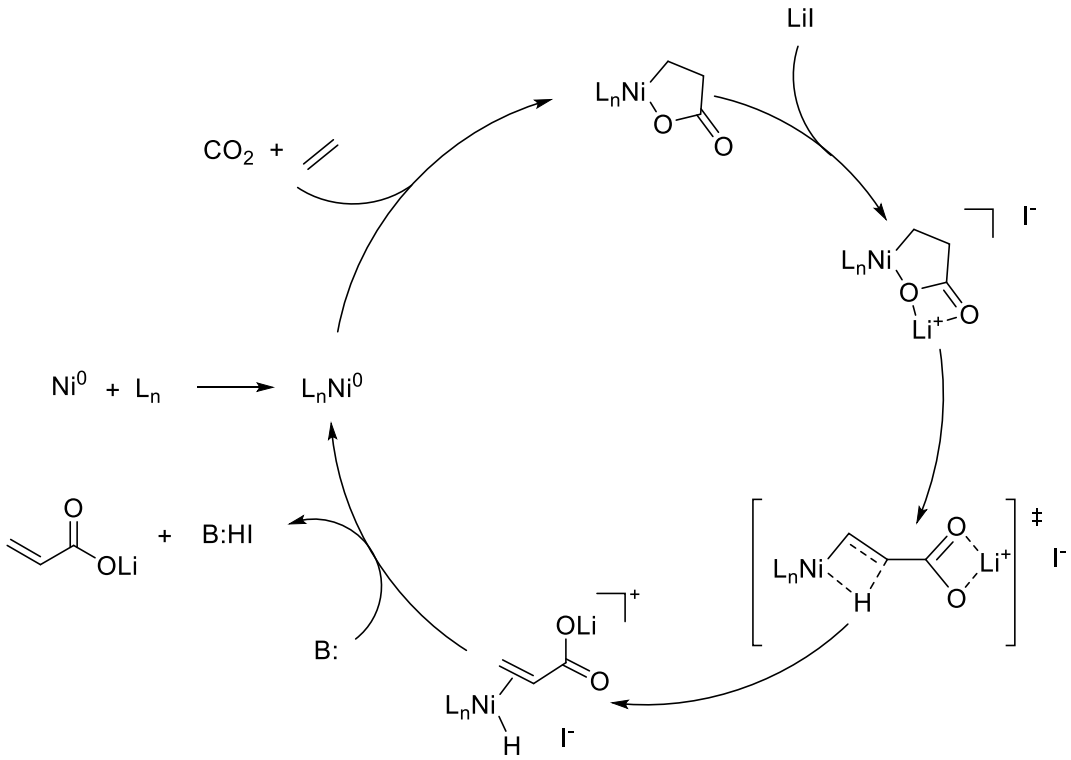


Scheme 4.12. Proposed catalytic cycle for the Lewis acid mediated formation of Li-acrylate from $CO_2$ and $C_2H_4$.[11]

A new perspective on the possible catalytic mechanism was opened, as the main difference between both approaches developed is that in the mechanism proposed by Limbach and co-workers the base is used to deprotonate the Ni-lactone that promotes the release of the acrylate; whereas in the mechanism proposed by the Vogt group the Lewis acid coordination to the carbonyl weakens the Ni–O bond and promotes the β-H elimination, and the base is used to close the cycle by elimination of the HI formed.

Shortly after, Limbach and co-workers revisited their approach to achieve a one-pot catalytic formation of acrylates (Scheme 4.13).[6] A screening of different bases was carried out. Phenolates were chosen as they are strong enough to deprotonate the Ni-lactone and less nucleophilic than alkoxides, resulting in lower reactivity towards carbon dioxide. Moreover, the steric and electronic influence can be modified by addition of different substituents. Phenolates bearing substituents with $^+$I inductive effect in *ortho* positions gave lower TONs; while substituents like fluorine, with $^-$I inductive effect, provided higher TONs for both in *ortho* and *meta* position. Sodium 2-fluorophenoxide gave the best results.

In addition, some ligands were screened resulting in higher TONs when using electron-rich P-stereogenic diphosphine ligands, carbon bridges of 2 or 3 carbons and substituents like *tert*-butyl or isopropyl on the phosphorus. The highest TON of 107 was reached with $Ni(cod)_2$ as catalyst precursor and BenzP* ((R,R)-(+)-1,2-bis(*tert*-butylmethylphosphino)benzene) as ligand. However, a large excess of Zn (50 equivalents relative to catalyst) was required.

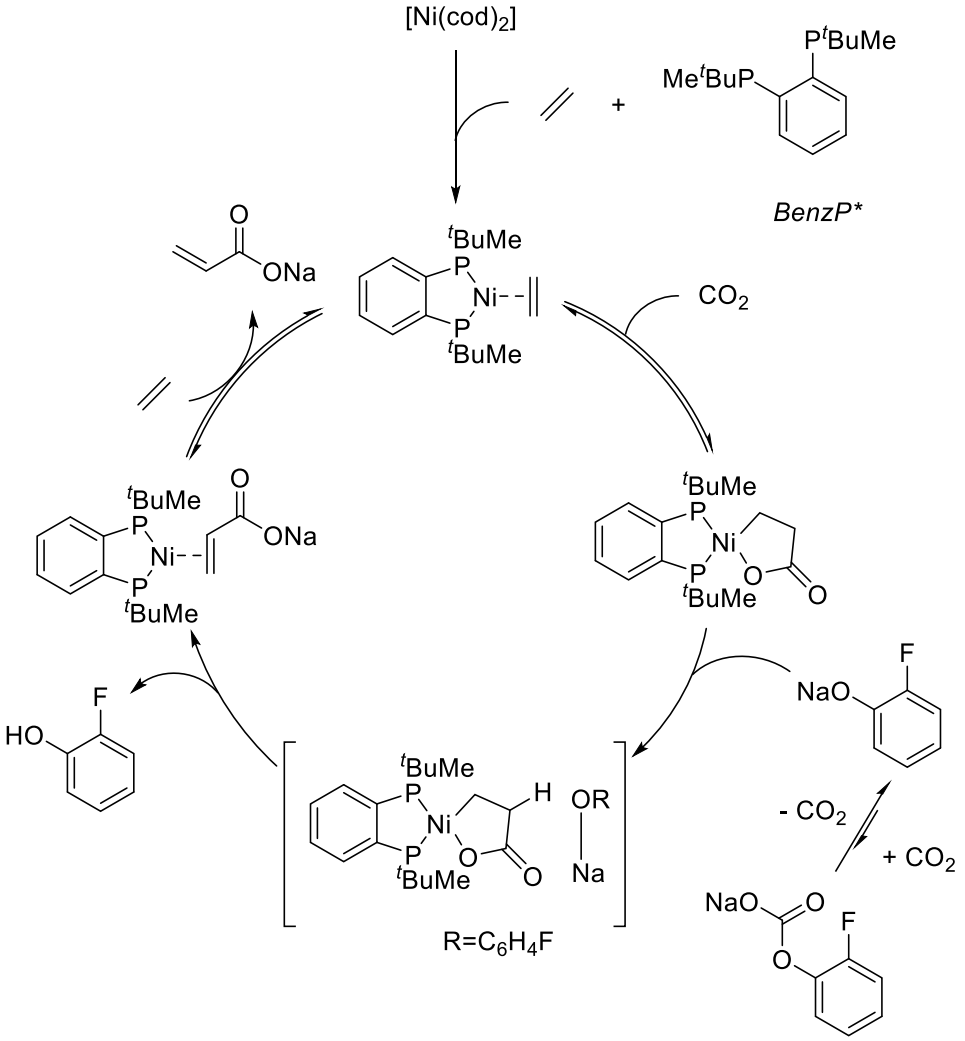


Scheme 4.13. Proposed catalytic cycle for the formation of Na-acrylate with the use of sodium 2-fluorophenoxide.[6]

The main drawback in the system is the use of an excess of Zn as a reductant. Therefore, further investigations on the reductant were carried out in a following report.[8] The main obstacles by using a solid reductant are the technical challenges in a continuous process, an increase in the cost of the production of Na-acrylate and the production of

waste. Moreover, DFT calculations have shown the formation of acrylates without the use of a reductant.[5, 17, 22] However, the activity decreased in the absence of Zn, indicating that the benefit is to prevent side reactions such as oxidations of the catalyst, confirming the role of Zn as regenerator of the catalyst. The addition of soluble $Zn^{II}$ species did not improve the catalysis.

The role of the solvent was also considered. A convenient solvent for an economic process (Figure 4.4) should provide: a) a phase separation with water, b) a high boiling point, as regeneration of the phenolate requires removal of water by distillation, c) solubility for sodium phenoxides, d) low toxicity.

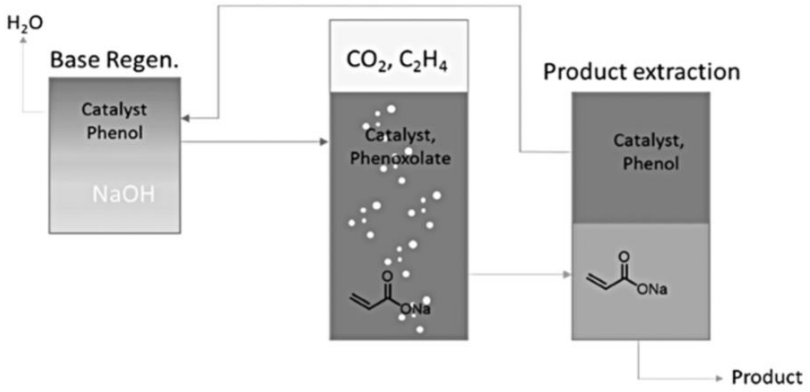


Figure 4.4. Process concept for the catalytic formation of Na-acrylate from $CO_2$, $C_2H_4$ and NaOH.[8]

The highest activity observed in previous results was achieved with non-protic, oxygen containing solvents.[5, 6, 11, 17, 22] Therefore a different range of solvents were tested, with THF, anhydrous anisole and butyl phenyl ether giving TONs of around 50. Moreover, the stability of the catalyst towards traces of water was tested, as this might be present in a continuous system. A negative impact on the catalysis was observed as the activity dropped significantly, e.g. TON dropped from 44 to 22 when wet anisole was used.[8]

Finally, a study on the improvement on the leaching of the base into the aqueous phase was carried out. Two parameters were taken into account in order to reduce the phenoxide loss into the aqueous phase: a) the amount of base was reduced by half without significant loss of activity; b) the lipophilicity of the base was tuned to reduce its solubility in water. However, increasing the steric hindrance in the *ortho*-position and the presence of *para*-substituents reduced the activity considerably.[8]

## 4.2. Pd-based systems

Since nickel was known to be active in the catalytic synthesis of acrylates from carbon dioxide and ethene, there was a growing interest in expanding the scope of metals used in catalysis. Metals which could form metallalactones were targeted as Ni-lactones have been identified as key intermediates.

When palladium was first investigated, some examples of substituted Pd-lactones had been reported,[24-26] but none had been generated by the direct reaction of an alkene and $CO_2$. However, seminal work on acrylic acid and its derivatives had been carried out. Jutand and co-workers, and Walther and co-workers reported the formation of the acrylic ester and acrylic acid palladium complexes respectively only in the presence of a rigid and bulky ferrocenyl-diphosphine ligand.[27, 28] The synthesis was carried out through reaction of [(d$^i$Prpfc)Pd(nb)] (d$^i$Prpfc = 1,1'-bis(di-*iso*-propylphosphino)ferrocene, nb = 2,5-norbornadiene) with an excess of acrylic acid in THF. (Scheme 4.14) Single X-ray crystal revealed that in [(d$^i$Prpfc)Pd($CH_2$=CHCOOH)] the ligands had the same arrangements as the related nickel acrylic acid complexes, and the formation of a dimer in the solid state with hydrogen bonding between the −COOH groups was observed.

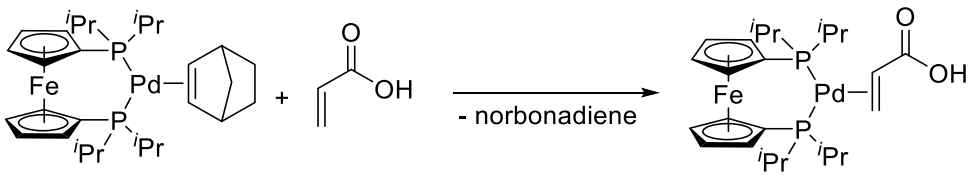


Scheme 4.14. Synthesis of low-valent palladium acrylic acid complex.[28]

Similarly to Ni-lactones, the ring opening of Pd-lactones might be the key step of the catalytic conversion of $CO_2$ and $C_2H_4$ to acrylates. Kühn and co-workers investigated the ring opening of Pd-lactones with different methylating agents.[23] As there were no reports of direct formation of Pd-lactones by reaction of $CO_2$ and $C_2H_4$, two model Pd-lactones **AK** and **AL** (Scheme 4.15) were synthesized. They differ in the denticity of the phosphine ligands and the substituents on the α-carbon. Both Pd-lactones were treated with methyl iodide and methyl triflate as methylating agents, enabling the ring opening, followed by β-H elimination. When treating **AK** with MeOTf, methyl crotonate was obtained selectively, while MeI also afforded methyl vinylacetate. On the other hand, the treatment of **AL** with methyl iodide proved to be almost ineffective in the ring opening.

MeOTf provided moderate yields of the dimethyl fumarate. It could be concluded that the cleavage of Pd-lactones depends on the chosen methylating agents and the ligands.

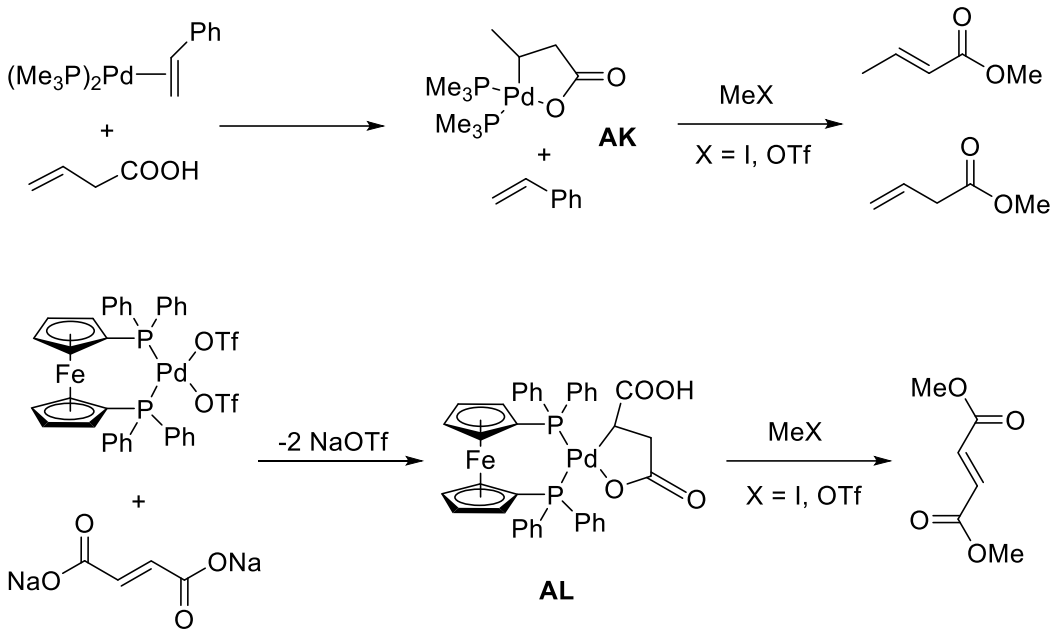


Scheme 4.15. Synthesis and liberation of acrylate derivatives from Pd-lactones.[23]

## 4.2.1. Catalysis with palladium

Limbach and co-workers published the first Pd-based catalytic formation of acrylates from $CO_2$ and ethene.[7] Using a similar approach as for the nickel system TONs up to 29 were achieved. Various Pd precursors were screened with [$PdCl_2$(cod)] and [Pd(Cp)($\eta^3$-allyl)] being the two most promising. As very few differences were observed [$PdCl_2$(cod)] was chosen for further screening experiments due to its easy availability and high stability.

The screening for suitable ligands was carried out in a reaction with two differentiated steps (Scheme 4.16): a) the autoclave was charged with the pre-catalyst, the ligand, 30 bar of $C_2H_4$ and was left stirring for one hour; b) the ethene pressure was released, sodium 2-fluorophenoxide was added and the autoclave was charged with further 5 bar of ethene and 10 bar of carbon dioxide. The reaction was carried out at 120°C for 20 hours to obtain the Na-acrylate. The best results were obtained when dcpe was used as ligand.

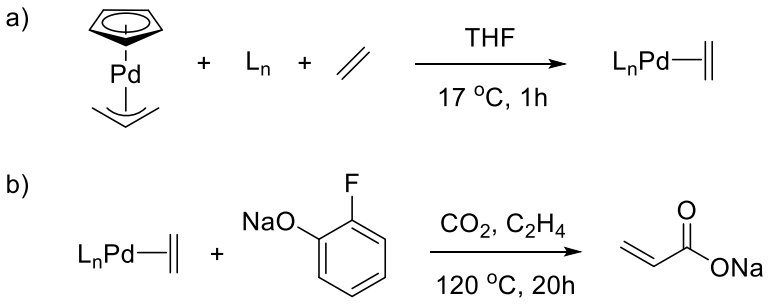


Scheme 4.16. Catalytic formation of Na-acrylate with Pd precursor. Screening of ligands.[7]

In order to gain a better understanding of the catalytic cycle, the isolation of some reaction intermediates was targeted. Only the side product **AM** (Scheme 4.17) was isolated from the reaction mixture. Therefore, it was reasoned that the reducing agent (Zn) not only generates the catalytic species, but also reduces the side products.

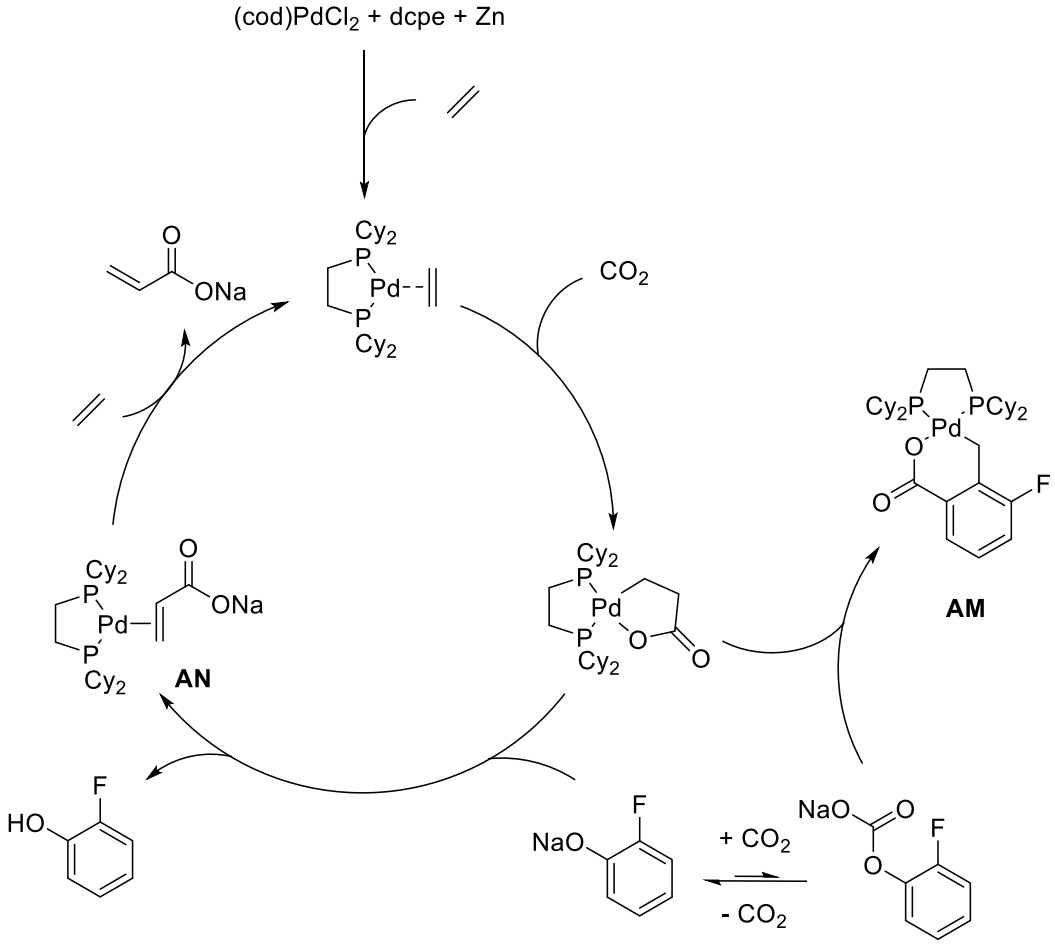


Scheme 4.17. Proposed catalytic cycle for the formation of Na-acrylate from $CO_2$ and $C_2H_4$ using Pd as catalyst.[7]

As reported with the nickel system, Schaub and co-workers investigated the use of Zn as the reductant, the role of the solvent and the leaching of the base in order to achieve an economic process concept.[8] The use of zinc could be reduced to a tenth (from 10 mmol to 1 mmol) and the TON was reduced only a quarter. However, when the catalysis was performed without the use of Zn, the activity was halved.

Moreover, the screening of different solvents showed anisole to be the best, with a TON of 45. In addition, the stability towards traces of water was also tested. When wet anisole was used, no significant drop in activity was observed, implying that Pd catalysts can tolerate a certain amount of water.

The base leaching was also reduced when the loading was decreased. Modifications on the substituents led to similar results to the nickel system, as the activity was greatly reduced when the steric hindrance in the *ortho* position was increased and when substituents in the *para* position were added. However, for [$Pd(PPh_3)_4$/dcpe] catalyst a TON of 50 was achieved when sodium 2,6-di-*tert*-butyl-4-methylphenoxide (NaBHT) was used. Therefore, further investigations were carried out with this system.

Another crucial point investigated was the metal leaching into the aqueous phase. For the development of an appropriate process concept the catalyst should be soluble in the organic phase and insoluble in the product phase after the addition of water to the reaction mixture, in order to enable a simple separation and a high product purity. Therefore, screening of ligands was performed, as the solubility of the catalyst strongly depends on the lipophilicity of the ligand. It was seen that chelating and alkyl-substituted ligands are necessary to obtain catalytically active Pd species. As seen for the Ni system, the bite angle plays an important role; spacers longer than $C_3$ and shorter than $C_2$ are not suitable for this transformation. Moreover, the effect of the substituents was also investigated. σ-Donating ligands such as alkyl substituted ligands were found to be crucial as no catalytic activity could be observed when aryl substituted phosphines were used. The best conditions were obtained with [$Pd(PPh_3)_4$/dcpe] catalyst with a catalyst loading of 0.01 mmol where a TON of 106 was achieved. Moreover, for these conditions only 1 ppm of palladium was found in the aqueous phase, which is a good compromise for useful activity and simple catalyst separation.

Finally, the possibility of recycling the catalyst was investigated. After the reaction

was performed, water was added in order to achieve phase separation where the Na-acrylate could be extracted from the aqueous phase, and the catalyst remained in the organic phase. Therefore, the organic phase with the catalyst was reused for further catalysis with fresh base and Zn if required. Two cycles with TON from 1 to 18 could be observed for both Ni and Pd.

In a following report by Schaub and co-workers a screening of different bases was carried out, as the main drawback of the previous approach is the use of a base with a high molecular weight.[9] Another problem seen with the use of alkoxides is the formation of stable carbonates. Therefore, the thermal stability of different sodium alkoxides and phenoxides and their respective carbonates was tested. It was seen that the bases which form stable carbonates at the reaction temperature are inactive for the catalytic synthesis of Na-acrylate. Among the bases examined, sodium *tert*-butoxide showed similar TONs to the phenoxide system. Moreover, the effect of the counterion was also considered by using lithium and potassium *tert*-butoxides. However, lower activity was observed.

Several advantages were seen with the use of sodium *tert*-butoxide, which has a lower molecular mass, therefore higher base loadings were allowed. Moreover, recyclability was easier, as the corresponding alcohol is water soluble and has a low boiling point. Therefore, the base could be separated from the product by distillation, regenerated in an independent step using less expensive base like sodium methoxide, and entered back to the catalysis (Figure 4.5).

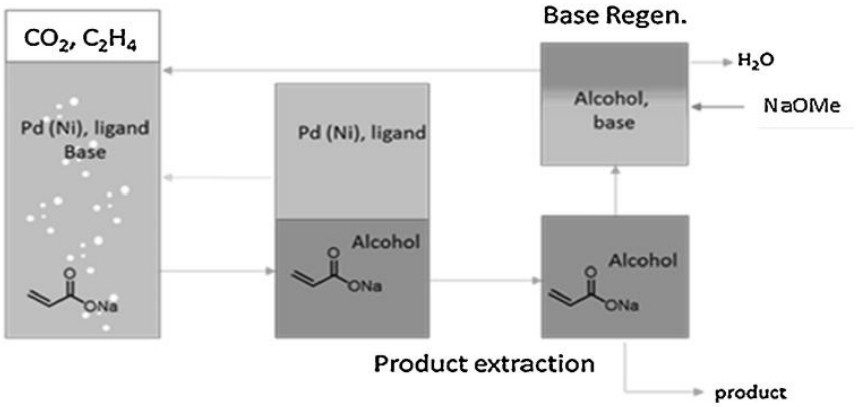


Figure 4.5. Continuous process concept using sodium *tert*-butoxide.[9]

A TON of 20 was achieved in the second cycle after regeneration of the catalyst by stirring under ethene with Zn. Moreover, a Zn-free recycling protocol was achieved by

regeneration of the catalyst only with ethene as inherent reductant with a TON of 19.

In a subsequent report, Schaub and co-workers studied the effect of the sodium acrylate palladium complex (**AN**, Scheme 4.17) in hampering the recyclability, as a resting state for the catalysis.[10] Therefore, complex **AN** was synthesised and used as catalyst with and without the presence of additives. When no additives were used, only very limited catalytic activity in the carboxylation of ethene was achieved. The addition of phosphine ligands had a positive effect, as they can help prevent catalyst decomposition.[29] Moreover, addition of Zn or $^t$BuOH did not result in better activity.

The agglomeration of Pd-acrylate complex **AN** through the sodium carboxylate group was thought to be a plausible reason for the lack of activity. Therefore, an increase in the concentration of $CO_2$ could be beneficial, as it can accelerate the catalytic cycle. Moreover, solvents with more coordinating properties and with higher solubility for $CO_2$, such as amides were targeted.

With higher $CO_2$ pressure (40 bar instead of 20) and by using N,N-dibutylformamide (DBF) and N-cyclohexylpyrrolidone (CHP) much higher TONs, 130 and 514 respectively, were observed.

The disadvantage of using amide solvents is their higher water content when wet, and the consequent loss of catalytic activity under these conditions. Therefore, the removal of the water from the organic phase is required in the continuous process concept before recycling. Evaporation of the water from the high-boiling catalyst containing DBF or CHP phase was proven to be sufficient (Figure 4.6).

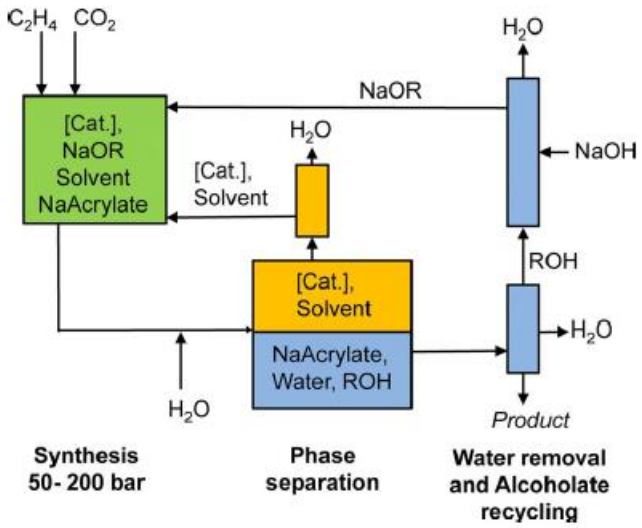


Figure 4.6. Modified continuous process concept for the Pd-catalysed formation of Na-acrylate.[10]

Recently, Liu, Liu and co-workers have reported extensive DFT studies in the catalytic formation of acrylates with both nickel and palladium catalyst in order to gain a better understanding in the differences and similitudes of these systems.[30, 31] In general trends, palladium showed to behave similarly to nickel although with higher energy barriers expect when bulkier ligands were used.

In conclusion, the catalytic formation of acrylates from $CO_2$ and ethene has been proven to be achievable. Since the pioneering work of Hoberg and Carmona, a number of groups have been working in order to understand the reaction mechanism and to achieve catalytic conversions. Two different approaches have been reported by Limbach, Schaub and co-workers, and by Vogt and co-workers. The highest TON reported so far is 514 and was obtained using palladium as catalyst.

## 4.3. Project objectives

As showed before, the catalytic conversion of carbon dioxide and ethene to provided acrylic acid and its derivatives has been widely studied for the past decades and has been an incentive to pursue chemistry in this direction in order to obtain industrially viable methods for this synthesis.

The primary objective of this project is to achieve reasonable catalytic turnovers with commercially available reagents. The addition of different additives is sought in order to facilitate the catalysis. Lewis acids are of interest as it has been showed that they can destabilise the metallalactone and therefore facilitate the β-hydride elimination step, in which the presence of a weak base such as $NEt_3$ is necessary. The addition of a reductant has been proven to be of use to regenerate the catalytic active specie. Therefore, this parameter is also taken into account.

Finally, increasing the scope of metals which can perform the catalytic formation of acrylates is carried out through the use of different palladium precursors. Moreover, a screening on different ligands is carried out.

## 4.4. Bibliography

[1] T. Sakakura, J. C. Choi, H. Yasuda, *Chem. Rev.* **2007**, *107*, 2365-2387.

[2] C. Martín, G. Fiorani, A. W. Kleij, *ACS Catalysis* **2015**, *5*, 1353-1370.

[3] M. Hollering, B. Dutta, F. E. Kühn, *Coord. Chem. Rev.* **2016**, *309*, 51-67.

[4] H. Hoberg, Y. Peres, C. Krüger, Y.-H. Tsay, *Angew. Chem. Int. Ed.* **1987**, *26*, 771-773.

[5] M. L. Lejkowski, R. Lindner, T. Kageyama, G. É. Bódizs, P. N. Plessow, I. B. Müller, A. Schäfer, F. Rominger, P. Hofmann, C. Futter, S. A. Schunk, M. Limbach, *Chem. – A Eur. J.* **2012**, *18*, 14017-14025.

[6] N. Huguet, I. Jevtovikj, A. Gordillo, M. L. Lejkowski, R. Lindner, M. Bru, A. Y. Khalimon, F. Rominger, S. A. Schunk, P. Hofmann, M. Limbach, *Chem. – A Eur. J.* **2014**, *20*, 16858-16862.

[7] S. C. E. Stieber, N. Huguet, T. Kageyama, I. Jevtovikj, P. Ariyananda, A. Gordillo, S. A. Schunk, F. Rominger, P. Hofmann, M. Limbach, *Chem. Commun.* **2015**, *51*, 10907-10909.

[8] S. Manzini, N. Huguet, O. Trapp, T. Schaub, *Eur. J. Org. Chem.* **2015**, *2015*, 7122-7130.

[9] S. Manzini, N. Huguet, O. Trapp, R. A. Paciello, T. Schaub, *Catal. Today* **2017**, *281*, 379-386.

[10] S. Manzini, A. Cadu, A. C. Schmidt, N. Huguet, O. Trapp, R. Paciello, T. Schaub, *ChemCatChem* **2017**, *9*, 2269-2274.

[11] C. Hendriksen, E. A. Pidko, G. Yang, B. Schäffner, D. Vogt, *Chem. – A Eur. J.* **2014**, *20*, 12037-12040.

[12] R. Fischer, J. Langer, A. Malassa, D. Walther, H. Görls, G. Vaughan, *Chem. Commun.* **2006**, 2510-2512.

[13] A. Dedieu, F. Ingold, *Angew. Chem. Int. Ed.* **1989**, *28*, 1694-1695.

[14] I. Pápai, G. Schubert, I. Mayer, G. Besenyei, M. Aresta, *Organometallics* **2004**, *23*, 5252-5259.

[15] D. C. Graham, C. Mitchell, M. I. Bruce, G. F. Metha, J. H. Bowie, M. A. Buntine, *Organometallics* **2007**, *26*, 6784-6792.

[16] G. Yang, B. Schäffner, M. Blug, E. J. M. Hensen, E. A. Pidko, *ChemCatChem* **2014**, *6*, 800-807.

[17] P. N. Plessow, A. Schäfer, M. Limbach, P. Hofmann, *Organometallics* **2014**, *33*, 3657-3668.

[18] C. Bruckmeier, M. W. Lehenmeier, R. Reichardt, S. Vagin, B. Rieger, *Organometallics* **2010**, *29*, 2199-2202.

[19] S. Y. T. Lee, M. Cokoja, M. Drees, Y. Li, J. Mink, W. A. Herrmann, F. E. Kühn, *ChemSusChem* **2011**, *4*, 1275-1279.

[20] D. Jin, T. J. Schmeier, P. G. Williard, N. Hazari, W. H. Bernskoetter, *Organometallics* **2013**, *32*, 2152-2159.

[21] D. Jin, P. G. Williard, N. Hazari, W. H. Bernskoetter, *Chem. – A Eur. J.* **2014**, *20*, 3205-3211.

[22] P. N. Plessow, L. Weigel, R. Lindner, A. Schäfer, F. Rominger, M. Limbach, P. Hofmann, *Organometallics* **2013**, *32*, 3327-3338.

[23] S. Y. T. Lee, A. A. Ghani, V. D'Elia, M. Cokoja, W. A. Herrmann, J.-M. Basset, F. E. Kühn, *New J. Chem.* **2013**, *37*, 3512-3517.

[24] K. Osakada, M. K. Doh, F. Ozawa, A. Yamamoto, *Organometallics* **1990**, *9*, 2197-2198.

[25] R. D. W. Kemmit, S. Mason, D. R. Russell, *J. Organomet. Chem.* **1991**, *415*, C9-C13.

[26] R. Kakino, K. Nagayama, Y. Kayaki, I. Shimizu, A. Yamamoto, *Chem. Lett.* **1999**, *28*, 685-686.

[27] A. Jutand, K. K. Hii, M. Thornton-Pett, J. M. Brown, *Organometallics* **1999**, *18*, 5367-5374.

[28] J. Langer, R. Fischer, H. Görls, D. Walther, *Eur. J. Inorg. Chem.* **2007**, *2007*, 2257-2264.

[29] J. F. Hartwig, *Organotransition metal chemistry : from bonding to catalysis*, University Science Books, Sausalito, Calif., **2010**.

[30] Y. Li, Z. Liu, R. Cheng, B. Liu, *ChemCatChem* **2018**, *10*, 1420-1430.

[31] Y. Li, Z. Liu, J. Zhang, R. Cheng, B. Liu, *ChemCatChem* **2018**, *10*, 5669-5678.

# Chapter 5 : Ni- and Pd-catalysed formation of acrylates from $CO_2$ and $C_2H_4$

Acrylic acid is an industrially important key intermediate for the production of poly-acrylates, e.g. in superabsorbent polymers, paints and colorants. It is typically prepared by the oxidation of propene with oxygen over a molybdenum catalyst.[1] In search for more environmentally benign methods for the production of acrylic acid, the catalytic oxidative coupling of ethene with carbon dioxide and subsequent β-H elimination has been intensively studied for decades.[2-10] Up to this date, the highest reported TON for this reaction is 514, achieved using $Pd(PPh_3)_4$, dcpe and sodium *tert*-butoxide.[11]

## Acrylate formation

As mentioned in the previous chapter, two different catalytic approaches have been reported. In the Vogt group path (Scheme 5.1), a Lewis acid such as $Li^+$ is added in order to facilitate the β-H elimination through coordination to the carbonyl moiety, therefore decreasing the overall free energy barrier. In order to regenerate the catalyst by reductive elimination of HI and to close the catalytic cycle, a weak base such as $NEt_3$ is added. Moreover, the addition of a reductant such as Zn dust is favourable as it allows the regeneration of the catalyst by reducing the side-product $[L_nNiI_2]$ back to $[(L_n)Ni^0]$ ($L_n$ = diphosphine). [12]

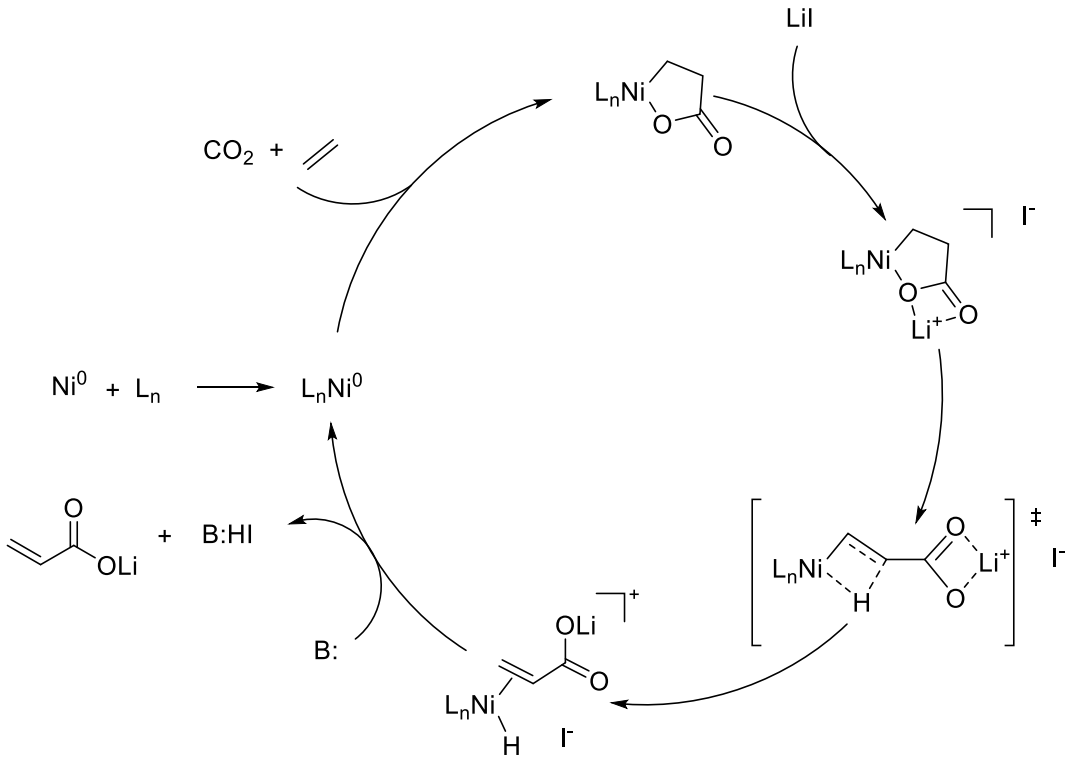


Scheme 5.1 Proposed catalytic cycle for the formation of Li-acrylate from $CO_2$ and $C_2H_4$.[12]

Herein we report a screening of different parameters for the oxidative coupling of ethene and $CO_2$ and subsequent β-H elimination to acrylates in the presence of a hard Lewis acid and a moderately weak base, such as LiI and $NEt_3$.

## 5.1. Nickel catalysed formation of acrylates

As mentioned in the previous chapter, the formation of acrylic acid from $CO_2$ and ethene is endergonic without additives.[13] The addition of auxiliaries was motivated as a way to cleave the kinetically inert Ni-lactone and to make the overall reaction exergonic, allowing the possibility to make this reaction catalytic.[14] Since Walther and co-workers successfully cleaved the 5-membered ring in 2006 via β-H elimination by the reaction with an appropriate ligand,[15] the addition of alkyl halides,[16-19] strong bases,[20] and Lewis acids[21, 22] has proved the ability to promote this step.

### 5.1.1. Screening of different parameters

Continuing the studies published by our group in 2014,[12] where the addition of a hard Lewis acid allowed the β-H elimination of the Ni-lactone and formation of lithium

acrylate, further screening of Lewis acidic salts was carried out (Table 5.1). Based on previous knowledge and studies[20] a strongly basic, preferably chelating ligand was anticipated to be favourable for the oxidative coupling of ethene and $CO_2$. Therefore, dcpe was chosen together with $Ni(cod)_2$ as catalyst precursor. Salts MX were used to promote the β-H elimination step. Moreover, as the formation of undesired [(dcpe)NiH] and [(dcpe)$NiI_2$] by-products has been observed, the addition of $NEt_3$ and Zn-dust is required in order to minimise these Ni inactive species. $NEt_3$ was chosen as a weak base to reductively eliminate HI from the Ni and regenerate the active catalyst, similar to Ni-catalysed Heck-type reactions.[23, 24] Zn-dust is added to regenerate the active catalyst by reducing the side-product [(dcpe)$NiI_2$] back to [(dcpe)$Ni^0$].

Table 5.1. Effect of the Lewis acid (MX), and reducing agent on the catalytic formation of acrylates from $C_2H_4$ and $CO_2$.

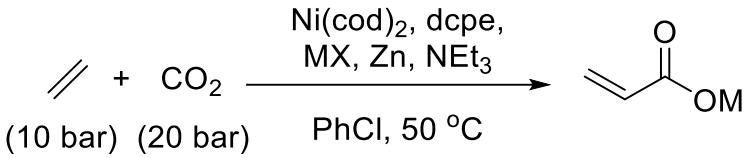


| Entry | Salt (MX) | Reductant | Time (h) | TON[a] |
|---|---|---|---|---|
| 1 | LiI | - | 72 | 1 |
| 2 | LiI | Zn | 72 | 8 |
| 3 | $ZnI_2$ | - | 24 | 5 |
| 4 | $ZnI_2$ | Zn | 24 | 5 |
| 5 | NaI | Zn | 72 | <1 |
| 6 | $CaI_2$ | - | 24 | <1 |
| 7 | $CaI_2$ | Zn | 24 | 1 |

| | | | | |
|---|---|---|---|---|
| 8 | $MgI_2$ | Zn | 72 | <1 |
| 9 | NaCl | Zn | 72 | 0 |
| 10 | NaBr | Zn | 72 | 0 |
| 11 | $NaBAr_4^F$ | Zn | 72 | 0 |
| 12 | LiCl | Zn | 72 | <1 |
| 13 | LiBr | Zn | 72 | 1 |
| 14 | LiOTf | - | 72 | <1 |
| 15 | LiOTf | Zn | 72 | <1 |
| 16 | LiIm | - | 72 | <1 |

Conditions: 50 µmol $Ni(cod)_2$, 50 µmol dcpe, 1.25 mmol Salt, 2.5 mmol Zn, 2.5 mmol $NEt_3$, 10 bar $C_2H_4$, 20 bar $CO_2$; 2 mL PhCl, 50 °C. [a]TON determined by NMR with $LiOAc{\cdot}2H_2O$ as internal standard.

Different cations were tested, such as $Li^+$, $Zn^{2+}$, $Na^+$, $Ca^{2+}$ and $Mg^{2+}$ with iodide as counter ion. As predicted in the previously reported DFT calculations for Na and Li,[12] the combination of the hard Lewis acid $Li^+$ with the soft anion $I^-$ gave the best results with a TON up to 8 (Table 5.1, entry 2). Surprisingly, $Zn^{2+}$ also gave catalytic conversions, despite its softer character, with a TON up to 5 (Table 5.1, entry 3 and 4), whereas the other iodine salts led to no catalytic conversions (Table 5.1, entries 5-8). The effect of the counter ion was examined for both $Na^+$ and $Li^+$. TONs decreased from $I^->Br^->Cl^-$ as expected when going from a soft to a hard ion, when the lithium halides were used (Table 5.1, entries 2, 12 and 13). Despite $Na^+$ has proven to be a good auxiliary for the β-H elimination step from Ni-lactones by Limbach and co-workers, with the use of sodium alkoxides and phenoxides,[20, 25] and by Bernskoetter and co-workers with the use of $NaBAr_4^F$;[22] NaCl, NaBr and $NaBAr_4^F$ showed no conversion towards acrylates in our system (Table 5.1, entries 9-11). This is probably due to the softer character of $Na^+$ when compared to $Li^+$, which seems to have a considerable influence in our catalytic system. Some other lithium salts which are typically used for lithium ion batteries applications

were tested. Lithium trifluoromethanesulfonate (LiOTf) and lithium bis(trifluoromethanesulfonyl)imide (LiIm) were chosen as easily available and cheap lithium salts (Table 5.1, entries 14-16). LiIm formed more lithium acrylate than LiOTf, even without Zn as reducing agent, although under these conditions no TONs were observed for any salt.

As reported in 2014, further optimization was carried out by modifying the ligand and the gas ratio. The use of a diphosphine with a bigger bite angle like dcpp (1,2-bis(dicyclohexylphosphino)propane) and changing the gas ratio from 10/20 to 25/5 bar of $C_2H_4/CO_2$ led to TONs up to 16.[12] With these optimised conditions different salts were screened (Table 5.2). In order to facilitate the screening, reaction times were decreased to 24 hours.

Table 5.2. Salt effect on the catalytic formation of acrylates from $CO_2$ and $C_2H_4$, improved conditions.

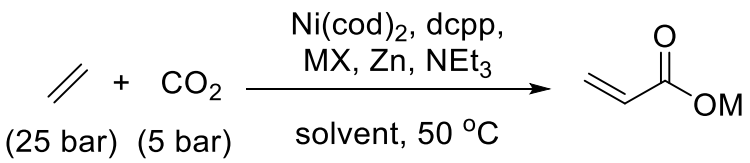


| Entry | Salt (MX) | Reductant | Solvent | TON[a] |
|---|---|---|---|---|
| 1 | LiI | - | PhCl | 1 |
| 2 | LiI | Zn | PhCl | 10 |
| 3 | LiI | - | toluene | 2 |
| 4 | LiI | Zn | toluene | 11 |
| 5 | $ZnI_2$ | - | PhCl | 2 |
| 6 | $ZnI_2$ | Zn | PhCl | 5 |

| | | | | |
|---|---|---|---|---|
| 7 | $ZnI_2$ | - | toluene | 2 |
| 8 | $ZnI_2$ | Zn | toluene | 2 |
| 9 | $ZnBr_2$ | - | PhCl | 2 |
| 10 | $ZnBr_2$ | Zn | PhCl | 2 |
| 11 | $ZnBr_2$ | - | toluene | 1 |
| 12 | $ZnBr_2$ | Zn | toluene | <1 |
| 13 | $ZnCl_2$ | - | PhCl | 1 |
| 14 | $ZnCl_2$ | Zn | PhCl | 1 |
| 15 | $ZnOTf_2$ | - | PhCl | <1 |
| 16 | $ZnOTf_2$ | Zn | PhCl | 1 |

Conditions: 50 μmol $Ni(cod)_2$, 50 μmol dcpp, 1.25 mmol Salt, 2.5 mmol Zn, 2.5 mmol $NEt_3$, 25 bar $C_2H_4$, 5 bar $CO_2$; 2 mL solvent, 50 °C, 24 h. [a]TON determined by NMR with $LiOAc{\cdot}2H_2O$ as internal standard.

The two Lewis acids with the best performance, $Li^+$ and $Zn^{2+}$ were examined. LiI proved to be the most active salt, giving a TON up to 11 (Table 5.2, entries 1-4). Variation of the halide counterion for the $Zn^{2+}$ salts resulted in lower TONs for $Cl^-<Br^-<I^-$ as seen previously for the $Li^+$ salts. Therefore, the highest activity (TON of 5) was observed when $ZnI_2$ was used (Table 5.2, entry 6), and it decreased with $ZnBr_2$, $ZnCl_2$ and the triflate salt $ZnOTf_2$ (Table 5.2, entries 9-16). Moreover, the use of toluene showed similar activity when compare to chlorobenzene. The use of toluene is preferable over a chlorinated solvent as it avoids formation of side-products such as [(dcpp)Ni(Ph)Cl] and additionally, is more suitable for industrial applications.

A further optimization was carried out by reducing the amount of catalyst loaded to the reaction. The use of 0.025 mmols of Ni catalyst led to higher TONs as seen in Table 5.3. The most promising salts, LiI and $ZnI_2$ were tested in these reaction conditions. Both

salts gave better results using these conditions, with LiI giving TONs of 24 and 26, in toluene and chlorobenzene respectively (Table 5.3, entries 4 and 6).

Table 5.3. Optimization of the formation of acrylates by modifying the catalyst loading.

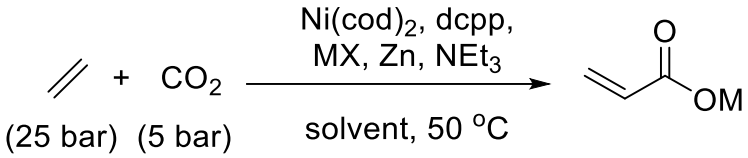


| Entry | Salt (MX) | Reductant | Solvent | TON[a] |
|---|---|---|---|---|
| 1 | $ZnI_2$ | - | PhCl | 9 |
| 2 | $ZnI_2$ | Zn | PhCl | 14 |
| 3 | LiI | - | PhCl | 14 |
| 4 | LiI | Zn | PhCl | 26 |
| 5 | LiI | - | toluene | 1 |
| 6 | LiI | Zn | toluene | 24 |

Conditions: 25 µmol $Ni(cod)_2$, 50 µmol dcpp, 1.25 mmol Salt, 2.5 mmol Zn, 2.5 mmol $NEt_3$, 25 bar $C_2H_4$, 5 bar $CO_2$; 2 mL solvent, 50 °C, 72 h. [a]TON determined by NMR with $LiOAc{\cdot}2H_2O$ as internal standard.

Finally, the effect of the base was screened. As mentioned before, Limbach, Schaub and co-workers have showed the use of alkoxides and phenoxides for both nickel and palladium catalysed systems with promising results.[11, 25-28] One of the prominent bases in their research is sodium 2-fluorophenoxide, which gave TONs up to 107 for the nickel system and 106 for palladium, yet a huge excess of base (300 equivalents) was needed.[25] This base was used in our catalytic system although, as seen in Table 5.4, entry 1, only traces of sodium acrylate were observed. Two more sodium bases were screened, $Na_2CO_3$ and Na(acac) (acac = acetylacetonate), although neither showed reactivity towards acrylate formation (Table 5.4, entries 2 and 3). $NEt_3$ seems to be the most suitable base for our catalytic system. These differences in activity might be due to

the strength of the base. Although mild bases are required, 2-F-PhONa, $Na_2CO_3$ and Na(acac) might not be strong enough to eliminate HI.

Table 5.4. Effect of base in the catalytic formation of acrylates.

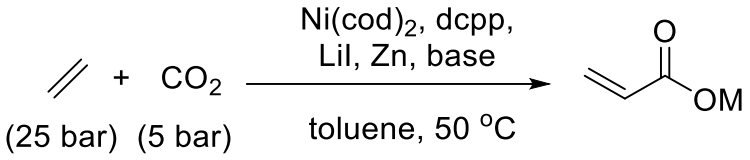


| Entry | Salt (MX) | Reductant | Base | TON[b] |
|---|---|---|---|---|
| 1[a] | - | Zn | 2-F-PhONa | <1 |
| 2 | LiI | Zn | $Na_2CO_3$ | 0 |
| 3 | LiI | Zn | Na(acac) | 0 |
| 4[c] | LiI | - | $NEt_3$ | 1 |
| 5[c] | LiI | Zn | $NEt_3$ | 24 |

Conditions: 25 µmol $Ni(cod)_2$, 25 µmol dcpp; [a] 50 µmol $Ni(cod)_2$, 50 µmol dcpp; 1.25 mmol LiI, 2.5 mmol Zn, 2.5 mmol base, 25 bar $C_2H_4$, 5 bar $CO_2$; 2 mL solvent, 50 °C, 24 h. [b] TON determined by NMR with $LiOAc{\cdot}2H_2O$ as internal standard. [c] Results showed in Table 5.3, entries 5 and 6.

All studies for the nickel-catalysed formation of acrylates from ethene and carbon dioxide were carried out in collaboration with Dr. Coen Hendriksen, Dr. Maria D. Segarra-Maset and Dr. Veronica Forcina at the University of Edinburgh.

## 5.2. Palladium catalysed formation of acrylates

Expanding the scope of the metal catalyst for the synthesis of acrylates from $CO_2$ and ethene was one of the main objectives of this project. Since our first screenings, several reports describing the catalytic activity of palladium have been published.[11, 26-28]

The use of palladium as catalyst was considered due to its capacity to form Pd-lactones, as the formation of Ni-lactones has been identified as key intermediates for

these reactions. Therefore, metals which could form metallalactones were thought to be good candidates for the catalytic coupling of $CO_2$ and alkenes.

### 5.2.1. Screening of different parameters

Following the nickel studies, a range of catalytic experiments were undertaken in order to examine the activity of palladium as catalyst for the formation of acrylates from $CO_2$ and $C_2H_4$.

$Pd(PPh_3)_4$ was chosen as a reasonable bench-stable $Pd^0$ precursor, as no prior reduction is needed. Shortly after, Schaub and co-workers reported the catalytic synthesis of acrylates using $Pd(PPh_3)_4$ as catalyst. [11, 27, 28]

The following catalytic reactions (Table 5.5 - Table 5.7) were performed using the best conditions obtained by our group for the Ni system,[12] where 25 µmol of catalyst, 25 µmol of ligand, 1.25 mmol of LiI as Lewis acid, 2.5 mmol of Zn as reductant and 2.5 mmol of $NEt_3$ as base were used. The reactions were carried out in toluene as solvent, at a pressure of 25 bar of ethene and 5 bar of $CO_2$, for 24 hours at 50 °C.

The nickel system showed bests results with chelating and alkyl-substituted diphosphines such as dcpp. Therefore, a first screening on the effect of the bite angle and the substituents of different diphosphines was carried out, testing both cyclohexyl and phenyl substituents with $C_1$ to $C_4$ bridged phosphines (Figure 5.1).

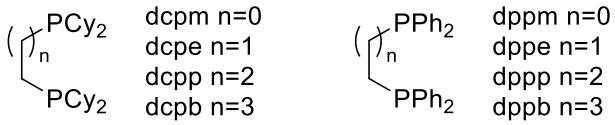


Figure 5.1. Phosphines investigated in the Pd-catalysed formation of acrylates.

When these phosphines were screened in the catalysis with $Ni(cod)_2$ as metal precursor, the diphosphines bearing cyclohexyl substituents, dcpe, dcpp and dcpb (1,2-bis(dicyclohexylphosphino)butane), showed catalytic conversions. Only the smallest dcpm did not present any catalytic conversion. Whereas diphosphines bearing phenyl substituents, only the $C_2$ bridged dppe presented catalytic activity. As seen in Table 5.5, no formation of acrylates was achieved when $Pd(PPh_3)_4$ was used. However, shortly after, Schaub and co-workers reported a TON of 106 when using dcpe and $Pd(PPh_3)_4$, sodium

2,6-di-*tert*-butyl-4-methylphenolate as a base and a temperature of 145 °C. Moreover, lower TONs (22 and 9) were reported for the same catalytic system with dcpp and dcpb respectively.[27]

Table 5.5. Ligand effect on the Pd-catalysed formation of acrylates.

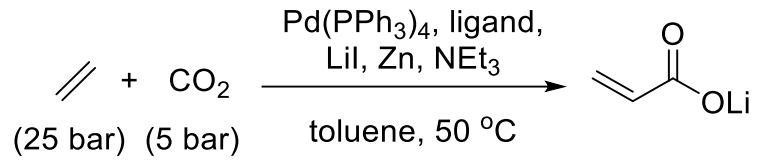


| Entry | Ligand | TON[a] |
|---|---|---|
| 1 | dcpm | 0 |
| 2 | dppm | 0 |
| 3 | dcpe | 0 |
| 4 | dppe | 0 |
| 5 | dcpp | 0 |
| 6 | dppp | 0 |
| 7 | dcpb | 0 |
| 8 | dppb | 0 |

Conditions: 25 µmol $Pd(PPh_3)_4$, 25 µmol Ligand, 1.25 mmol LiI, 2.5 mmol Zn, 2.5 mmol $NEt_3$, 2 mL toluene, 50 °C, 24h. [a]TON determined by NMR with $LiOAc{\cdot}2H_2O$ as internal standard.

Further studies on the backbone and substituents of the phosphines were performed. The use of the following phosphines for the formation of acrylates was examined (Figure 5.2).

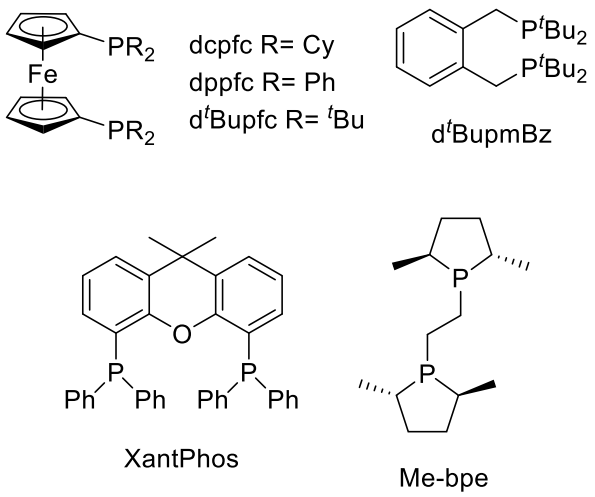


Figure 5.2. Phosphines investigated in the Pd-catalysed formation of acrylates.

The use of a phosphine bearing a ferrocene as backbone has shown a TON of 4 when $Ni(cod)_2$ was used as a metal precursor and dcpfc (1,1'-bis(dicyclohexylphosphino)ferrocene) as ligand in our catalytic system. Moreover, Schaub and co-workers reported a TON of 5 with dcpfc using $Pd(PPh_3)_4$, sodium 2,6-di-*tert*-butyl-4-methylphenolate as a base and a temperature of 145 °C.[27] In our system, only the ferrocene derivative phosphine dppfc presented some activity, although no turnover number was achieved (Table 5.6, entry 2). As $Pd(PPh_3)_4$ is only slightly soluble in toluene, preformation of the diphosphine palladium precursor was carried out overnight. However, as seen in Table 5.6 entry 3, the performance was not improved. The more rigid backbone phosphine XantPhos (4,5-bis(diphenylphosphino)-9,9-dimethylxanthene) did not present any activity towards the formation of acrylates. This is in agreement to previously reported results, as the use of the similar phosphine bis(dicyclohexylphosphinophenyl)ether by Schaub and co-workers did not present any catalytic activity.[27] In addition, d$^t$BupmBz (1,2-bis(di-*tert*-butylphosphinomethyl)benzene) and Me-bpe (1,2-bis((2S,5S)-2,5-dimethylphospholano)ethane) did not form any lithium acrylate under these reaction conditions.

Table 5.6. Ligand effect on the Pd-catalysed formation of acrylates.

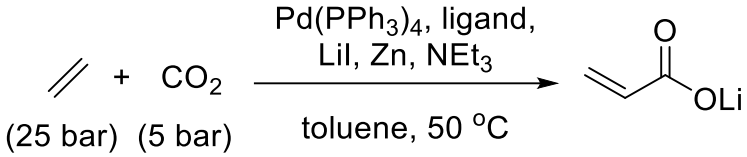


| Entry | Ligand | TON[a] |
|---|---|---|
| 1 | dcpfc | 0 |
| 2 | dppfc | <1 |
| 3[b] | dppfc | <1 |
| 4 | d$^t$Bupfc | 0 |
| 5 | d$^t$BupmBz | 0 |
| 6 | XantPhos | 0 |
| 7 | Me-bpe | 0 |

Conditions: 25 µmol $Pd(PPh_3)_4$, 25 µmol Ligand, 1.25 mmol LiI, 2.5 mmol Zn, 2.5 mmol $NEt_3$, 2 mL toluene, 50 °C, 24h. [a]TON determined by NMR with $LiOAc{\cdot}2H_2O$ as internal standard. [b] Preformation of catalyst overnight.

The influence of the donating atom was also investigated by testing P-N bidentate ligands such as dppEtPy (2-(2-(diphenylphosphino)ethyl)pyridine) and dpppa (3-(diphenylphosphino)-1-propylamine). Finally, the use of monophosphines such as $PPh_3$ and XPhos (2-dicyclohexylphosphino-2',4',6'-triisopropylbiphenyl) was also investigated (Figure 5.3).

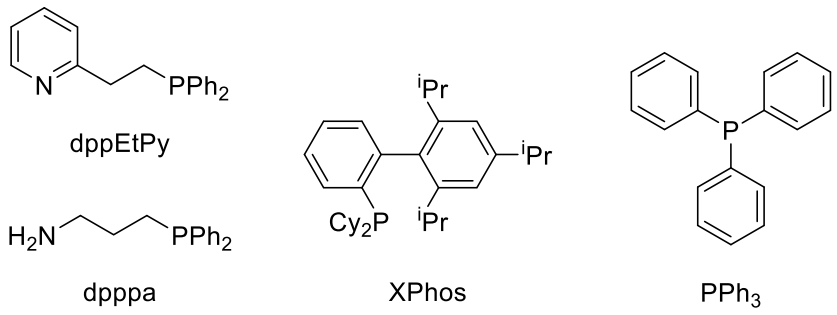


Figure 5.3. P-N ligands and phosphines examined for the catalytic formation of acrylates.

The substitution of a phosphorus for a less donating atom such as nitrogen did not have a positive effect on the catalytic reaction as no formation of lithium acrylate was observed (Table 5.7, entries 1 and 2). Moreover, the use of monophosphines did not give better results either, although $PPh_3$ has previously showed a TON of 2 when $Ni(cod)_2$ was used as catalyst precursor.

Table 5.7. Ligand effect for the formation of acrylates.

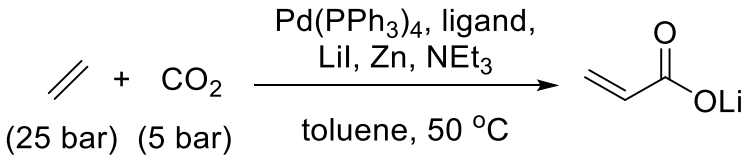


| Entry | Ligand | TON[b] |
|---|---|---|
| 1 | dppEtPy | 0 |
| 2 | dpppa | 0 |
| 3 | - | 0 |
| 4[a] | XPhos | 0 |

Conditions: 25 µmol $Pd(PPh_3)_4$, 25 µmol Ligand; [a]50 µmol Ligand, 1.25 mmol LiI, 2.5 mmol Zn, 2.5 mmol $NEt_3$, 2 mL toluene, 50 °C, 24h. [b]TON determined by NMR with $LiOAc{\cdot}2H_2O$ as internal standard.

These results seem to indicate that $Pd(PPh_3)_4$ is a not suitable precursor in our reaction conditions.

After the lack of activity shown by the phosphine ligands, some N-heterocyclic carbenes provided by Evonik were tested as ligands for the formation of lithium acrylate (Figure 5.4).

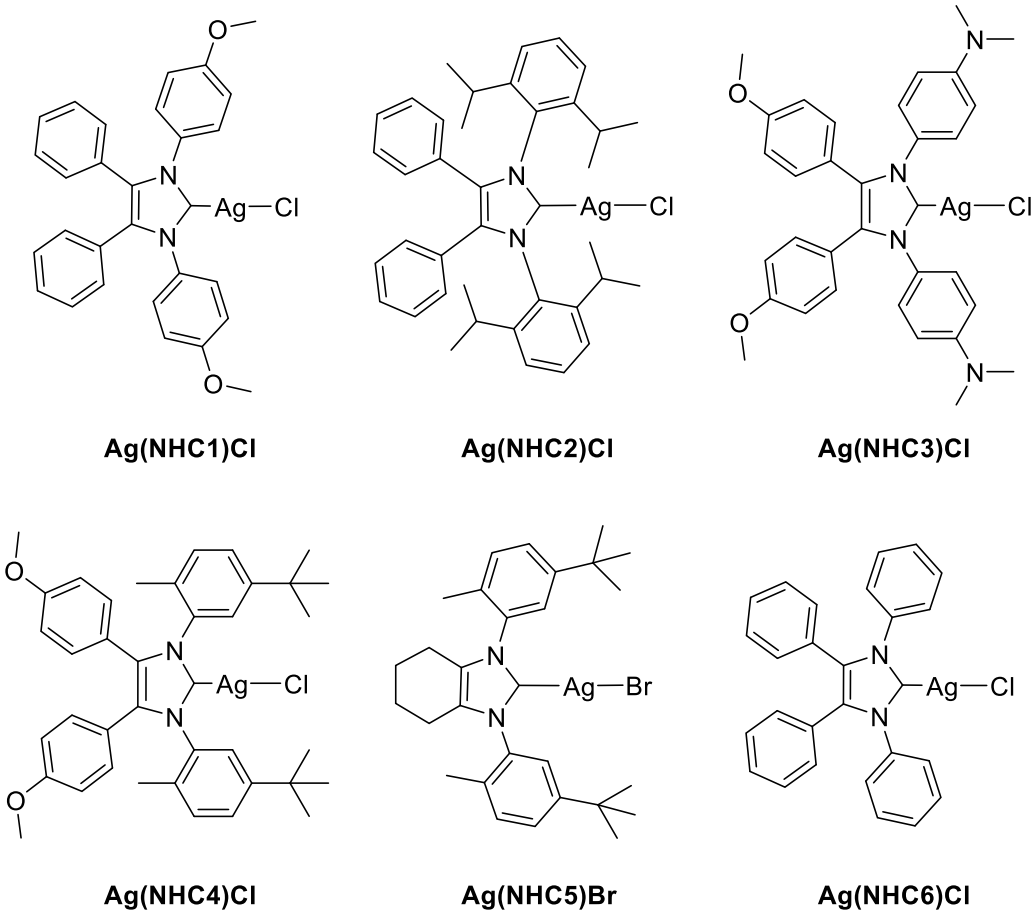


Figure 5.4. NHC silver salts tested in the Pd-catalysed formation of acrylates from $CO_2$ and $C_2H_4$.

Palladium complexes of the NHCs were synthesised by reacting $Pd(CH_3CN)_2Cl_2$ with the silver salt of the carbene ligands in DCM. The reaction was left stirring for two hours in the dark, as silver NHC salts can be light sensitive (Scheme 5.2). Pd-NHC complexes were characterised by $^{1}H$ and $^{13}C$ NMR spectroscopies.

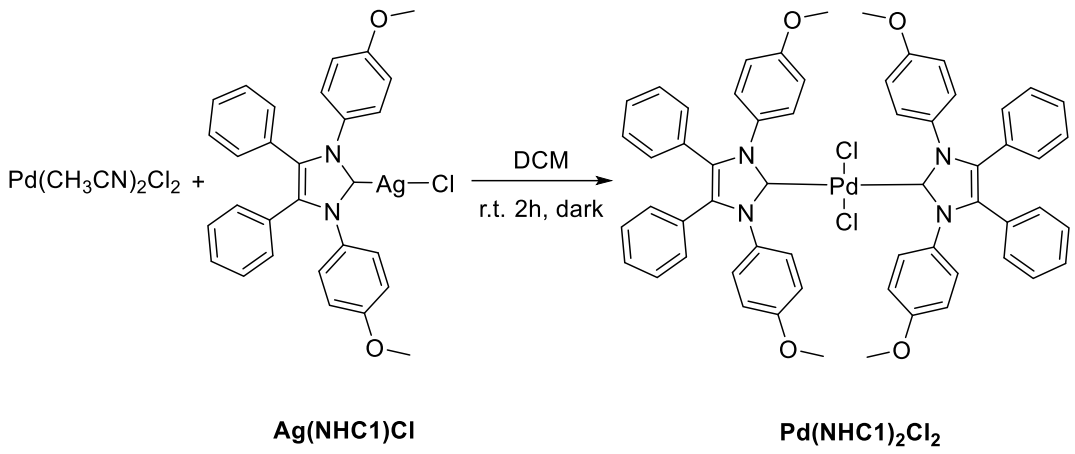


Scheme 5.2. Synthetic route for the formation of Pd-NHC catalysts.

As seen in Table 5.8 Pd-NHC complexes were used as catalysts for the formation of acrylates from carbon dioxide and ethene with the best conditions obtained by our group for the Ni system,[12] where 25 μmol of catalyst, 1.25 mmol of LiI as Lewis acid, 2.5 mmol of Zn as reductant and 2.5 mmol of $NEt_3$ as base were used. Toluene was used as solvent and a pressure of 25 bar of ethene and 5 bar of $CO_2$ were used. The reactions were stirred for 24 hours at 50 °C. However, formation of lithium acrylate was not observed for any Pd-NHC catalyst.

Table 5.8. Screening of Pd-NHC complexes as catalysts for the formation of acrylates.

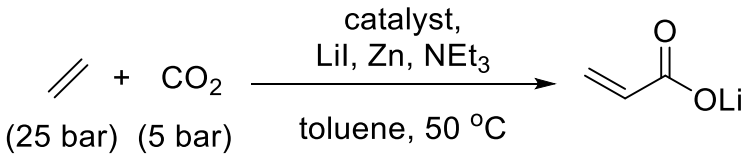


| Entry | Catalyst | TON[a] |
|---|---|---|
| 1 | $Pd(NHC1)_2Cl_2$ | 0 |
| 2 | $Pd(NHC2)_2Cl_2$ | 0 |
| 3 | $Pd(NHC3)_2Cl_2$ | 0 |
| 4 | $Pd(NHC4)_2Cl_2$ | 0 |

| | | |
|---|---|---|
| 5 | $Pd(NHC5)_2Cl_2$ | 0 |
| 6 | $Pd(NHC6)_2Cl_2$ | 0 |

Conditions: 25 µmol catalyst, 1.25 mmol LiI, 2.5 mmol Zn, 2.5 mmol $NEt_3$, 2 mL toluene, 50 °C, 24h. [a]TON determined by NMR with $LiOAc{\cdot}2H_2O$ as internal standard.

Despite the absence of reactivity exhibited for palladium catalysts so far, $Pd_2(dba)_3$ was used as another $Pd^0$ precursor. As seen for $Pd(PPh_3)_4$, $Pd_2(dba)_3$ does not require any prior reduction. An interesting aspect about $Pd_2(dba)_3$ is that it has proven to be a good catalyst for carbon-carbon cross-coupling reactions, among other reactions.[29]

The reaction optimisations were performed using dppp as ligand, as an accessible and commercially available phosphine. For the first reaction (Table 5.9, entry 1), same conditions as for $Pd(PPh_3)_4$ were used. Although catalytic turnover was not achieved, the formation of lithium acrylate was observed. Higher TONs (up to 106) had been reported by Schaub and co-workers when temperatures of 145 °C were used.[27] Therefore, the effect of the increment of the temperature was considered. Increasing the temperature up to 100 °C had a positive effect as a TON of 3 was achieved (Table 5.9, entry 2). The catalyst loading was also investigated. Reducing by half the amount of catalyst led to the highest turnover seen so far (TON of 4; Table 5.9, entry 3). Encouraged by these results, a further increment of the temperature to 150 °C was performed for both dppp and dcpp ligands (Table 5.9, entries 4 and 5). However, it had a negative effect as no formation of acrylates was observed, probably due to the decomposition of the catalyst.

Table 5.9. Effect of the temperature and catalyst loading.

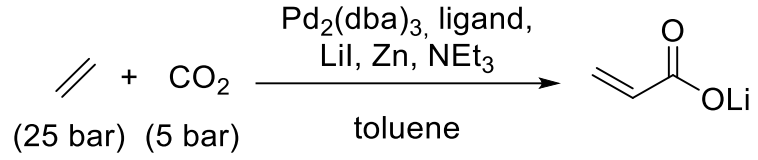


| Entry | Ligand | Temperature (°C) | TON[b] |
|---|---|---|---|
| 1 | dppp | 50 | <1 |
| 2 | dppp | 100 | 3 |
| 3[a] | dppp | 100 | 4 |
| 4[a] | dppp | 150 | 0 |
| 5[a] | dcpp | 150 | 0 |

Conditions: 25 µmol $Pd_2(dba)_3$, 50 µmol dppp; [a] 12.5 µmol $Pd_2(dba)_3$, 25 µmol dppp; 1.25 mmol LiI, 2.5 mmol Zn, 2.5 mmol $NEt_3$, 2 mL toluene, 24h. [b]TON determined by NMR with $LiOAc{\cdot}2H_2O$ as internal standard.

A few more tests were done with dppp as ligand and using 12.5 µmol of $Pd_2(dba)_3$ (Table 5.10). The amount of phosphine was doubled in order to prevent catalyst decomposition during the catalytic reaction. However, this resulted in a lower TON (Table 5.10, entry 1).

Another parameter that was studied was the ratio of gases. So far, the best conditions for the nickel system were used, e.g. 25 bar $C_2H_4$ and 5 bar $CO_2$. However, other palladium systems have shown better catalytic activity with higher $CO_2$ pressures.[11, 27, 28] Therefore, pressures of 20 bar $C_2H_4$ and 10 bar $CO_2$ were used (Table 5.10, entry 2). However, a lower turnover was obtained. These reactions are carried out in 4 mL vials closed with a screw cap with PTFE/silicon septum, and the septum is punctured with a small needle in order to allow the gases into the reaction mixture. The effect of having open vials was also studied (Table 5.10, entry 3), although no appreciable difference was observed.

Table 5.10. Effect of the phosphine loading and pressure.

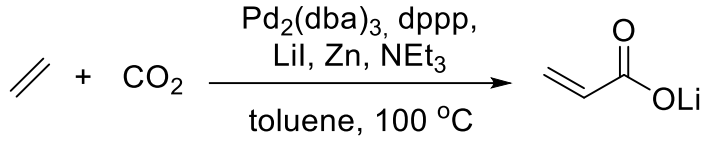


| Entry | P $C_2H_4$ (bar) | P $CO_2$ (bar) | TON[b] |
|---|---|---|---|
| 1[a] | 25 | 5 | 2 |
| 2 | 20 | 10 | 2 |
| 3[c] | 20 | 10 | 2 |

Conditions: 12.5 µmol $Pd_2(dba)_3$, 25 µmol dppp; [a] 12.5 µmol $Pd_2(dba)_3$, 50 µmol dppp; 1.25 mmol LiI; 2.5 mmol Zn; 2.5 mmol $NEt_3$; 2 mL toluene, 100 °C, 24 h. [b]TON determined by NMR with $LiOAc{\cdot}2H_2O$ as internal standard. [c] Open vials.

After the preliminary screening, the set of ligands used for the $Pd(PPh_3)_4$ was also examined with $Pd_2(dba)_3$ as catalyst precursor. Cyclohexyl and phenyl substituted diphosphines with $C_1$ to $C_4$ bridged backbone were tested (Table 5.11).

Table 5.11. Ligand effect for the formation of acrylates using $Pd_2(dba)_3$.

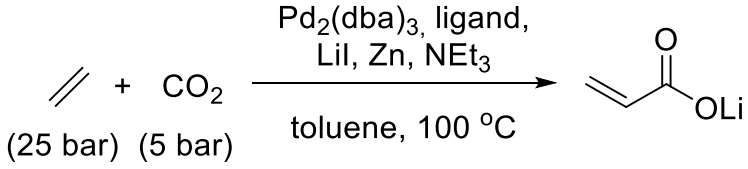


| Entry | Ligand | TON[a] |
|---|---|---|
| 1 | dcpm | <1 |
| 2 | dppm | <1 |
| 3 | dcpe | <1 |

| | | |
|---|---|---|
| 4 | dppe | 1 |
| 5 | dcpp | 2 |
| 6[b] | dppp | 4 |
| 7 | dcpb | <1 |

Conditions: 12.5 µmol $Pd_2(dba)_3$, 25 µmol Ligand, 1.25 mmol LiI, 2.5 mmol Zn, 2.5 mmol $NEt_3$, 2 mL. toluene, 100 °C, 24 h. [a]TON determined by NMR with $LiOAc{\cdot}2H_2O$ as internal standard. [b] Result showed in Table 5.9, entry 3.

It can be observed that modifications on the bite angle appear to influence on the formation of acrylates, with the best results obtained with propene bridged diphosphines dcpp and dppp (Table 5.11, entries 5 and 6). Moreover, the aryl substituted phosphines seem to have better activity than the alkyl substituted, towards the formation of lithium acrylate. However, the differences in the TONs are so marginal that no clear trend should be deduced from that.

Two more solvents were screened for this reaction (Table 5.12). Both NMP (1-methyl-2-pyrrolidone) and THF are polar aprotic solvents, although THF has a low boiling point and NMP a high boiling point. Moreover, THF has been successfully used for the formation of acrylates by Schaub and co-workers.[26, 27]

Variation of the solvent did not provide an improvement on the synthesis of lithium acrylate from carbon dioxide and ethene as no catalytic conversion could be observed when dppe, dppp, dcpp and dppb were used as ligands (Table 5.12).

Table 5.12. Solvent effect for the formation of acrylates using $Pd_2(dba)_3$.

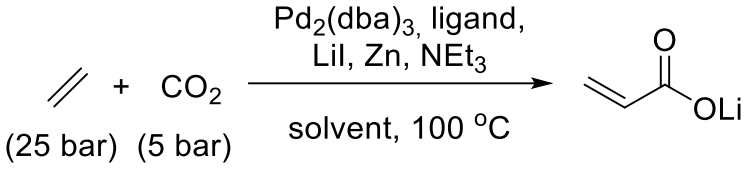


| Entry | Ligand | Solvent | TON[a] |
|---|---|---|---|
| 1 | dppe | THF | 0 |
| 2 | dppe | NMP | 0 |
| 3 | dppp | THF | 0 |
| 4 | dppp | NMP | <1 |
| 5 | dcpp | THF | 0 |
| 6 | dcpp | NMP | 0 |
| 7 | dppb | THF | 0 |
| 8 | dppb | NMP | 0 |

Conditions: 12.5 µmol $Pd_2(dba)_3$, 25 µmol Ligand, 1.25 mmol LiI, 2.5 mmol Zn, 2.5 mmol $NEt_3$, 2 mL of solvent, 100 °C, 24 h. [a]TON determined by NMR with $LiOAc{\cdot}2H_2O$ as internal standard.

Diphosphines bearing more rigid backbone were screened using toluene as solvent. In contrast with $Pd(PPh_3)_4$, when $Pd_2(dba)_3$ is used as catalyst, formation of acrylates is observed not only with dppfc, but also when dcpfc and d$^t$BupmBz are used. However, no catalytic turnovers were observed (Table 5.13). Alkyl-bulky substituents such as *tert*-butyl in the ferrocene backboned phosphines had a negative effect, as lithium acrylate formation was not observed.

Table 5.13. Ligand effect in the catalytic formation of acrylates using $Pd_2(dba)_3$.

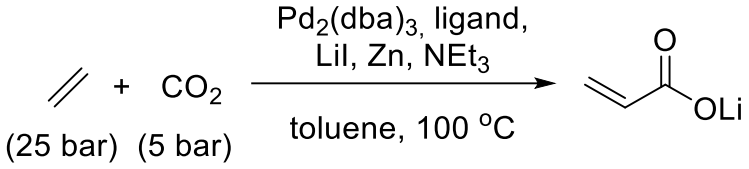


| Entry | Ligand | TON[a] |
|---|---|---|
| 1 | dcpfc | <1 |
| 2 | dppfc | <1 |
| 4 | d$^t$Bupfc | 0 |
| 5 | d$^t$BupmBz | <1 |

Conditions: 12.5 µmol $Pd_2(dba)_3$, 25 µmol Ligand, 1.25 mmol LiI, 2.5 mmol Zn, 2.5 mmol $NEt_3$, 2 mL toluene, 100 °C, 24 h. [a]TON determined by NMR with $LiOAc{\cdot}2H_2O$ as internal standard.

The effect of the donor atom was also screened (Table 5.14). Although no catalytic TON was observed, when dpppa, which bears a $C_3$ bridge, was used, formation of small amounts of lithium acrylate was detected by $^1$H NMR spectroscopy (Table 5.14, entry 2).

Table 5.14. Effect of P-N ligands in the catalytic formation of acrylates using $Pd_2(dba)_3$.

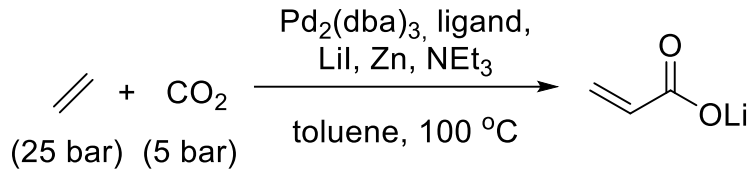


| Entry | Ligand | TON[a] |
|---|---|---|
| 1 | dppEtPy | 0 |
| 2 | dpppa | <1 |

Conditions: 12.5 µmol $Pd_2(dba)_3$, 25 µmol Ligand, 1.25 mmol LiI, 2.5 mmol Zn, 2.5 mmol $NEt_3$, 2 mL toluene, 100 °C, 24 h. [a]TON determined by NMR with $LiOAc{\cdot}2H_2O$ as internal standard.

After these optimizations, a few more tests were carried out with $Pd(PPh_3)_4$. The catalysis was performed at 100 °C and dppfc, which gave formation of acrylates in the previous tests with $Pd(PPh_3)_4$ (Table 5.6, entry 2); and dppp, which gave the best results for $Pd_2(dba)_3$ (Table 5.9, entry 3) were used. Interestingly, increasing the temperature did not affect the reaction performance when dppfc was used (Table 5.15, entry 1). However, it had a positive effect on the reaction with dppp as formation of lithium acrylate was achieved (Table 5.15, entry 2), while there was no conversion when the catalysis was performed at 50 °C.

Although an improvement on the catalytic conversion of $CO_2$ and ethene to acrylate was seen with dppp as ligand, it seems to indicate that $Pd_2(dba)_3$ might be a better catalyst for these reactions than $Pd(PPh_3)_4$.

Table 5.15. Ligand effect for the formation of acrylates using $Pd(PPh_3)_4$ and the improved conditions

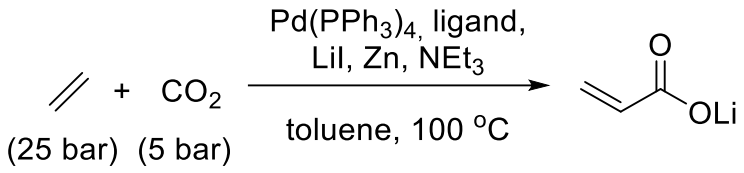


| Entry | Ligand | TON[a] |
|---|---|---|
| 1 | dppfc | <1 |
| 2 | dppp | 1 |

Conditions: 12.5 µmol $Pd(PPh_3)_4$, 25 µmol Ligand, 1.25 mmol LiI, 2.5 mmol Zn, 2.5 mmol $NEt_3$, 2 mL toluene, 100 °C, 24h. [a]TON determined by NMR with $LiOAc{\cdot}2H_2O$ as internal standard.

## 5.3. Chapter summary and conclusions

The screening for the optimization of the catalytic conversion of carbon dioxide and ethene to lithium acrylate has been carried out.

The addition of LiI or $ZnI_2$, together with $NEt_3$ has been proven to be necessary in order to achieve higher TONs when $Ni(cod)_2$ is used as a pre-catalyst. Moreover, increasing the portion of ethene and decreasing the carbon dioxide pressure, e.g. a gas ratio of 25 bar $C_2H_4$ and 5 bar $CO_2$ led to better conversions. Moving towards non-chlorinated solvents such as toluene, showed similar turnovers. Therefore, toluene was chosen as the solvent for further optimizations.

Regarding the catalytic experiments using Pd as catalyst, two different metal precursors were screened, $Pd(PPh_3)_4$ and $Pd_2(dba)_3$. Moreover, screening of different commercially available phosphines was carried out. Aryl substituted $C_3$ bridged diphosphine dppp showed the best results. The highest TON achieved was 4 using 12.5 µmol $Pd_2(dba)_3$, 25 µmol dppp, 1.25 mmol LiI, 2.5 mmol Zn and 2.5 mmol $NEt_3$. Carrying out the reaction in toluene, 25 bar $C_2H_4$ and 5 bar $CO_2$ for 24 hours. Increasing the temperature from 50 °C to 100 °C had a positive effect for the palladium system.

Although this process is certainly not developed to the extent of industrial application, these results show that acrylate formation is possible and the ease with which the reaction can be performed leaves a lot of room for future development.

## 5.4. Bibliography

[1] B. Cornils, W. A. Herrmann, I. Wiley, *Applied homogeneous catalysis with organometallic compounds : a comprehensive handbook in three volumes*, Wiley-VCH, Weinheim, Germany, **2002**.

[2] H. Hoberg, D. Schaefer, *J. Organomet. Chem.* **1983**, *251*, c51-c53.

[3] H. Hoberg, D. Schaefer, G. Burkhart, C. Krüger, M. J. Romão, *J. Organomet. Chem.* **1984**, *266*, 203-224.

[4] H. Hoberg, D. Schaefer, B. W. Oster, *J. Organomet. Chem.* **1984**, *266*, 313-320.

[5] H. Hoberg, B. W. Oster, *J. Organomet. Chem.* **1984**, *266*, 321-326.

[6] H. Hoberg, B. Apotecher, *J. Organomet. Chem.* **1984**, *270*, c15-c17.

[7] H. Hoberg, Y. Peres, A. Milchereit, *J. Organomet. Chem.* **1986**, *307*, C38-C40.

[8] H. Hoberg, Y. Peres, A. Milchereit, *J. Organomet. Chem.* **1986**, *307*, C41-C43.

[9] H. Hoberg, Y. Peres, C. Krüger, Y.-H. Tsay, *Angew. Chem. Int. Ed.* **1987**, *26*, 771-773.

[10] H. Hoberg, A. Ballesteros, A. Sigan, C. Jegat, A. Milchereit, *Synthesis* **1991**, *1991*, 395-398.

[11] S. Manzini, A. Cadu, A.-C. Schmidt, N. Huguet, O. Trapp, R. Paciello, T. Schaub, *ChemCatChem* **2017**, *9*, 2269-2274.

[12] C. Hendriksen, E. A. Pidko, G. Yang, B. Schäffner, D. Vogt, *Chem. – A Eur. J.* **2014**, *20*, 12037-12040.

[13] D. C. Graham, C. Mitchell, M. I. Bruce, G. F. Metha, J. H. Bowie, M. A. Buntine, *Organometallics* **2007**, *26*, 6784-6792.

[14] P. N. Plessow, A. Schäfer, M. Limbach, P. Hofmann, *Organometallics* **2014**, *33*, 3657-3668.

[15] R. Fischer, J. Langer, A. Malassa, D. Walther, H. Görls, G. Vaughan, *Chem. Commun.* **2006**, 2510-2512.

[16] C. Bruckmeier, M. W. Lehenmeier, R. Reichardt, S. Vagin, B. Rieger, *Organometallics* **2010**, *29*, 2199-2202.

[17] S. Y. T. Lee, M. Cokoja, M. Drees, Y. Li, J. Mink, W. A. Herrmann, F. E. Kühn, *ChemSusChem* **2011**, *4*, 1275-1279.

[18] S. Y. T. Lee, A. A. Ghani, V. D'Elia, M. Cokoja, W. A. Herrmann, J.-M. Basset, F. E. Kühn, *New J. Chem.* **2013**, *37*, 3512-3517.

[19] Z. Zhang, F. Guo, F. E. Kühn, J. Sun, M. Zhou, X. Fang, *Appl. Organometal. Chem.* **2017**, *31*, e3567.

[20] M. L. Lejkowski, R. Lindner, T. Kageyama, G. É. Bódizs, P. N. Plessow, I. B. Müller, A. Schäfer, F. Rominger, P. Hofmann, C. Futter, S. A. Schunk, M. Limbach, *Chem. – A Eur. J.* **2012**, *18*, 14017-14025.

[21] D. Jin, T. J. Schmeier, P. G. Williard, N. Hazari, W. H. Bernskoetter, *Organometallics* **2013**, *32*, 2152-2159.

[22] D. Jin, P. G. Williard, N. Hazari, W. H. Bernskoetter, *Chem. – A Eur. J.* **2014**, *20*, 3205-3211.

[23] M. Oestreich, *The Mizoroki-Heck Reaction*, Hoboken, NJ : John Wiley & Sons, Hoboken, Chichester, **2009**.

[24] S. Z. Tasker, E. A. Standley, T. F. Jamison, *Nature* **2014**, *509*, 299.

[25] N. Huguet, I. Jevtovikj, A. Gordillo, M. L. Lejkowski, R. Lindner, M. Bru, A. Y. Khalimon, F. Rominger, S. A. Schunk, P. Hofmann, M. Limbach, *Chem. – A Eur. J.* **2014**, *20*, 16858-16862.

[26] S. C. E. Stieber, N. Huguet, T. Kageyama, I. Jevtovikj, P. Ariyananda, A. Gordillo, S. A. Schunk, F. Rominger, P. Hofmann, M. Limbach, *Chem. Commun.* **2015**, *51*, 10907-10909.

[27] S. Manzini, N. Huguet, O. Trapp, T. Schaub, *Eur. J. Org. Chem.* **2015**, *2015*, 7122-7130.

[28] S. Manzini, N. Huguet, O. Trapp, R. A. Paciello, T. Schaub, *Catal. Today* **2017**, *281*, 379-386.

[29] A. R. D. Moln r, *Palladium-catalyzed coupling reactions : practical aspects and future developments*, First edition.. ed., Weinheim, Germany : Wiley-VCH, Weinheim, Germany, **2013**, p445-489.

# Chapter 6 : Experimental details

## 6.1. General procedures and techniques

Standard high vacuum Schlenk-line techniques and MBraun and Vac glove boxes were used to store and manipulate air- and moisture-sensitive compounds under an atmosphere of air free and dried dinitrogen or argon. Reactions and manipulations were carried out under an inert atmosphere unless stated otherwise. All gases were purchased from BOC Industrial gases UK. All chemicals were purchased by Sigma Aldrich, Fisher Scientific or VWR International Ltd and were used as received unless otherwise noted. All glassware was dried in an oven at 160 °C, cooled under vacuum and purged with nitrogen or argon prior to use. All Fisherbrand® 1.2 μm retention glass microfiber filters and cannula were dried in an oven at 160 °C before use.

Toluene, THF, diethyl ether and hexane for use with air- and moisture-sensitive compounds were stored in ampules containing activated 4 Å molecular sieves from the Vac Atmospheres solvent tower drying system, where they had been passed over a column of molecular sieves for a minimum of 12 hours prior to collection. Anhydrous chlorobenzene, toluene, tetrahydrofuran and 1-methyl-2-pyrrolidone were purged with argon and stored over 4 Å molecular sieves or distilled over sodium and benzophenone under an argon atmosphere and stored over 4 Å molecular sieves. Triethylamine was purchased from Romil Ltd and was purified by distillation over $CaH_2$ and stored over 4 Å molecular sieves. 1,4-dioxane and benzene were refluxed over potassium for 3 days, distilled and collected in an ampoule containing activated 4 Å molecular sieves. All solvents were degassed prior to use and stored. The solvents $C_6D_6$, THF-$d_5$ and pyridine-$d_5$ were heated under reflux over potassium for 24 hours, degassed and distilled by trap to trap distillation and stored under an atmosphere of nitrogen prior to use. All solvents were purchased by Sigma Aldrich or Fisher Scientific.

All NMR spectroscopic analyses were recorded at 298 K using Bruker Avance III 500.12 MHz spectrometers with $^{1}H$ NMR spectra run at 500.12 MHz, $^{13}C$ NMR spectra run at 125.76, $^{29}Si$ NMR spectra run at 99.37 MHz, $^{11}B$ NMR spectra run at 160.46 MHz and $^{19}F$ NMR spectra run at 470.59 MHz. The $^{1}H$ and $^{13}C$ NMR spectra are referenced

internally to the residual solvent peaks or an external standard ($Me_4Si$ for $^{29}Si$, $Et_2O{\cdot}BF_3$ for $^{11}B$, $CFCl_3$ for $^{19}F$).

Elemental analyses were performed by Mr. Stephen Boyer at the London Metropolitan University.

Mass spectra measurements were carried out on a 12T SolariX FT-ICR-MS with an Infinity cell (Bruker Daltonics); fitted with an APPI II ion source (Bruker Daltonics) equipped with krypton lamp. Samples were prepared in a glovebox in toluene (10 μM) in a sealed sample vial. Infrared spectra were recorded on a Perkin Elmer Spectrum 65 FT-IR spectrometer as nujol mulls between KBr disks.

### 6.1.1. Preparation of reagents

All commercially available solid reagents were dried under vacuum and liquids were either dried with alkali metal and purified by trap to trap distillation, or activated molecular sieves when appropriate.

$NaN(SiMe_3)_2$,[1] $[U(N(SiMe_3)_2)_3]$,[2] $HOBMes_2$,[3] $HOBMes_2^F$,[4] $[Y(N(SiMe_3)_2)_3]$[5] were synthesised according to literature procedures, in some cases with slight modifications. Sodium salts of the boroxide ligands were prepared by deprotonation of the appropriate conjugate acid with $NaN(SiMe_3)_2$ in toluene. Sodium 2-fluorophenoxide, 2-F-$C_6H_4ONa$, was synthesised using the literature procedure reported for the synthesis of sodium pentafluorophenoxide.[6]

Carbon dioxide CP Grade N 4.5, carbon monoxide research grade N 3.7, nitrous oxide research grade N 4.7 and ethene research grade N 3.2 were used.

### 6.1.2. High pressure vessels

High pressure vessels were used for the catalytic conversion of $CO_2$ and $C_2H_4$ to acrylates. Stainless steel 75 mL autoclaves equipped with a rising plug valve inlet, a manometer, a pressure relief valve and a thermocouple were used. The autoclaves can withstand a maximum pressure of 100 bar and a maximum temperature of 250 °C.

## 6.2. Experimental details for uranium boroxide complexes

### 6.2.1. Synthesis of $[U(OBMes_2)_2(\mu\text{-}OBMes_2)]_2$ (1)

A Schlenk flask was charged with $[U(N(SiMe_3)_2)_3]$ (1.08 g, 1.5 mmol) and $HOBMes_2$ (1.20 g, 4.5 mmol, 3 eq.) and a stir bar. The reaction mixture was dissolved in toluene (40 mL) to yield a purple solution, which was allowed to stir at room temperature for 4 hours. Volatiles were removed by evaporation to dryness. The residue was washed with cold hexane (-78 °C, 4 mL) and recrystallized from hexane providing dark block crystals suitable for single-crystal X-ray crystallography. The resulting purple solid was dried under vacuum and stored in the glovebox for no longer than one month due to its sensitivity towards water and oxygen. Clean starting materials and precise control of the stoichiometry is key to the formation of pure samples, as complex **1** is very air sensitive. Yield: 634 mg, 41%

$^1$H NMR (500 MHz, $C_6D_6$): $\delta_H$ 8.3 (Ar-**H** terminal Mes, 16H); 7.2 (*o*-C**H**$_3$ terminal Mes, 48H); 2.5 (*p*-C**H**$_3$ terminal Mes, 24H); -3.7 (*o*-C**H**$_3$ bridging Mes, 12H); -9.2 (Ar-**H** and *p*-C**H**$_3$ bridging Mes, 20H); -15 (*o*-C**H**$_3$ bridging Mes, 12H).

$^{11}$B NMR (106 MHz, $C_6D_6$): $\delta_B$ 74 and 51 (O**B**Mes).

Elemental analysis: C 62.75 %, H 6.44 % calculated. C 62.63 %, H 6.47 % found.

MS (APPI): $C_{54}H_{66}B_3O_3U^{+\bullet}$ $[M]^{+\bullet}$ requires 1033.5799, found 1033.5675 (+12.4 ppm).

FTIR ($cm^{-1}$): 3612, 2728, 1721, 1608, 1552, 1280, 1228, 1176, 1151, 1081, 1029, 960, 928, 847, 745, 672.

### 6.2.2. Synthesis of $[U(OBMes_2)_4(Py\text{-}O)_2]$ (2)

A Young's NMR tube was charged with $[U(OBMes_2)_2(\mu\text{-}OBMes_2)]_2$ (25 mg, 0.012 mmol), $C_5H_5NO$ (5 mg, 0.048 mmol, 4 eq.) and $C_6D_6$ (0.4 mL). The reaction mixture turned dark brown immediately and was allowed to react for 72 hours, during which time dark orange crystals of $[U(OBMes_2)_4(Py\text{-}O)_2]$ suitable for XRD analysis

deposited on the reaction vessel walls. The resulting orange solid was dried under vacuum and stored in the glovebox Yield: 19 mg, 65%

$^{1}$H NMR (500 MHz, $C_6D_6$): $\delta_H$ 6.8 (Ar-**H** Mes, 12H); 4.4 (Py-O **H**, 6H); 2.3 (*o*-C**H**$_3$ Mes, 36H); 2.2 (*p*-C**H**$_3$ Mes, 18H); 1.9 (Py-O **H**, 4H).

$^{11}$B NMR (160 MHz, $C_6D_6$): $\delta_B$ 50 (O**B**Mes).

MS (APPI): $C_{64}H_{76}B_3N_2O_5U^{+\bullet}$ $[M]^{+\bullet}$ requires 1223.6541, found 1223.6552 (-1.1 ppm).

### 6.2.3. Synthesis of [U(OBMes$_2$)$_3$(OPPh$_3$)$_2$] (3)

$[U(OBMes_2)_2(\mu\text{-}OBMes_2)]_2$ (25 mg, 0.012 mmol) and $OPPh_3$ (7 mg, 0.024 mmol, 2 eq.) were placed in a Young's NMR tube. The tube's contents were dissolved in $C_6D_6$ (0.4 mL). $^{1}$H NMR spectroscopy confirmed the formation of the title compound. Co-crystals of this and the side product $[U(k_2\text{-}\{OB(Mes)\}_2O)(OBMes_2)_3]$ (**4**) suitable for X-ray diffraction studies were grown by slow diffusion of hexane into a concentrated benzene solution of $[U(OBMes_2)_3(OPPh_3)_2]$. Yield: 23 mg, 60%

$^{1}$H NMR (500 MHz, $C_6D_6$): $\delta_H$ 6.9 (Ar-**H** Mes, 12H); 6.5 (*p*-Ph **H**, 6H); 5.9 (*o*-Ph **H**, 12H); 3.6 (*o*-C**H**$_3$ Mes, 36H); 2.9 (*m*-Ph **H**, 12H); 1.9 (*p*-C**H**$_3$ Mes, 18H).

$^{11}$B NMR (160 MHz, $C_6D_6$): $\delta_B$ 56 (O**B**Mes).

$^{31}$P NMR (202 MHz, $C_6D_6$): $\delta_P$ -18(O**P**Ph$_3$).

MS (APPI): $C_{90}H_{96}B_3O_5P_2U^{+\bullet}$ $[M]^{+\bullet}$ requires 1589.7520, found 1589.7790 (-27.0 ppm).

### 6.2.4. Synthesis of [{(OBMes$_2$)$_3$U}$_2$(μ-η$^2$:η$^2$-S$_2$)$_2$] (5)

To a magnetically stirred, dark purple solution of $[U(OBMes_2)_2(\mu\text{-}OBMes_2)]_2$ (165 mg, 0.08 mmol) in 2 mL of toluene in a 7 cm$^3$ vial elemental sulfur (10 mg, 0.04 mmol, 0.5 eq.) was added. The reaction was allowed to stir for 2 hours. Dark red crystals of $[\{(OBMes_2)_3U\}_2(\mu\text{-}\eta^2\text{:}\eta^2\text{-}S_2)_2]$ suitable for X-ray diffraction can be obtained from storage of a concentrated benzene solution at room temperature. Yield: 32 mg, 18%

$^{1}$H NMR (500 MHz, $C_6D_6$): $\delta_H$ 6.9 (Ar-**H** Mes, 24H); 2.4 (*p*-C**H**$_3$ Mes, 36H); 2.2 (*o*-C**H**$_3$ Mes, 72H)

$^{11}$B NMR (160 MHz, $C_6D_6$): $\delta_B$ 50 (O**B**Mes).

MS (APPI): $C_{54}H_{66}B_3O_3S_2U^{+\cdot}$ $[M]^{+\cdot}$ requires 1097.5240, found 1097.5259 (-1.9 ppm).

### 6.2.5. Synthesis of [U(η$^2$-N(C$_6$H$_{11}$)C(=NC$_6$H$_{11}$)N(C$_6$H$_{11}$))(OBMes$_2$)$_3$] (6)

A solution of *N*,*N*′-Dicyclohexylcarbodiimide (DCC) (10 mg, 0.048 mmol, 2 eq.) in benzene (1 mL) was added dropwise to a stirring benzene solution of $[U(OBMes_2)_2(\mu\text{-}OBMes_2)]_2$ (50 mg, 0.024 mmol) in a 7cm$^3$ vial. The solution turned green immediately and was allowed to stir for 18 hours. The solution was then filtered and evaporated to dryness. $^{1}$H NMR spectroscopy confirmed the formation of the title compound. Yield: 22 mg, 69 %.

$^{1}$H NMR (500 MHz, $C_6D_6$): $\delta_H$ 58 (Cy **H**, 1H); 43 (Cy **H**, 1H); 28 (Cy **H**, 3H); 14 (Cy **H**, 2H); 12 (Cy **H**, 1H); 11 (Cy **H**, 2H); 9.7 (Cy **H**, 1H); 9.0 (Cy **H**, 3H); 7.6 (Cy **H**, 2H); 7.3 (Cy **H**, 1H); 6.8 (Ar-**H** Mes, 12H); 6.5 (Cy **H**, 2H); 3.9 (Cy **H**, 1H); 3.0 (*p*-C**H**$_3$ Mes, 18H); 2.9 (Cy **H**, 4H); 2.5 (Cy **H**, 1H); 2.2 (Cy **H**, 1H); 1.8 (Cy **H**, 1H); -4.7 (Cy **H**, 1H); -6.6 (Cy **H**, 1H); -10 (*o*-C**H**$_3$ Mes, 36H); -11 (Cy **H**, 4H).

MS (APPI): $C_{73}H_{100}B_3N_3O_3U^{+}$ $[M + H]^{+}$ requires 1337.8552, found 1337.8577 (-2.5 ppm).

### 6.2.6. Reaction with N$_2$O (compound 7)

A purple solution of $[U(OBMes_2)_2(\mu\text{-}OBMes_2)]_2$ (25 mg, 0.012 mmol) in $C_6D_6$ (0.4 mL) was prepared in situ in a Young's NMR tube. The solution was then degassed by three freeze pump thaw cycles and exposed to 1 bar pressure of $N_2O$. The mixture was agitated to give an immediate colour change to light brown. Formation of complex $[(OBMes_2)_3U\text{-}O\text{-}]_n$ in quantitative yield was confirmed by NMR spectroscopies and elemental analysis.

Analogous formation is observed when the complex $[U(OBMes_2)_2(\mu\text{-}OBMes_2)]_2$ is stored as a solution or when solutions are heated, due to reaction with traces of oxygen.

$^1$H NMR (500 MHz, $C_6D_6$): $\delta_H$ 5.9 (Ar-**H** Mes); 1.9 (*p*-C**H$_3$** Mes); -0.52 (*o*-C**H$_3$** Mes).

$^{11}$B NMR (160 MHz, $C_6D_6$): $\delta_B$ 89 (O**B**Mes).

$^{13}$C NMR (126 MHz, $C_6D_6$): $\delta_C$ 166 (*o*-**C** Mes); 137 (*p*-**C** Mes); 134 (**C**-B Mes); 127 (Ar-**C**H Mes); 21 (*p*-**C**H$_3$ Mes); 5.1 (*o*-**C**H$_3$ Mes).

Elemental analysis: C 61.80 %, H 6.34 % calculated. C 61.75 %, H 6.37 % found.

FTIR (cm$^{-1}$): 3617, 2728, 1721, 1608, 1552, 1280, 1228, 1175, 1152, 1081, 1029, 960, 928, 840, 745, 670.

### 6.2.7. Reaction with CO

A purple solution of $[U(OBMes_2)_2(\mu\text{-}OBMes_2)]_2$ (25 mg, 0.012 mmol) in $C_6D_6$ (0.4 mL) was placed in a Young's NMR tube and degassed by three freeze pump thaw cycles. The solution was then exposed to 1 bar pressure of CO. The mixture was agitated and an immediate colour change was observed to light brown. $^1$H, $^{11}$B and $^{13}$C NMR spectroscopies showed the formation of complex $[(OBMes_2)_3U\text{-}O\text{-}]_n$ from oxygen traces.

### 6.2.8. Reaction with $CO_2$

A Young's NMR tube was charged with a purple solution of $[U(OBMes_2)_2(\mu\text{-}OBMes_2)]_2$ (25 mg, 0.012 mmol) in $C_6D_6$ (0.4 mL). The NMR tube was then degassed by three freeze pump thaw cycles and exposed to 1 bar pressure of $CO_2$. The reaction was allowed to react at room temperature, and at 80 °C for one day. No change was detected in the $^1$H NMR spectrum except for trace decomposition.

### 6.2.9. Synthesis of $[\{(dmpm)(OBMes_2)_2U\}_2(\mu\text{-}\eta^6\text{:}\eta^6\text{-}C_7H_8)]$ (8)

Dmpm (10 µL, 0.064 mmol, 2 eq.) was added to a stirring toluene or benzene solution (1 mL) of $[U(OBMes_2)_2(\mu\text{-}OBMes_2)]_2$ (66 mg, 0.032 mmol) in a 7cm$^3$ vial and

the solution was allowed to stir for 15 min providing a black solution which contained the tittle product, and an off-white precipitate which contained by-products. Crystals suitable for X-ray diffraction studies were grown by slow diffusion of hexanes into the reaction mixture.

$^{1}$H NMR (500 MHz, $C_6D_6$): $\delta_H$ 7.6 (Ar-**H** Mes, 16H); 6.7 (*o*-C**H$_3$** Mes, 48H); 2.1 (*p*-C**H$_3$** Mes, 24H); -5.6 (dmpm 24H); -26 (dmpm 2H); -77 ($C_6H_6$).

$^{11}$B NMR (160 MHz, $C_6D_6$): $\delta_B$ -17 (O**B**Mes).

MS (APPI): $C_{41}H_{58}B_2O_2P_2U^+$ $[M + H]^+$ requires 905.4684, found 905.4692 (0.8 ppm)

### 6.2.10. Synthesis of [{(dmpm)(OBMes$_2$)$_2$U}$_2$(μ-η$^6$:η$^6$-C$_6$H$_6$)] (10)

A Young's NMR tube was charged with $[U(OBMes_2)_2(\mu\text{-}OBMes_2)]_2$ (66 mg, 0.032 mmol) and dmpe (10 μL, 0.064 mmol, 2 eq.) in $C_6D_6$ (0.4 mL). The reaction mixture was allowed to stand for 10 days, after which reaction is complete. Formation of the title compound was confirmed by $^{1}$H and $^{11}$B NMR spectroscopies.

$^{1}$H NMR (500 MHz, $C_6D_6$): $\delta_H$ 7.8 (Ar-**H** Mes, 16H); 4.8 (*o*-C**H$_3$** Mes, 48H); 2.6 (*p*-C**H$_3$** Mes, 24H); -14 (C**H$_3$** dmpe 24H); -42 (C**H$_2$** dmpe 8H); -75 (C$_6$**H$_6$**)

$^{11}$B NMR (160 MHz, $C_6D_6$): $\delta_B$ -17 (O**B**Mes).

### 6.2.11. Reaction with dcpm

To a purple solution of $[U(OBMes_2)_2(\mu\text{-}OBMes_2)]_2$ (50 mg, 0.024 mmol) in benzene (1 mL) dcpm (20 mg, 0.048 mmol, 2 eq.) was added in a 7 cm$^3$ vial. The solution was allowed to stir for 18 hours at room temperature. No formation of inverse arene sandwich complex was detected in $^{1}$H or $^{11}$B NMR spectra, but only formation of $[(OBMes_2)_3U\text{-}O\text{-}]_n$ complex, due to the presence of traces of oxygen.

### 6.2.12. Reaction with dppm

Dppm (18 mg, 0.048 mmol, 2 eq.) was added in a 7 $cm^3$ vial to a purple solution of $[U(OBMes_2)_2(\mu\text{-}OBMes_2)]_2$ (50 mg, 0.024 mmol) in benzene (1 mL). The reaction was allowed to stir for over 18 hours at room temperature. The formation of complex $[(OBMes_2)_3U\text{-}O\text{-}]_n$ from oxygen traces was confirmed by $^1H$ and $^{11}B$ NMR spectroscopies.

### 6.2.13. Reaction with dppe

A Young's NMR tube was charged with $[U(OBMes_2)_2(\mu\text{-}OBMes_2)]_2$ (25 mg, 0.012 mmol) and dppe (19 mg, 0.024 mmol, 2 eq.) in $C_6D_6$ (0.4 mL). The reaction was allowed to stand for 5 days. $^1H$ and $^{11}B$ NMR spectroscopies showed only the formation of $[(OBMes_2)_3U\text{-}O\text{-}]_n$, due to the presence of traces of oxygen.

### 6.2.14. Synthesis of $[(OBMes_2)_3U(\mu\text{-}\eta^6\text{:}\eta^6\text{-}C_6H_6)U(PMe_3)(OBMes_2)_2]$ (14)

To a purple solution of $[U(OBMes_2)_2(\mu\text{-}OBMes_2)]_2$ (62 mg, 0.03 mmol) in benzene (1 mL) in a 7$cm^3$ vial, $PMe_3$ (9 µL, 0.09 mmol, 3 eq.) was added. The reaction was allowed to stir for 18 hours. $^1H$ and $^{11}B$ NMR spectroscopies confirmed the formation of the inverse arene sandwich complex.

$^1H$ NMR (500 MHz, $C_6D_6$): $\delta_H$ 6.8 (Ar-**H** Mes, 24H); 2.2 (*p*-C**H₃** Mes, 36H); -0.63 (*o*-C**H₃** Mes, 72H); -80 ($C_6$**H₆**)

$^{11}B$ NMR (160 MHz, $C_6D_6$): $\delta_B$ -16 (O**B**Mes).

### 6.2.15. Synthesis of $[\{(OBMes_2)_3U\}_2(\mu\text{-}\eta^6\text{:}\eta^6\text{-}C_6H_6)]$ (16) with $PEt_3$

$PEt_3$ (12 µL, 0.012 mmol, 0.5 eq.) in THF was added to a stirring benzene solution (1 mL) of $[U(OBMes_2)_2(\mu\text{-}OBMes_2)]_2$ (50 mg, 0.024 mmol) in a 7$cm^3$ vial and the solution was allowed to stir for 18 hours. $^1H$ and $^{11}B$ NMR spectroscopies confirmed the formation of the inverse arene sandwich complex.

$^{1}$H NMR (500 MHz, $C_6D_6$): $\delta_H$ -80 ($C_6\mathbf{H_6}$)

$^{11}$B NMR (160 MHz, $C_6D_6$): $\delta_B$ -16 (O**B**Mes).

### 6.2.16. Synthesis of [{(OBMes$_2$)$_3$U}$_2$(μ-η$^6$:η$^6$-C$_6$H$_6$)] (16) with PCy$_3$

$PCy_3$ (28 mg, 0.1 mmol, 2 eq.) was added to a stirring benzene solution (1 mL) of $[U(OBMes_2)_2(\mu\text{-}OBMes_2)]_2$ (103 mg, 0.05 mmol) in a 7cm$^3$ vial and the solution was allowed to stir for 18 hours. Crystalline $[\{(OBMes_2)_3U\}_2(\mu\text{-}\eta^6\text{:}\eta^6\text{-}C_6H_6)]$ was obtained from slow diffusion of hexane into the reaction mixture. Yield: 20 mg, 19%

$^{1}$H NMR (500 MHz, $C_6D_6$): $\delta_H$ 6.4 (Ar-**H** Mes, 24H); 2.1 (*p*-C**H$_3$** Mes, 36H); -0.63 (*o*-C**H$_3$** Mes, 72H); -82 ($C_6\mathbf{H_6}$)

### 6.2.17. Reaction with PPh$_3$

In a 7 cm$^3$ vial $PPh_3$ (13 mg, 0.048 mmol, 2 eq.) was added to a purple solution of $[U(OBMes_2)_2(\mu\text{-}OBMes_2)]_2$ (50 mg, 0.024 mmol) in benzene (1 mL). After stirring over 18 hours at room temperature, the formation of complex $[(OBMes_2)_3U\text{-}O\text{-}]_n$ from oxygen traces was confirmed by $^{1}$H and $^{11}$B NMR spectroscopies.

### 6.2.18. Synthesis of [U(OBMes$_2$)$_4$] (17)

A toluene solution (1.5 mL) of $NaOBMes_2$ (115 mg, 0.4 mmol, 4 eq.) was added dropwise over 10 mins to a solution of $UI_4(dioxane)_2$ (92 mg, 0.1 mmol) in toluene (1.5 mL) in a 7 cm$^3$ vial with stirring for 18 hours. The reaction was then centrifuged and filtered. Colourless plates suitable for single-crystal X-ray crystallography were grown from slow diffusion of hexanes into the reaction mixture. Yield: 16.7 mg, 12%

$^{1}$H NMR (500 MHz, $C_6D_6$): $\delta_H$ 6.7 (Ar-**H** Mes, 16H); 2.2 (*o*-C**H$_3$** Mes, 48H); 2.0 (*p*-C**H$_3$** Mes, 24H).

$^{11}$B NMR (160 MHz, $C_6D_6$): $\delta_B$ 50 (O**B**Mes).

MS (APPI): $C_{72}H_{88}B_4O_4U^{+\cdot}$ $[M]^{+\cdot}$ requires 1298.7563, found 1298.7595 (-3.2 ppm).

### 6.2.19. Synthesis of $K_2[\{(OBMes_2)_3U\}_2(\mu\text{-}O)_2]$ (18)

To a dark purple solution of $[U(OBMes_2)_2(\mu\text{-}OBMes_2)]_2$ (50 mg, 0.024 mmol) in benzene (1 mL) in a 7 $cm^3$ vial, $KC_8$ (8 mg, 0.06 mmol, 2.5 eq.) was added. The suspension was allowed to react for 18 hours. The reaction was centrifuged and the supernatant was filtered. Light brown crystals of $K_2[\{(OBMes_2)_3U\}_2(\mu\text{-}O)_2]$ suitable for single-crystal X-ray crystallography were grown by slow diffusion of hexanes into the reaction mixture, but in very low yield; NMR spectra on this small sample are complicated and poorly resolved, so full characterisation was not pursued further.

### 6.2.20. Reaction with $P_4$

$[U(OBMes_2)_2(\mu\text{-}OBMes_2)]_2$ (62 mg, 0.03 mmol) and $P_4$ (4 mg, 0.03 mmol, 1 eq.) were placed in a Young's NMR tube in 0.4 mL of $C_6D_6$. The reaction was allowed to stand for one day at room temperature. No change was detected in the $^1H$ NMR spectrum except for the formation of $[(OBMes_2)_3U\text{-}O\text{-}]_n$ complex due to reaction with oxygen traces.

### 6.2.21. Reaction with $Me_3SiN_3$

$Me_3SiN_3$ (10 µL, 0.076 mmol, 3 eq.) was added to a purple solution of $[U(OBMes_2)_2(\mu\text{-}OBMes_2)]_2$ (52 mg, 0.025 mmol) in benzene (1 mL) in a 7 $cm^3$ vial. The reaction was allowed to stir for 18 hours, after which the reaction had turned brown. $^1H$ and $^{11}B$ NMR spectra showed resonances of complex $[(OBMes_2)_3U\text{-}O\text{-}]_n$ from the reaction with traces of oxygen.

### 6.2.22. Synthesis of $[U(OBMes_2)_3Cl]$ (19)

An excess of $Ph_3CCl$ (25 mg, 0.09 mmol, 7.5 eq.) was added to a solution of $[U(OBMes_2)_2(\mu\text{-}OBMes_2)]_2$ (25 mg, 0.012 mmol) in $C_6D_6$ (0.4 mL) in a Young's NMR tube. The solution turned pale red immediately leading to the formation of $[U(OBMes_2)_3Cl]$. $^1H$ and $^{11}B$ NMR spectroscopies confirmed the formation of the title compound.

$^{1}$H NMR (500 MHz, $C_6D_6$): $\delta_H$ 8.7 (Ar-**H** Mes, 12H); 3.5 (*p*-C**H**$_3$ Mes, 18H); 2.3 (*o*-C**H**$_3$ Mes, 36H).

$^{11}$B NMR (160 MHz, $C_6D_6$): $\delta_B$ 50 (O**B**Mes).

### 6.2.23. Synthesis of [U(N(SiMe$_3$)$_2$(OBMes$_2$)] (20)

[U(N(SiMe$_3$)$_2$)$_2$($\kappa^2$C:N-N(SiMe$_3$)SiMe$_2$CH$_2$)] (10 mg, 0,014 mmol) and dimesitylborinic acid (3.5 mg, 0,014 mmol, 1 eq.) were placed in an NMR tube and dissolved in $C_6D_6$ (0.4 mL). $^{1}$H NMR showed that quantitative formation of [U(N(SiMe$_3$)$_2$(OBMes$_2$)] had occurred. Crystals suitable for X-ray diffraction studies were grown by slow evaporation of a toluene solution of [U(N(SiMe$_3$)$_2$(OBMes$_2$)].

$^{1}$H NMR (500 MHz, $C_6D_6$): $\delta_H$ 7.5 (Ar-**H** Mes, 4H); 4.9 (*o*-C**H**$_3$ Mes, 12H); 2.5 (*p*-C**H**$_3$ Mes, 6H); -6.6 (C**H**$_3$ N(SiMe$_3$)$_2$, 54H).

$^{29}$Si NMR (99 MHz, $C_6D_6$): $\delta_{Si}$ -132 (N(**Si**Me$_3$)$_2$).

Anal. Calc for $C_{36}H_{76}B_1N_3O_1Si_6U_1$: C, 52.58 H, 8.01 N, 3.41%. Found: C, 52.39 H, 7.34 N, 3.53%.

### 6.2.24. Reaction of [U(N(SiMe$_3$)$_2$)$_3$] with HOBMes$_2^F$ to target [U(OBMes$_2^F$)$_3$]

[U(N(SiMe$_3$)$_2$)$_3$] (25 mg, 0.035 mmol) and HOBMes$_2^F$ (53 mg, 0.105 mmol, 3 eq.) in $C_6D_6$ (0.4 mL) were added to a Young's NMR tube. The reaction proceeded immediately to form a brown precipitate. $^{1}$H and $^{19}$F NMR spectroscopies indicated that a mixture of products had formed.

## 6.3. Experimental details for [Y(OBMes$_2$)$_3$]

### 6.3.1. Synthesis of [Y(OBMes$_2$)$_3$] (21)

A colourless solution of NaOBMes$_2$ (750 mg, 2.6 mmol, 2.8 eq.) in THF (15 mL) was added dropwise over a colourless solution of [YCl$_3$(THF)$_2$] (316 mg, 0.93 mmol) in THF (15 mL) over an ice bath. The solution was allowed to stir for 18 hours. The reaction was evaporated to dryness and the white residue was washed with hexane. Yield: 649 mg, 83%

$^1$H NMR (500 MHz, $C_6D_6$): $\delta_H$ 6.70 (Ar-**H** Mes, 12H); 2.36 (*o*-C**H$_3$** Mes, 36H); 2.15 (*p*-C**H$_3$** Mes, 18H).

$^{11}$B NMR (160 MHz, $C_6D_6$): $\delta_B$ 50.58 (O**B**Mes).

Elemental analysis: C 73.33 %, H 7.52 % calculated. C 73.06 %, H 7.66 % found.

### 6.3.2. Reaction with S$_8$

A Young's NMR tube was charged with [Y(OBMes$_2$)$_3$] (53 mg, 0.06 mmol) and elemental sulfur (4 mg, 0.015 mmol, 0.25 eq.) in $C_6D_6$ (0.4 mL). The reaction was allowed to stand for 4 days at room temperature. No change could be detected by $^1$H and $^{11}$B NMR spectroscopies.

### 6.3.3. Reaction with Me$_3$SiN$_3$

To a colourless solution of [Y(OBMes$_2$)$_3$] (66 mg, 0.075 mmol) in $C_6D_6$ (0.4 mL) in a Young's NMR tube, $Me_3SiN_3$ (10 µL, 0.075 mmol, 1 eq.) was added. The reaction was allowed to stand for 4 days after which no difference was appreciated in the $^1$H and $^{11}$B NMR spectra.

### 6.3.4. Reaction with dmpm

[Y(OBMes$_2$)$_3$] (57 mg, 0.065 mmol) and dmpm (10 µL, 0.064 mmol, 1 eq.) in $C_6D_6$ (0.4 mL) were placed in a Young's NMR tube. The resulting solution was stored at room temperature for 4 days. $^1$H, $^{11}$B and $^{31}$P NMR spectroscopies showed no change.

### 6.3.5. Reaction with dmpe

Dmpe (10 µL, 0.064 mmol, 1 eq.) was added to a colourless solution of [Y(OBMes$_2$)$_3$] (53 mg, 0.064 mmol) in $C_6D_6$ (0.4 mL) and placed in a Young's NMR tube. The reaction was allowed to stand for 4 days. No new resonances were observed in the $^1$H, $^{11}$B and $^{31}$P NMR spectra indicating no reaction had occurred.

## 6.4. Experimental details for [Y(OBMes$_2^F$)$_3$]

### 6.4.1. Synthesis of [Y(OBMes$_2^F$)$_3$] (22)

To a stirring colourless solution of [Y(N(SiMe$_3$)$_2$)$_3$] (177 mg, 0.31 mmol) in toluene (10 mL) in an ice bath, a solution of HOBMes$_2^F$ (468 mg, 0.92 mmol, 3 eq.) in toluene (15 mL) was added dropwise. The off-white solution was allowed to stir for 2 hours. The solution was then evaporated to dryness. The residue was washed with cold toluene (-78 °C, 5 mL) and recrystallized from toluene providing colourless crystals suitable for single-crystal X-ray crystallography. Yield: 263 mg, 46%

$^1$H NMR (500 MHz, THF-$d_8$): $\delta_H$ 8.04 (Ar-**H** Mes$^F$, 12H).

$^{11}$B NMR (160 MHz, THF-$d_8$): $\delta_B$ 32.87 (O**B**Mes$_2^F$).

$^{19}$F NMR (471 MHz, THF-$d_8$): $\delta_F$ -56.91 (*o*-C**F$_3$** Mes$^F$, 36H); -64.13 (*p*-C**F$_3$** Mes$^F$, 18H).

Elemental analysis: C 34.95 %, H 0.65 % calculated. C 34.95 %, H 0.71 % found.

### 6.4.2. Reaction with $KC_8$

To an off-white solution of $[Y(OBMes_2^{F}{}_2)_3]$ (50 mg, 0.027 mmol) in THF (1 mL) $KC_8$ (4 mg, 0.027 mmol, 1 eq.) and 18-crown-6 (7 mg, 0.027 mmol, 1 eq.) were added with stirring in a 7 $cm^3$ vial. The reaction was allowed to stir for 90 minutes. The suspension was then centrifuged and the supernatant was filtered into a vial and layered with hexane. Pale pink crystals were obtained which resulted in a mixture of $[Y(OBMes_2^{F})_3]$ and other unidentified minor products.

### 6.4.3. Reaction with $CO_2$

A Young's NMR tube was charged with an off-white solution of $[Y(OBMes_2^{F})_3]$ (22 mg, 0.012 mmol) in $C_6D_6$ (0.4 mL). The NMR tube was then degassed by three freeze pump thaw cycles and exposed to 1 bar pressure of $CO_2$. The reaction was heated at 80 °C for 2 hours. No change was detected in the $^{1}H$ and $^{19}F$ NMR spectra.

### 6.4.4. Reaction with dmpm

Dmpm (2 µL, 0.012 mmol, 1 eq.) was added to a solution of $[Y(OBMes_2^{F})_3]$ (22 mg, 0.012 mmol) in $C_6D_6$ (0.4 mL) in a Young's NMR tube. The reaction was heated at 80 °C for 2 hours after which no visible change was observed in $^{1}H$, $^{11}B$, $^{31}P$ and $^{19}F$ NMR spectra.

### 6.4.5. Reaction with dmpe

$[Y(OBMes_2^{F})_3]$ (22 mg, 0.012 mmol) and dmpe (2 µL, 0.012 mmol, 1 eq.) were added in a Young's NMR tube in $C_6D_6$ (0.4 mL). The reaction was heated for 2 hours at 80 °C. No change could be detected in $^{1}H$, $^{11}B$, $^{31}P$ and $^{19}F$ NMR spectra.

The same reaction was attempted twice more, by using THF (0.4 mL) or pyridine-$d_5$ (0.4 mL). However, no change could be detected with NMR spectroscopies. Colourless crystals suitable for single-crystal X-ray crystallography were grown from slow diffusion of hexane into pyridine reaction mixture, which shown the formation of the boroxine ring $[(Mes_2^{F}BO)(NaPy)]_3$ (**23**).

## 6.5. Experimental details for catalysis

All catalytic experiments involving $Ni(cod)_2$, $Pd(PPh_3)_2$ and $Pd_2(dba)_3$ were carried out using the same procedure. Therefore, an example is described in this section.

### 6.5.1. Example procedure for the synthesis of lithium acrylate ($H_2C=CHCO_2Li$)

To four oven-dried 4 mL vial charged with LiI (167 mg, 1.25 mmol), Zn-dust (163 mg, 2.5 mmol) and a magnetic stirrer bar, a solution of $Pd_2(dba)_3$ (12 mg, 12.5 µmol) and dppp (10 mg, 25 µmol) in toluene (2 mL) was added at room temperature. The vials were closed with a screw cap with a PTFE/silicon septum, and to each vial $NEt_3$ (0.35 mL, 2.5 mmol) was added via syringe. The vials were transferred to a 75 mL stainless steel autoclave and the septum was punctured with a small needle. The autoclave was closed and pressurised to the required ethene pressure (25 bar). After stirring for 30 min at room temperature, the autoclave was pressurised with additional $CO_2$ pressure (5 bar) to a final total pressure of 30 bar. The autoclave was heated to 100 °C for 24 h. After cooling to ambient temperature, the pressure was gradually released from the autoclave. The vials were removed from the autoclave and to each vial 1 mL of a 0.25 M solution of $LiOAc{\cdot}2H_2O$ in $D_2O$ was added as an internal standard. After vigorous stirring for 30 minutes, the combined phases were filtered through cotton wool and the $D_2O$ layer was separated from the organic phase. The turnover number was determined by $^1H$ NMR spectroscopy of the $D_2O$ layer according to the previous reported procedure:

mmol Acrylate = (mmol $LiOAc{\cdot}2H_2O$ * area Acrylate resonance)/ area $LiOAc{\cdot}2H_2O$ resonance, TON = mmol Acrylate/mmol catalyst.[7]

When NMP or THF were used as solvent for the catalytic formation of acrylates, the volatiles were removed under vacuum after the catalysis and 1 mL of a 0.25 M solution of $LiOAc{\cdot}2H_2O$ in $D_2O$ was added afterwards as an internal standard.

$^1H$ NMR (500MHz, $D_2O$): $\delta_H$ 6.19 – 6.12 (dd, $^3J$ = 10.51, 17.51 Hz, 1H, COC**H**); 6.06 – 6.01 (dd, $^3J$ = 17.51, $^2J$ = 1.88 Hz, 1H, COCHC**H**$_2$); 5.71 – 5.68 (dd, $^3J$ = 10.51, $^2J$ = 1.88 Hz, 1H, COCHC**H**$_2$).

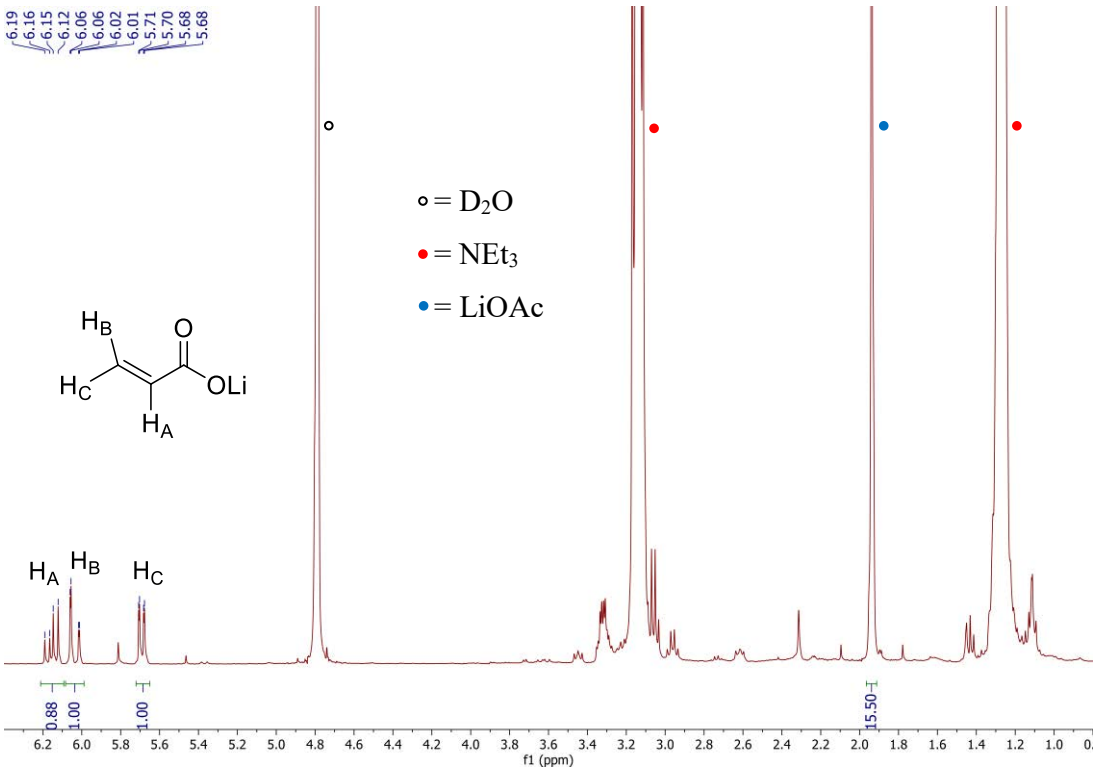


Figure 6.1. Example of $^{1}$H NMR spectrum (298 K, $D_2O$, 500 MHz) of lithium acrylate from the catalytic conversion of $C_2H_4$ and $CO_2$, using the conditions mentioned above.

## 6.6. Synthesis and catalysis of Pd-NHC complexes

### 6.6.1. Synthesis of $Pd(NHC1)_2Cl_2$

A Schlenk flask was charged with $Pd(CH_3CN)_2Cl_2$ (97 mg, 0.375 mmol) and Ag(NHC1)Cl (433 mg, 0.75 mmol, 2 eq.) and a stirrer bar. The reaction mixture was dissolved in $CH_2Cl_2$ (10 mL) to yield a dark brown solution, which was allowed to stir at room temperature for 2 hours in the dark. The solution was then filtered through celite and evaporated to dryness to afford $Pd(NHC1)_2Cl_2$ as a brown solid. The product was recrystallised from $CH_2Cl_2$/hexane at -20 °C.

Yield: 128 mg, 33%.

$^{1}$H NMR (500MHz, $CDCl_3$): $\delta_H$ 7.36 – 7.32 (d, $^{2}J$ = 8.93 Hz, 8H); 7.09 – 7.06 (tt, $^{2}J$ = 7.41, $^{3}J$ = 1.32 Hz, 4H); 7.02 – 6.99 (m, 8H); 6.73 – 6.71 (m, 8H); 6.63 – 6.60 (d, $^{2}J$ = 8.93 Hz, 8H); 3.83 (s, 12H).

$^{13}$C NMR (126 MHz, $CDCl_3$): $\delta_C$ 169.43, 158.87, 132.75, 131.16, 130.72, 130.15, 128.62, 128.03, 127.87, 113.40, 55.27.

### 6.6.2. Synthesis of $Pd(NHC2)_2Cl_2$

$Pd(NHC2)_2Cl_2$ was synthesised with analogous procedure to $Pd(NHC1)_2Cl_2$. $Pd(CH_3CN)_2Cl_2$ (97 mg, 0.375 mmol) and Ag(NHC2)Cl (387 mg, 0.75 mmol, 2 eq.) were used to afford $Pd(NHC2)_2Cl_2$ as a dark brown solid.

Yield: 102 mg, 29%.

$^1$H NMR (500MHz, $CDCl_3$): $\delta_H$ 7.41 – 7.39 (m, 8H); 7.24 – 7.21 (tt, $^2J$ = 7.54, $^3J$ = 1.24 Hz, 4H); 7.09 – 7.04 (m, 12H); 7.01 – 6.98 (m, 8H); 6.73 – 6.70 (m, 8H).

$^{13}$C NMR (126 MHz, $CDCl_3$): $\delta_C$ 169.32, 138.01, 132.74, 130.68, 128.98, 128.52, 128.38, 128.28, 128.02, 110.12.

### 6.6.3. Synthesis of $Pd(NHC3)_2Cl_2$

$Pd(NHC3)_2Cl_2$ was synthesised with analogous procedure to $Pd(NHC1)_2Cl_2$. $Pd(CH_3CN)_2Cl_2$ (130 mg, 0.5 mmol) and Ag(NHC3)Cl (685 mg, 1 mmol, 2 eq.) were used to afford $Pd(NHC3)_2Cl_2$ as a brown solid.

Yield: 146 mg, 23%.

$^1$H NMR (500MHz, $CDCl_3$): $\delta_H$ 7.63 – 7.61 (m, 8H); 7.20 – 7.17 (tt, $^2J$ = 7.61, $^3J$ = 1.15 Hz, 4H); 7.14 – 7.12 (m, 4H); 7.05 – 7.01 (m, 8H); 6.80 – 6.78 (m, 8H); 2.84 – 2.74 (m, 8H); 0.94 – 0.92 (d, $^3J$ = 6.89 Hz, 24H); 0.61 – 0.59 (d, $^3J$ = 6.89 Hz, 24H).

$^{13}$C NMR (126 MHz, $CDCl_3$): $\delta_C$ 169.73, 142.05, 133.54, 133.32, 130.15, 129.03, 128.91, 128.04, 124.06, 29.54, 23.43, 23.15.

### 6.6.4.Synthesis of $Pd(NHC4)_2Cl_2$

$Pd(NHC4)_2Cl_2$ was synthesised with analogous procedure to $Pd(NHC1)_2Cl_2$. $Pd(CH_3CN)_2Cl_2$ (195 mg, 0.75 mmol) and Ag(NHC4)Cl (903 mg, 1.5 mmol, 2 eq.) were used to afford $Pd(NHC4)_2Cl_2$ as a yellow solid.

Yield: 231 mg, 31%.

$^1$H NMR (500MHz, $CDCl_3$): $\delta_H$ 7.30 – 7.24 (m, 4H); 7.18 – 7.15 (m, 4H); 6.98 – 6.96 (m, 4H); 2.08 – 2.05 (m, 12H); 1.93 – 1.80 (m, 8H); 1.56 (br, 8H); 1.31 – 1.30 (m, 36H).

$^{13}$C NMR (126 MHz, $CDCl_3$): $\delta_C$ 148.68, 144.81, 133.54, 138.71, 129.24, 128.26, 124.98, 116.57, 103.07, 35.27, 33.48, 23.96, 21.92, 17.57.

### 6.6.5. Synthesis of $Pd(NHC5)_2Cl_2$

$Pd(NHC5)_2Cl_2$ was synthesised with analogous procedure to $Pd(NHC1)_2Cl_2$. $Pd(CH_3CN)_2Cl_2$ (106 mg, 0.41 mmol) and Ag(NHC5)Br (543 mg, 0.82 mmol, 2 eq.) were used to afford $Pd(NHC5)_2Cl_2$ as a dark brown solid.

Yield: 105 mg, 21%.

$^1$H NMR (500MHz, $CDCl_3$): $\delta_H$ 7.40 – 7.38 (m, 8H); 7.37 – 7.35 (m, 8H); 6.76 – 6.74 (m, 8H); 6.58 – 6.56 (m, 8H); 3.70 – 3.69 (m, 12H); 2.97 – 2.95 (m, 24H).

$^{13}$C NMR (126 MHz, $CDCl_3$): $\delta_C$ 166.54, 145.72, 130.67, 130.24, 125.98, 125.47, 124.95, 116.34, 115.56, 98.01, 56.73, 44.12.

### 6.6.6. Synthesis of $Pd(NHC6)_2Cl_2$

$Pd(NHC6)_2Cl_2$ was synthesised with analogous procedure to $Pd(NHC1)_2Cl_2$. $Pd(CH_3CN)_2Cl_2$ (195 mg, 0.75 mmol) and Ag(NHC6)Cl (1.07 g, 1.5 mmol, 2 eq.) were used to afford $Pd(NHC6)_2Cl_2$ as a pale brown solid.

Yield: 317 mg, 32%.

$^{1}$H NMR (500MHz, $CDCl_3$): $\delta_H$ 7.34 – 7.31 (m, 4H); 7.16 – 7.13 (m, 4H); 6.86 – 6.82 (m, 4H); 6.70 – 6.66 (m, 8H); 6.58 – 6.53 (m, 8H); 3.61 (t, $^{4}J$ = 1.83 Hz, 12H); 1.26 – 1.24 (m, 36H).

$^{13}$C NMR (126 MHz, $CDCl_3$): $\delta_C$ 166.49, 149.98, 137.22, 130.44, 129.83, 126.61, 125.72, 125.58, 123.32, 119.74, 115.68, 106.13, 56.84, 35.11, 31.25, 19.03.

### 6.6.7. Example procedure for the synthesis of lithium acrylate catalysed by Pd-NHC complexes 1-6

To four oven-dried 4 mL vial charged with LiI (167 mg, 1.25 mmol), Zn-dust (163 mg, 2.5 mmol) and equipped with a magnetic stirrer bar, a solution of $Pd(NHC1)_2Cl_2$ (26 mg, 25 μmol) in toluene (2 mL) was added. The vials were closed with a screw cap with a PTFE/silicon septum, and to each vial $NEt_3$ (0.35 mL, 2.5 mmol) was added via syringe. The vials were transferred to a 75 mL stainless steel autoclave and the septum was punctured with a small needle. The autoclave was closed and pressurised to the required ethene pressure (25 bar). After stirring for 30 min at room temperature, the autoclave was pressurised with additional $CO_2$ pressure (5 bar) to a final total pressure of 30 bar. The autoclave was heated to 50 °C for 24 h. After cooling to ambient temperature, the pressure was gradually released from the autoclave. The vials were removed from the autoclave and to each vial 1 mL of a 0.25 M solution of $LiOAc{\cdot}2H_2O$ in $D_2O$ was added as an internal standard. After vigorous stirring for 30 minutes, the combined phases were filtered through cotton wool and the $D_2O$ layer was separated from the organic phase. The turnover number was determined by $^{1}$H NMR spectroscopy of the $D_2O$ layer according to the previous reported procedure:

mmol Acrylate = (mmol $LiOAc{\cdot}2H_2O$ * area Acrylate resonance)/ area $LiOAc{\cdot}2H_2O$ resonance, TON = mmol Acrylate/mmol catalyst.[7]

## 6.7. Crystallographic details

X-ray crystallography data on compound **1** was collected on a Rigaku Oxford diffraction SuperNova diffractometer fitted with an Atlas CCD detector with Mo Kα radiation (λ = 0.7107 Å). Compounds **2**, **3**, **4**, **5**, **8**, **16**, **17**, **18**, **20**, **22** and **23** were collected

using an Oxford Diffraction Excalibur Eos diffractometer with Mo Kα radiation at 120(2), 170(2) or 293(2) using a Mo Kα source radiation source (λ = 0.71073 Å). All structures were solved using SHELXT in Olex2.[8, 9] Absorption corrections were completed using *CrysAlis PRO* 1.171.38.46 (Rigaku Oxford Diffraction, 2015) software. Analytical numeric absorption corrections used a multifaceted crystal model based on expressions derived by Clark and Reid.[10] Numerical absorption correction was based on a Gaussian integration over a multifaceted crystal model. Empirical absorption correction using spherical harmonics, implemented in SCALE3 ABSPACK scaling algorithm.

Unless otherwise stated, all non-H atoms were refined anisotropically and all H atoms were placed in calculated positions and refined using a riding model. No restraints were applied during the refinement of **2**, **3**, **4**, **5**, **8**, **16**, **17**, **18** and **20** The $CF_3$ groups in **22** and **23** were restrained using the SHELX software package SADI and RIGU.

Table 4.1.Crystallographic data summary for complexes **1**, **2** and **3** and **4**.

| Complex | **1** | **2** | **3 and 4** |
|---|---|---|---|
| **Local code** | Po17030_refinalized | p17082_imono081 | p18047 |
| **Chemical formula** | $0.67(C_{108}H_{132}B_6O_6U_2)\cdot 1.33(C_6H_{14})$ | $0.5(B_4C_{72}O_8U)\cdot 2(C_5N)$ | $C_{90}H_{96}B_3O_5P_2U\cdot C_{72}H_{88}B_5O_6U\cdot 5$(toluene) |
| $M_r$ | 1492.93 | 999.37 | 3233.95 |
| **Crystal system, space group** | Monoclinic, $P2_1/c$ | Monoclinic, $I2/m$ | Triclinic, $P$-1 |
| **Temperature (K)** | 120 | 120 | 293 |
| **$a$, $b$, $c$ (Å)** | 13.8450 (2)<br>14.9545 (2)<br>31.6940 (4) | 17.2362 (5)<br>13.7651 (8)<br>16.4420 (5) | 17.2121 (4)<br>23.0300 (4)<br>23.4449 (6) |
| **α, β, γ (°)** | 96.521 (1) | 90.156 (2) | 72.304 (2)<br>80.146 (2)<br>70.091 (2) |
| **$V$ (Å$^3$)** | 6519.63 (15) | 3901.0 (3) | 8300.8 (4) |
| **$Z$** | 3 | 4 | 2 |
| **Radiation type** | Mo $K\alpha$ | Mo $K\alpha$ | Mo $K\alpha$ |
| **μ (mm$^{-1}$)** | 2.53 | 4.21 | 2.03 |
| **Crystal size (mm)** | 0.34 × 0.22 × 0.17 | 0.23 × 0.11 × 0.04 | 0.19 × 0.15 × 0.08 |
| **Diffractometer** | SuperNova, Dual, Cu at zero, Atlas | Xcalibur, Eos | Xcalibur, Eos |
| **Absorption correction** | Gaussian | Analytical | Multi-scan |
| **$T_{min}$, $T_{max}$** | 0.519, 0.880 | 0.978, 0.995 | 0.951, 1.000 |
| **No. of measured, independent and observed [$I > 2s(I)$] reflections** | 139328<br>17270<br>13836 | 31319<br>3992<br>2962 | 190301<br>33882<br>21873 |
| **$R_{int}$** | 0.072 | 0.128 | 0.141 |
| **$(\sin\theta/\lambda)_{max}$ (Å$^{-1}$)** | 0.698 | 0.617 | 0.625 |
| **$R[F^2 > 2s(F^2)]$, $wR(F^2)$, $S$** | 0.041, 0.075, 1.04 | 0.335, 0.658, 4.80 | 0.058, 0.123, 1.00 |
| **No. of reflections** | 17270 | 3992 | 33882 |
| **No. of parameters** | 624 | 74 | 1708 |
| **No. of restraints** | 0 | 0 | 0 |
| **H-atom treatment** | H-atom parameters not refined | - | H-atom parameters constrained |
| **$\Delta)_{max}$, $\Delta)_{min}$ (e Å$^{-3}$)** | 1.00, -1.42 | 33.67, -13.92 | 1.51, -1.04 |

Table 4.2. Crystallographic data summary for complexes **5**, **8** and **16**.

| Complex | **5** | **8** | **16** |
|---|---|---|---|
| **Local code** | p18033 | p18005 | P18056a |
| **Chemical formula** | $C_{54}H_{66}B_3O_3S_2U \cdot C_6H_6 \cdot C_3$ | $C_{44.5}H_{61.5}B_2O_2P_2U$ | $0.75(C_{114}H_{132}B_6O_6U_2) \cdot 5(C_6H_{12})$ |
| $M_r$ | 1211.78 | 950.02 | 1503.67 |
| **Crystal system, space group** | Triclinic, *P*-1 | Monoclinic, $P2_1/n$ | Trigonal, *P*-3 |
| **Temperature (K)** | 293 | 170 | 293 |
| ***a*, *b*, *c* (Å)** | 12.3086 (2)<br>14.3349 (2)<br>21.6092 (4) | 13.4507 (4)<br>14.9327 (4)<br>22.0650 (6) | 23.0864 (5)<br><br>17.2733 (3) |
| **α, β, γ (°)** | 77.206 (1)<br>87.126 (1)<br>84.907 (1) | 99.940 (2) | |
| ***V* (Å$^3$)** | 3701.62 (11) | 4365.3 (2) | 7972.9 (4) |
| ***Z*** | 2 | 4 | 4 |
| **Radiation type** | Mo *K*α | Mo *K*α | Mo *K*α |
| **μ (mm$^{-1}$)** | 2.28 | 3.83 | 0.61 |
| **Crystal size (mm)** | 0.38 × 0.27 × 0.05 | 0.66 × 0.33 × 0.25 | |
| **Diffractometer** | Xcalibur, Eos | Xcalibur, Eos | Xcalibur, Eos |
| **Absorption correction** | Analytical | Analytical | Multi-scan |
| $T_{min}$, $T_{max}$ | 0.267, 0.814 | 0.667, 0.828 | 0.854, 1.000 |
| **No. of measured, independent and observed [$I > 2s(I)$] reflections** | 78705<br>15098<br>12610 | 37396<br>9975<br>7472 | 184529<br>15273<br>8504 |
| $R_{int}$ | 0.077 | 0.046 | 0.135 |
| **(sin θ/λ)$_{max}$ (Å$^{-1}$)** | 0.625 | 0.649 | 0.713 |
| ***R*[$F^2 > 2s(F^2)$], *wR*($F^2$), *S*** | 0.044, 0.111, 0.96 | 0.046, 0.103, 1.09 | 0.079, 0.219, 1.02 |
| **No. of reflections** | 15098 | 9975 | 15273 |
| **No. of parameters** | 638 | 494 | 682 |
| **No. of restraints** | 0 | 0 | 0 |
| **H-atom treatment** | H-atoms treated by a mixture of independent and constrained refinement | H-atoms treated by a mixture of independent and constrained refinement | H-atom parameters constrained |
| **Δ)$_{max}$, Δ)$_{min}$ (e Å$^{-3}$)** | 2.25, -0.77 | 2.40, -1.50 | 13.32, -2.15 |

Table 4.3. Crystallographic data summary for complexes **17**, **18** and **20**.

| Complex | **17** | **18** | **20** |
|---|---|---|---|
| **Local code** | p18061 | p18089 | p18053_tri |
| **Chemical formula** | $C_{74}H_{92}B_4O_5U$ | $0.67(C_{108}H_{132}B_6K_2O_8U_2)$ | $2(C_{36}H_{76}BN_3OSi_6U)$ |
| $M_r$ | 1342.74 | 1451.50 | 1968.75 |
| **Crystal system, space group** | Triclinic, *P*-1 | Monoclinic, $P2_1/n$ | Triclinic, *P*-1 |
| **Temperature (K)** | 170 | 293 | 293 |
| ***a*, *b*, *c* (Å)** | 14.1285 (10)<br>15.8427 (12)<br>16.6496 (12) | 15.3907 (2)<br>22.7218 (2)<br>16.9809 (3) | 12.0703 (2)<br>13.1641 (2)<br>15.6746 (3) |
| **α, β, γ (°)** | 103.798 (6)<br>105.012 (6)<br>98.607 (6) | 109.680 (2) | 102.222 (2)<br>98.270 (1)<br>90.122 (1) |
| ***V* (Å$^3$)** | 3405.7 (5) | 5591.43 (13) | 2407.48 (7) |
| ***Z*** | 2 | 3 | 1 |
| **Radiation type** | Mo *K*α | Mo *K*α | Mo *K*α |
| **μ (mm$^{-1}$)** | 2.43 | 3.02 | 3.55 |
| **Crystal size (mm)** | 0.21 × 0.10 × 0.01 | 0.28 × 0.24 × 0.16 | 0.79 × 0.33 × 0.08 |
| **Diffractometer** | Xcalibur, Eos | Xcalibur, Eos | Xcalibur, Eos |
| **Absorption correction** | Analytical | Analytical | Multi-scan |
| $T_{min}$, $T_{max}$ | 0.714, 0.972 | 0.743, 0.840 | 0.483, 1.000 |
| **No. of measured, independent and observed [$I > 2s(I)$] reflections** | 78218<br>15623<br>11506 | 109506<br>10220<br>8129 | 51203<br>9835<br>8900 |
| $R_{int}$ | 0.152 | 0.061 | 0.049 |
| **(sin θ/λ)$_{max}$ (Å$^{-1}$)** | 0.649 | 0.602 | 0.625 |
| **$R[F^2 > 2s(F^2)]$, $wR(F^2)$, $S$** | 0.069, 0.087, 0.99 | 0.030, 0.069, 1.02 | 0.024, 0.055, 1.07 |
| **No. of reflections** | 15623 | 10220 | 9835 |
| **No. of parameters** | 781 | 586 | 457 |
| **No. of restraints** | 0 | 0 | 0 |
| **H-atom treatment** | H-atom parameters constrained | H-atom parameters constrained | H-atom parameters constrained |
| **Δ)$_{max}$, Δ)$_{min}$ (e Å$^{-3}$)** | 2.04, -1.09 | 0.80, -0.68 | 0.80, -0.60 |

Table 4.4. Crystallographic data summary for complexes **22** and **23**.

| Complex | **22** | **23** |
|---|---|---|
| **Local code** | p17130_100_tri | p18066 |
| **Chemical formula** | $C_{58}H_{20}B_3F_{54}O_4Y$ | $3(C_{69}H_{27}B_3F_{54}N_3Na_3O_3)$ |
| $M_r$ | 1813.13 | 6219.51 |
| **Crystal system, space group** | Triclinic, *P*-1 | Trigonal, *R*-3*c* |
| **Temperature (K)** | 120 | 293 |
| ***a*, *b*, *c* (Å)** | 13.3660 (8)<br>15.5824 (7)<br>22.4158 (19) | 20.7121 (3)<br>20.7121 (3)<br>34.5400 (7) |
| **α, β, γ (°)** | 81.135 (5)<br>89.536 (6)<br>72.310 (4) | |
| ***V* (Å$^3$)** | 4391.0 (5) | 12832.2 (5) |
| ***Z*** | 2 | 2 |
| **Radiation type** | Mo *K*α | Mo *K*α |
| **μ (mm$^{-1}$)** | 0.75 | 0.19 |
| **Crystal size (mm)** | 0.40 × 0.31 × 0.07 | 0.26 × 0.23 × 0.16 |
| **Diffractometer** | Xcalibur, Eos | Xcalibur, Eos |
| **Absorption correction** | Analytical | Analytical |
| $T_{min}$, $T_{max}$ | 0.797, 0.952 | 0.893, 0.938 |
| **No. of measured, independent and observed [$I > 2s(I)$] reflections** | 56779<br>9171<br>6195 | 10441<br>2335<br>1732 |
| $R_{int}$ | 0.114 | 0.066 |
| **(sin θ/λ)$_{max}$ (Å$^{-1}$)** | 0.500 | 0.581 |
| **$R[F^2 > 2s(F^2)]$, $wR(F^2)$, $S$** | 0.112, 0.271, 1.03 | 0.051, 0.118, 1.04 |
| **No. of reflections** | 9171 | 2355 |
| **No. of parameters** | 1318 | 262 |
| **No. of restraints** | 1059 | 186 |
| **H-atom treatment** | H-atom parameters constrained | H-atom parameters constrained |
| **Δ)$_{max}$, Δ)$_{min}$ (e Å$^{-3}$)** | 0.59, -0.60 | 0.15, -0.17 |

## 6.8. Bibliography

[1] S. M. Mansell, B. F. Perandones, P. L. Arnold, *J. Organomet. Chem.* **2010**, *695*, 2814-2821.

[2] M. J. Monreal, R. K. Thomson, T. Cantat, N. E. Travia, B. L. Scott, J. L. Kiplinger, *Organometallics* **2011**, *30*, 2031-2038.

[3] A. Pelter, B. Singaram, L. Warren, J. W. Wilson, *Tetrahedron* **1993**, *49*, 2965-2978.

[4] S. M. Cornet, K. B. Dillon, C. D. Entwistle, M. A. Fox, A. E. Goeta, H. P. Goodwin, T. B. Marder, A. L. Thompson, *Dalton Trans.* **2003**, 4395-4405.

[5] D. C. Bradley, J. S. Ghotra, F. A. Hart, *J. Chem. Soc., Dalton Trans.* **1973**, 1021-1023.

[6] S. Y. Lee, S. Neufeind, G. C. Fu, *J. Am. Chem. Soc.* **2014**, *136*, 8899-8902.

[7] C. Hendriksen, E. A. Pidko, G. Yang, B. Schäffner, D. Vogt, *Chem. – A Eur. J.* **2014**, *20*, 12037-12040.

[8] G. Sheldrick, *Acta Crystallogr. Sect. A* **2015**, *71*, 3-8.

[9] O. V. Dolomanov, L. J. Bourhis, R. J. Gildea, J. A. K. Howard, H. Puschmann, *J. Appl. Cryst.* **2009**, *42*, 339-341.

[10] R. C. Clark, J. S. Reid, *Acta Crystallogr. Sect. A* **1995**, *51*, 887-897.